Università degli studi di Modena e Reggio Emilia

PhD "Enzo Ferrari" in Industrial and Environmental Engineering XXXIV° Cycle

Coordinator: Prof. Alberto Muscio

HIGH-EFFICIENCY AND ENVIRONMENTALLY FRIENDLY PROPULSION AND POWER GENERATION SYSTEMS

Academic Discipline (SSD) ING-IND/08

Candidate: Francesco Legrottaglie

Supervisor: Prof. Carlo Alberto Rinaldini

Thanks

I thank all the people who supported me to achieve this important goal, in particular Professor Carlo Rinaldini and fellow engineers Francesco Scrignoli, Tommaso Savioli and Filippo Vecchio. I also thank Silena, Leonardo and Lorenzo who have been very patient with me.

Abstract

The European Commission has adopted a package of legislative proposals aimed at achieving climate neutrality in the EU by 2050. The new ambitious European targets provide the strategic framework for the evolution of the national system, also in regulatory and planning terms. The Italian National Recovery and Resilience Plan (PNRR) includes important investments for the reduction of greenhouse gas emissions, focusing on the circular economy, the decarbonisation of the economy and energy efficiency.

Both biogas and hydrogen can help address increasing waste and substantially reduce the use of fossil fuels. They could be used in the transportation field, as well as in combined heat and power generation in compression ignition engines, or, in the case of hydrogen, in fuel cells.

In this context, their use in compression-ignition engines as a full or partial alternative to fossil fuels will in some cases require minor changes to the engine control management parameters or, in other cases, may require structural, but modest, combinations so that existing engines can be powered by a wide range of alternative fuel blends to conventional ones.

This research work explores the potentials of innovative combustion concepts. The task was developed based on the results of experimental tests of a compression-ignition engine conducted on the engine test bench of the Engineering Department of the University of Modena and Reggio Emilia. The diesel cycle engine was adapted to operate in dual-fuel (DF) mode, and specifically set up to work in the reactivity-controlled combustion (RCCI) condition.

In this configuration, a portion of diesel fuel is replaced by a low-reactivity fuel injected indirectly into the intake manifold, forming a homogeneous, lean premixed charge; a small amount of high-reactivity fuel is injected directly into the cylinder for fuel ignition.

Following the analysis of the experimental tests, the investigation was conducted on the basis of the results of 3D CFD modelling of combustion.

Summary

List of figures

List of tables

Dissemination

1. Mattarelli E, Rinaldini CA, Savioli T, Scrignoli F, Legrottaglie F. Experimental investigation on a diesel engine operated in RCCI combustion mode. AIP Conference Proceedings. 2019;2191(1):020096. doi:10.1063/1.5138829

2. Legrottaglie F, Mattarelli E, Rinaldini CA, Scrignoli F. Application to Micro-Cogeneration of an Innovative Dual Fuel Compression Ignition Engine Running on Biogas. International Journal of Thermofluids, doi.org/10.1016/j.ijft.2021.100093

3. Mattarelli, E.; Rinaldini, C.A.; Marmorini, L.; Caprioli, S.; Legrottaglie, F.; Scrignoli, F. 2-Stroke RCCI Engines for Passenger Cars. Energies 2022, 15, 1173. https://doi.org/10.3390/en15031173

4. Scrignoli, F., Vecchio, F., Legrottaglie, F., Mattarelli, E., & Rinaldini, C. A. (2022). Numerical Investigation of Dual Fuel Combustion on a Compression Ignition Engine Fueled with Hydrogen/Natural Gas Blends. Fuels, 3(1), 132-151.

Nomenclature

ATDC	After top dead centre
BDC	bottom death centre
BMEP	Brake mean effective pressure
BP	Brake power/net power
BSEC	Brake specific energy consumption
BSFC	Brake specific fuel consumption
BSU	Bosch smoke unit
BTDC	Before top dead centre
BTE	Brake Thermal Efficiency
CFD	Computational fuel dynamics
CFR	Cooperative fuel research
CI	Compression ignition
CNG	Compressed natural gas
COV	Coefficient of variation
CR	Compression ratio
DF	Dual fuel
DICI	direct injection compression ignition
EGR	Exhaust gas recirculation
ER	Equivalence ratio
FTD	Fischer–Tropsch diesel
HCCI	Homogeneous charge compression ignition
HHV	Higher heating value
HSU	Hartridge smoke unit
HV	Heating value/calorific value
ICE	Internal combustion engine
IDI	Indirect injection
IMEP	Indicated mean effective pressure
IMEP*	Indicated mean effective pressure from -40 [CA°] to 114 [CA°]
IP	Indicated power/gross power
ISEC	Indicated specific energy consumption
KL	Knock-limited power output
LFL	Lower/lean flammability limit
LHV	Lower heating value

LNG	Liquefied natural gas
LPG	Liquefied petroleum gas
MN	Methane number
PLC	Programmable logic control
PM	Particulate matter
RCCI	Reactivity controlled compression ignition
RON	Research octane number
SCR	Selective catalytic reduction
SI	Spark ignition
SOF	Soluble organic fraction
T	Absolute temperature
TDC	Top dead centre
WN	Wobbe number
WTW	Well-to-wheel
3D-CFD	Three-dimensional fluid dynamics
B	Mole fraction of heptane in mixtures with methane
Φ	Equivalence ratio on fuel-to-air basis
Λ	Equivalence ratio on air-to-fuel basis
CH4	Methane
CO	Carbon Monoxide
CO_2	Carbon Dioxide
NOx	Nitrogen Oxides (NO+NO2)
O2	Oxygen
a_{ii}	as it is
c	combustion
CO	carbon monoxide
D	Diesel fuel
Dm	dry matter
lw	live weight
NG	Natural Gas
vs	volatile substance
m_D	Mass of Diesel fuel provided to the engine per cycle in normal Diesel operation, mg
m_{NG}	Mass of natural gas provided to the engine per cycle in dual fuel operation, mg

m'_D	Mass of Diesel fuel provided to the engine per cycle in dual fuel operation, mg
$\dot{m}_{NG}$	Natural gas mass flow rate, g/s
$\dot{m}_{air}$	Air mass flow rate, kg/s
P_{in}	Power provided to the engine by means of fuel(s), kW
S_D	Substitution rate of high reactivity fuel,%
X_D	Fraction of energy introduced with Diesel fuel in dual fuel mode,%
X_{NG}	Fraction of energy introduced with natural gas in dual fuel mode,%
AFR	Air to Fuel Ratio
AHRR	Apparent Heat Release Rate, J/°
CAD	Crank Angle Degree, °
CN	Cetane Number
CO	concentration of carbon monoxide, ppm
FMEP	Friction Mean Effective Pressure, bar
HC	Concentration of methane equivalent unburnt hydrocarbons, ppm
LHV_{CO}	Carbon monoxide lower heating value, MJ/kg
LHV_D	Diesel fuel lower heating value, MJ/kg
LHV_{NG}	Natural Gas lower heating value, MJ/kg
PPRR	Peak Pressure Rise Rate, bar/°
RI	Ringing Intensity, MW/m^2
RoHR	Rate of Heat Release, J/°
WI	Wobbe Index, MJ/Nm^3

INTRODUCTION

The environmental problem that has been created with industrialisation, transport, and, in general, human activities is now known to all; it has now moved so far in one direction that it will be difficult to backtrack against the current continuous growth of global warming, if significant interventions are not taken immediately.

Moreover, the problem of energy security is a very current issue, due to the lack of resources in national territories, especially in the case of Italy, where most of the major energy carriers are imported from abroad. The very recent situation related to the Russia/Ukrainian crisis is a classic example, as faced with sanctions imposed on the distributor country there is an increasing risk of higher costs, as well as supply difficulties.

Most of the world's industrialised nations agree that everyone should do their part, but in relation to the trends indicated by the international scientific communities, the results are not being achieved as they should. It is not easy to implement rapid actions to contain climate-changing emissions, because if first and foremost, energy efficiency is not improved, it will be necessary to reduce either production or transport, or both. Clearly this is not possible for anyone, as it would mean slowing the growth of a country. The only way is therefore to improve the effectiveness with which energy is transformed and made available to industrial, civil or transport users.

The main European objectives are to reduce greenhouse gas emissions, first of all CO_2, setting very precise thresholds to be reached, initially until 2050, if we want to contain the atmospheric temperature values within certain limits; for this reason, the European Commission is allocating funds to investments to tackle the problem.

Consequently, the Italian National Plan of Resistance and Resilience also provides for investments in this sense: some issues being tackled in this direction are energy efficiency, the abandonment of obsolete systems, the limitation of fossil fuel usage, the increment of renewable energy sources and new energy carrier solutions that can be used simply, such as hydrogen.

The study of clean energy generation systems such as nuclear fusion is also a current issue, although it will take time to obtain solid results on the efficiency and stability of this method. Certainly, better developments have been achieved in fuel cell technology, but the reliability demanded for long-term applications has not yet been achieved.

Research in bio-fuels has already made good progress in trying to replace fossil fuels: this is a priority not only in terms of energy security, but especially to drastically reduce climate-changing greenhouse gas emissions. We must look to bio-fuels deriving from farming waste

and generally, processing by-products of organic origin; methods and processes for their transformation have been in place for some time, indeed today we talk of fourth-generation biofuels. The use of bio-fuels instead of fossil fuels can bring to the carbon-neutrality: the use of this source of energy would return to the environment the CO_2 (the main greenhouse gas produced by hydrocarbon combustion) absorbed during its production.

Renewable sources remain a very important element, and must be focused on without the speculation of the past, as they have now become a necessity. Programmable renewable sources are those for which the production of energy can be programmed over time. It is obviously important to be able to predict the availability of energy, without necessarily having to base this on statistics deriving from historical data, when for example we talk about wind or sun energy, also by virtue of the sudden climate changes we are experiencing.

Obviously, together with programmability, we need an energy distribution network that offers greater flexibility of zonal exchange. The future must include more and more micro-power plants for the generation of both heat and electricity, which will have to support combinations of programmable and non-programmable production centres, the well-known "smart-grids" will have to increasingly become intelligent exchange networks. Important progress is also being made in the installation various kinds of batteries to compensate for peaks in energy demands.

In the transport sector, powertrains are becoming electrified: the current regulated emissions thresholds have become far too restrictive to continue to use only thermal engines. For this reason, traditional engines are often coupled to an electric engine (hybrid powertrains) or even completely replaced (electric powertrains). However, we have to understand how much this is becoming a commercial fashion, and understand if electric powertrains are truly “zero-emission”. In fact, this is still not exactly the case today: more than half of the electricity is still produced from fossil fuels (in Europe or Italy), and the production of fundamental elements of an electric vehicle, such as batteries, seems far from low-environmental-impact. In addition, reliability, longevity and autonomy are some very important characteristics to consider, and today are not comparable with those achieved by combustion engines. Certainly, both for light and heavy vehicles on electric traction further developments are still needed in the field of electric powertrains to reach the well-known levels of technology of combustion engines.

In this scenario, with a view to a real "energy transition", it seems possible, if not necessary, to continue to use internal combustion engines, improving their efficiency, limiting their emissions and, above all, eliminating the use of fossil fuels in order to strongly limit CO_2

emissions. In recent decades, many experiments have been carried out in combustion techniques and with the combination of several fuels, also of non-fossil origin, to understand if there is room for improvement in terms of the polluting exhaust gases produced, while maintaining high performance levels.

With this in mind, for some time diesel engines have been converted to natural gas that can be produced from biomass, in this case we talk of biogas. Typically, however, the conversion takes place by replacing the injectors with spark plugs, converting the Diesel cycle to an Otto cycle. This necessarily requires the modification of the piston geometry to reduce the compression ratio and avoid knocking, with a consequent worsening of the overall efficiency of the engine.

To date, new combustion techniques that allow the combustion of a pre-mixed charge of a low-reactivity fuel (such as gasoline, natural gas or biogas) by auto-ignition of a small amount of diesel have been studied. In this way, the risk of detonation is limited and the engine can run at the original compression ratio; moreover, this type of ignition is able to efficiently burn even lean pre-mixed charges, a condition that would be critical for a spark ignition engine. Moreover, the combustion obtained is defined as "low temperature" and shifts from the areas that promote the formation of NOx while the pre-mixed combustion limits the formation of soot; in this way, the trade-off between NOx and soot emissions typical of traditional diesel engines is overcome Finally, the conversion does not require substantial changes to the engine, aside from the installation of indirect injectors for the fuel that is pre-mixed to the combustion air and the related electronic control hardware.

The work carried out in the three-year PhD programme focuses on the study of this innovative type of combustion that takes the name of Reactivity-Controlled Compression Ignition (RCCI) Dual Fuel (DF) combustion.

In detail, experiments were carried out on a compression ignition engine partially substituting diesel oil with different low-reactivity fuels (gasoline and natural gas) and evaluating the differences in terms of combustion. For each operating point, different levels of diesel replacement were tested, with calibrations to optimise the engine performance.

The data collected during the experimental campaign were then used to validate a 3D CFD combustion model of the engine for Dual-Fuel natural gas/diesel combustion. The validated model was then used for further investigations into both the phenomenology of this type of combustion and the possible use of other fuels such as bio-gas and hydrogen.

The first chapter of the thesis present an overview of the state of play in terms of climate and environmental trends, the policies currently in place on future strategies for reducing the main climate-altering gases.

Chapter two offers a summary of the low temperature combustion techniques adopted on compression ignition engines and describes some studies carried out on the use of biofuels.

Chapter three presents a brief discussion of the main alternative fuels for compression ignition engines, which have been applied in various experiments by different scientific communities, replacing or mixed with diesel oil, or in dual-fuel mode.

Chapter four describes the Unimore test bench on which the experimental tests were carried out. The diesel-gasoline tests, where gasoline fed the engine as a low-reactivity fuel, are described in Chapter five. Chapter six illustrates the experimental tests on dual-fuel combustion using natural gas, and the results are given in a potential gen set application compared to the current technologies on the market in this sector.

The following chapters describe the combustion modelling carried out. The software used (KIVA-3V) is introduced with a brief description in Chapter seven. Chapter eight presents the first application studied, concerning the numerical investigation of one of the experimental operating points described in Chapter six. Then, also biogas is investigated as a low-reactivity fuel, and the results obtained are reported in Chapter nine and in function of these results is recalled an application study on cogeneration. Chapter ten offers a broad discussion of the use of hythane (blend of methane and hydrogen) as a low-reactivity fuel; the results obtained using different levels of hydrogen in the blends and varying the diesel injection timing are reported.

1 Word Energy scenario

1.1 Climate change, primary energy sources and policy plans for future development

The latest report of the Intergovernmental Panel on Climate Change (IPCC) was approved on 6 August 2021 by its 195 member governments. The report, called Climate Change 2021: The Physical Science Basis, is the first part of a more comprehensive report, the Sixth assessment report (AR6), which will be presented in 2022. This report confirms important changes in the Earth's climate in every region and climate system. Many of these changes are unprecedented in hundreds of thousands of years, and some of those that are already in place, such as the continuing rise in sea level, are irreversible for the next hundreds of thousands of years.

However, we need strong and constant reductions in carbon dioxide (CO_2) and other important greenhouse gases to try to limit climate change. Thanks to these reductions, benefits for air quality could be quickly achieved, but it may still take 20-30 years to see global temperatures stabilise.

The report shows that greenhouse gas emissions from human activities are responsible for about 1.1 [°C] of warming compared to 1850-1900. On average over the next 20 years, the global temperature should reach or exceed 1.5 [ºC] of warming. This assessment is based on the data sets observed and used to assess past warming.

The latest report is based on the latest scientific advances in understanding the response of the climate system to greenhouse gas emissions from human activities.

An analysis of the report shows that an increase in climate change is expected in all regions in the coming decades. With 1.5°C of global warming, the number of heatwaves, longer warm seasons and shorter cold seasons is expected to increase. With global warming of 2 [°C], heat extremes would more often reach critical tolerance thresholds for agriculture and health.

These temperature rises are bringing transformations to different regions, and these will increase with further warming. The changes related to humidity values, winds, snow and ice, in coastal areas and in the oceans.

For example, these disturbances concern:

- The intensification of the water cycle. In some regions, this leads to more intense rains and associated floods, in many other regions to more intense droughts;

- The precipitation trends. At high latitudes, precipitation is likely to increase, while it is expected to decrease in most subtropical regions. Changes in monsoon rainfall are expected, with variations in different regions;
- For coastal areas, sea levels are expected to continue to rise throughout the 21st century, which would contribute to more frequent and severe coastal flooding in shallow areas than sea level and coastal erosion. Extreme sea-level events that used to occur once every 100 years could occur every year by the end of this century.
- Further warming will intensify the melting of permafrost, the loss of seasonal snow cover, the melting of glaciers and ice caps, and the loss of Arctic sea ice in summer.

The report also shows that human activities still have the potential to determine the course of the future climate. There is clear scientific evidence that carbon dioxide (CO_2) is the main driver of climate change, although other greenhouse gases and atmospheric pollutants also contribute to climate change.

It is clear that human influence has warmed the atmosphere, the ocean and the land surface. The observed increases in greenhouse gas (GHG) concentrations since about 1750 are unequivocally caused by human activity.

Since 2011, atmospheric concentrations have continued to increase, reaching annual averages of 410 ppm for carbon dioxide (CO_2), 1,866 ppb for methane (CH_4), and 332 ppb for nitrous oxide (N_2O) in 2019.

The global surface temperature in the period 2001-2020 was 0.99 [°C] higher than in the period 1850-1900, and was 1.09 [°C] higher in the period 2011-2020 than in the period 1850-1900, with higher increases on land (1.59 [°C]) than in the ocean (0.88 [°C])[1].

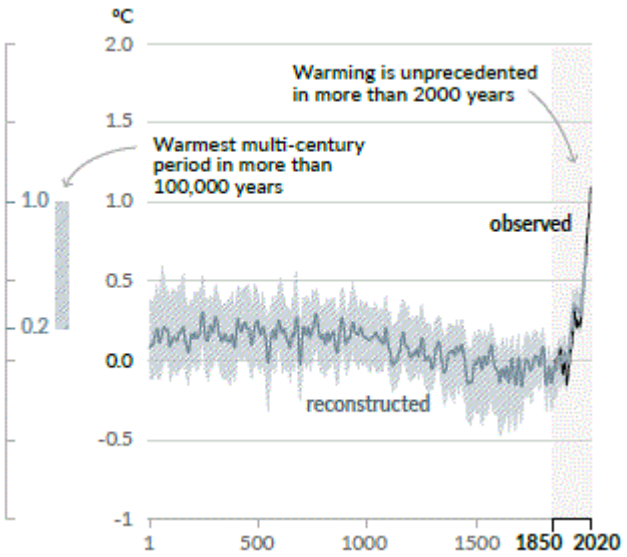

Figure 1.1 - Change in global surface temperature (decadal average) as reconstructed (1-2000) and observed (1850-2020)[1]

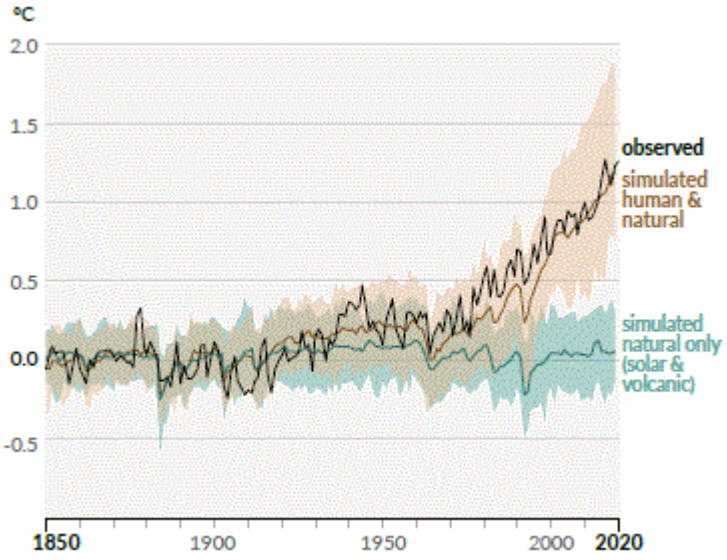

Figure 1.2 - Change in global surface temperature (annual average) as observed and simulated using human & natural and only natural factors (both 1850-2020)[1]

Figure 1.1: Changes in global surface temperature reconstructed from paleoclimate archives (solid grey line, 1–2000) and from direct observations (solid black line, 1850–2020), both relative to 1850–1900 and decadally averaged. The vertical bar on the left shows the estimated temperature (very likely range) during the warmest multi-century period in at least the last 100,000 years, which occurred around 6,500 years ago during the current interglacial period (Holocene). The Last Interglacial period, around 125,000 years ago, is the next most recent candidate for a period of higher temperatures. These past warm periods were caused by slow (multi-millennial) orbital variations. The grey shading with white diagonal lines shows the very likely ranges for the temperature reconstructions.

Figure 1.2: Changes in global surface temperature over the past 170 years (black line) relative to 1850–1900 and annually averaged, compared to CMIP6 climate model simulations (see Box SPM.1) of the temperature response to both human and natural drivers (brown), and to only natural drivers (solar and volcanic activity, green). Solid coloured lines show the multi-model average, and coloured shades show the very likely range of simulations. (see Figure SPM.2 for the assessed contributions to warming).

1.2 Possible future climate change

Five new emission scenarios have been used to explore the climate response to a wider range of GHG, soil uses and air pollutants than assessed in the previous IPCC Assessment Report (AR5).

It is expected that the global surface temperature will continue to increase at least until the middle of the century in all emission scenarios considered. Global warming of 1.5 [°C] and 2 [°C] will be overcome during the course of the 21st century unless significant reductions in CO_2 and other greenhouse gas emissions occur in the coming decades.

Compared to the 1850-1900 period, the average global surface temperature in 2081-2100 will most likely be higher than 1.0 [°C] - 1.8 [°C] in the very low GHG emission scenario (SSP1-1.9), 2.1 [°C] - 3.5 [°C] in the intermediate scenario (SSP2-4.5) and 3.3 [°C] - 5.7 [°C] in the very high emission scenario (SSP5-8.5). The last time the global surface temperature exceeded 2.5 [°C] was more than 3 million years ago.

Based on complex calculations and the scientific evidence gathered so far, the IPCC report uses five future scenarios - the Shared Socioeconomic Pathways (SSPs) - which describe how the Earth’s climate will evolve in the coming decades. In particular, they quantify how much the average temperatures of the planet could increase compared to the period before the industrial revolution. We recall that, according to the new estimates of the IPCC, human activities are already responsible for an increase in average temperatures of 1.1 [°C] compared to the period 1850-1900, a figure destined to grow.

The factors taken into consideration by the IPCC to develop the SSP scenarios include not only the increasing or decreasing trend of pollutant emissions that modify the climate, the “climate-changing gases”, but also socio-economic dynamics, such as demography and land use.

The SSP1-1.9 scenario is, so to speak, the most optimistic: it considers a world in which by 2050 the goal of climate neutrality, or "net zero emissions", in which there will be no more emissions than the amount reabsorbable by the planet, is achieved. In the SSP1-2.6 scenario, the goal of neutrality will be achieved, but after the middle of this century. The intermediate SSP2-4.5 scenario, on the other hand, considers a stabilisation of current emissions until 2050, then a slow decline, achieving neutrality only around 2100. Then there are the two worst-case scenarios, SSP3-7.0 and SSP5-8.5, where a doubling of emissions is considered by 2100 or 2050.

As the report points out, at the moment we do not know which scenario will be most likely, since future events depend on the political choices made in the short term. However, based on the five scenarios, scientists have calculated how much average temperatures could increase compared to the pre-industrial period (table 1.1).

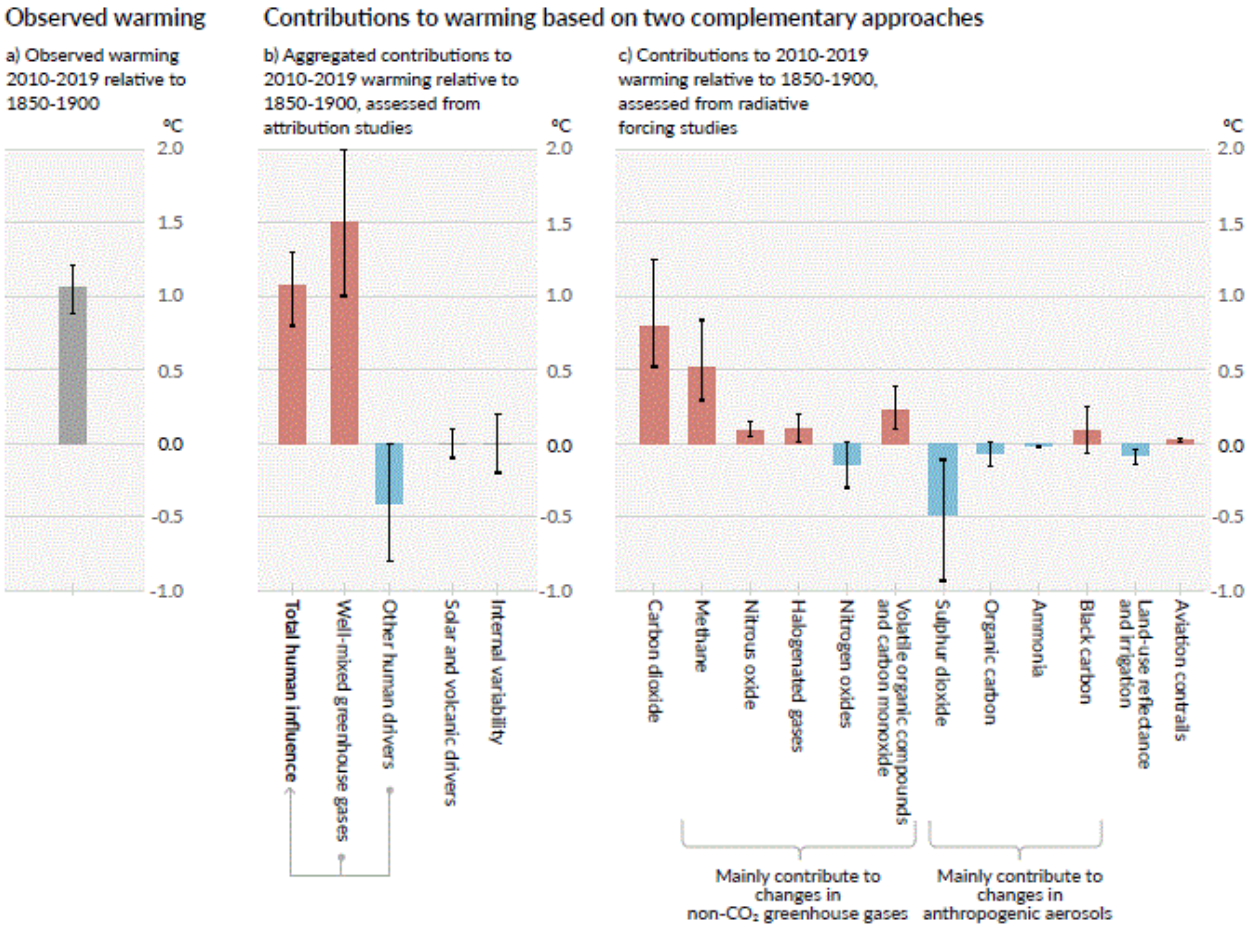

Figure 1.3 – Contributions to global warming[1]

Panel 1.3a): Observed global warming (increase in global surface temperature) and its very likely range

Panel 1.3b): Evidence from attribution studies, which summarise information from climate models and observations. The panel shows temperature change attributed to total human influence, changes in well-mixed greenhouse gas concentrations, other human drivers due to aerosols, ozone and land-use change (land-use reflectance), solar and volcanic drivers, and internal climate variability. Whiskers show likely ranges.

Panel 1.3c): Evidence from the assessment of radiative forcing and climate sensitivity. The panel shows temperature changes from individual components of human influence, including emissions of greenhouse gases, aerosols and their precursors; land-use changes (land-use reflectance and irrigation); and aviation contrails. Whiskers show very likely ranges. Estimates account for both direct emissions into the atmosphere and their effect, if any, on other climate drivers. For aerosols, both direct (through radiation) and indirect (through interactions with clouds) effects are considered.[1]

Scenario	Near term, 2021–2040		Mid-term, 2041–2060		Long term, 2081–2100	
	Best estimate (°C)	*Very likely* range (°C)	Best estimate (°C)	*Very likely* range (°C)	Best estimate (°C)	*Very likely* range (°C)
SSP1-1.9	1.5	1.2 to 1.7	1.6	1.2 to 2.0	1.4	1.0 to 1.8
SSP1-2.6	1.5	1.2 to 1.8	1.7	1.3 to 2.2	1.8	1.3 to 2.4
SSP2-4.5	1.5	1.2 to 1.8	2.0	1.6 to 2.5	2.7	2.1 to 3.5
SSP3-7.0	1.5	1.2 to 1.8	2.1	1.7 to 2.6	3.6	2.8 to 4.6
SSP5-8.5	1.6	1.3 to 1.9	2.4	1.9 to 3.0	4.4	3.3 to 5.7

Table 1.1 - Changes in global surface temperature, which are assessed based on multiple lines of evidence, for selected 20-year time periods and the five illustrative emissions scenarios considered. Temperature differences relative to the average global surface temperature of the period 1850–1900 are reported in °C. This includes the revised assessment of observed historical warming for the AR5 reference period 1986–2005, which in AR6 is higher by 0.08 [–0.01 to 0.12] [°C] than in the AR5. Changes relative to the recent reference period 1995–2014 may be calculated approximately by subtracting 0.85°C, the best estimate of the observed warming from 1850–1900 to 1995–2014[1].

All these considered emission scenarios suggest that the global surface temperature will continue to rise at least until the middle of the century. Global warming of 1.5 [°C] and 2 [°C] will be exceeded during the course of the 21st century unless significant reductions in CO_2 and other greenhouse gas emissions occur in the coming decades.

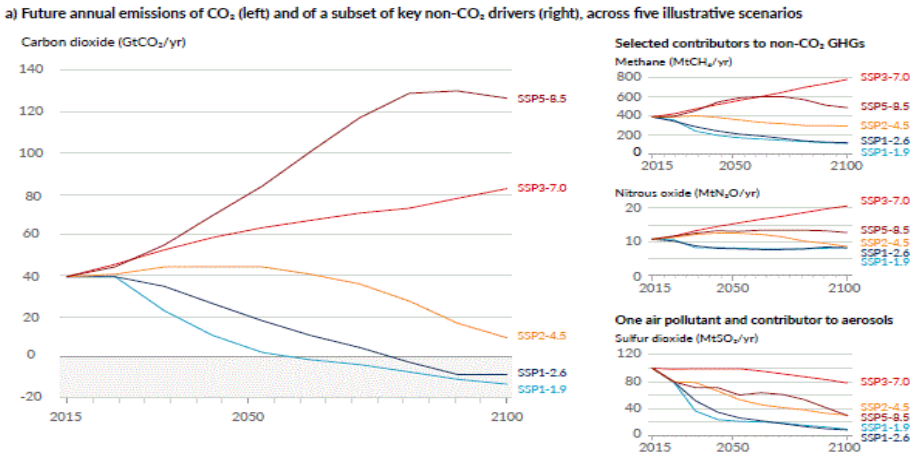

Figure 1.4 – Future emissions cause future additional warming, with total warming dominated by past and future CO2 emissions[1]

The overall surface temperature in each individual year may vary above or below the long-term human-induced trend due to substantial natural variability. The occurrence of individual

years with global average temperature variations above a certain level, such as 1.5 [°C] or 2 [°C], relative to the period 1850-1900 does not imply that this level of global warming has been reached.

1.3 Limiting future climate change

Possible future scenarios also include air pollution control actions to consistently assess the effects of different assumptions on climate projections and air pollution.

Limiting global warming to a specific level requires a limitation of cumulative CO_2 emissions reaching net zero emissions, together with major reductions in other greenhouse gas emissions. Significant reductions in methane emissions (CH_4) would also limit the warming effect resulting from the reduction of aerosol pollution and improve air quality.

In a few years, scenarios with low GHG emissions (SSP1-1.9 and SSP1-2.6) lead to perceptible effects on GHG and aerosol concentrations, and air quality.

- Emission reductions in 2020 associated with measures to reduce the spread of COVID-19 led to temporary but detectable effects on air pollution, and a temporary increase in total radiative forcing, mainly due to reductions in cooling caused by aerosols. Concentrations of CO_2 in the atmosphere continued to increase in 2020, without a detectable decrease in the observed CO_2 growth rate.
- GHG emission reductions also lead to improvements in air quality.
    - However, in the short term (2021-2040), even in scenarios with a significant reduction of GHG, these improvements are not sufficient to achieve the World Health Organisation's air quality guidelines in many polluted regions.
    - Scenarios with targeted reductions in air pollutant emissions lead to faster improvements in air quality than reductions in GHG emissions alone in the early years, but from 2040, major improvements are expected in scenarios combining efforts to reduce both air pollutants and GHG emissions.[2-3]

1.4 World energy situation

The pandemic that affected the whole world at the beginning of 2020 is a humanitarian tragedy. To date, at the time of writing this paper, more than five million people have died as a result of COVID-19. Unfortunately, the number will continue to increase.

For the global energy system, the presence of this pandemic, together with efforts to mitigate its impact, has generated unparalleled developments and results in modern peacetime. For energy, 2020 was a year like no other.

This emergency situation has been experienced in a context of growing social and political demands for an accelerated transition to a net zero energy system. Indeed, the COP26, probably the most important UN climate conference since Paris, hosted in Glasgow, Scotland, had to be postponed until November 2021.

Analyses have been conducted in the energy sector to compare what was expected from the Paris agreements to prepare the challenges and opportunities posed by the nations at this year's COP.

The main results are dramatic: global energy demand has been estimated to have fallen by 4.5% and global carbon emissions from energy consumption by 6.3%.

As far as we know from historical developments, they have fallen enormously: this is the biggest decrease in energy and in carbon emissions since World War II. The levels last observed in 2011 were like those of last year, i.e., with a decrease of over 2 Gt of CO_2.

Equally surprising is the reduction in the intensity of carbon in the energy mix - the average carbon emitted per unit of energy used - which fell by 1.8%, one of the largest events in post-war history. In weight, there was an estimated -2.1 Gt reduction in carbon emissions, bringing CO_2 emissions to the lowest level since 2011.

When observed in terms of industrial production, clearly this figure, which runs parallel to the lower energy demand, is dramatic. But according to what the future holds, the rate of decrease in carbon emissions observed last year is similar to what the world needs to average each year, and for the next 30 years, to be on the right track to achieve the climate goals of Paris and the recent COP26.

More concretely, if carbon emissions were to fall at the same average rate as last year for the next 30 years, global carbon emissions would fall by around 85% by 2050, which the IPCC has analysed as a possible scenario, roughly mid-way between the Rapid and Net Zero scenarios, which are broadly consistent with maintaining the rise in global temperature within the threshold of 2 [°C] and below 1.5 [°C] respectively.

Looking at last year's decline in carbon emissions from an economic point of view, we can see that this is a huge loss of economic production and activity. In the need to reduce climate-changing emissions, the challenge is to avoid causing serious hardship and damage to everyday life, without having to resort to cuts in investment that create progress .

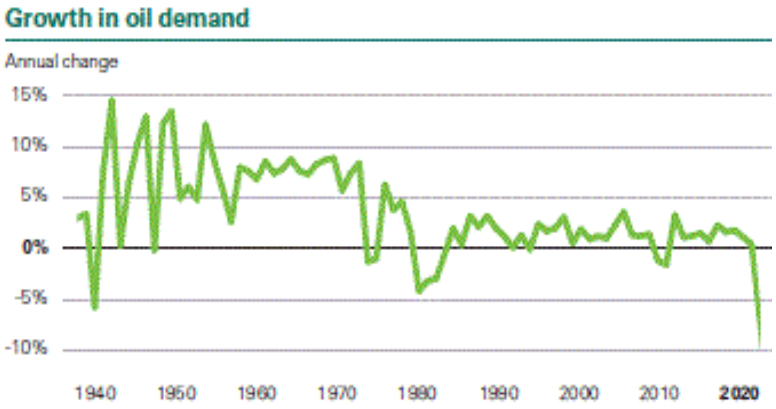

Figure 1.5 - Growth in oil demand[4]

The following graph shows the components of energy demand. As you can see, the decline in oil consumption in 2020 was much greater than expected based on past trends. The extent of this difference was far greater than any other component of demand[4].

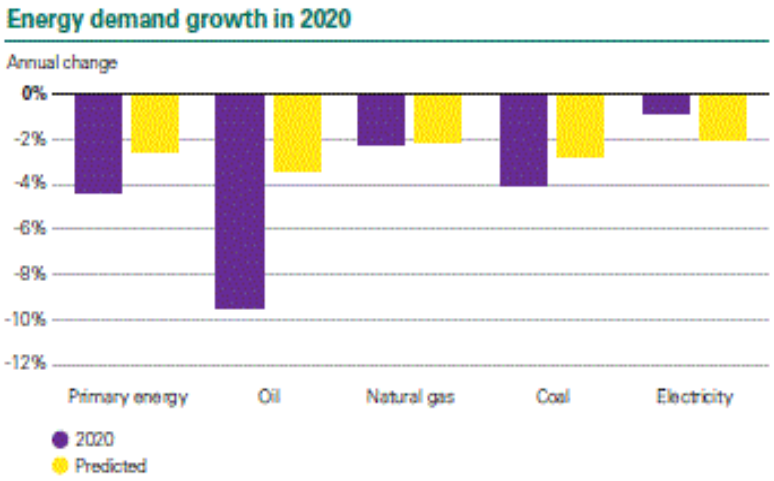

Figure 1.6 – Growth in energy demand in 2020[4]

Similarly, the demand for gasoline decreased by about 13% (3.1 Mb/day), and road mobility was greatly reduced. On the contrary, the products more closely related to the petrochemical sector (naphtha, ethane and LPG) remained partly supported by the growing demand for PPE and other medical hygiene supplies.

On the contrary, natural gas showed greater resilience. Gas demand is estimated to have decreased by 2.3% (81 billion m^3) in 2020, a decrease substantially similar to that recorded in 2009 as a result of the financial crisis. Consumption was recorded in most areas of the world, with the notable exception of China, where gas demand grew by almost 7%. The reason why natural gas has held is to be found in the sharp drops in prices, which have

allowed gas production to gain market shares in the US energy market and maintain its position in the EU.

Electricity consumption is estimated to have experienced the smallest fall across the main components of final energy demand, declining by just 0.9% in 2020. The relative resilience of electricity usage was aided by the nature of the lockdowns, with falling power demand in industry and commercial buildings, partially offset by increased domestic use by home-based workers and locked-down families.

Good resilience was recorded in overall power generation, but with a significant change in the generation mix. In particular, despite the fall in overall energy demand, production from renewable sources (wind, solar, bioenergy and geothermal energy, excluding hydropower) recorded its largest increase (358 [TWh_e]). This growth was driven by strong increases in both wind generation (173 [TWh_e]) and solar (148 [TWh_e]).

The share of renewable energy in global generation has been encouraging, as it has increased the most, improving the strong growth observed in recent years. Over the past five years, generation from renewable sources has accounted for about 60% of the growth of global energy generation; especially wind and solar energy has more than doubled.

Renewables grew last year largely at the expense of coal-fired generation, which recorded one of its highest record declines (405 [TWh_e], 4.4%). In addition to the general decline in energy demand, but at the same time the increase in the use of energy from renewable sources, coal has also suffered a loss of competitiveness relative to natural gas, especially in the United States and the EU.

These trends are exactly what the world needs to have and maintain in order to lead the transition to net zero: strong growth in renewable generation and the elimination of fossil fuel sources. Having said that, the doubling of wind and solar generation over the last five years has not substantially replaced total coal generation. The level of coal production in 2020 remained broadly unchanged compared to 2015, as last year's decline simply compensated for the increases in previous years. As we are seeing in global economic growth compared to last year's decline, strong growth in renewable energies is not enough to eliminate coal from the global energy sector, especially at the required pace. There is still a long way to go to remove coal from the energy sector.

More progress needs to be made on energy efficiency in developed countries. Many emerging market economies need to take important steps to avoid the use of coal. At the same time, better access to energy must be ensured, probably with the expansion of natural gas expand alongside renewable energies in the next 15 to 20 years.

The evolution of world energy consumption by source over the past 25 years is summarised below.[3]

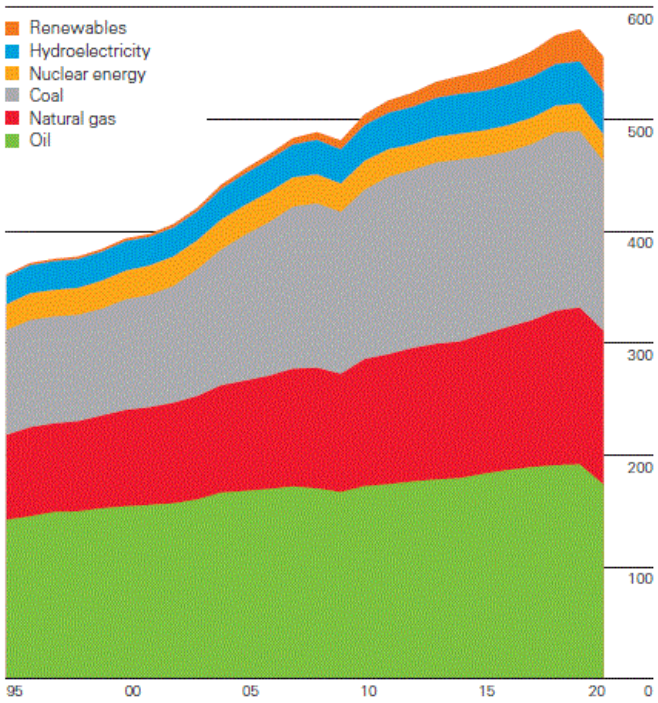

Figure 1.7 - Primary energy consumption decreased by 4.5% last year, the first decline in energy consumption since 2009. The decline was driven largely by oil (-9.7%), which accounted for almost three quarters of the decrease. Consumption for all fuels decreased, apart from renewables (+9.7%) and hydro (+1.0%). Consumption fell across all the regions, with the largest declines in North America (-8.0%) and Europe (-7.8%). The lowest decrease was in Asia-Pacific (-1.6%) due to the growth in China (+2.1%), the only major country where energy consumption increased in 2020. In the other regions, the decline in consumption ranged between -7.8% in South and Central America to -3.1% in the Middle East.[4]

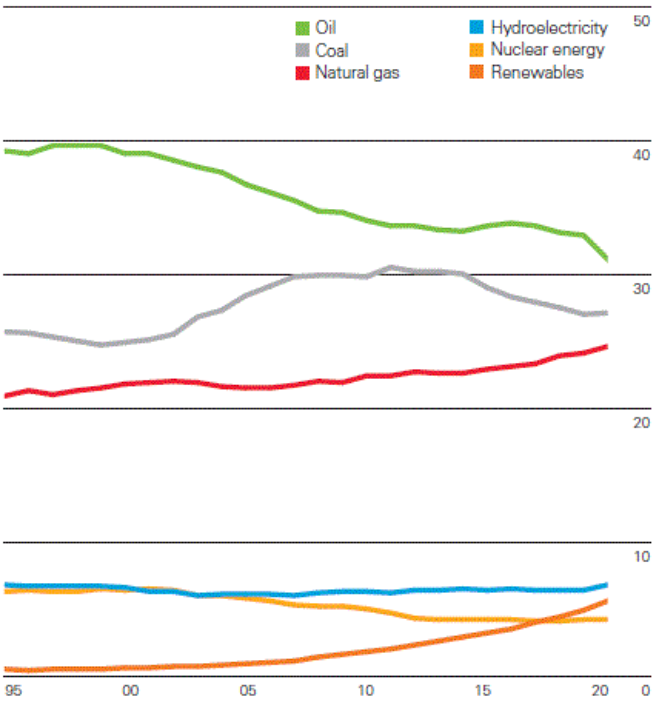

Figure 1.8 – Energy sources trend over the years. Oil continues to hold the largest share of the energy mix (31.2%). Coal is the second largest fuel in 2020, accounting for 27.2% of total primary energy consumption, a slight increase from 27.1% in the previous year. The share of both natural gas and renewables rose to record highs of 24.7% and 5.7% respectively. Renewables have now overtaken nuclear which makes up only 4.3% of the energy mix. Hydro's share of energy increased by 0.4 percent last year to 6.9%, the first increase since 2014.[4]

1.5 The strategy for a climate-neutral economy by 2050 and the European green deal

In December 2019, the European Council endorsed the objective of achieving a zero-climate EU by 2050, and the European Commission presented the Green Deal with the same objective. The implementation of the Green Deal and the achievement of climate neutrality by 2050 remain the priority objective of Union policies even after the crisis caused by the Covid-19 pandemic (Adapted Work Programme presented on 27 May 2020).

The European Green Deal contains many measures, including the adoption of a "European climate law", which entered into force with Regulation (EU) 2021/1119 of the European Parliament and of the Council of 30 June 2021 establishing the framework for achieving climate neutrality and amending Regulation (EC) No. 401/2009 and Regulation (EU) 2018/1999 (“European Climate Law”). This Regulation sets forth:

- The binding objective of climate neutrality in the EU by 2050, linked to the reduction of temperature increase as provided for in the Paris Agreement;
- A net reduction of at least 55% of the EU’s greenhouse gas emissions by 2030.

On 17 September 2020, the EU Commission presented the communication "A more ambitious 2030 climate target for Europe", which explains the plan to achieve the 2030 climate targets and what action is intended to achieve them. This is a more ambitious emissions reduction plan, with the 2030 Climate and Energy Framework being updated with stronger climate and energy legislation and interventions in all sectors of the economy, starting with the energy and construction sector, by revising the existing targets for renewable energy and energy efficiency.

On 14 July 2021, the European Commission adopted a package of legislative proposals setting out how to achieve EU climate neutrality by 2050, including the net reduction of at least 55% of greenhouse gas emissions by 2030 as a further intermediate target.

This package, called "Fit for 55%", therefore proposes to revise several EU climate laws, including the EU ETS, the Effort Sharing Regulation, transport legislation and land use, defining in real terms how the Commission intends to achieve the EU’s climate targets under the European Green Deal.

1.6 Italy’s actions to achieve the 2020 and 2030 targets and “PNRR” investments for ecological transition

In relation to the achievement of the new target set by the EU Council of December 2020, the report recalls that "in the framework of the Next Generation EU, the instrument established at European level to respond to the pandemic crisis caused by Covid-19, the Government is finalising the National Recovery and Resilience Plan (PNRR), the investment programme designed to make Italy a more equitable, green and inclusive country, with a more competitive, dynamic and innovative economy. The largest allocation of resources is foreseen for the mission 'Green Revolution and Ecological Transition', to which more than 31% of the total amount of the Plan will be allocated, approximately EUR 70 billion to step up Italy’s efforts in line with the ambitious objectives of the Green Deal on energy efficiency

and building upgrading issues, sustainable mobility, strengthening infrastructure and cycle routes and renewing the TPL fleet in a decisive way, to increase the share of energy produced from renewable sources and stimulate the industrial chain, including hydrogen, and digitize network infrastructure".

In addition, art. 4 of Italian Decree-Law No. 22/2021 provides for the establishment, at the Presidency of the Council of Ministers, of the Interministerial Committee for Ecological Transition (CITE), which will have to approve the Ecological Transition Plan (ETP), in order to coordinate a series of environmental policies, including the reduction of greenhouse gas emissions and mitigation and adaptation to climate change.

The main objectives of Italy's environmental policies are described in the PTE (pPTE) proposal. These include those set by the EU to combat the current climate change and require a 55% reduction in CO_2 emissions by 2030, compared to 1990, and the achievement of climate neutrality by 2050. Closely linked to these objectives are the energy objectives.

The pPTE highlights the need for the contribution of renewable energy to electricity generation, and that to do so this must reach at least 72% in 2030 and cover 2050 shares close to 100% of the overall primary energy mix. Another key issue in environmental policy is sustainable mobility, which should be based on the increased use of rail traffic, the use of low-impact fuels, and from 2030, to achieve the goal of full decarbonisation, at least 50% of engines will have to be electric.

The pPTE also recalls the commitment to publish, by June 2022, the new "National Strategy for the Circular Economy" with the aim of promoting an advanced circular economy and consequently significantly prevent the production of waste (-50%) by 2040. The measures to achieve these objectives are mainly those envisaged by the PNRR, in particular in mission 2 of the plan, "Green Revolution and Ecological Transition", to which some EUR 70 billion are allocated.[5]

1.7 Energy transition

The energy transition to decarbonisation has reached a huge media impact and now conditions energy policies (and not only) worldwide.

The process has led and will lead to significant investments in research and innovations in materials, components, systems and their use and to new business (and life) models in what are considered the 3 pillars of decarbonisation:

- Energy production free of fossil fuel inputs,

- Energy efficiency (supplying products and services with lower energy consumption thanks to technologies) combined with savings, even if these are different concepts: savings refer to lower consumption in parallel to a lower production, avoiding unnecessary waste, use of public transport instead of private cars, etc...
- Electric mobility/transport, not only stopping the use of fossil fuels, but also considering the complete life cycle for the production/transport of the fuel used, production and use of the vehicle with its final cycle.

A strong interaction between the three pillars is fundamental.

Decarbonisation is a global problem. All the more or less industrially developed nations must make their own contribution, but it must be borne in mind that some national situations differ greatly in the three pillars mentioned.

There must be a multidisciplinary systemic approach that analyses the three areas in an integrated way, with the aim of achieving the objectives, which are undoubtedly stimulating and at the same time reasonable, at an appropriate cost to the community.

Taking the example of Italy, the EU 2030 targets impose twice the current production of renewable energy at that date, and in just 8 years this an almost impossible challenge.

To reach the target by 2030, Italy would have to install photovoltaic systems for a power of 7 [GW_e] per year, while they are currently installing much less than one [GW_e].

Undoubtedly, simpler authorisation processes are needed, as is certainly the case today in Northern Europe, and the Italian Government is also working on this.

In general, however, and this is true of the nature of some renewable sources, such as sun or wind, these are not programmable, and for this reason high-performance energy storage technology is being developed, but it will take time to reach a good level, comparable not only to the storage of energy from fossil sources, but also from other renewable sources, such as biogas or hydrogen.

The intermittent production of energy, linked to the presence of the sun or wind, must necessarily also be managed through an exchange and greater interconnection between the European networks. For example, if there is more wind in Northern Europe, and there is a need for energy in Southern Europe because at that moment the sun cannot cover all needs, the wind energy can be channelled to that area, and vice versa, when there is more sun in the south and there is more need for energy in the north.

In doing this you can, for example, link thousands of electric cars to the grid, better regulating supply and demand. So there are many technologies and strategies to be examined.

International policy has therefore set very strict targets for the reduction of polluting and greenhouse emissions, which must be achieved in a short time. Despite the growth observed in recent years, the renewable energy sector still needs a strong boost, especially from an energy policy that must definitely be based on the development of these sources, dictating lean rules, providing large investments and creating a strong energy exchange network.

In the field of transport and energy generation, technologies that are not yet able to completely replace internal combustion engines for reliability, efficiency and longevity must be developed further. The current vehicles powered by electric engines have not yet reached the same potential, and even less so the batteries they use, which are powered by energy that still comes mostly from fossil sources.

In the field of energy generation and transformation, it is well known that thermal engines make a high level of efficiency available when used to generate thermal and electrical energy and, when coupled to absorbers, cooling energy.

Compression ignition engines have a good overall efficiency. They have been studied for a long time and a detailed control of their combustion has been achieved with highly advanced technology. Electronics together with precision mechanics now offer formidable levels of performance and efficiency, while also ensuring their longevity.

The studies carried out in recent years aim to achieve further reductions in the emissions of pollutants and greenhouse gases produced by thermal engines, without compromising their effectiveness, through the adoption of advanced low temperature combustion methodologies. These techniques can be coupled to suitable fuels, obtained from non-fossil sources. Hydrogen is also an excellent fuel that can make a great contribution, when used in power with other fuels.

The great availability of organic by-products and biofuel conversion techniques, which are advancing technologically and further improving, can be decisive for the longevity of environmentally friendly compression-ignition engines.

In this way, this geo-political period of "energy transition" could be faced with a real and gradual transition both in the traction sector and in that of energy generation, which must be really clean. Until new technologies are derived upstream from totally clean processes, they can be powered by renewable carriers and have achieved wide levels of reliability.

2 Low Temperature Combustion (LTC) strategies for Compression Ignition (CI) engines

2.1 Introduction to LTC

Cleaner and more efficient technologies are needed for future vehicles, to ensure better ambient air quality, a drastic reduction in greenhouse emissions and better energy security. In the transport sector, the challenges currently facing innovative fuels and engine technologies are to seek the best efficiency to save fuel and reduce emissions. The absolutely restrictive emission standards, which in fact prohibit the use of fossil fuels in the immediate future, as well as the general increasing scarcity of primary energy resources, lead to a strong need to exploit alternative fuels that can be used together with the development of new methods and highly efficient and environmentally friendly combustion systems.

In order to comply with the strict regulations on polluting emissions into the environment imposed on the transport sector, in recent years new combustion methodologies have been developed concerning the concept of low temperature combustion (LTC).

Compared to conventional combustion modes, the high potential of LTC technologies in reducing emissions and, at the same time, maintaining high overall efficiency has been observed. The main techniques usually included in this technology are: homogeneous charge compression ignition (HCCI), premixed charge compression ignition (PCCI), reactivity-controlled compression ignition (RCCI), etc.

The fundamental principle behind these techniques is the same, even though there are differences in the method by which they are implemented, i.e., to produce combustions with reduced peak temperatures acting on the formation of tendentially lean mixtures.

LTC engines can have a higher CR than traditional diesel engines, depending on the quality of the fuel used. In addition, the combustion duration may be shorter (similar to a constant volume combustion) and, even for the lower temperatures reached in combustion, can reach a high thermal efficiency.

NOx and PM emissions can be simultaneously reduced because there are no localised areas with high temperatures or rich blends due to the greater homogeneity of the mixture. Thus, LTC techniques are not affected by the classic soot-NOx trade-off of diesel combustion.

LTC engines allow the use of various alternative fuels that could compensate for the rapid depletion of oil reserves. In addition, these engines can be coupled with advanced hybrid engines, to combine the advantages of high efficiency IC engines with hybrid electric powertrains.

Despite its high potential, and although the technique has been known for many years, this combustion mode is not yet ready to be put on the market. In fact, several technical aspects must be addressed before mass production can be achieved. Some aspects certainly deserve attention to ensure the proper functioning of LTC techniques. A major challenge is certainly to have control of LTC combustion over the entire range of engine operation.

Chemical kinetics is the main parameter that affects start of combustion (SOC) in LTC, therefore the physical and chemical properties of the fuel and the evolution of the fuel-air mixture temperature over time control LTC combustion.

A number of factors characterising the LTC combustion phases are decisive, such as the auto-ignition properties of the fuel, relative fuel-air ratio, flow rate and reactivity of residual gases, fuel-air mixture homogeneity, test fuel latent heat of vaporization, CR, intake air temperature, engine temperature, heat transfer from the cylinder, and a few other engine-dependent parameters.

To better manage LTC modes, first of all auto-ignition must occur in the proximity of TDC, throughout the engine operating range, and optimum thermal efficiency must be ensured.

Usually, LTC engines operate satisfactorily only at low-medium loads, while they encounter difficulties at high loads. At high loads, the high rate of combustion leads to a very high increase in pressure (RPR – rate of pressure rise) and thus pressure oscillation.

These oscillations not only result in unacceptable noise, but can lead to potential engine damage and increased NOx emissions. This leads to limiting power/density as well as engines with a more robust structure.

Although LTC engines produce significantly lower NOx and PM emissions, they emit relatively higher hydrocarbon (HC) and carbon monoxide (CO) emissions. In homogeneous combustion, a significant part of the charge enters the crevices during the compression stroke, and escapes with the expansion stroke together with the combustion gases, without having participated in the combustion process. Therefore, HC and CO emissions are higher than conventional diesel combustion. Furthermore, peak temperatures are low (below 1,500 [K]) and this limits the oxidation reactions from CO to carbon dioxide (CO_2), especially at low loads, thus worsening combustion efficiency[6].

In an LTC engine, cyclic variations affect the power at low load and the control of the combustion phase. As mentioned, LTC techniques do not directly control the combustion phase, as can be done by timing the injection into a traditional diesel engine. Therefore, the lack of combustion control may increase due to cycle-cycle variations in LTCs, and this is even more marked in transitional operations.

2.1.2 Homogenous Charge Compression Ignition

The homogenous charge compression-ignition engine (HCCI) is a new engine concept, which lies between conventional spark-ignition (SI or gasoline) and compression-ignition (CI or diesel) engines[7–9]; this engine, avoiding a throttle valve and maintaining high compression ratios as in diesel engines, is able to obtain high efficiency[10,11].

HCCI engines use a premixed charge of fuel and air in the engine, similar to SI engines, but in this case no spark plug is used, and ignition is induced exclusively through the compression of the gas resulting from piston motion.

A lean fuel-air blend is formed, or even diluted with exhaust gas, to support a flame and the gas ignition takes place in many small "hot spots", or "ignition pits" distributed throughout the engine, thus becoming a combustion process controlled by low temperature combustion chemistry [7,10,12,13]. Very low combustion temperatures have the advantage of reducing NOx emissions, while premixed charges avoid a local high Fuel to Air ratio, eliminating soot formation. On the other hand, unburned hydrocarbon and carbon monoxide emissions can increase due to the fuel trapped in the piston and cylinder cracks, and as the conversion of CO to CO_2 is not complete.

In the category of LTC engines, the HCCI technique, which involves extremely lean blends, in the graph Φ-T[14] is placed in the lower area than the operating area of low temperature combustion techniques. It can be seen that soot formation conditions are very distant, as well as the area that facilitates the formation of NO.

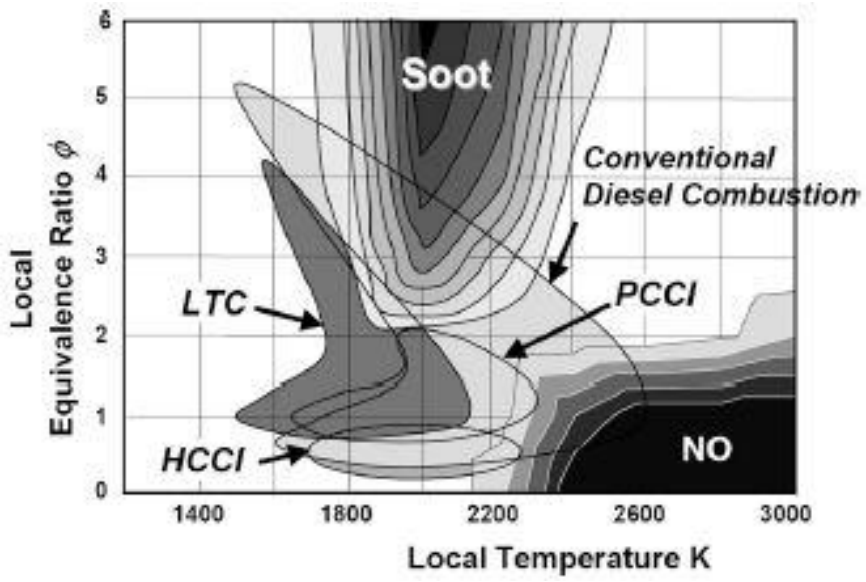

Figure 2.1 - Φ–T Soot and NOx generation map: homogeneous charge compression ignition (HCCI), premixed charge compression ignition (PCCI), low temperature diesel combustion (LTC), conventional diesel combustion (CDC)[14]

The advantage of HCCI engines is that they can achieve high efficiencies, like CI engines, and very low emission levels, if special exhaust after-treatment technologies are used, especially for the completion of CO and HC reactions[13].

HCCI engine performance limitations occur at high loads when combustion becomes uncontrollable due to rapid pressure increases, which result in engine noise, knocking and potential engine damage; in addition, at low loads cyclic variability increases due to the very lean blend. Therefore, HCCI engines cannot cover the full range of operation required for a typical passenger vehicle[10,15].

In the HCCI technique, in order to obtain a homogeneous charge, the diesel fuel must be injected early in the compression stroke. Basically, the problem in HCCI engines is that there is no direct ignition control mechanism such as a spark in a SI engine or fuel injection timing in a CI engine and, hence, low temperature combustion chemistry controls ignition and strongly influences engine stability[10,13,16].

2.1.3 Premixed Charge Compression Ignition

Then, with the aim of increasing combustion control, a second case of LTC was developed: the Premixed Charge Compression Ignition (PCCI) combustion. As can be seen in the Phi-T map, the PCCI concept works halfway between HCCI and traditional diesel combustion: the premixed blend is not completely homogenous (such as HCCI) and usually a significant

amount of EGR can be used. Also in the case of PCCI, the fuel must be injected into the combustion chamber with adequate advance (usually lower than HCCI) in the compression process to make the premixed charge mixture. In order to allow time for the air-fuel mixing to take place and to optimise the combustion phase, a multi-injection injection strategy can be adopted. Usually, PCCI combustion leads to a reduction of NOx and soot, like HCCI combustion, but the inhomogeneity of the charge improves ignition control, increasing combustion stability and extending the operating range. While using multiple high-pressure fuel injection events, it is possible to cause highly turbulent jets that promote rapid mixing, resulting in a more homogeneous blend that burns in premixes, distributing the action zone spatially and reducing the flame temperature[10,11,13]

2.2 Dual Fuel and Reactivity Controlled Compression Ignition

Thirdly, Dual Fuel (DF) LTC engines have been introduced as an alternative to single-fuel techniques, in order to better control the combustion phase while maintaining low NOx and PM emissions.

Dual-fuel LTC techniques use two fuels with different reactivity, and are referred to as LRF (Low Reactivity Fuel – high octane number), low reactivity fuel, and high reactivity fuel HRF (High Reactivity Fuel – high cetane number). For example, CNG (biogas, ethanol, methanol, etc.) which is an LRF, and diesel (or biodiesel, dimethyl-ether) can be adopted as HRF. Dual-fuel PCCI combustion can be classified into pilot DF and RCCI according to the combustion stage control method. In the case of RCCI, the LRF is injected into the intake manifold, while the HRF is injected directly into the cylinder during compression with appropriate advance. On the other hand, in the case of DF-pilot combustion, the LRF is introduced during the aspiration process through the intake port, the HRF is injected directly into the combustion chamber near the TDC to ignite. Therefore, the timing of the HRF injection is the determining factor of the combustion phase[17].

Figure 2.2 shows the different concepts of advanced combustion compared to conventional diesel combustion according to the injection advances and the EGR strategy used.

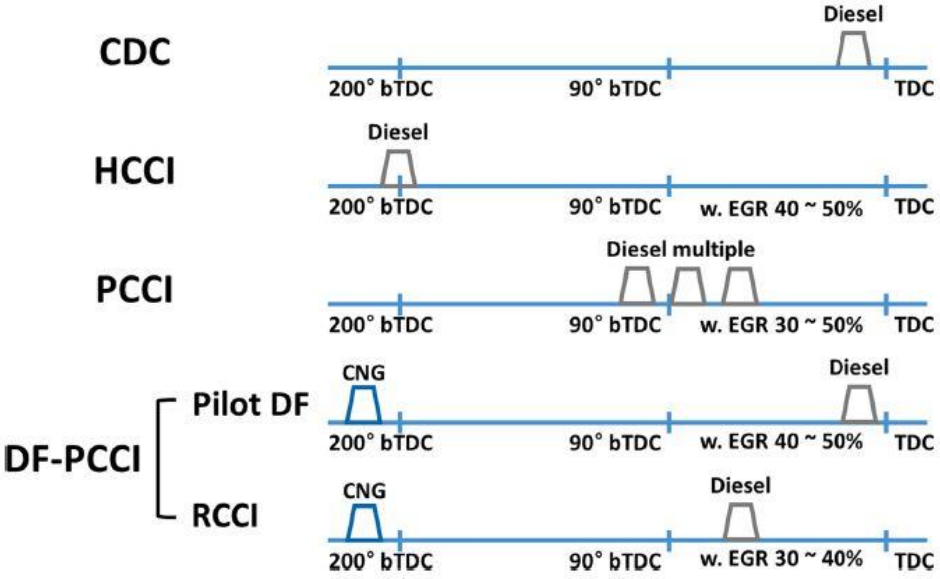

Figure 2.2 - Various combustion technologies advanced compared to conventional diesel combustion depending on EGR and supply strategy[17].

For example, using natural gas as a low reactivity fuel, figure 2.3 schematically shows the conceptual operating area for five combustion concepts based on diesel injection time and natural gas replacement ratio.

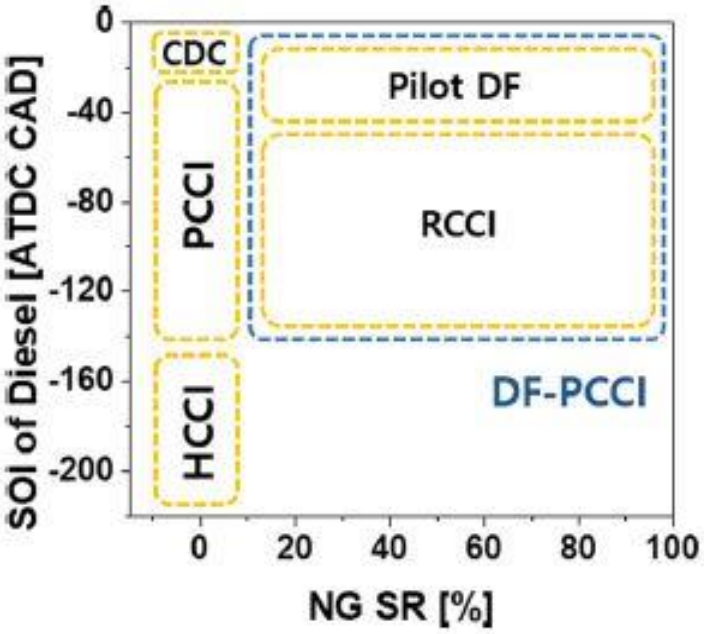

Figure 2.3 - Five combustion concepts represented in a conceptual operating area depending on the replacement ratio of natural gas and diesel injection times[17].

Generally, for the design of LTC techniques, which can be increasingly high-performing, important control strategies based on exhaust gas recirculation (EGR), fuel stratification, as

well as in-depth knowledge of the chemistry of combustion of possible fuels that can burn in lean environments and at low temperatures, including the potential use of alternative fuels to fossil fuels, such as biofuels.

Fuel chemistry affects the control of ignition in the engine, and must therefore be optimised; in addition, another important control parameter is the mixture between different fuel types[16]; by varying the amount of fuel, the overall reactivity of the final charge of the cylinder can be altered and the subsequent combustion phase controlled[10].

2.2.1 Operation of Dual Fuel Engines

The pre-mixed dual-fuel engine is basically a conventional compression-ignition engine where the injection of HRF, usually a liquid fuel (i.e., diesel fuel, biodiesel), normally in fairly small doses, is used to provide the source of ignition. The LRF can be injected at very high pressures directly into the engine cylinder (figure 2.4b) or injected at low pressure into the intake manifold and then premixed to the oxidising air before it reaches the cylinder (figure 2.4a).

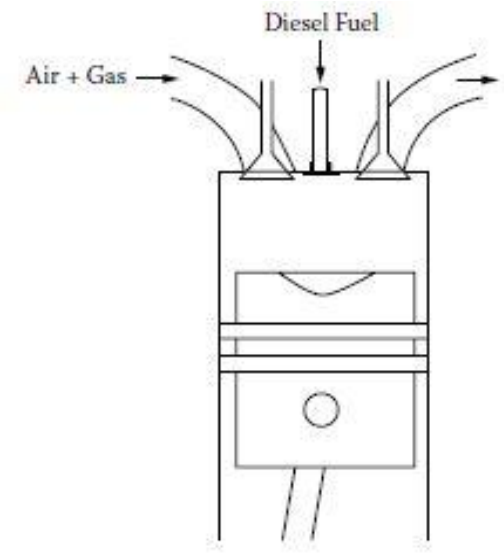

Figure 2.4a - Simplified representation of a dual-fuel premixed engine with direct diesel injection as a pilot for ignition.[18]

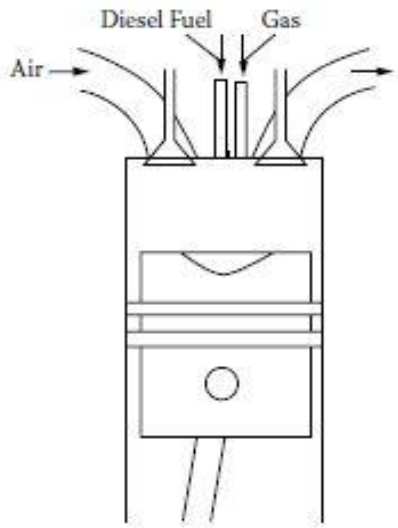

Figure 2.4b - Simplified representation of a dual-fuel engine in which the combustible gas is introduced directly into the chamber and the fuel injection serves as a pilot for ignition.[18]

Normally, in dual-fuel engine applications much of the energy release comes from the combustion of the LRF, while only a small amount of HRF is injected with timing according to conventional diesel engine calibration.

Adopting some optimal conversions, especially for the feed of gas fuel, it has been shown that operating characteristics can be obtained that are often comparable or even higher than the original ones when the engine is powered with diesel only. This is achieved by improved exhaust emission characteristics, i.e., quieter, smoother and improved operation with reduced thermal load. Higher performance can only be achieved by adopting effective measures, such as eliminating knocking problems at high loads or using an excessively lean mix at low loads.

Usually, with this use combined with diesel, the goal is to maximise the replacement of the original fuel with gaseous fuel, normally cheaper and more abundant, maintaining acceptable exhaust emission levels and engine performance. For this dual power supply, we can expect a sufficiently high-power density and efficiency and a reduction in lost heat.

The operating method may fall under different fuel injection management modes, depending on how much fuel is replaced with gaseous fuel. The most common and simple strategy is to have a relatively small pilot amount injected over the entire load and speed range. As shown schematically in figure 2.5a, most of the energy release is therefore increasingly derived from the combustion of gaseous fuel.

Another method of operation is to inject a variable amount of liquid fuel beyond the low load zone, with increasing addition of the gaseous fuel to the engine air, as illustrated schematically in figure 2.5b.

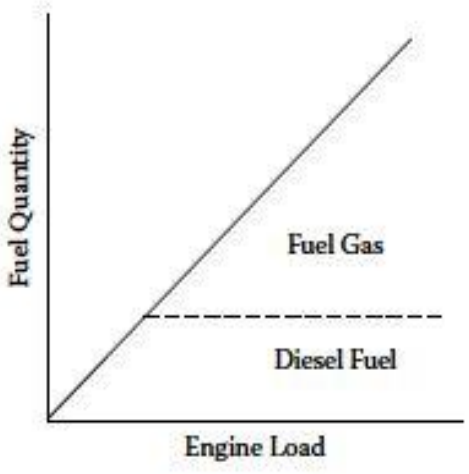

Figure 2.5a - Variations in the amount of gaseous fuel compared to constant amount of liquid pilot fuel as a function of the load[18].

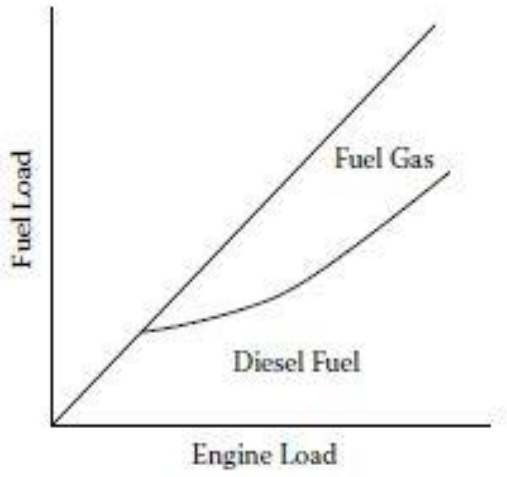

Figure 2.5b - Variations in the amount of gaseous fuel compared to a constant amount of liquid pilot fuel as a function of the load[18].

It is, however, more useful to vary the amount of liquid fuel optimally than the amount of gaseous fuel, depending on the operating conditions and the type of fuel used. In fact, it is

not useful to have greater quantities of pilot with the increase of the engine load (figure 2.5c), while the quantity of the gaseous mixture is increasingly maintained. This results in superior performance across all load and speed ranges. This approach requires better control of injections for both pilot and gaseous fuel.

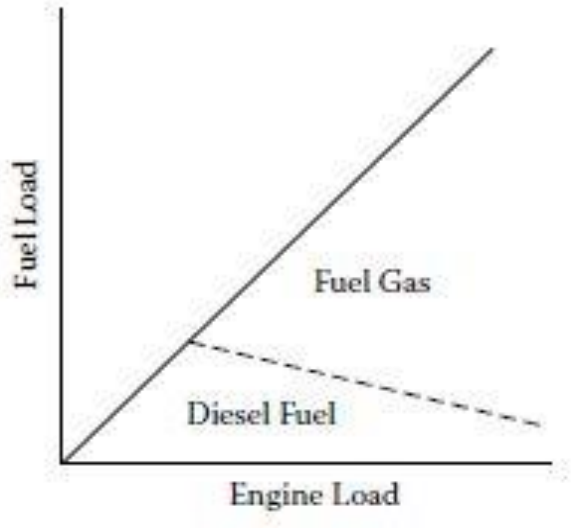

Figure 2.5c - Increasing amount of gaseous fuel and variation of the pilot fuel with the load.[18]

The modern CI high compression ratio engine is well suited to dual-fuel operation, especially when using a fuel such as methane, the main component of a wide range of products such as mainly natural and biogas. In addition, different pure gases, such as ethane, propane, butane, hydrogen and ethylene, have been used in recent years in studies and various experiments in dual-fuel engine applications. Different liquid fuels were also used, including liquefied natural gas, gasoline and alcohols, which were always introduced premixed in air into the intake manifold, rather than injected directly into the cylinder during the first part of the compression stroke, always with pilot ignition of diesel fuel.

The dual power supply is separate and at any time it is possible to switch to conventional diesel operation without interrupting the energy production if necessary. This flexible feature in the traditional drive of the engine, rather than with dual power, avoids the limitations imposed by the storage limits of gaseous fuel on board the vehicle and the refuelling distance between stations during long journeys.

The combination of low-cost fuels and a well-developed primary engine proves to be a very attractive investment opportunity, while at the same time offering general advantages of efficiency over engine operation, and therefore in environmental terms.

Most turbocharged diesel engines of recent design can perform equally well when converted to dual-fuel operation. Two-stroke diesel engines normally require excess scavenging air to clear the cylinder adequately of residual gases. In their corresponding dual-fuel applications, when the gaseous fuel is fumigated into the intake air before entering the cylinder, special procedures need to be adopted to ensure the elimination of the discharge of some unburned fuel into the exhaust. Otherwise, there will be both significant fuel wastage and increased contribution to exhaust emissions.[18]

2.2.2 Conversion of diesel engines to Dual Fuel mode

Although DICI engines are made in very different sizes, have applications in many sectors, and the operating field is very wide, the conversion to dual-fuel operation is always quite challenging, especially when aiming for optimal performance. The operating conditions should be well related to the gaseous fuel characteristics, for example by carefully dosing the quantity of the pilot fuel and its injection timing, to optimise nitrogen oxide emissions.
In addition, the operation of these dual-fuel modes with gaseous fuels can lead to knocking, and there is a need for careful dosing as well as injection timing if the compression ratio is not to be revised.
Despite the numerous positive operational, environmental and economic characteristics, in the past the use of dual-fuel engines for energy production has not seen such a wide application as could be expected. Similarly, there have been very few applications in the transport sector. Some factors that have prevented commercial development are listed below:

- The combustion process in the dual-fuel diesel engine is quite complex;
- Until relatively recently, exhaust emissions in the wide operating range of the diesel engine, for all load and speed ranges, were not easy to manage, especially when combined with other fuel. However, much recent progress has been made, making these difficulties much more manageable;
- The current electronic control systems for managing engine conditions have also only recently been developed. The past mechanical controls did not allow the simple management of the dual power supply;
- In addition, adequate storage and control systems are required for the related fuel systems of the two fuels with widely different properties;

- It was also a challenge to maintain the flexibility of the engine in being able to be fuelled also with diesel fuel, as originally designed and according to its nature, in the case of the unavailability of gaseous fuel in the storage system;
- Diesel cycle engines have always been used for stationary applications for electricity generation. Their fuel consumption is high and the need to reduce their costs while maintaining high levels of efficiency has always been an important consideration. The latest generation diesel engines have reached a very advanced stage of sophistication and reliability. They are turbocharged and their performance is well optimised. However, dual-fuel engines were used only when relatively cheap and abundant supplies of fuel gas were available;
- The low efficiency and sensitivity to changes in the fuel gas composition of the low-compression-ratio spark ignition gas engine made it fall quickly out of favour in comparison to the gas-fuelled diesel engine. However, with their continued improvements in the control of their emissions, efficiency and reliability, diesel engines tended to relegate the dual-fuel engine to a secondary role, confining it increasingly to special applications where economic advantages can be assured through the exploitation of much cheaper gaseous fuels. The increased attention in recent years to reduce greenhouse gas emissions is facilitating the widespread application of dual-fuel engines in transport applications.[18]

2.3 State of the art of LTC combustion

Many research has been carried out by various scientific communities to investigate the phenomena governing LTC techniques, seeking to optimise strategies for the correct management of the control of the combustion process and thus make them concretely effective and applicable to vehicles on the market.

Various studies concerning LTC techniques have shown the deviation from the classic production of NOx and soot of traditional compression ignition engines, but with some problems on the stability and regularity of combustion, even though the use of the EGR is necessary.

The PPCI combustion strategy was tested by researchers at the University of Lund (Noehre et ai., 2006). The experimentation conducted showed that the traditional NOx-soot trade-off that exists with conventional diesel combustion can be avoided with the PPCI diesel strategy, but requires EGR shares above 70% and the use of a reduced compression ratio

(for example, 12.4), which also means the complex management of the intake air used to maintain the engine stable in this condition[19].

Another approach used to achieve a condition of partial pre-mixing, and which can lead to a better combustion stability, uses low reactivity fuels (i.e., high octane number) to allow a longer mixing time before ignition and thus reduce the demand for EGR. Kalghatgi et al. (2006) conducted an in-depth study comparing a DICI engine powered by gasoline and diesel separately. The results showed that for a given set of operating conditions and for the same combustion phase, operation with gasoline produced a much longer ignition delay, which facilitated a combustion event with a more premixed charge.[20]

Researchers at Lund University (Kalghatgi et al. - 2009) developed a PPCI operational strategy in a diesel engine for heavy-duty vehicles, by investigating the entire load range using a variety of different gasolines (Manente et al., 2009, 2010). In their operational strategy, depending on the gasoline used and therefore on the octane number, a single or double injection was used. For low to medium engine loads, the main injection event is separated from the start of combustion by 5 to 20 degrees crank angle, due to the low reactivity of the gasoline. This means extremely low soot emissions. However, to achieve acceptable NOx emission levels (below 0.3 g/kWh), EGR rates of ~50 % were still needed. Compared to PPC operation with the use of diesel oil was achieved a reduction of EGR, but further developments were necessary in order to properly manage the intake air and pumping losses (Suresh et al., 2013) and improved operating stability, especially at low loads.[21]

The quality of the fuel in its propensity to auto-ignite is important. Since studies carried out by Bessonette et al. (2007) on the management of the controllability of combustion in the HCCI mode, it has been demonstrated that HCCI has a relatively narrow operating window on a single fuel, and that therefore a better control of combustion is achieved when the fuel used has autoignition qualities between that of diesel fuel and that of gasoline, depending on the operating conditions. For example, it was found in their experimentation, that at relatively high load the most suitable fuel had a derived cetane number of ~27. However, at low load, close to the engine idling, it requires a cetane number of ~45 (i.e., a traditional diesel fuel) to ensure stable operation. From these considerations on the quality of autoignition, it follows that it would have been important to explore other fuel blends in order to understand which might have brought advantages in terms of controllability of combustion, depending on engine conditions.[22]

Different studies have been carried out on engines powered by two fuels with different flammability. This mode of combustion, Dual Fuel HCCI and Dual Fuel PCCI, was effectively useful in the control of the combustion phase and RoHR. In particular, Inagaki et al.[20], using isooctane as LRF and diesel as high reactivity fuel, studied a stratified combustion of PCCI DF. To form a homogeneous mixture with air, the first fuel was injected into the port, while the second was injected directly into the combustion chamber at early timing, in order to create a slight stratification in terms of equivalence ratio (Φ) and research octane number (RON). It has been shown that the ignition timing is controlled by changing the ratio between the two fuels, while the combustion process develops gradually thanks to the stratification of the flammability[23].

By what was initially inferred from Bessonette et al. and Inagaki et al, the Reactivity-Controlled Compression Ignition (RCCI) was subsequently developed by Kokjohn et al. (2009).[24] Using optical diagnostic tools, Kokjohn (2012)[25] demonstrated, in fact, that the RCCI strategy is a chemically controlled combustion process that follows the principle of the HCCI mode. During the compression stroke, direct injection events are carried out in a sufficiently early mode so that the equivalence ratio remains very low at the start of combustion (equivalence ratio < 0.5). This results in sequential auto-ignition events that begin in regions of higher fuel reactivity and progress towards a lower reactivity gradient.[25] For a given set of operating conditions and the same combustion phase, Kalghatgi et al. used less reactive gasoline, which resulted in a much longer delay on ignition, which facilitated premixed combustion, resulting in a reduction in NOx and soot emissions.[20]

2.4 Natural gas supplied to dual fuel engines

Natural gas is a mixture of methane (usually > 90%), other hydrocarbons, such as ethane, propane and butane, and small quantity of carbon dioxide and nitrogen. Due to its low ignition characteristics, its high auto-ignition temperature and its low cetane number compared to diesel fuel[26,27], natural gas does not appear to be suitable for combustion in the diesel engine. It is used in dual fuel mode injected into the intake manifold to mix evenly with air and is then fed into the cylinder and ignited by fuels injected directly with high cetane number[28].

When used in dual fuel mode, at low and intermediate loads the BTE is a little lower than that of the normal diesel mode, while under high engine load conditions the BTE is similar to or a little higher than normal diesel mode. The reduction of BTE can be caused by the

very lean natural gas/air mixture at partial loads under dual-fuel combustion, as well as by the low burning rate due to the slower flame propagation speed, which increases the heat loss during the combustion process. Indeed, the BTE of a high-speed dual-fuel diesel engine operating in a wide range of natural gas/diesel proportions was examined by Papagiannakis et al.[29]. As the mass fraction of natural gas increases, the relative air-fuel ratio decreases, which leads to a higher BTE than in normal diesel operation. This was most noticeable at low and intermediate loads, while at high loads and high mass fractions of natural gas the BTE was slightly improved.

NOx emissions are usually lower with dual-combustion natural gas/diesel than with normal diesel operation. The lean premixed condition, which causes poor quality natural gas combustion, as well as the longer ignition delay of the dual-fuel natural gas/diesel combustion, also reduces the combustion temperature, resulting in a reduction in NOx emissions; moreover, the introduction of natural gas reduces the available oxygen concentration in the cylinder charge, with a negative effect on the oxygen available for NOx formation.

Increases in NOx production were sometimes observed as the amount of pilot diesel and engine load increased. Experimentally, it was found by Abd Alla et al.[30] that, by increasing the amount of pilot diesel in the entire engine operating range, NOx emissions increased. This increase also occurred by advancing the injection times.

The increase of NOx can be attributed to a higher intensity of heat release in the premixed combustion stage caused by the improvement of natural gas combustion, which raises the maximum combustion temperature peak, resulting in increased NOx emissions.

In dual combustion, natural gas/diesel produces much more HC and CO emissions than normal diesel combustion. During the valve overlap period, a small part of the natural gas-air mixture is directly discharged during the scavenging process and this leads to an increase in HC emissions. In addition, as for the CO emission formation mechanism, the partially combusted blend remains trapped in the cracks and, with the extinguishing of the flame, it is difficult to ignite in the last part of the combustion process. Another case is when, with natural gas, there is a very lean mixture, especially in low load conditions, and the propagation of combustion for the whole charge inside the cylinder is not facilitated. On the other hand, increasing the load, combustion is improved, the temperature is raised, as well as an extensive pilot diesel spray that strengthens the combustion of the air mixture of natural gas, resulting in a decrease in HC emissions.

The effect of certain operational parameters on HC emissions in a single-cylinder dual-fuel engine was examined by Shioji et al.[31]. To reduce HC emissions, especially at low-medium loads, the amount of pilot diesel must be increased and the injection timing advanced. It has also been observed how these emissions are further improved by avoiding too lean a mixture of natural gas, limiting the intake charge air.

PM emissions are significantly reduced in dual-fuel mode. In fact, the amount of pilot diesel is very small, because most of the diesel fuel has been replaced by natural gas, and most of the fuel is burned in premixed combustion. Therefore, less soot is formed. Moreover, since natural gas does not contain C-C bonds and is free of aromatics and sulphur, it has a very low tendency to produce soot. In addition, the soot formed by the combustion of the pilot diesel is oxidised by the combustion of the homogeneous mixture of natural gas and air.

Among several experimental studies carried out, the reduction in soot production is always confirmed. In particular, Papagiannakis et al.[32] noted that, with the increase in the mass ratio of natural gas, soot emissions decreased sharply at partial load, and even at high load, soot reduction was significant.

In dual fuel mode with natural gas supply, the following general conclusion can be drawn:

- Especially at low and intermediate loads, in dual-fuel mode, the BTE is reduced; conversely, the BTE is similar to or slightly higher than normal diesel mode, under high engine load conditions. In these last engine conditions, the observed maximum increase was about 3%;
- There is a decrease in engine power in dual-fuel mode compared to diesel combustion alone. This loss can be recovered by modifying the pilot quantity, for example, by increasing the temperature and pressure of the aspirated mixture;
- PM emissions can be significantly reduced, but HC and CO emissions can increase significantly;
- In dual-fuel mode, engine loads and the amount of pilot diesel affect NOx emissions, which can be higher or lower in comparison with standard diesel operation.

2.5 Biogas supplied to dual fuel engines

Biogas normally consists of a concentration varying between 50 and 70% methane and the remaining part almost totally carbon dioxide, with negligible percentages of other gases. A natural gas, biogas can be applied to diesel engines in Dual Fuel mode.

In the dual fuel engine supplied with high biogas flows, the BTE decreases especially at low and medium load, but at full load improves. A negative impact is also given by higher values of the fuel air equivalence ratio.

According to experimental tests by Rahman and Ramesh[33], the brake thermal efficiency was lower due to decelerated combustion, especially for replacements of more than 60% of biogas. Kalsi and Subramanian[34], Nathan et al.[35] found that BTE decreases significantly especially with low methane ratios, also resulting in lower heat release due to low combustion and a high ignition delay.

However, an increase in full load was recorded due to improved combustion and higher temperature values, as reported by some authors[36,37]. In addition, preheating the charge can lead to an improvement in BTE, and if high compression ratios are used BTE improves to a certain extent. This preheating should facilitate the slower combustion of biogas in the premixed phase, as has been observed by some authors[38,39].

The brake power of the dual-fuel engine is identical to the diesel engine, and is further improved by increasing the engine speed and the flow of biogas in the cylinder, as observed by Girish et al.[40]. With an increase in the methane content of biogas, Prabhu et al.[41] noted increased brake power.

Compared to the diesel engine, higher biogas consumption leads to a decrease in load due to the low calorific value of biogas and the presence of CO_2 in biogas that slows down the combustion process[40,42]. With the increased load, BSFC decreases for better combustion. However, it is possible to recover this by advancing the injection times or improving the equivalence ratio.

In dual-fuel mode, in all load conditions, lower NOx emissions are produced than in diesel mode alone due to the high specific heat of the biogas. A reduction in NOx emissions was observed due to the lower heat release rate of the gaseous fuel, leading to a reduction in the combustion temperature caused by the high thermal capacity of CO_2 in biogas[34,43,44]. Another cause is the reduced combustion rate and the lower temperature in the cylinder due to the presence of CO_2[43,45].

It is possible to achieve lower smoke emissions, according to Verma et al.[46], by improving the compression ratio, which leads to better combustion and oxidation due to the short ignition delay and high temperature in the cylinder.

The use of biogas in dual-fuel mode offers the following conclusions:

- in general, by powering the DICI engine in dual feed with biogas, there is a reduction in thermal efficiency, which can be partially recovered by acting, for example, on the injection timing or on the higher compression ratio;
- at low and medium loads, the BSFC is higher than traditional combustion, while there is an improvement at higher loads due to better combustion, as well as acting on appropriate injection timing or on the air mixture ratio;
- there is a significant decrease in NOx and smoke emissions, while HC and CO emissions increase.

2.6 Alcohol supplied to dual-fuel engines

Ajav et al.[47] used vaporised ethanol mixed with air at room temperature and preheated to 50 [ºC] before injection. No significant variation was recorded in BSFC; the BSFC decreased only when the load was increased, as the brake power increases as the load increases. In addition, this BSFC reduction contributes to the lower calorific value of alcohol and to the cooling of the premixed charge due to the evaporation of alcohol which, although increasing in density, requires more fuel to support full combustion and provide the amount of power required.

In alcohol fumigation, BTE is reduced in low load conditions, while it increases in medium-high load conditions. The reduction in low load conditions occurs for the following reasons: at low engine loads, the excess air ratio is very high and alcohol fumigation forms a mixture that may be too lean to sustain combustion, resulting in the deterioration of combustion efficiency and thus reduced BTE; alcohol has a very high heat vaporisation, which could cool the fuel blend resulting in a reduction of BTE.

Higher values of BTE at medium to high loads can be explained by the following reasons: premixed air/alcohol charge tends to be homogeneous and burns faster, thus providing combustion that tends to increase BTE; the ignition delay increases, as alcohol has a lower cetane number, which involves the release of energy in a very short time, resulting in a reduction of heat loss through the walls, because there is not enough time to transfer the heat to the coolant. The effect of methanol fumigation on the brake thermal efficiency of a four-cylinder CD engine, in dual-fuel mode, was studied by Zhang etal.[48]. Replacement rates of 10%, 20% and 30% methanol fumigation were tested. The tests were carried out at constant speed and at different loads. With the maximum percentage of replacement (30%), in low load conditions, they recorded reductions of BTE of 10% at 0.13 [MPa] and of 11% at 0.27 MPa, while no significant changes were found in the medium and high loads. In another

experimental study conducted by Zhangetal.[49], using 10% and 20% methanol and ethanol fumigation, BTE reduction at low engine load was recorded (2-5% for 0.08 [MPa] and 3-8% for 0.39 [MPa]) along with an increase at high load (at 0.70 [MPa], 10% and 9% with 10% and 20% with methanol replacement only - 3% for 20% with ethanol replacement only).

For many experiments carried out on alcohol fumigation, different results were found on the production of NOx compared to the engine supplied with pure diesel. NOx emissions tend to be lower at low loads, but higher at medium and high loads. Various authors also found that NOx formation depends greatly on the combustion temperature, as well as the concentration of oxygen present in the combustion process.

The positive effect of alcohol fumigation on NOx emissions can be attributed to the following reasons: with the high latent heat of alcohol vaporisation, lower temperature are reached during the combustion process, thus preventing the formation of NOx, especially in conditions of lean blends and low loads; at high load conditions, the fumigation mode contributes to the reduction of the air/fuel ratio, and this could have a negative effect on the oxygen available for NOx formation. As alcohol contains more oxygen than diesel, the oxygen supply has increased, which could help increase NOx emissions. Fumigated alcohol has poor auto-ignition properties, and this leads to an increase in the fuel burned in premixed mode with a consequent increase in the combustion temperature and therefore NOx emissions. The effect of methanol fumigation on NOx emission at different replacement rates (10%, 20% and 30%) was studied by Zhang etal.[48]. All fumigation levels produced lower NOx emissions than traditional diesel combustion. However, NOx emission increases with the level of fumigation, but this is reduced with increased engine loads.

The increase in HC emissions in alcohol fumigation mode can be found in the following reasons. In the fumigation mode, an unburned fumigated alcohol layer may form inside the cylinder. Alcohol tends to have a cooling effect on the combustion process, and as a result the combustion temperature is reduced and may not ignite unburned fumigated alcohol during the expansion stroke, thus leading to the increase in HC emissions.

Due to the large amount of excess air present especially at low loads, with poor fuel distribution and low temperature values maintained throughout the combustion process, create the conditions for maintaining unburnt fractions resulting in increased HC emissions. An increase in HC emissions, as for CO emissions, has been reported by several authors. The effects of alcohol fumigation on HC emissions also affect CO emissions. The alcohol fumigation effect on HC emissions was studied by Zhang et al.[48], who tested five constant-speed engine conditions. The conclusions of their investigation were that HC emissions are

higher than traditional diesel combustion when methanol fumigation increases. It has also been noted that the emissions increase with the level of fumigation, while they decrease with the increase in engine loads.

Compared to clean diesel, alcohol fumigation significantly reduces smoke and PM emissions. This may be for the following reasons. As a large part of diesel fuel is replaced by alcohol, less diesel fuel is consumed. Thus, a smaller amount of diesel fuel is burned in diffusion mode, and that present burns along with the homogeneous alcohol/air mixture, which burns faster and with a greater availability of oxygen, leading to a reduction in PM emissions. The ignition delay is increased by alcohol fumigation and therefore the mixing of diesel fuel with the alcohol-air mixture is improved, thus air usage is improved and smoke is reduced. Alcohol contains no aromatics, is sulphur-free, has a lower C/H ratio than diesel fuel and also increases the hydrogen content in the mixture, resulting in a reduction in PM emissions.

This tendency has been found in experiments. In the experimental tests conducted by Zhang et al.[48], PM emissions were reduced compared to diesel. With 10% methanol fumigation, between 14 and 31% reduction was recorded, reaching 27-57% with 30% ethanol fumigation.

Among the conclusions it can be stated that:

- when the diesel engine is subjected to alcohol fumigation, BSFC increases with the percentage of alcohol fumigation at all engine loads. About 7-12% increase in BSFC on a mass basis was found on average for many experiments conducted, a consequence of the lower calorific value of alcohol;
- BTE is reduced at low engine loads (5-13%), but a slight increase at medium and high engine loads (2-9%) has been observed;
- NOx emissions are reduced by alcohol fumigation compared to standard diesel operation. Engine loads affect these emissions. In most experiments, compared to pure diesel fuel, the maximum reduction was found to be 20%, at low load with a 30% amount of fumigated alcohol;
- in comparison to diesel fuel combustion alone, alcohol fumigation increases specific emissions of CO and HC over wide ranges;
- smoke and PM emissions are reduced by alcohol fumigation. Reductions were observed in a wide range of 14 to 57%.

3 Alternative fuels for diesel engines

3.1Main characteristics of Diesel Oil

The general requirements which engine fuels should meet are listed below:

1. abundant availability, ease of preparation, low cost and respect for the environment;
2. high heating value per unit mass and volume and easy storage and transportation;
3. complete combustion without toxic products;
4. absence of carbon deposits on the walls of the combustion chamber and of corrosive products.

Today, most combustion engines are powered by fuels derived from oil distillation. Crude oil from which they are made consists of a mixture of several types of hydrocarbons of different molecular weight, including a small fraction of organic compounds containing sulphur, nitrogen, etc. The actual composition of crude oil varies greatly depending on the region of origin.

Depending on the characteristics of its residue at the end of the distillation process, which may mainly contain paraffins, naphthenes or a mixture of the two, crude oil is called paraffinic, naphthenic or mixed, with a wide variety in terms of the relative weight of each hydrocarbon group.

Products derived from the refining of petroleum may be classified according to their use and their density and volatility.

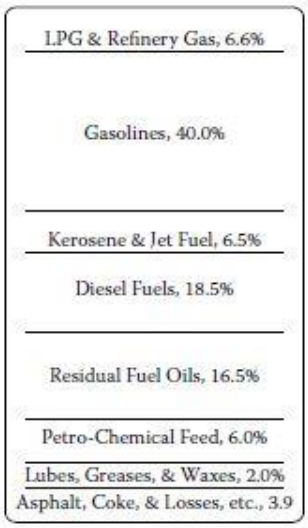

Figure 3.1 - Typical distribution of the products of refining crude petroleum. (From Karim, G.A., Fuels, Energy, and the Environment, CRC Press, Boca Raton, FL, 2012.)

In particular, diesel fuels, are fractions of distillate between kerosene and lubricating oils, covering a wide range of densities (0.815 [kg/dm^3] 0,855 [kg/dm^3]) and distillation temperatures (180 and 360 [ºC]). They are divided into different classes based on their physical characteristics, which are tightly controlled to make them suitable for use in various types of diesel engines.

A number of properties meet standard specifications that characterise the suitability of a diesel fuel. These properties include cetane number, density, distillation characteristics, viscosity, lower heating value, flash point, cloud and pour points, nitrogen and sulphur content, carbon residues and ash, water and sediment content and overall composition. Most of these features are defined in fuel standards, such as those of the American Society for Testing and Materials (ASTM).
These physical and chemical characteristics are determined by the chemical composition and molecular structure of the constituents of petroleum-derived fuels and influence their evaporation, ignition and combustion processes.

The cetane number represents a measure of the ignition characteristic of a fuel. It is calculated comparing the ignition delay of the fuel with a binary mixture of liquid fuel consisting of cetane (n-hexadecane) and iso-hexadecane (Heptamethylonane) when tested in a standard engine under the same standard operating conditions. In this rating scale, n-hexadecane has a cetane number of 100, while the isohexadecane is 15, i.e., cetane number = n-cetane (%) + 0.15 Heptamethylnonane (%).
A low cetane number indicates the difficulty a fuel has in auto-igniting in the times dictated by the engine, and therefore is less suitable as a fuel for diesel engines. This type of fuel corresponds to a high-octane number, which therefore reflects the resistance to auto-ignition.
Normally, most commercial fuels used in CI engines have a cetane number between 45 and 60. Diesel fuel normally has cetane number values around 50-52. Long-chain normal hydrocarbons, which are easily oxidisable, tend to have high cetane numbers, while aromatic fuels, which are relatively less prone to auto-ignition reactions, have low cetane numbers. Appropriate additives are used to improve the properties of fuels for diesel engine applications. After refining from crude oil, the yield of a fuel depends on the fraction of the products constituting it[50].

Consequently, the ignitability of diesel fuel is therefore a very important factor in determining performance, efficiency, operating smoothness, particulate emissions, noise and engine starting ease. It depends on the chemical characteristics of the fuel (structure and size of the molecule, which is therefore more or less easily attacked by oxygen) and on the physical characteristics (volatility, viscosity, heating value, etc.) which influence the processes of vaporisation and diffusion.

The heating value is another important parameter that defines the quality of a fuel; this is defined as the amount of heat developed during the complete combustion of the mass unit of the fuel considered. The heating value of diesel fuel is between 42 and 43.5 [MJ/kg].

Volatility is an important fuel property, because it influences the engine behaviour, especially during cold starts and acceleration, as well as the correct operation of the fuel supply circuit. In the case of the diesel engine, it plays an important role in the spray evolution in the combustion chamber, conditioning the vaporisation of the drops and the consequent mixing of air and fuel. It is also important for fast engines that the diesel fuel contains a sufficiently volatile fraction, also to avoid difficulties in cold starting, when the charge cannot benefit from heating by the walls.

Another parameter that intervenes in the fuel jet breaking and pulverising processes at the exit of the injector is viscosity. It also ensures the lubrication and sealing of the main mechanical couplings of the injection apparatus and directly influences the value of the power absorbed by the circulation pumps and fuel injection. The gas oil viscosity is contained within limits that make this fuel suitable to ensure these specificities[50].

The compatibility of materials with existing engine hardware or fuel infrastructure is important for the penetration of alternative fuels in the market. Otherwise, studies must be undertaken to see what and how many changes are needed and how much they cost, and evaluate if they can actually be used on a large scale. In other words, there must be an economic balance between the necessary adaptations, yields and benefits and consequent commercialisation. For example, lubrication differences are one of the typical examples when it comes to compatibility. Low fuel lubrication, as in the case of dimethyl ether (DME), can cause malfunctions in sophisticated fuel injection equipment, such as the common-rail direct injection system (DICI) in diesel engines. Another example is the additives that are

necessary to obtain a suitable biodiesel, or even clean a biogas resulting from a gasification process. Therefore, to avoid possible damage to the hardware, lubricants, additives and treatments are needed.

The cost of production is one of the practical issues for both producers and consumers. Production costs have fallen in recent decades as technology has improved, but the price of alternative fuels is still high compared to conventional gasoline and diesel fuel. The prices of the main alternative fuels are still high, precisely because they are normalised with equal energy content compared to traditional fossil fuels.

3.2Biofuels

Biofuels are fuels whose energy is obtained through the biological carbon fixation process. They are the most effective and efficient form of renewable energy. They are extracted from biomass, are biodegradable and more environmentally friendly than the combustion of fossil fuels, as they produce less toxic fuels.

When biomass grows, the CO_2 cycle takes place, as it absorbs carbon dioxide from the atmosphere, while when it is burned it releases carbon dioxide back into the atmosphere[51]. The global CO_2 emissions emitted during biomass combustion can then be considered zeroed.

Biofuels are a renewable form of energy and they have low environment impact. Their production has been increasing for many years, and this growth is expected to continue in the near future. Following the trends in recent years and the distribution on production by geographical areas of biofuels[52].

Usually, biofuels are classified into 4 different categories:

- First generation fuels come from special crops belonging to the food chain. First-generation biodiesel comes from the trans-esterification of vegetable oils (mainly rapeseed, palm, sunflower) while bioethanol comes from microbial fermentation (mainly by yeasts such as Saccharomyces cerevisiae and bacteria such as Zymomonas mobilis) sugars in cultivated plants (mainly maize, rapeseed and sugar cane). This technology, less complex and expensive, is still the most widely used.
- The second generation includes biofuels derived from residual and/or lignocellulosic biomass, such as agricultural and forestry waste. This preserves crops for food purposes, as sugars to produce biofuels are derived from the polysaccharides constituting the plant cell wall, namely cellulose, hemicellulose and pectin. However, to make these available for micro-organisms for the fermentation step, they first have

to be freed from the lignin matrix and subsequently be depolymerised. This step is often complex and requires the use of high temperatures, pressures and/or chemical compounds or enzymes. This causes an increase (sometimes limiting for the development on an industrial scale) in production costs and environmental impacts. Second-generation biodiesel usually derives from the trans-esterification of oils of microbial origin (mainly by yeast), obtained by fermenting the second-generation sugars.

- Third-generation biofuels are based on further improvements in the production of biomass. It takes advantage of specially engineered energy crops such as algae as its energy source. The algae are cultured to act as a low-cost, high-energy and entirely renewable feedstock. Algae can also be grown using land and water unsuitable for food production, therefore reducing the strain on already depleted water sources. Conceptually, the third generation is a giant step forward in the production of biofuels, as it would act directly and quickly on atmospheric carbon dioxide levels. CO_2 is fixed by algae which use it to synthesise mainly lipids and other cellular components. These lipids can then be extracted and trans-esterified into biodiesel.
- Finally, the fourth generation of biofuels represents a further evolution of the third generation in that the origin of carbon atoms remains atmospheric, but the conversion of carbon into biofuel already takes place within the cell, in the sense that the post-processing concerns only the purification and concentration of biofuel. The direct conversion of carbon dioxide into ethanol by the use, for example, of cyanobacteria, produces remarkable results. Their nature makes them easy and fast to engineer compared to more complex organisms, increasing their productivity[53].

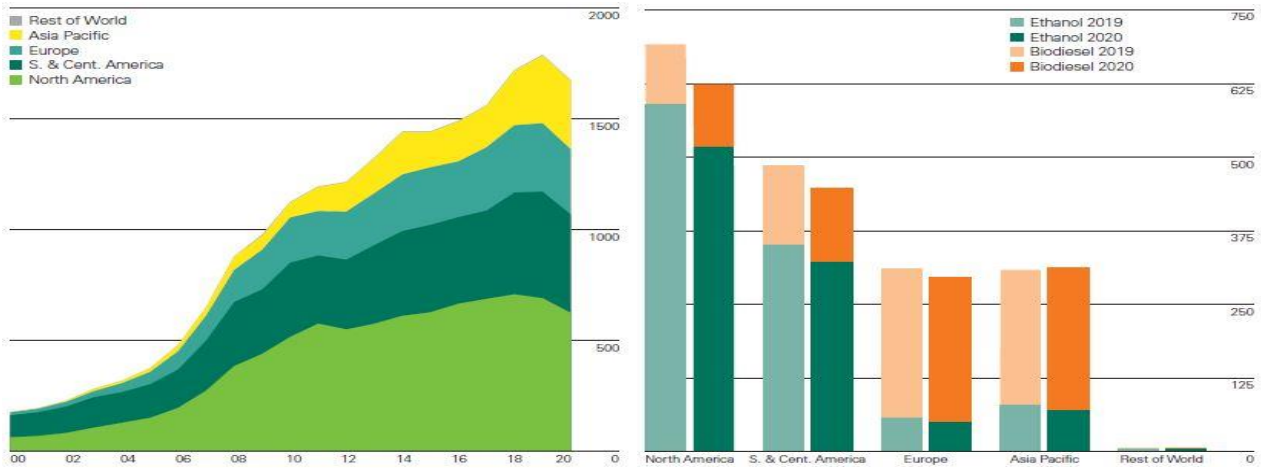

Figure 3.2 - World biofuels production (Thousand barrels of oil equivalent per day) - Biofuels production fell 6% globally in 2020 (113,000 barrels of oil equivalent per day or boe/d) in contrast to the 6% average growth for the 10 years prior. Moderate growth in Asia (4,000 boe/d) was more than compensated by a decline in the US (64,000 boe/d), Argentina (19,000 boe/d) and Brazil (16,000 boe/d). Asia's production was resilient due to an increase in biodiesel whereas ethanol production decreased in all major regions by 7 to 12% (107,000 boe/d globally). Biodiesel is the dominant fuel[4].

A real shift from first-generation to second-generation biofuels has been made thanks to the advancement of technology and processes, production efficiency has been improved and the use of non-edible organic raw materials has been promoted; important steps still have to be taken for third- and fourth-generation biofuels.

Ethanol is considered an ecological fuel, as stocks of traditional feed, such as molasses, sugar cane juice and maize, can act as a CO_2 sink[54]. In particular, corn and sugar cane are the main raw materials of the United States and Brazil, which are the largest producers of ethanol in the world.

Several researchers have carried out extensive WTW (well-to-wheel) CO_2 emissions and LCA-based efficiency research of major alternative fuels. Although the energy needs of WTW for biofuels are higher than for conventional gasoline and diesel, their greenhouse gas emissions are relatively lower[55]. For example, the greenhouse gas reduction range for biodiesel derived from soybean methyl ester was around 50% that of conventional diesel[56]. However, the extent of the CO_2 reduction for bioethanol was lower than for other biofuels. The transition from cereal-based or seed-based biofuels to biofuels derived from high-yield lignocellulosic energy crops has been suggested to further reduce the impact of biofuel greenhouse gas emissions[57].

Figure 3.3 summarises the ways available to produce liquid fuels and some gaseous fuels from fossil fuels or biomass[58]. Most transport fuels have always been derived from the refining of crude oil with well-established technologies, although the production of non-conventional raw materials such as oil sands, oil shale and shale gas continues to increase. Fuels with similar properties to petroleum products, such as synthetic liquids, can be

produced by the gasification and Fischer-Tropsch (FT) process of any hydrocarbon or coal raw material.

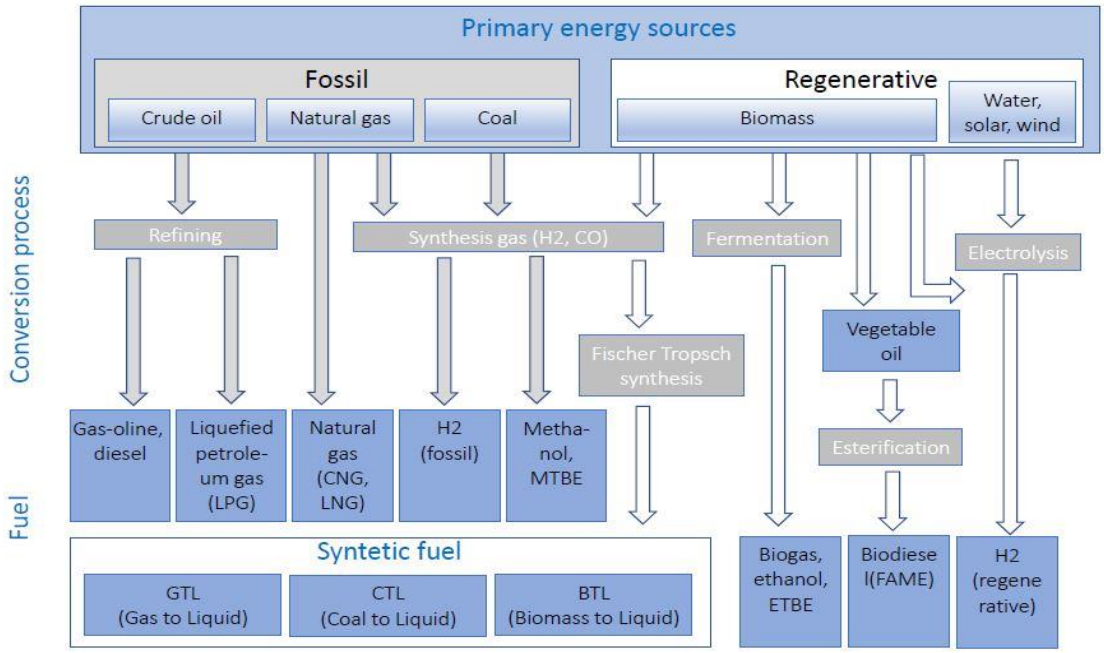

Figure 3.3 - Schematic flow process producing trench and regenerative fuels[58]

Table 3.1 shows the characteristics of some conventional and alternative fuels[59]. A number of known alternative fuels, such as ethanol (bioethanol) and advanced biodiesel, which show moderate compatibility with existing DICI vehicles, are in production on a moderate scale and meet greenhouse gas emissions in a moderate manner.

The following is a brief description of the supply of compression ignition engines with biodiesel and dimethyl fuels, which can be mixed with or completely replace diesel fuel. The fuels discussed below, based on alcohol and gas, feed the engine in dual-fuel mode by injection at low pressure in the intake manifold.

Fuel	Energy density	Production cost oil at USD 100 / bbl	Ditribution infrastructure	Current production and retail availability for vehicles	Compatibility with existing ICE vehicles	Typical GHG emissions	Feedstock	Process
Gasoline	H	Mod	Comp	Comp	Comp	High	Oil from both conventional sources and non-conventional sources, such as heavy crudes and tar sands	Refining
Distillate	H	Mod	Comp	Comp	Comp	High		
CTL diesel	H	Hmod	Cpt	VL	Comp	VH	NG, coal	Gasification / FT
GTL diesel	H	Hmod	Cpt	VL	Comp	H		
Grain ethanol	M	Hmod	Par	Lmod	Par	HMod	Grain crops	Saccharification and distillation
Cane ethanol	M	Lmod	Pal	Lmod	Par	Low	Sugar crops (cane)	Distillation
Advanced ligno-cellulosic ethanol	M	H	Par	None	Par	Low	-	-
Oil-seed biodiesel	H	Hmod	Par	Lmod	Par	Mod	Oil-seed crops	Esterification, hydrogenation
Advanced BTL diesel	H	H	Cpt	None	Comp	Low		
CNG	L	Lmod	Par	VL	RC	Hmod	Natural gas	Gasification / FT
LPG	L	Lmod	Par	VL	RC	Hmod		
Methanol from NG	L	Mod	VL	VL	RC	Hmod	Natural gas	
DME from NG	M	Mod	VL	VL	RC	Hmod		
H2 from fossil sources	L	Mod	VL	VL	RC	Hmod	Natural gas	Reforming, compression
H2 from renewable sources	L	H	VL	None	RC	VL		

Acronyms: H: high; M: medium; L: low; VH: very high; VL: very low; Mod: moderate; Lmod: low-moderate; Hmod: moderate high; Par: partial; WS: widespread; RC: requires conversion; Cpt: compatible with existing; Comp: complete Note: Table classifications are indicative, based on current characteristics and estimates, and apply only to near-term. There may be situations and regions in which these classifications do not apply.

Table 3.1 - Production process and characteristics of various fuels[60]

3.3Biodiesel

Biodiesel is an alternative fuel derived from the processing of raw materials of biological origin. Many raw materials from this derivation can be transformed into fuel. Among them, vegetable oil, animal fat and cooking oil. The most commonly used raw materials are rapeseed and soybean oils. The disposal problem has drawn attention to the possibility of reusing waste oils. Furthermore, biodiesel derived from cooking oils has shown the lowest Well to Wheel (WTW) greenhouse gas emissions, and compared to conventional diesel it saves around 82% of greenhouse gas emissions[60]. The choice of raw materials differs in different countries, according to the cost of regional production, environmental impact and agricultural strategies adopted by each nation.

WTW greenhouse gas emissions depend on raw material and production technology, as biodiesel production cycles are complex. It has been shown that if grassland and/or

deforested land are not used, compared to conventional diesel, WTW greenhouse gas emissions can be reduced to around 50%[60].

There are regulations in some countries which prescribe the use of biodiesel alone or blends with conventional diesel[61]. When biodiesel is mixed with diesel in small portions, no major changes to the engine are required, as the physiochemical characteristics of biodiesel are generally similar to those of diesel. However, there are some differences that need to be considered. The following table shows some types of biodiesels named after the raw material of origin and, in some cases, the geographical area of origin; this table shows the main chemical and physical characteristics[62].

Biodiesel Types	Trends Compared to Conventional Diesel						
	Density (kg/m^3)	Kinematic Viscosity at 40 °C (mm^2/s)	Calorific Value (MJ/kg)	Flash Point (°C)	Cetane Number	Oxidation Stability (h) or (%)	Acid Value (mg KOH/g)
Argemone mexicana biodiesel	870/830 (15 °C)	4.38/2.8	37.5/44.5	193/65.5			
Moringa oleifera biodiesel	866.1/834.3 (40 °C)	4.03/3.63	39.9/45.21	189.0/71.5	54.3/52.4	10.8/0.1 h	0.24/-
Karanja biodiesel	881/831 (40 °C)	4.42/2.78	37.98/43.79		50.8/51.2		
Jatropha oil biodiesel	865/841	5.2/4.5	34.5/42	175/50	51/49		
Calophyllum inophyllum biodiesel	871.8/834.7 (40 °C)	4.9762/3.4926	39.17/45.6	92.6/68.5	56/48	2.53/35 h	0.41/0.072
Water hyacinth biodiesel	887/838 (15 °C)	3.96/2.76	36.9/42.7	212/68	52.5/48		0.42/-
Pongamia biodiesel	912/824 (15 °C)	10.29/2.3	912/824	175/53		2.3–11.6/- h	>1.53
Citrullus colocynthis L. biodiesel	886/830 (15 °C)	3.45/2.43	37.64/42.82	134/69	66.89/60.82		0.27/-
Fish oil biodiesel	885/850	4.741/3.05	40.057/42.8	114/56	52.6/52		
Rice bran oil biodiesel	887/843	4.98/3.58	38.725/43.2		55.7/48	11.25%/0	
Neem oil biodiesel	871/843	4.63/3.58	41/43.2		53.5/48	11%/0	
Cottonseed oil biodiesel	864/843	4.14/3.58	36.8/43.2		52/48	−10%/0	
Linseed oil biodiesel	924/842 (15 °C)	16.23/2.44	39.750/45.343	108/47	35/>50		
Fleshing oil biodiesel	876.7/829 (15 °C)	4.7/3	37.3/43.2	168/63	58.8/56.8		
Chicken fat biodiesel	889.7/829 (15 °C)	5.3/3	37.1/43.2	169/63	52.3/56.8		
Canola-safflower biodiesel	884.3/831.7 (15 °C)	4.35/2.58	40.10/45.98	168/63			
Rapeseed oil biodiesel	874/850	4.8/2.6	37.6/42	>140/68	54/51	10.2/- h	

Table 3.2 - Physical and chemical characteristics of some biodiesel types [65]

Compared to conventional diesel fuel, the LHV of biodiesel is lower, while it generally has a higher cetane number. Biodiesel also has a higher flash point, which is beneficial for fuel storage and transport safety. Due to the greater portion of saturated fatty acids, biodiesel has higher cloud and pour points than conventional diesel. These characteristics indicate

the lowest temperature values at which a fuel can be pumped, before turning into a crystal wax[63]. Cloud and pour points have disadvantages when the engine is started cold, and this causes some inconvenience especially with the use of larger portions of biodiesel.
Compared to conventional diesel, biodiesel is denser and more viscous and has a higher surface tension. This results in longer injection delays than conventional diesel due to viscosity[64]. The viscosity of biodiesel slows down the rate at which the injector opens and decreases its flow performance during transient injection behaviour.
Due to the presence of intrinsic oxygen atoms in the fuel molecule, the equivalence ratio is lower than that of diesel, and this characteristic is dominant for soot formation.
The lower LHV of biodiesel may not allow the maximum torque to be reached at full load.

Many authors have found that the lower power output is slightly lower than can be expected due to the lower heating value. Kaplan et al.[65] compared sunflower oil biodiesel and diesel fuels at full load and partial loads and at different engine speeds in a 2.5 [l] - 53 [kW] engine. The torque and power loss varied between 5% and 10%, and especially at full load, the power loss was closer to 5% at low speed and 10% at high speed.
Due to the higher cetane number, the start of combustion (SOC) for pure biodiesel or biodiesel blends should be advanced compared to conventional diesel[66]. A higher ignition delay was also observed, for example with biodiesel WCO, with a cetane number difference between fuel and conventional diesel being less than 1[67]. In addition, the early formation of the flammable air-fuel mixture is made difficult by the poor evaporation characteristics.
A review of the published data on biodiesel emissions for heavy engines was produced by the U.S. EPA. The overall CO, HC, NOx and PM emissions are reported in the figure 3.4 below[61]. With the increase in the concentration of biodiesel in diesel, the tendency to reduce CO and HC emissions is clear, which means increased combustion efficiency. This is due to the oxygenated nature of biodiesel, where more oxygen is available for combustion[68].

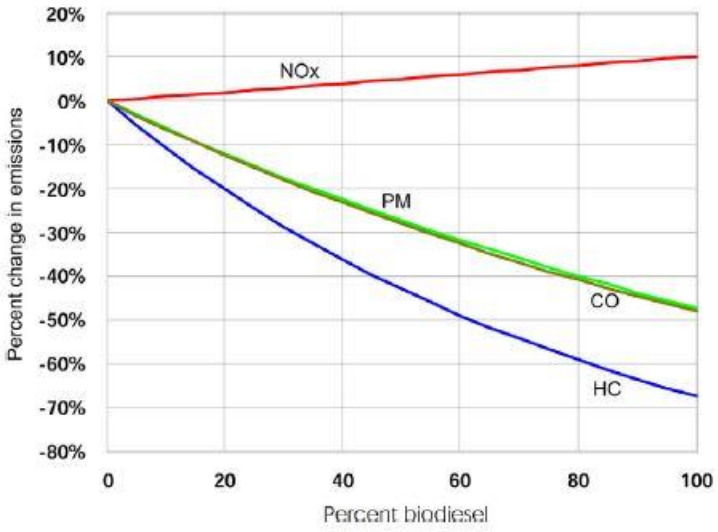

Figure 3.4 - Average emission impacts of biodiesel fuels in compression ignition engines[64]

The presence of oxygen helps to promote stable and complete combustion by facilitating combustion in the pyrolysis zone. Locally over-rich regions can be reduced and the formation of soot particles limited. In addition, it was demonstrated by chemical kinetics studies carried out by Westbrook et al., how the strong bond of oxygen and carbon remained intact, preventing it from becoming available for the production of soot[69].

Detailed investigations carried out using different technologies have compared the size of primary soot particles, and it was observed that WCO biodiesel particles were composed of smaller particles than those in conventional diesel. The particles contained a more soluble organic fraction (SOF) than diesel, with an oxygen content of over 9%, 6% higher than the primary particles produced by diesel, showing a faster oxidation process and with fewer carbonaceous species[70].

The increase in flame temperature with the burning of biodiesel may be the main cause of the increase in NOx emissions. The increase in temperature can be explained by a decrease in the dissipation of heat through radiation, as a consequence of the reduced amount of soot emitted[71].

3.4 Dimethyl ether

DME is a colourless, non-toxic, slightly narcotic and highly flammable gas in environmental conditions, and if slightly pressurised it changes state and can be managed as a liquid. Dimethyl ether (DME) may be produced by indirect or direct synthetic methods. Indirect

synthetic methods occur by a dehydration reaction after the synthetic reaction of methanol, while direct synthetic methods produce DME directly from natural gas.

DME is not a greenhouse gas and has a high cetane number (>>55, diesel fuel: 40-55). DME is therefore considered to be a clean alternative fuel to diesel oil[72]. However, the physical nature and peculiarities of this fuel, with its combustion characteristics, need to be further investigated to understand whether it can really be an alternative fuel and suitable for diesel IC engines, and to determine what the optimal operating conditions for the actual application to the vehicle may be.

DME is a simple chemical compound with the chemical formula CH_3-O-CH_3 and with a low carbon-hydrogen (C/H) ratio[73]. The physical properties of DME are similar to those of LPG, which is basically propane and butane. Therefore, storage, handling and transport operations are similar to those for LPG. DME exists as an invisible ether compound in the gas phase. In the atmospheric conditions of 0.1 MPa and 298 K, it passes from vapour phase to liquid phase when pressurised above 0.5 MPa at standard atmospheric temperature. Therefore, it is necessary to pressurise the DME above its vapour pressure at ambient temperature to keep the DME in liquid phase in a fuel tank.

Gaseous DME is denser than dry air, while at normal temperature and pressure the density of liquid DME is 668 kg/m^3. The liquid density of DME is two thirds that of water and DME dissolves in water up to 6% by mass[74]. In terms of fuel density and viscosity characteristics, DME differs significantly from conventional diesel.

The low density and viscosity of DME cause leakage from the fuel tanks and fuel supply system from the tank to the injection system in the engines. The physical and chemical properties of DME and LPG fuels are listed in Table 3[73,75].

Property	DME	Diesel	LPG	
			Butane	Propane
Chemical formula	CH_3OCH_3	C_8 to C_{25}	C_4H_{10}	C_3H_8
Molecular weight	46.07	96~	58.13	44.11
Vapor pressure at 20 °C (bar)	5.1	<0.01	8.4	2.1
Boiling temperature (°C)	−25	≈150–380	−0.5	−42.1
Liquid density at 20 °C (kg/m^3)	660	800–840	610	501
Liquid viscosity at 25 °C (kg/ms)	0.12–0.15	2–4	0.2	0.2
Gas specific gravity (vs air)	1.59	–	2.01	1.52
Lower heating value (MJ/kg)	28.43	42.5	45.74	46.36
Cetane number	55–60	40–55	–	5
Stoichiometric A/F ratio (kg/kg)	9.0	14.6	14.8	15.7
Enthalpy of vaporization at NTP[a] (kJ/kg)	460 (−20 °C)	250[a]	390	426

[a] Normal temperature and pressure.

Table 3.3 - Physical and chemical properties DME, Diesel, LPG [78,80].

DME has no direct carbon-carbon bonds (C-C) and contains about 34.8% oxygen. The absence of C-C bonds allows combustion without smoke production, as well as a high rate of oxidation reaction of particulates and combustible materials. In addition, C-O bonds in DME break more easily than C-H bonds, and the lower binding energy of C-O bonds than C-H bonds results in a shorter ignition delay.

From the chemical point of view, it is quite stable and reacts only in particular conditions. The lower explosion limit is 3.4% by volume in air (refer to table 3.4)[76].

Items	DME	Diesel	Propane	Butane
Auto-ignition temperature (K)	508	523	743	638
Lower explosion limit (vol.%)	3.0–3.4	0.6	2.1	1.9
Upper explosion limit (vol.%)	17–18.6	6.5–7.5	9.4	8.4
Minimum ignition energy (mJ)	0.29	–	0.26	0.305

Table 3.4 - Explosion and hazard characteristics of DME [77].

LHV (lower heating value) of DME has a value (LHV DME: 28.3 [MJ/kg]) significantly lower than that of diesel (LHV diesel fuel: 42.5 [MJ/kg]), but a LHV higher than methanol (LHV methanol: 19.5 [MJ/kg]) and ethanol (LHV ethanol: 27.0 [MJ/kg]), as shown in figure 3.5[76]. This property means that a larger amount of fuel per cycle is required to generate the same engine output when conventional diesel is used. In fact, for the low LHV value and the lower density compared to diesel, in the experimental tests carried out by Kim et al.[77] it was necessary to introduce 48% more mass of DME fuel than the mass of diesel fuel to produce the same heat as diesel fuel, and therefore the injection duration was 37% longer than diesel.

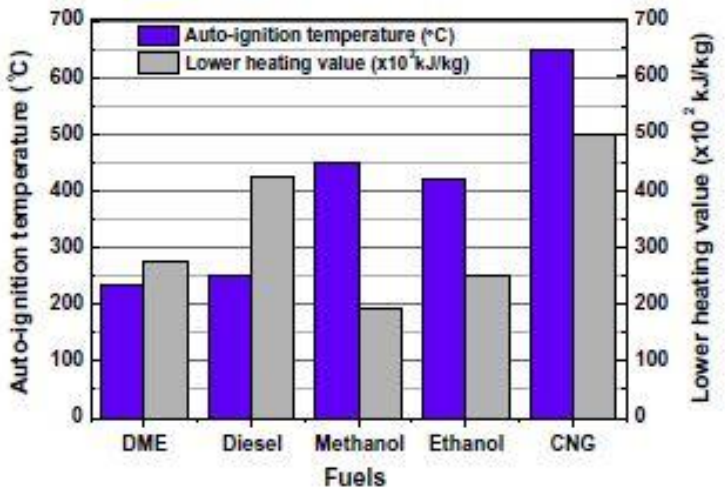

Figure 3.5 - Auto-ignition temperature and heating values of various fuels[76]

The DME has a cetane number greater than 55, close to the upper limit of that of diesel. The high cetane number of DME indicates that it is suitable for use in a diesel engine, because a high cetane number corresponds to a shorter ignition delay.

The disadvantages of DME are its low viscosity and low lubrication characteristics, which cause fuel losses and surface wear of moving parts in the fuel injection system. Therefore, appropriate additives must be added to prevent leakage and surface wear. On the other hand, DME is not corrosive to the structure of the feed system and the metal surfaces.

To use DME fuel, injection capacities such as the displacement volume have to modify and changes have to be made to prevent leakage from the sealing of moving parts. To increase the displacement of the injection pump, the plunger diameter and stroke can be increased, an anti-dissolving material should be used for the seals and nozzle dimensions appropriate to a DME fuel system should be used. Most of the sealing materials used in conventional fuel pumps and high-pressure injection pumps dissolve and swell when DME is used, resulting in leakage of high-pressure DME fuel[76].

Once injected into the combustion chamber, DME vaporisation is immediate due to its low boiling temperature. It has a faster mixing of the fuel vapour, which allows a reduced ignition delay. This plays an important role in the combustion characteristics and determination of exhaust emissions.

Experimental tests conducted by Youn et al.[72] on a total DME power on a DICI light duty engine, at constant load and speed, showed how the peak pressure of diesel fuel was higher than that of DME at the same injection rate, due to the higher LHV of diesel fuel (about 42.5 [MJ/kg]) than that of DME (about 28.43 [MJ/kg]). The amount of injected DME fuel should be increased to the amount corresponding to the same input energy as diesel, in order to improve both the combustion characteristics, in-cylinder pressure and heat release. The maximum pressure of DME has reached values higher than those of diesel fuel, when the injection timing is anticipated. They indicated that the ignition delay of DME was lower than that of diesel, due to differences in vaporisation characteristics and higher cetane number. In addition, the combustion reaction was promoted by the higher oxygen content of DME fuel. Advancing DME fuel ignition led to fast fuel burning and an early increase in accumulated heat release. In DME combustion, the homogeneous fuel and air mixture created in the premixed area is the dominant factor for cumulative heat release.

However, due to the use of additives to improve lubrication, impurities present in the fuel or lubricating oil in the fuel pump, very small amounts of soot emissions are sometimes detected in DME fuels.

HC emissions from DME combustion are generally lower than or equal to those from the combustion of diesel fuel[78]. Due to the already stated characteristics of evaporation, atomisation, mixing, cetane number, the ignition delay of DME is shorter, which makes it difficult to form regions that are too rich or too lean due to insufficient mixing time. This does not favour the formation of areas that are too rich or too lean due to the insufficient mixing period[79]. However, the oxygen content of DME produces relatively less fuel-rich regions than diesel. Therefore, DME combustion results in lower HC emissions than diesel combustion.

CO emissions from DME combustion are normally lower than those from diesel combustion, as DME has a low C/H ratio, lacks C-C bonds and has a high oxygen content, characteristics that promote mixing and rapid oxidation of intermediate species[77,80].

According to many researchers, NOx emissions have a contrasting trend[72,81].

The main reason for lower NOx emissions compared to diesel combustion is the lower heating value, the high cetane number and a higher latent heat capacity than diesel [78]. In addition, low NOx emissions are related to the short ignition delay, which results in a small amount of pre-mixed burnt DME and the resulting low peak combustion temperature. However, when the injection system is modified and the timing is optimised to recover the performance of the engine running on diesel oil, NOx may even increase when DME is used.

3.5 Alcohol fuels (ethanol and methanol)

Ethanol can be produced from starch cultures after conversion to simple sugars by fermentation and distillation. Varieties of cellulosic raw materials such as rice straw, corn stalks, sugarcane bagasse, switch grass and pulp wood can be used. Considering the life cycle, ethanol derived from wood waste has considerable potential to reduce CO_2 emissions from greenhouse gases[82]. It blends perfectly with water. It causes corrosion problems on metal parts such as aluminium, brass and copper. It also reacts with rubber, which means that, in engines, it may cause obstructions in the supply line. Fluorocarbon rubber is used for this purpose[83].

Most methanol is produced from fossil fuels such as coal and natural gas, and research is currently being carried out into the feasibility of its production from renewable and

sustainable sources. In this regard, considerable attention has been paid to forest biomass as a sustainable and environmentally friendly source of methanol production[84].
Among the simplest of alcohols, methanol (CH OH) is a light, colourless, volatile, flammable liquid with a characteristic odour[85]. Methanol is free of sulphur and complex organic compounds.

Alcohols such as ethanol and methanol usually have very high cetane number (greater than gasoline) and so they can be successfully employed in spark ignition engines. However, some modalities have been also studied for the operation with dual alcohol-diesel feeding in compression-ignition engines, and the most known methods are:
1. alcohol injection into the intake manifold upstream of the port valve, when mixed with the oxidising air[47];
2. alcohol-diesel blend, premixed and then injected into the cylinder directly through the fuel injector[86].
In the mixture mode, alcohol and diesel are premixed before injection into the cylinder. The amount of alcohol is limited due to the poor miscibility of alcohol with diesel. In fact, the blends are not stable and can be separated in the presence of water.
In order to increase the miscibility, and thus prevent the phase separation of two fluids, additional additives are used in alcohol-diesel mixing, but these reduce the energy input to the engine. Therefore, the mixing mode provides less energy-based alcohol (25%) than the injection mode (50%)[87]. Furthermore, with the addition of alcohol, diesel oil partially changes its physical characteristics: it decreases its viscosity and reduces the cetane number and heating value.
In the other mode, alcohol is injected into the intake manifold and vaporises by mixing with the intake air flow. This involves additional injectors, as well as a separate fuel tank line and controls for combined operation with diesel operation. Alcohol vaporisation decreases the mixture temperature, increasing its density. As there is no need to use additives in this mode, the miscibility with diesel is better and it is possible to replace up to 50% of diesel with alcohol[87], resulting in cleaner combustion.

Reference is made to the chapter describing low temperature combustion techniques (chapter 2) for a brief discussion of the behaviour of alcohols which supply compression-ignition engines in dual-fuel mode.

3.6 Fuelling gaseous fuels for dual-fuel engine

3.6.1 Methane and Natural Gas

Natural gas has always been used to power engines for economic and environmental benefits. Its availability has increased because, in recent years, the search for natural gas has grown in the rocky structures of the subsoil with low permeability, which are normally narrow and deep. This has led to increased extraction costs, as well as environmental costs, as machines are used for extensive hydraulic fracturing of rock structures to facilitate gas mobility.

In addition to traditional deposits, the natural gas industry can be produced gas from different resources: sour gas, tight gas, shale gas, coal-bed methane, and methane gas hydrate[88].

Although methane, known to be a greenhouse gas, is its main component, as natural gas has the lowest carbon-hydrogen ratio of all fossil fuels it can contribute to the reduction of CO_2 emissions. The potential contribution of methane gas in the formation of photochemical smog is reduced. But when present in the atmosphere, it represents a source of greenhouse gases with a significant contribution to global warming. Therefore, it is very important to control leaks and releases, identified as fugitive gas emissions, which can be natural, such as due to biodegradation processes, or anthropic releases, mainly linked to industrial emissions, in particular those associated with the refining and processing of fossil fuels such as oil and gas.

Depending on the extraction site and the long route it takes to reach the utilities, natural gas can have a different composition. These variations can affect the performance of engines powered by them and the emissions produced by their combustion, as well as the resistance to auto-ignition and the consequent stresses. The main treatments carried out on natural gas concern the sulphur content, reduced to almost zero values. Water content is also monitored in order to reduce the possibility that over time it can create fouling due to the formation of solid hydrates or the possibility of corrosion along the pipes, in storage tanks or in the same power supplies as engines. Some adjustments can be made in its composition, with elements such as propane or air, depending on the climatic season, in order to regulate its density and average specific heat.

Natural gas normally consists of a blend of some main gases, mainly methane, and including some types of light alkanes, such as ethane, propane, n-butane and isobutane, and

pentanes. Small parts of carbon dioxide, nitrogen and traces of water vapour may be present. The composition and content varies slightly depending on the source and production process (table 3.5)[89].

Component	Typical analysis (vol%)	Range (vol%)
Methane	94.9	87.0–96.0
Ethane	2.5	1.8–5.1
Propane	0.2	0.1–1.5
Isobutane	0.03	0.01–0.3
n-Butane	0.03	0.01–0.3
Isopentane	0.01	Trace to 0.14
n-Pentane	0.01	Trace to 0.14
Hexane	0.01	Trace to 0.06
Nitrogen	1.6	1.3–5.6
Carbon dioxide	0.7	0.1–1.0
Oxygen	0.02	0.01–0.1
Hydrogen	Trace	Trace to 0.02

Table 3.5 - Usual components of natural gas[91]

Methane content is usually between 87% and 96%. Methane is a much lighter gas than air, odourless, colourless and relatively non-toxic; in fact, its effects on health are associated with being a simple asphyxiant that removes oxygen from the lungs. In its distribution points, for instance, ethyl mercaptans are added to make it odorous and therefore guarantee easy detection up to reduced concentrations in the environment. It is treated to remove almost all of the hydrogen sulphide that may be present, while reducing the water content to an acceptable level, as well as minimising the presence of inert gases, to ensure effective combustion.

The physical-chemical properties of natural gas are very similar to those of pure methane. A comparison with gasoline and diesel is shown in table 3.6[89].

Fuel properties	Natural gas	Diesel	Gasoline
Low heating value (MJ/kg)	48.6	42.5	43.5
Heating value of stoichiometric mixture (MJ/kg)	2.67	2.79	2.78
Cetane number	–	52.1	13–17
Octane number	130	–	85–95
Auto-ignition temperature (°C)	650	180–220	310
Stoichiometric air–fuel ratio (kg/kg)	17.2	14.3	14.56
Carbon content (%)	75	87	85.5

Table 3.6 - Main physiochemical properties of natural gas, diesel, gasoline[91]

Due to the low ignition characteristics, the high auto-ignition temperature, and low cetane number compared to diesel fuel, natural gas does not appear to be suitable in compression

ignition engines as a substitute of diesel oil. It is used in dual-fuel mode injected into the intake manifold to mix evenly with air and is then fed into the cylinder and ignited by fuels injected directly with high cetane number[28]. Reference is made to the chapter 2, describing low temperature combustion techniques for a brief discussion of the behaviour of natural gas which supplies compression-ignition engines in dual fuel mode.

3.6.2 Biogas

Producing a combustible gas by transforming organic materials, for example by-products of agricultural processes, often considered waste, into a useful economic asset is economically and environmentally advantageous, especially if this gas then powers conventional engine systems, which require minimum changes, to produce thermal and electrical energy. Clearly, this would also collectively represent a significant global environmental benefit.

The term biogas refers to gaseous products formed by processes of pyrolysis, gasification or anaerobic digestion of organic matter from animal and plant sources, described as biomass or sometimes as non-hazardous by-products or waste. Gasification of this material produces a mixture of gases such as methane, hydrogen, carbon monoxide, carbon dioxide, nitrogen, water and some simple hydrocarbons, mainly lower olefins. The occasional presence of hydrogen tends to compensate for the low combustion rate associated with fuel caused by the presence of some diluents.

Biogases are common fuel blends with low and medium heating values. Basically, all organic material can be used for the production of this gas. It is considered a renewable energy source derived from organic waste on an ongoing basis, for example by knowing the farm's livestock and agricultural production, it can be defined as a renewable and programmable energy source, unlike other renewable sources that cannot be said to be programmable, such as the energy produced by the sun, wind or waves.

The gas produced by most biomass sources must be thoroughly cleaned of any tar, alkaline metal compounds and dust before it can be used, particularly in engines.

Typically, the composition of the blend by volume is 50-80% methane, 15-45% carbon dioxide, water, traces of hydrogen sulphide and traces of gaseous nitrogen. The relative amount of each gas varies depending on the maximum temperature, pressure, heating rate, size and porosity of the biomass bed. In order to reduce the gas content and allow satisfactory operation in engines, part of the CO_2 must be removed.

Figure 3.6 shows an example of the variety of processes and products resulting from the transformation of biomass to produce a wide range of products, with most combustible products in the form of combustible gases.

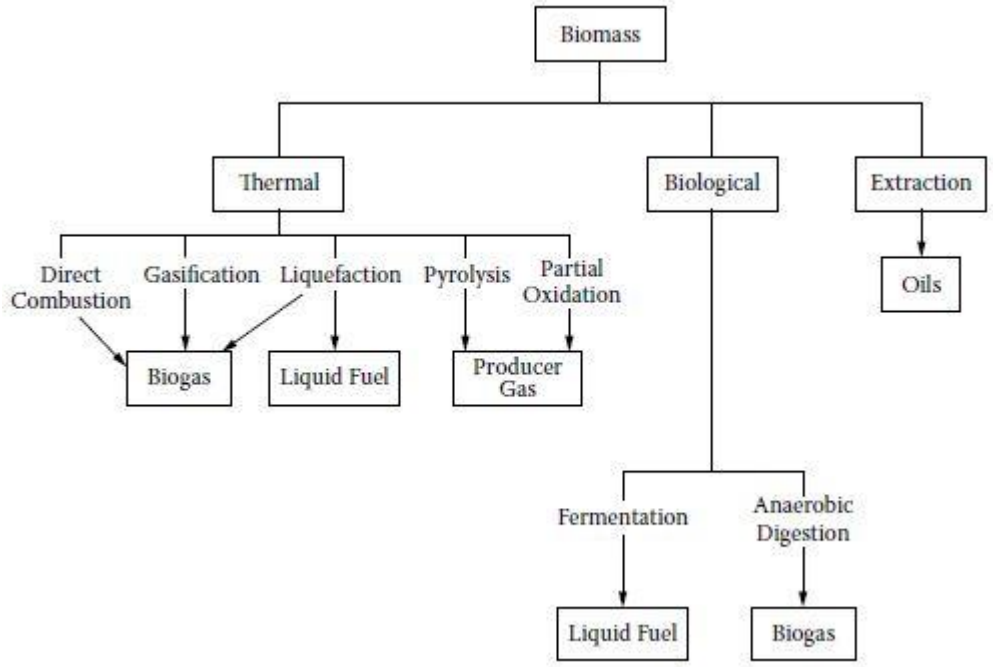

Figure 3.6 - Main biomass processes for the production of renewable fuels

In general, the production rate and composition of biogas depend on a number of variables. These include temperature, available nutrients, retention time, pH value, solid content, agitation, etc. Moderately increasing the average temperature tends to increase the speed of gas production. The required external heat input is often provided by the combustion of part of the gas produced.

There are a number of basic requirements for the efficient use of biogas for energy production in engine applications. It must have an adequate heating value and be free of dust and tar in order to produce a constantly sufficient power at satisfactory efficiency and minimise engine wear, deposits and maintenance problems in compliance with the required exhaust emission controls. The maximum power an engine can produce during biogas operation depends on the heating value of the gas, its composition and the specific characteristics of the engine.

Compared to natural gas operation, larger engines and power lines would be needed to compensate for the low specific energy content of the gas. Combustion devices, including engines, must be suitably modified to allow efficient biogas combustion. These changes, for

example, include an adequate increase in the size of the fuel lines and injector to allow the management of larger flows.

For effective use of biogas as a fuel, it may be necessary to enrich their methane and other combustible components by measures such as water purification, glycol absorption, application of molecular sieves and membrane separation. These are used in wastewater treatment plants, where water does not need to be regenerated or recycled. The presence of any hydrogen sulphide in the gas has detrimental effects, for example, on lubricating oil, cylinder surfaces, valves and exhaust gas treatment measurements. It is also necessary, when using natural gas and other gaseous fuels, to ensure that they are sufficiently dry.

Waste gases and biogas frequently contain silicon and halogen vapour compounds in small concentrations, which require removal, for example by activated carbon adsorption systems. These compounds can form unwanted deposits of silica in the engine, increasing component maintenance requirements and wear and affecting the operation of oxidising catalytic exhaust gas converters. Biogas-powered engines may contain some siloxanes and tend to lose efficiency and require more maintenance. In addition, silicon dioxide contaminates the lubricating oil, increasing the accumulation of deposits.[18]

The presence of CO_2 reduces the energy content of the gas. This increases fuel consumption, in fact CO_2 is an inert gas, and in a dual-fuel engine it contributes to increasing the specific heat of the pre-mixed intake charge, causing a reduction in the speed of flame propagation[90]. Generally, due to the presence of CO_2, dual-fuel biogas-diesel engines achieve low BTE and high BSFC. These results were confirmed by experimental tests conducted by Makareviciene et al.[91], which observed a reduction of BTE from 30% to 27% and by Bari[92], which reported an increase in BSFC for a percentage of CO_2 above 30% (vol. base) of biogas. This may be due to the decrease in the combustion temperature that involves the presence of inerts such as CO_2, and the influence that this has on the rate of combustion of the mixture. It has also been said by Nathan et al.[35] that the CO_2 content in biogas up to 40% does not affect the performance of the dual-fuel IC engine, but beyond this threshold, CO_2 affects the ignition delay due to dissociation in O_2 and CO.

As mentioned above, the main component in the composition of biogas is methane (CH_4) (up to 65%); therefore, the higher the methane content, the greater resistance to detonation of the biogas, as methane has a high octane number. In addition, the presence of methane makes biogas suitable for engines with high CR, as well as allowing the recovery of BTE for higher heat release speed[93]. Due to the lower carbon content of methane compared to

diesel, less pollutant emissions are produced at the same time[94]. In addition, in order to achieve further improvements in terms of BTE and emission control, it is possible to replace the pilot fuel with biodiesel, increase compression ratios, use H_2 enriched biogas and use EGR technology to preheat the input charge.

On the other hand, the presence of CO_2 limits the conversion of CO and HC to finished combustion products, so a suitable technology has to be developed to overcome this problem.

Therefore, by appropriate adaptations and by treating biogas appropriately before being used in existing diesel engines, dual-fuel mode offers clear environmental and economic benefits, especially when the biogas comes from by-products of the local territory. This is undoubtedly a system that must be invested in to optimise its performance.

3.6.3 Biomethane

Among gaseous fuels, biomethane (BM) is an excellent fuel for its combustion characteristics and bio-nature. Biomethane is also referred to as green gas or bio-CNG.

Biomethane is a renewable energy source obtained from agricultural biomass (dedicated crops, agricultural by-products and waste and animal manure), agro-industrial (waste from the food chain processing chain) and the organic fraction of municipal solid waste. Biomethane is acquired in two phases: production of raw biogas - mainly through anaerobic digestion of biomass - and subsequent removal - upgrading - of components not compatible with the network (CO_2).

Biomethane meets emission reduction targets by exploiting existing gas networks and helping to increase national production. This development would also have positive effects on the agri-food sector, promoting an economic model based on sustainability and circularity in the use of resources.

The contribution of biomethane to decarbonisation objectives is not limited to the energy consumption stage alone. Its production process can significantly contribute to reducing agricultural sector emissions (14% of greenhouse gases) and to returning organic matter to the soil. The digestate (what remains after the anaerobic digestion process of the agricultural matrices) is in fact an excellent natural fertiliser that can be used as an alternative to those of fossil origin. Farmers could therefore substantially reduce their production costs and increase their competitiveness. Biomethane produced with sustainability criteria is able to increase the capacity to absorb and store soil carbon.

Compared to gasoline, greenhouse gas (GHG) emissions during the biomethane life cycle can reach levels below 80%, and also achieve significantly lower CO_2 production than natural gas (about 250 [g/km])[95].

Chandra et al.[27] and Subramanian et al.[96] observed that there are no significant differences between normal CNG and biomethane in engine applications in terms of thermal efficiency, specific gas consumption, brake power output, vehicle fuel economy or emissions.

Some advantages of biomethane in internal combustion engines include:

- it can contribute to the reduction of CO_2 emissions due to the low carbon-hydrogen ratio;
- it can significantly reduce NOx emissions and at the same time produce almost negligible smoke and particulates;
- it is better than gasoline for the higher octane number and lower cetane number;
- due to the low production costs, it is cheaper than gasoline or diesel;
- it has a higher combustion enthalpy per unit mass than gasoline or diesel;
- the operating and maintenance costs of vehicles powered by biomethane gas are lower than those of vehicles powered by diesel/ gasoline[89].

In addition to some drawbacks such as natural gas storage, there are two limitations for biogas:

- the production process by refining, transport and storage involves leakage into the atmosphere and therefore environmental pollution;
- in the gaseous phase, the energy density of biomethane is much lower than that of gasoline and diesel; although it is an energy-consuming process, its density can be increased by the process of liquefaction. To obtain liquefied biomethane, it is estimated that biogas should contain less than 25 ppm, 1 ppm and 4 ppm respectively of CO_2, H_2O and H_2S, otherwise the presence of these impurities complicates the liquefaction process and the presence of oxygen may cause explosions[89,97].

3.6.4 Hydrogen

The amount of hydrogen on the Earth is very small and indeterminable as its density is very low and it is pushed out of the gravitational attraction of the planet. Therefore, hydrogen must be produced from other components where it exists as natural gas, oil and water. Hydrogen is an energy carrier and its production requires a source of energy such as fossil fuels (coal, oil or natural gas) or nuclear or renewable energy (solar, wind, biomass, geothermal and hydroelectric). However, in recent years, around 95% of hydrogen has been

produced by fossil-based methods and only a small fraction comes from renewable resources. Therefore, hydrogen generation is still considered expensive and produced through high-emission processes. The question of whether hydrogen can be produced abundantly and economically by renewable sources is critical to the successful transition to a the new era of hydrogen.

In recent years there has been significant progress on technological developments applied to the internal combustion engine and the use of renewable energy for hydrogen production; in an economy of international policies that also include the use of hydrogen, this fuel has been considered a short-term option for its use in the transport sector.

Hydrogen is a colourless, odourless, zero-emission fuel when burned with oxygen. In fact, the combination and reaction of two atoms of hydrogen and one of oxygen leads to energy release and the formation of water only, while if it is burnt in air, it may also produce NOx. The combustion reaction can occur either in the form of a chemical reaction with the help of an anode from a fuel cell, or by its combustion under high temperature and pressure conditions. The main characteristics of hydrogen fuel compared to other fossil fuels commonly used in internal combustion engines such as natural gas, gasoline or diesel are given in table 3.7[98].

		Hydrogen	Natural gas	Gasoline[b]	Diesel[b]
Density at NTP[a]	(kg/m^3)	0.09	0.7–0.9	737	820–950
Energy content	(MJ/kg)	120–142	53.6	46.4	48
Autoignition temperature	(K)	858	813	520–583	473
Flammability limits	(% gas-to-air volume ratio)	4–75	5–15	1.4–7.6	0.6–7.5
Minimum ignition energy	(mJ)	0.02	0.29	–	–
Quenching gap at NTP[a]	(mm)	0.64	2.1	–	–
Diffusion coefficient into air at NTP[a]	(cm^2/s)	0.61	0.24[c]	–	–

[a] Normal temperature and pressure conditions, P = 1 bar, T = 293.15 K.
[b] Liquid fuels.
[c] Diffusion coefficient of methane.

Table 3.7 – Main characteristics of hydrogen versus natural gas, gasoline and diesel liquid fuels[100].

One of the main advantages of hydrogen fuel is its large energy content. The energy density of hydrogen is one of the largest fuels commonly used in internal combustion engines. For example, 1 kg of hydrogen can provide at least three times more energy than gasoline and diesel fuels. However, the significant low density of hydrogen gas is a limit for the space required for its storage to power a vehicle with adequate travel distances. In addition, low fuel density reduces the energy density of the air-fuel mixture. In fact, its energy density in terms of volume is extremely low, equal to 0.11 [MJ/l] in atmospheric conditions. This is one of the disadvantages of this fuel, because even at high pressures (750 [bar]) or at low

temperatures (liquefied to 20 [K]) its energy density remains much lower than that of most other liquid fuels (4.7 and 8.6 [MJ/l], respectively). It also requires high energy to pressurise or liquefy it, which is an important share of its own calorific value LHV.

Another characteristic that must be taken into account in its storage and distribution is its tiny molecule, which can pass through materials that are normally not permeable to other gases. This requires the use of special sealing materials, including special welding.

The wide flammability range of hydrogen ensures wide tolerance in the ratio of air-fuel mixture, up to the extreme low value of the ratio of equivalence $\Phi = 0.1$. The operation of lean mixture with hydrogen improves the economy of the engine, with complete combustion and few fuel residues.

In addition, its high diffusivity and flame speed helps to form a faster and more uniform mixture of fuel and air and improve combustion in a wide range within the cylinder. On the other hand, the high auto-ignition temperature of the fuel requires the implementation of a combustion trigger such as a spark or an additional low-temperature fuel auto-ignition.

Hydrogen shows a very high RON, allowing compression ratios (CR) above 14.5:1 without knocking, probably aided by its very high burning speeds[90]; for this reason its application to spark ignition engine seems very promising. However, in recent years some research groups have also studied its application in also in compression ignition engines running in dual-fuel mode. In the latter case, depending on the load and speed of the engine, hydrogen can be introduced with different gas/oil replacement fractions. Most of the experiments were carried out with a proportion of hydrogen between 10 and 40%[98].

Referring to the Hydrogen/Diesel dual-fuel combustion, some researchers saw that the brake-specific fuel consumption (BSFC), in case of hydrogen-diesel dual-fuel, shows a general improvement over operation with pure diesel [99].

In high-load engine conditions, the addition of hydrogen produces a sharp increase in the peak pressure in the cylinder and the peak heat release speed[100]. This often leads to an increase in the brake thermal efficiency compared to operating with only diesel. Sandalci and Karagooz[101] demonstrated that partial hydrogen enrichment does not significantly affect the specific consumption and general diesel engine efficiency, while slightly decreasing the volumetric efficiency.

Hydrogen enrichment usually has a negative effect on NOx emissions, as a significant increase is observed, due to the increase of the peak heat release rate and the in-cylinder pressure reached.

The introduction of exhaust gas recirculation (EGR) compensates for the increase in pressure and the rate of heat release and inhibits the formation of NOx emissions. However, the increase in the EGR rate leads to increased production of smoke, CO and HC emissions due to the lower availability of O_2 in the cylinder[99]. However, even if there is an increase in these emissions due to the use of EGR, compared to neat diesel emissions they are often significantly lower. Therefore, dual-fuel operation with hydrogen injection premixed to oxidising air, coupled with exhaust gas recirculation, could generally result in lower emissions and improved performance than when the engine is powered by diesel only[99].

An experimental study conducted by Wu and Wu[102], where an EGR fraction of 40% was applied and a hydrogen input in energy terms of 20%, showed a simultaneous reduction of NOx and smoke emissions compared to the use of pure diesel fuel. There was also a clear simultaneous containment of these NOx and smoke emissions from Suzuki and Tsujimura[103], which carried out experimental tests on a dual-fuel engine with high hydrogen rates above 70% without the use of EGR. The brake thermal efficiency increased by almost 13% compared to operating with only diesel. But the engine also recorded uncontrolled combustion. The test demonstrated a 42% smoke reduction for hydrogen enrichment alone, as well as CO_2, CO and HC emissions which were reduced by 40.5%, 45.8% and 57.7% respectively.

4 Engine setup test bed installation

4.1 Dual fuel gasoline system installation

Lean combustion concepts are particularly interesting for gen-set applications or generally for fixed-load engines. In this scenario, heavy-duty diesel engines are typically adopted. These engines run typically at 1500 [rpm]; in particular, these engines are quite heavy and it can be quite attractive to find a lighter solution in order extend the fields of application.
Taking into account these considerations, an automotive engine can be quite attractive for this application, because of its weight and reliability. Furthermore, the automotive engine control system of the injection completely fulfil the needs for dual-fuel operation as far as the high reactivity fuel is concerned. Only a simple and low-cost indirect injection system with its own control has to be installed in order to complete the conversion.
The engine chosen for the activity is a light-duty direct-injection common rail euro IV diesel engine. This engine is called VM RA428 and is designed for the automotive market (figure 4.1). The main characteristics of the engine are given in table 4.1.

Figure 4.1 - VM 428 Diesel Engine

Engine	HSDI 4-S Diesel, EURO IV
N. of cylinders and arrangement	4 in-line
Total displacement [L]	2.78
Bore x Stroke [mm]	94 x 100
Compression ratio	17.5:1
N. of valves per cylinder	4
Air Metering	VGT + Intercooler
Injection system	Common Rail
Max. Injection press. [MPa]	160
Injector hole diameter [mm]	0.153
Number of injector holes	6
EGR system	High Pressure with EGR cooler
Max. brake power [kW@rpm]	130@3800
Max. brake torque [Nm@rpm]	440@1750
Max. Peak cylinder pressure [bar]	150
Max. engine speed [rpm]	4600

Table 4.1 - VM 428 Tech specs

Thanks to the Common rail high-pressure injection system and the relatively small stroke of the pistons, this engine can normally operate at over 4,000 [rpm]. This leads to a smaller displacement in order to obtain the same power of a generic gen-set engine. The small displacement decreases the weight and overall dimensions.

The first part of the presented work consists in an initial modification of the engine in order to run in RCCI combustion with diesel and gasoline.

In RCCI combustion, the gasoline is injected into the intake manifold in order to form a premixed lean charge. The gasoline injection pressure is set at 4 [bar], and the injectors can run from 3.5 [bar] to 5 [bar]. The chosen injectors are commercial gasoline injectors available on the market. A typical PFI injector is shown in the figure below.

Diesel oil is directly injected at high pressure using the original diesel injection system.

Figure 4.2 - Common PFI injector

The RCCI combustion process is achieved with a premixed lean charge of gasoline, and the charge is ignited by the direct diesel injection; in this scenario it is fundamental to generate a homogeneous charge of the low reactivity fuel. Thanks to this consideration, the PFI injectors were placed just after the intercooler system.

In addition, PFI injectors inject a liquid that must be able to evaporate within the charge without having impingement phenomena that would lead to the formation of a fluid film in the intake manifold. This fluid film can act by disturbing the air-fuel cycle-cycle ratio, thus generating irregularities in the dosage.

Taking these constraints into account, a specific spray duct was designed using free CAD software. The prototype was then made using a Filament Deposition Moulding (FDM) 3D printing, the prototype of which is shown in the following figures:

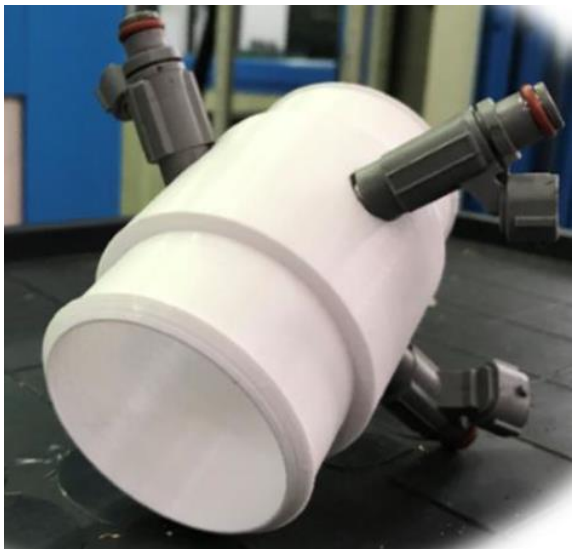

Figure 4.3 - PFI injector manifold detail 1

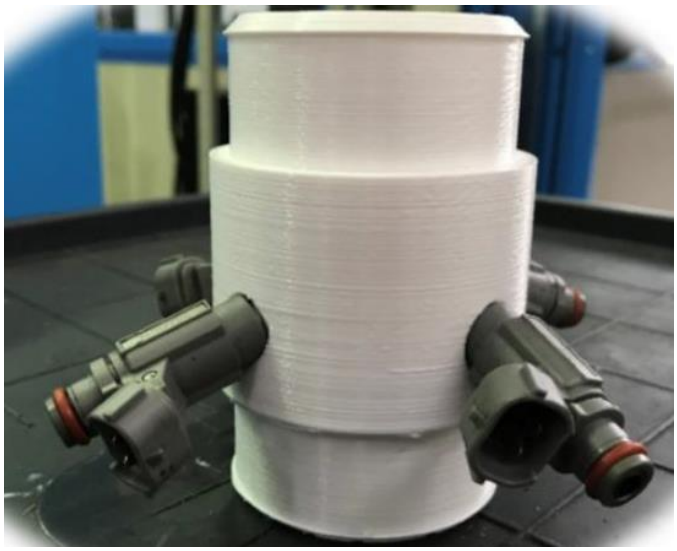

Figure 4.4 - PFI injector manifold detail 2

The PFI injectors are inclined by 30° in relation to the shaft of the duct and by 20° in relation to the direction perpendicular to it. The last inclination is used to create a swirl motion in the injector jet in order to obtain a better vaporisation of the charge and prevent the formation of the fluid film. Four injectors were installed to minimise the average diameter of the holes to improve atomisation. The figure below shows the injector mass flow rate as a function of the injection pressure.

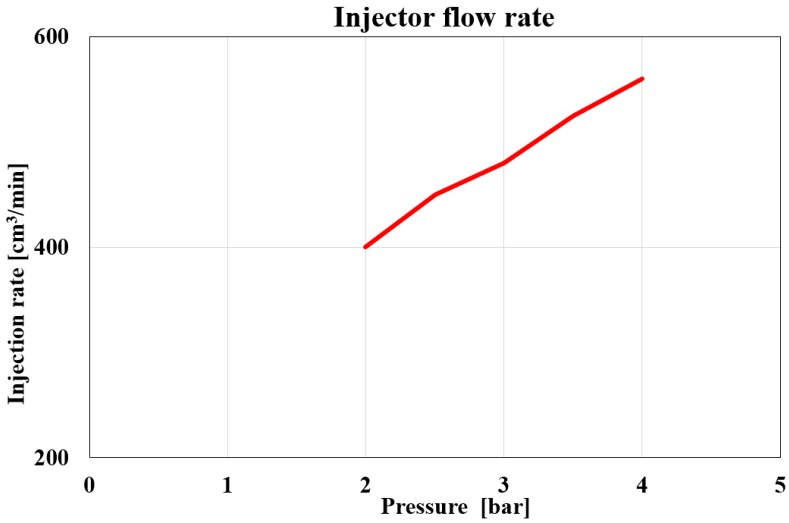

Figure 4.5 - Injector flow rate

The engine is controlled by a development ECU driven by the ETAS INCA calibration software while the PFI injection is controlled by the control system "Drivven". The system is a development control system implemented with Lab View; this system is modular and meets different needs and can drive for example direct injectors, throttle bodies, hall sensors, code wheels, PFI injectors, EGR valves, etc. In this case, the PFI injector module and the engine position sensor are used in order to have a correct injection phase.
Figure 4.6 shows the Drivven system.

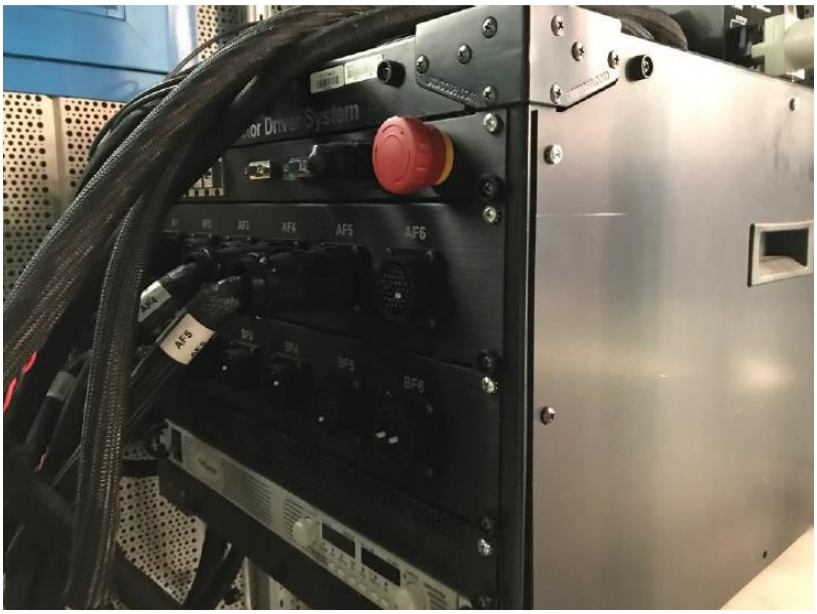

Figure 4.6 - NI Drivven control system cabinet

The Drivven system is run by a specific software provided by NI called SCM. With this instrument it is possible to programme custom algorithms for the injection strategy, in other words it is a rapid prototyping software for injection control. In this study, an injection timing is calibrated and the energising time of the injectors is controlled according to engine load. A diagram of the control system is reported in the figure below:

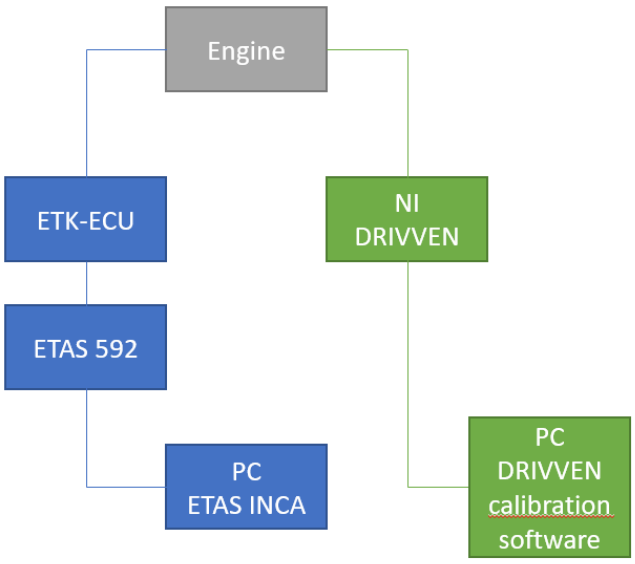

Figure 4.7 - Engine control system diagram

4.2 Indicating system

The Indicating system is an apparatus dedicated specifically to the acquisition of pressure in the combustion chamber when the engine is running. It is used to obtain fundamental engine parameters: PME, PMI, maximum pressure, heat released.

The system consists of several components. The first is the piezoelectric pressure transducer, which measures in-cylinder pressure; the second sensor is an optical encoder, installed on the crankshaft in order to detect the instant position of the piston. These two sensors are recorded by an acquisition module, which sends data packages to the PC via an Ethernet cable.

A diagram of the whole system is given ed in the figure below:

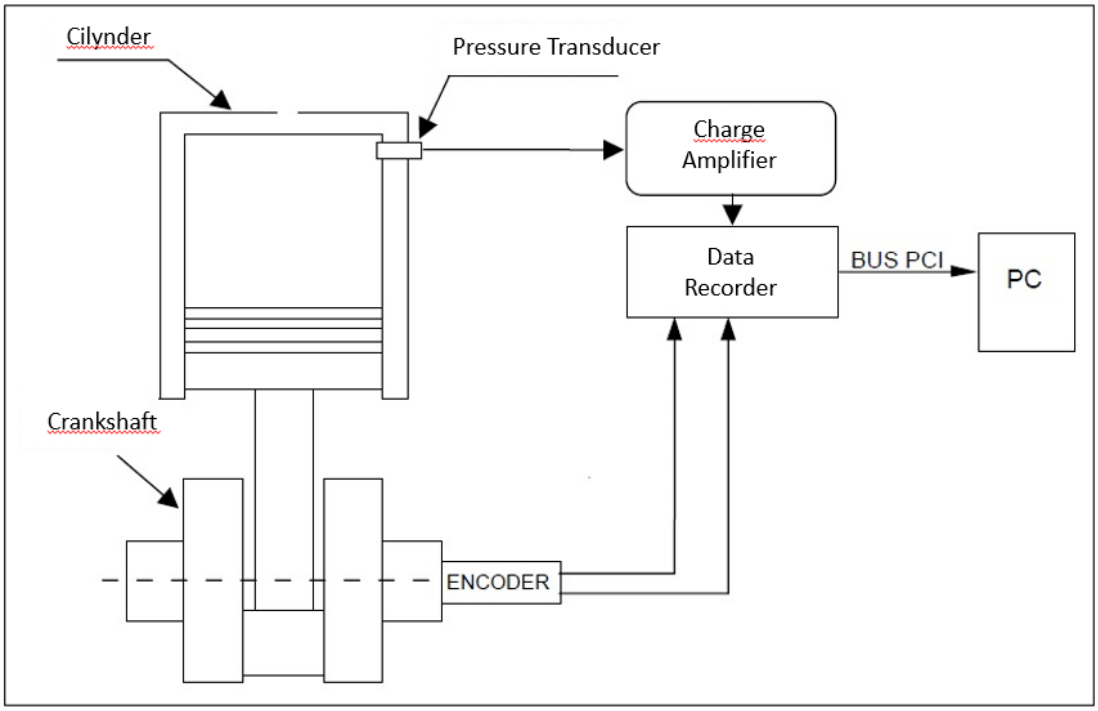

Figure 4.8 – Indicating system diagram

4.1.2 Pressure sensors in the combustion chamber

The pressure in the combustion chamber is recorded by a piezoelectric transducer, positioned on the head and facing directly into the combustion chamber, mounted in place of the spark plug of cylinder #1.

Piezoelectric pressure transducers are characterised by a very high frequency and high thermal and mechanical resistance; their principle of operation is based on the ability of quartz crystals to emit electrical charges in quantities proportional to the force they are subjected to. They are composed of a quartz foil that, compressed between two metal

plates, generates equal and opposite surface charges on its ends. Due to the piezoelectricity phenomenon, in fact, if a traction, compression or cut is applied to a crystal or a quartz plate, the deformation obtained generates a surface charge proportional to the stress forces.
The sensor used in the tests is a Kistler 6058, adapted with a specific plug to the VM428 engine, as shown in the figure below. The sensor port must ensure the right exposure to pressure but must preserve the piezoelectric transducer.

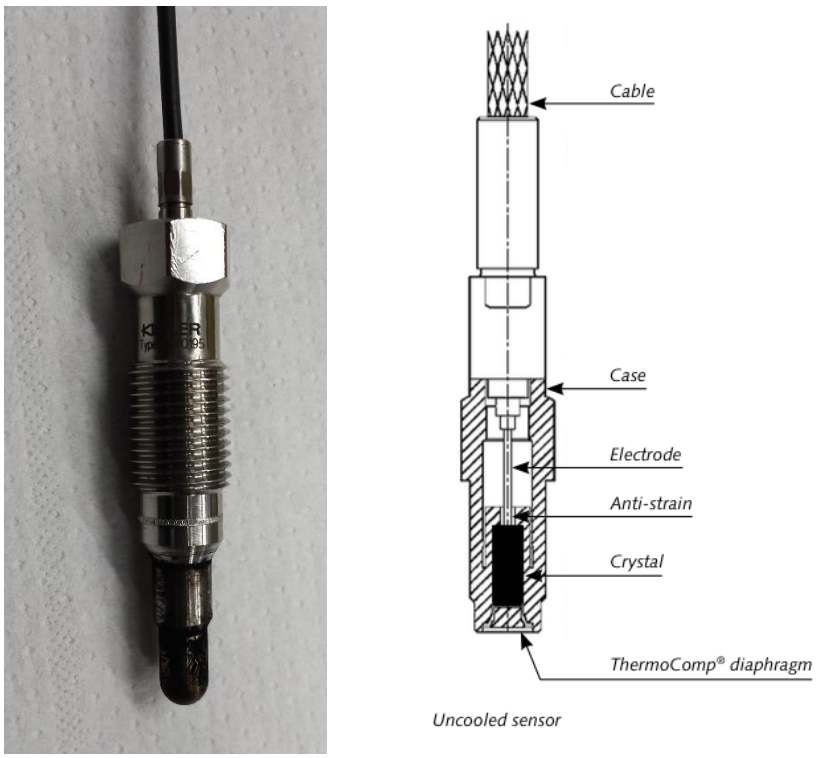

Figure 4.9 – Kistler sensor used

A specific high impedance charge amplifier then converts the electric charge into the output voltage detectable by the data acquisition hardware of the room.
The main features of piezoelectric translators include:

- very high mechanical tensile strength (pressures up to 10000 [bar]);
- temperature resistance (up to 500 [ºC]);
- constant sensitivity to temperature over a wide range;
- high own pulsation (suitable for measuring frequencies up to 500 [kHz]);
- excellent linearity;
- absence of hysteresis;
- very small dimensions, for easier installation in the combustion chamber.

In addition, the resulting minimum inertia ensures the ability to measure quantities that vary rapidly over time.
However, piezoelectric transducers always require field calibration, as the measured values are given up to a constant to be determined from time to time; they are not suitable for measuring constant pressures over time; they are not suitable for measuring low pressures, bar order (low sensitivity).

4.1.3 Encoder

The optical encoder is an angular position transducer that records the rotational speed of the engine. A support is fitted on the flange of the joint closest to the crankshaft to mount a code wheel, to which this sensor is coupled, as shown in figure 4.10.

Figure 4.10 - Optical encoder and sound wheel located on the drive shaft exit

Equidistant slits are present along the entire circumference of the code wheel; this enables an optical sensor to detect the clear to dark transition by means of a light source, which is shielded or not during the rotation of the disc, and sends a voltage pulse recorded later by an electronic meter. In this way, the number of pulses sent by the electromechanical transducer to the time unit, expressed in voltage variation, added to the known dimensions of the code wheel, allow the speed of rotation of the crankshaft to be measured. The slits

are all transparent except for one, which is closed; this enables to detect the angular position of the crankshaft.

The National Instruments CompactRIO hardware and the Alma Automotive OBI software were used to acquire the pressure traces inside the cylinder and monitor the related parameters calculated in real time; 100 consecutive engine cycles are sampled for each operating point and examined to calculate the averaged in-cylinder pressure trace.

The CompactRio communicates via an ethernet cable with a PC on which the Alma Automotive Software OBI Client runs.

A screenshot of this software is given below.

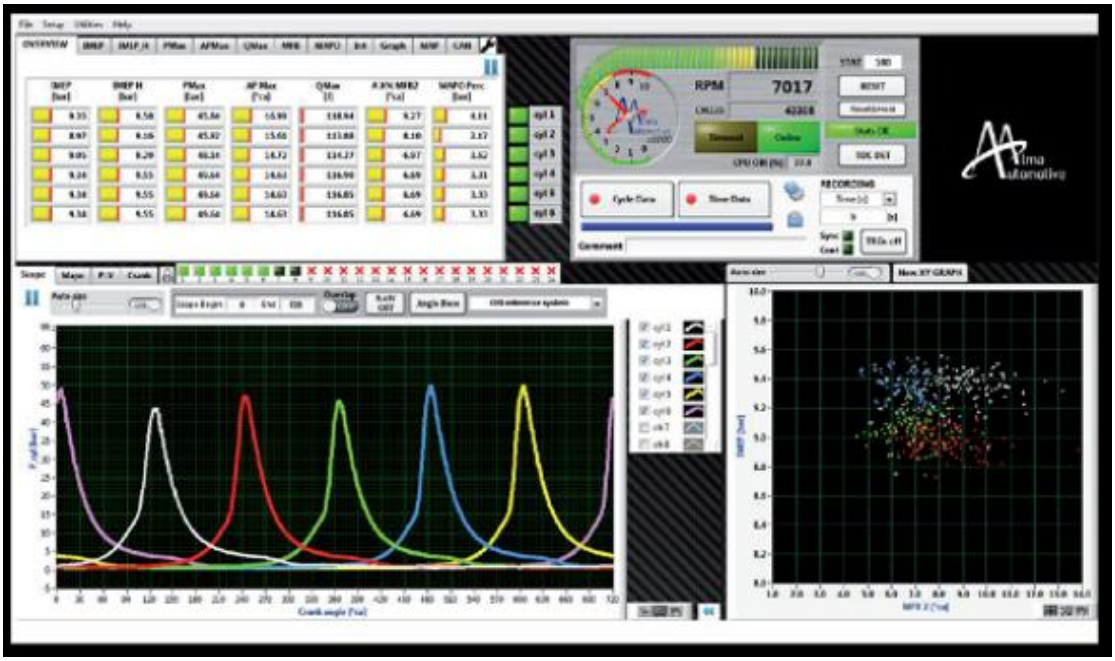

Figure 4.11 - Obi client Indicating Software by Alma Automotive

The Obi client software can directly show the pressure traces in the cylinder and calculate the mean value of each cycle e.g., IMEPH IMPEP and cumulative heat release; furthermore, it can calculate MFB 10,50,90 and MAPO. This last parameter is fundamental when RCCI combustion is running. MAPO monitors the pressure oscillation and, when a threshold is exceeded, knocking phenomena are present in the combustion chamber. In order to avoid damage to the engine and perform the correct calibration of the combustion process, the MAPO limit is set at 5 [bar].

4.2 Experimental Setup

The engine is installed at the Unimore test bed. This is provided with the Apicom FR 400 BRP eddy-current brake (maximum power 260 [kW], maximum torque 900 [Nm], maximum rotation speed 12,000 [rpm] – figure 4.12) and Apicom Horus software was used for the system control and data acquisition. The figure below gives the data sheet of the dynamometer.

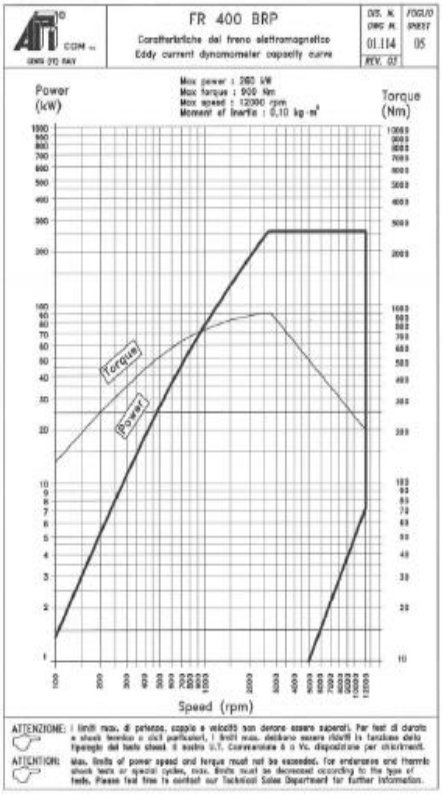

Figure 4.12 - Apicom FR 400 BRP

A diagram of the test bench installation and measuring equipment is given in the following figure:

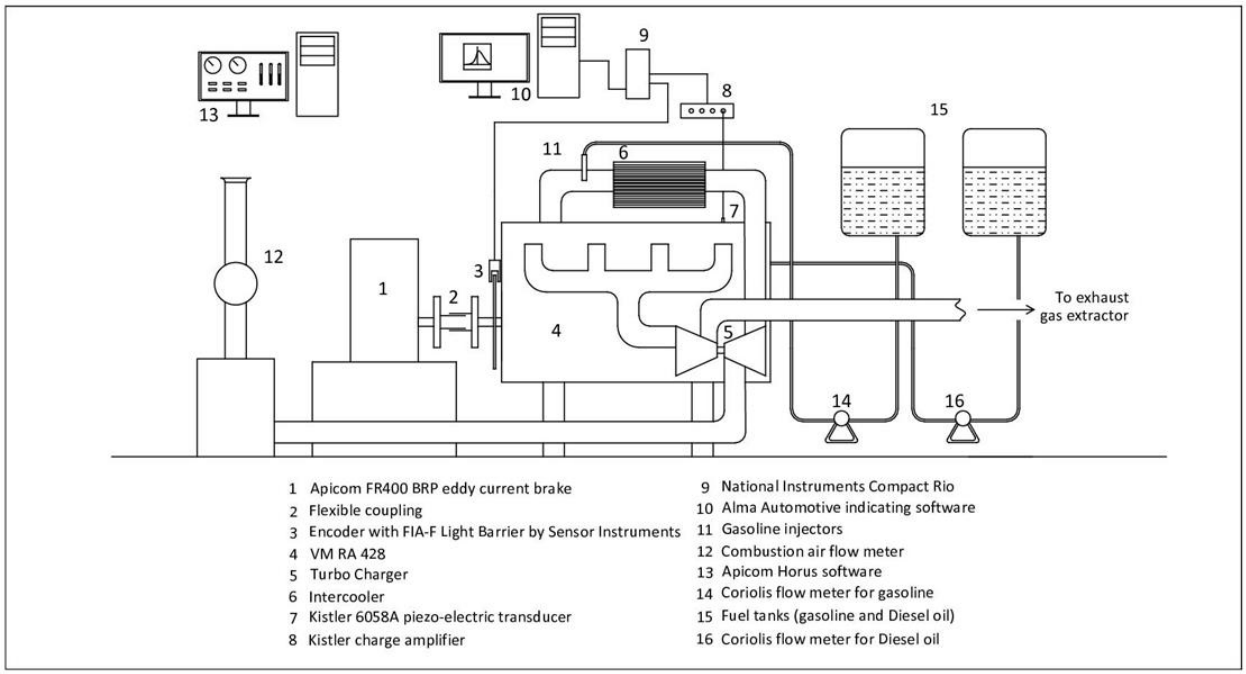

Figure 4.13 – Diagram of the test bench

The figure lists the main sensors used to measure the main engine parameters. Firstly, the air flow meter (12) was installed before the compressor (5). Two Coriolis flow meters were installed to measure fuel consumption. In addition, pressure and temperature were measured in many points (before and after the compressor, the intercooler and the turbine) in order to monitor the gas transformation. In the figure, the indicating system can also be observed, only one pressure sensor is present due to cost constraints. In order to obtain information on the distribution of the charge between the cylinders, the piezoelectric sensor at the beginning of the experimental campaign was moved from one cylinder to the other, to measure each one and observe the differences.

4.3 Dual fuel CNG system installation

After the conversion to diesel/gasoline Dual Fuels, the engine was equipped with a CNG injection system in order to test also the diesel/natural gas Dual Fuels combustion. CNG injectors are very simple: they consist of a solenoid actuator that drives a gas valve with a calibrated hole. Compared to a liquid fuel injector, the diameter of the hole is quite large, about 1.5 mm; this is due to the fact that the gaseous fuel has a lower density than liquid fuel; moreover, as the injection pressure is also lower, to obtain the correct mass flow rate

and limit the injection time, you need to enlarge the hole. The following figure shows the CNG injector:

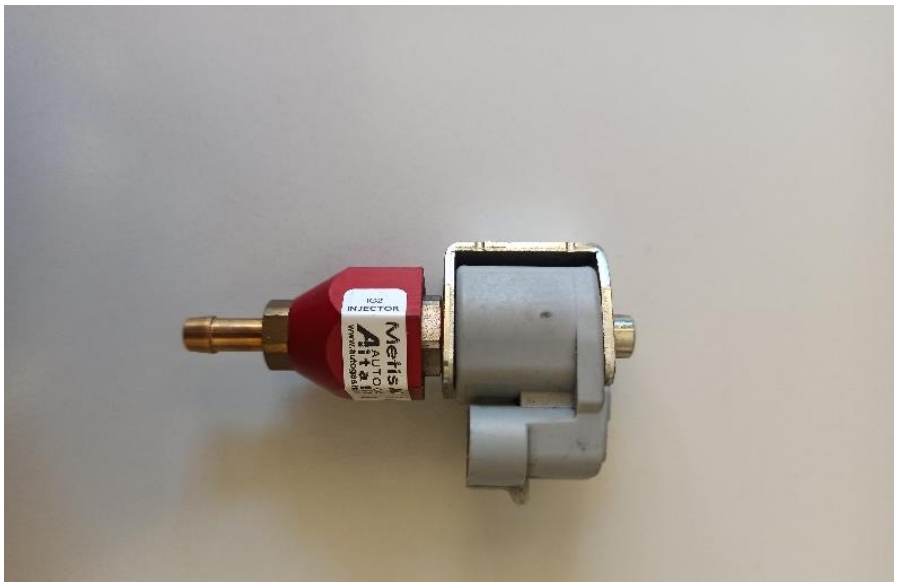

Figure 4.14 - Methane injector

On the engine intake manifold, just downstream of the intercooler and about 500 [mm] before the intake plenum, four NG injectors are installed, with a nominal flow rate of 1.5 [g/s] at 3 [bar].

In order to improve air-to-NG mixing, each injector is installed in such a way that it forms an angle of 30° with the radius of the duct cross section, passing from the nozzle. To obtain a homogeneous NG-air mixture before the flow between the cylinders is split, the injectors are placed at an appropriate distance from the plenum.

Because the injectors are slightly different from each other, this solution is preferred to installing the injectors on the intake manifold, as this guarantees greater uniformity between the cylinders. By switching the position of the piezoelectric pressure sensor and comparing the pressure traces, the uniformity of the charge composition between the cylinders was verified; the difference recorded was below the acceptable threshold of the IMEP cycle-by-cycle variation (2%).

The installation of the CNG injectors is reported in figure 4.15:

Figure 4.15 - Methane injection system installed after the intercooler

The CNG injection system consists of a 250 [bar] pressurised tank and two pressure reduction stages, the last one determining the injection pressure. CNG used for the experiments is commercial CNG for transportation and it is mainly composed of methane.

A specific ECU manufactured from Ecomotive Solutions controls the NG injectors; the main input signals required are engine speed, engine load, pressure and charge temperature, exhaust gas temperature.

In fact, dual-fuel operation is not included in the control unit of the original engine, as it only handles the diesel engine. The ECU driving the VM428 engine is a MED EDC16 and is a "standard" ECU supplied by BOSCH. Then, a specific development unit is used to modify all the calibration parameters of the engine.

Through the original engine control software, the system intervenes on instantaneous changes in any calibration, enabling or disabling strategies or diagnoses that may be inadequate during dual mode operation feeding.

As an example, an image of an ETK ECU is given in the following figure. A specific hardware configuration and a specific calibration programme is used to correctly configure this ECU.

ETAS provides the necessary hardware to calibrate the parameters and take measurements, made specifically for the ETK: ETAS592 is the module used. ETAS INCA is the software adopted to calibrate the measurements and manage the datasets; this software represents a standard for the calibration of automotive controls.

Figure 4.16 - ETK-ECU development

The company Ecomotive Solution supplies the CNG injection development controller; through this, it is possible to control and modify the relevant parameters, as already described for the BOSCH ETK: this is essential for the optimisation of the dual-fuel combustion process.

Figure 4.17 - ETAS592 module

Figure 4.18 - D-GID ECU

Below is a diagram representing the entire controller (figure 4.19). Two parallel controllers work as stand-alone systems, this is useful for the calibration of the test bench at fixed operating points and not for transient conditions. Communication between parallel controls via the can bus protocol should be implemented to manage transitional conditions. For these reasons, it is not necessary to carry out this communication.

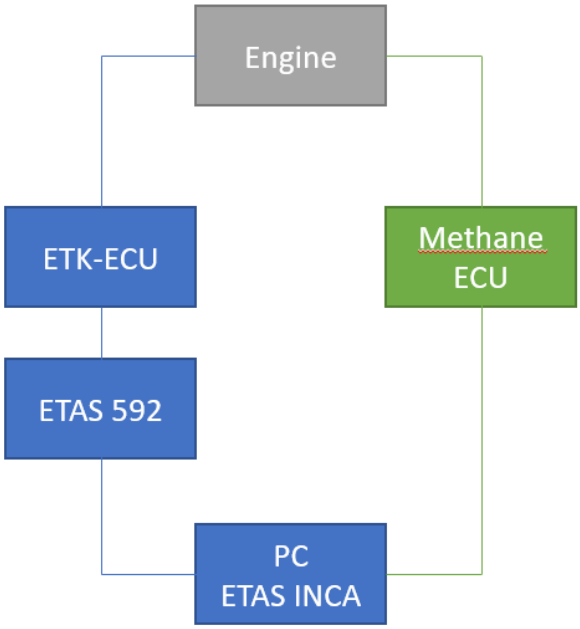

Figure 4.19 - Engine control diagram

Compared to figure 4.13, what described on the installation of the engine, the hardware and software instrumentation necessary for this DF trial, with the engine powered by CNG, are reported below.

In addition to standard pressure and temperature transducers, the laboratory instruments include a Coriolis flow meter to measure diesel fuel consumption and an Alicat MCE gas mass flow controller to measure NG consumption. The air flow rate is measured using a hot-wire anemometer.

A series of ETAS tools supports the optimisation of the engine control parameters, including INCA software. The VARIOplus Industrial MRU was used to measure engine gaseous emissions; this instrument, using non-dispersive infrared (NDIR) technology, records the concentration of O_2, CO, CO_2, NO, NO_2, NOx and CH_4.

Soot emissions are measured with the AVL Dismoke 4000 opacimeter. It should be noted that, since the after-treatment system is not installed, all measured concentrations of pollutants are raw. Finally, a current clamp is installed on the diesel injector power supply cables, this measurement determines the time and duration of each shot ad it is measured using an oscilloscope connected to the current clamp and the optical encoder.

The whole installation of the engine on the test bench is reported in the figure below:

Figure 4.20 - Engine installed on the Unimore test bench

5 Experimental analysis of diesel/gasoline Dual Fuel combustion

5.1 Introduction

As mentioned in the introductory chapter, the main advantages offered by the LTC combustion mode include a reduced production of smoke and NOx, as a lean and/or highly diluted charge (i.e., with a high EGR rate) is adopted. It has been observed from several experimental tests that the classic NOx-soot exchange, which hinders the standard diesel combustion, does not occur.

Other important advantages are found in achieving higher thermal efficiencies. This is because, compared to conventional combustion, the rate of combustion is considerably higher, approaching the ideal combustion at constant volume of the Otto cycle. In addition, the reduction in the rate of heat transfer between the hot gases and the walls of the combustion chamber is due to the low temperature of the combustion process.

On the other hand, there are also some disadvantages with this mode, which are basically: a) control of combustion at high loads and speeds; b) despite the introduction of port fuel injection (PFI), no perfectly homogeneous charge is sometimes obtained[10,104,105].

The research activity presented in this chapter relates to experimental tests carried out using low and high cetane-number gasoline and diesel fuel, respectively. The study was conducted on a suitably modified light diesel engine (see previous chapter for engine conversion process), aiming to better understand the details of this new combustion concept. In order to identify the upper threshold beyond which diesel injection is no longer sufficient to maintain regular combustion in RCCI mode, the experimental activity was carried out without the use of external EGR.

The reference engine and experimental setup are presented in the section related to this thesis work.

5.2 The experimental campaign

Two operating points were studied, identified by the torque at 150 and 300 [Nm] (corresponding to BMEP of 6.75 and 13.5 [bar]), both at 1500 [rpm].

For each operating point, starting from the original diesel (DICI) operating condition, the RCCI mode is implemented by replacing an increasing amount of diesel oil with gasoline. During this passage, in order to maintain the same engine load, a closed-loop control on

torque is applied to decrease in the quantity of diesel with the increase of the quantity of gasoline.

In order to ensure the same conditions for the transition from DICI to DF, the EGR valve is blocked, and a constant boost pressure is manteined through the use of ETAS INCA software. The engine speed is controlled by a second closed-loop control applied to the eddy current brake.

The case studies are shown in table 5.1. For some of these cases, a calibration process was necessary, by modifying the fuel injection strategy.

1500 rpm – 150 Nm		1500 rpm – 300 Nm
Cases with original injection law	Cases with modified injection law	Cases with original injection law
CD	CD	CD
-16.9% Diesel oil	-27.6% Diesel oil	-14% Diesel oil
+25% gasoline	+26.4% gasoline	+17.2% gasoline
-24.6% Diesel oil	-37.6% Diesel oil	-18.5% Diesel oil
+36.8% gasoline	+38.8% gasoline	+22.8% gasoline
-42.8% Diesel oil	-62.1% Diesel oil	-30% Diesel oil
+42.7% gasoline	+59.3% gasoline	+33.5% gasoline
-	-73.4% Diesel oil	-
	+71.6% gasoline	

Table 5.1 - Investigated cases

The different cases are identified using the percentage of diesel energy that is subtracted (equation 2) from the corresponding percentage of replacement gasoline (equation 3).

Then, the fraction of energy introduced with diesel in RCCI mode compared to the original condition CD is evaluated with the following formula:

1) $$\mathrm{X}_{Diesel}[\%] = \left(\frac{\dot{m}_{D,RCCI}}{\dot{m}_{D,CD}}\right) \cdot 100$$

Thus, the percentage of energy subtracted from diesel is:

2) $$\mathrm{X}_{Diesel,sub}[\%] = 100 - \mathrm{X}_{Diesel}[\%]$$

In the same way, the fraction of energy supplied with gasoline in RCCI mode compared to the amount of energy that was introduced with diesel in the original mode of operation CD, is obtained with the following formula:

3) $$\mathrm{X}_{Gasoline}[\%] = \left(\frac{\dot{m}_G.LHV_G}{\dot{m}_{D,CD}.LHV_D}\right) \cdot 100$$

5.3 Experimental results

The results of the experimental campaign, comparing at each operating point those obtained in RCCI mode compared to the basic DICI mode, are given below.

The comparison is carried out mainly in terms of pressure inside the cylinder, burnt mass fraction (referring to the parameter x_b shown in the graphs below), RoHR (referred to as $dx_b/d\theta$ in the graphs) and BTE.

The experimental results are shown in figures below.

The first point analysed is at 150 [Nm] (BMEP = 6.75 [bar]) - 1500 [rpm].

This first engine operating point was acquired without any modification to the Diesel injection law. As the amount of gasoline in place of diesel fuel is introduced, there is an increase in the burning rate in the injection area of the pre- and pilot diesel fuel (figure 5.1a), an increase of the combustion irregularities and a decrease in-cylinder heat release in the next phase of main, a shift towards the TDC of the pressure peak. The burnt mass fraction curve is shifted to the left (figure 5.1c), which leads to a peak pressure in the highest cylinder (figure 5.1b).

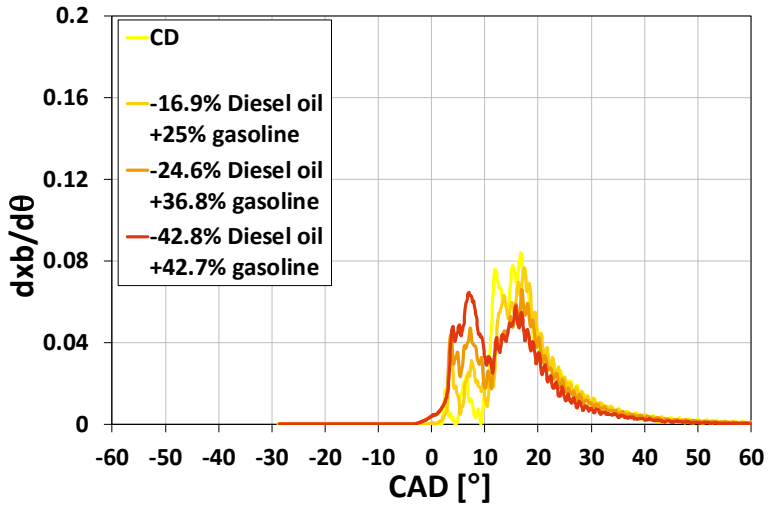

Figure 5.1a - Case with original injection law - 150 [Nm] - 1500 [rpm] RoHR

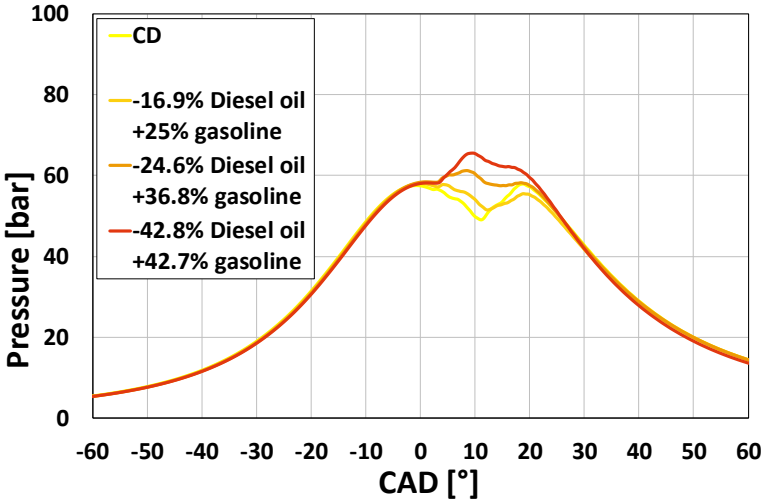

Figure 5.1b - Case with original injection law - 150 [Nm] - 1500 [rpm] pressure

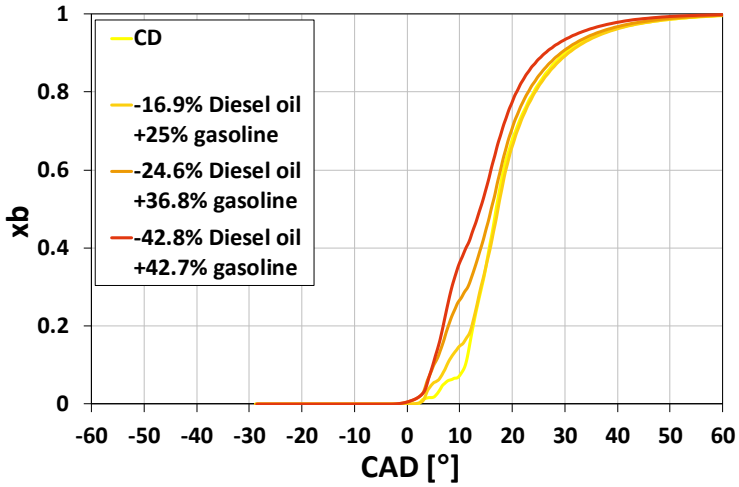

Figure 5.1c - Case with original injection law - 150 [Nm] - 1500 [rpm] burnt mass fraction xb

Therefore, by not adopting a specific calibration, the brake thermal efficiency of the RCCI reaches values lower than that of the DICI mode. The main reason is the low flame rate that occurs through the homogeneous lean blend, which leads to a high amount of unburned. However, with the increase in the proportion of gasoline replacing diesel, BTE tends to improve (figure 5.1d).

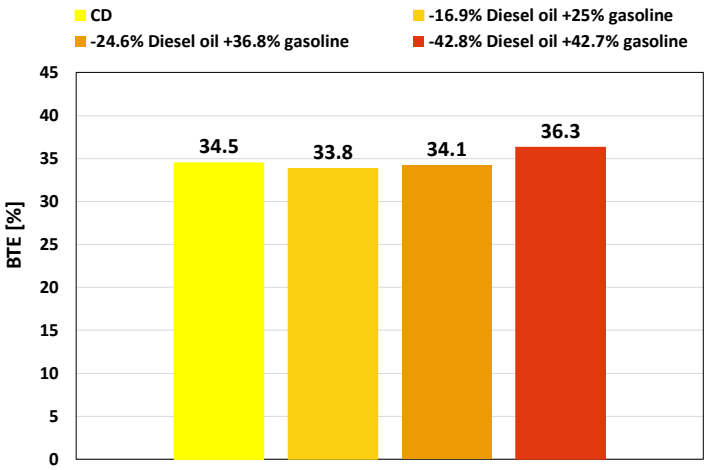

Figure 5.1d - Case with original injection law - 150 [Nm] - 1500 [rpm] BTE

No other percentage of diesel can be replaced except by obtaining a cyclic dispersion of the pressure that would lead to greater irregularity of combustion. So, in this case a limited use of the RCCI strategy.

In the second case, the same engine operating point, maintained constant by means of boost pressure control and completely closed EGR, is carried out with the modification of the injection law: the diesel fuel injection advance has been reduced and the pre- and pilot phases are eliminated. A rapid increase in the burning rate is achieved by increasing the diesel replaced with gasoline, and consequently a faster in-cylinder heat release (figure 5.2a). Also in this case, there is a shift of the pressure peak towards the TDC (figure 5.2b) and the shift to the left of the burnt mass fraction curve (figure 5.2c). Good combustion quality is therefore maintained in terms of rapidity and completeness.

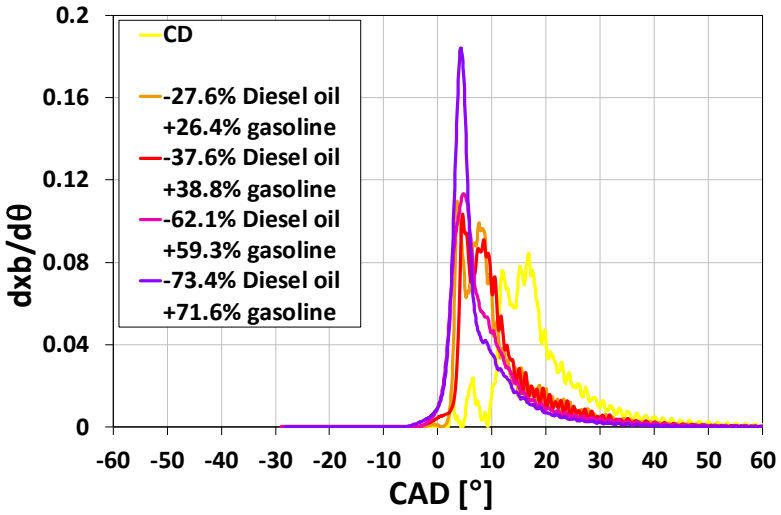

Figure 5.2a - Case with modified injection law - 150 [Nm] - 1500 [rpm] RoHR

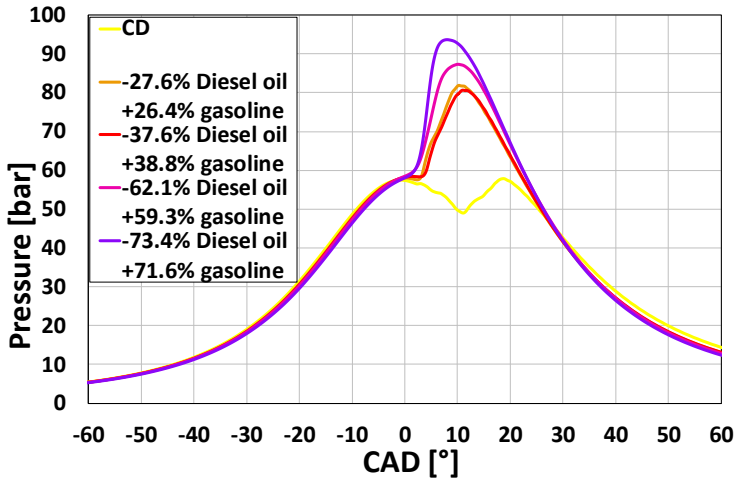

Figure 5.2b - Case with modified injection law - 150 [Nm] - 1500 [rpm] pressure

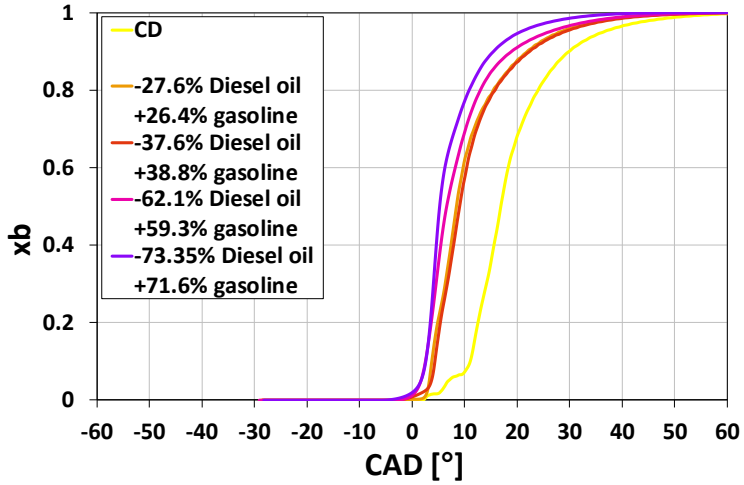

Figure 5.2c - Case with modified injection law - 150 [Nm] - 1500 [rpm] burnt mass fraction xb

In this way, we can observe a continuous improvement of the general efficiency (up to 4%) (figure 5.2d) with the increase of the quantity of diesel replaced, even if with lower values than the previous test, but this test certainly involves a greater operativity in the engine map on the gasoline-diesel mix.

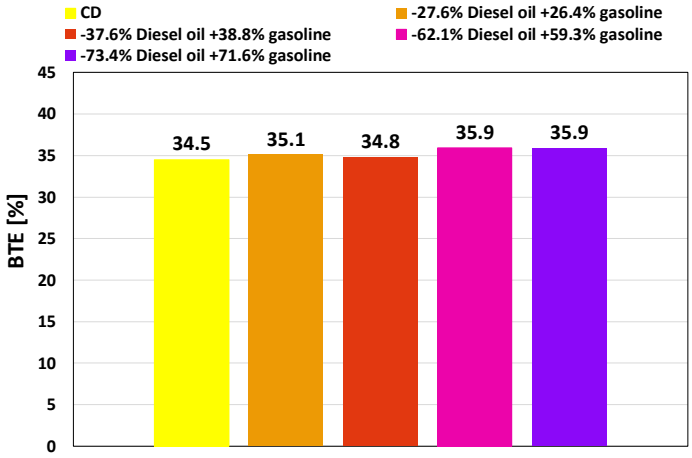

Figure 5.2d - Case with modified injection law - 150 [Nm] - 1500 [rpm] BTE

The second operating point tested is 300 [Nm] (BMEP = 13,5 [bar]) – 1.500 [rpm].

Even before the injection of diesel fuel, the auto-ignition of the air-gasoline mixture is observed, because in this condition, in the combustion chamber there are high charge temperature and pressure values (figure 5.3b), therefore the chemical reactions between air and fuel are accelerated.

The higher the proportion of diesel replaced, the richer the homogeneous air-gasoline mixture. This results in a higher peak heat release (figure 5.3a). Auto-ignition is slightly anticipated, as the reactivity of the mixture is richer.

Switching from DICI operation to DF operation, the BTE worsens (figure 5.3d), as partially observed for the previous point.

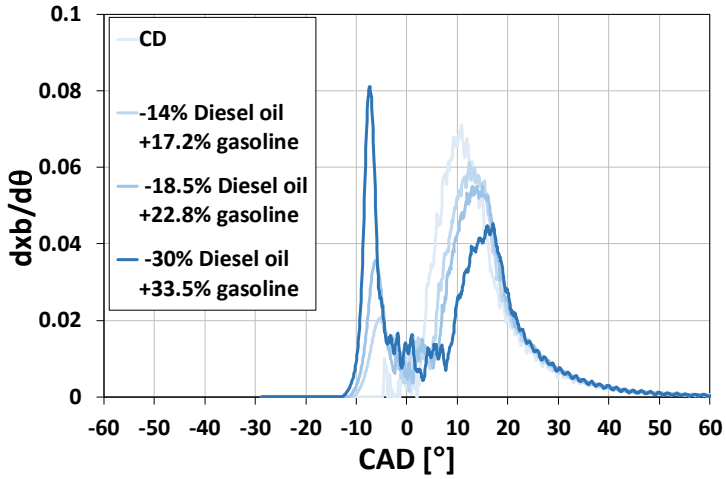

Figure 5.3a - Case with original injection law - 300 [Nm] - 1500 [rpm] RoHR

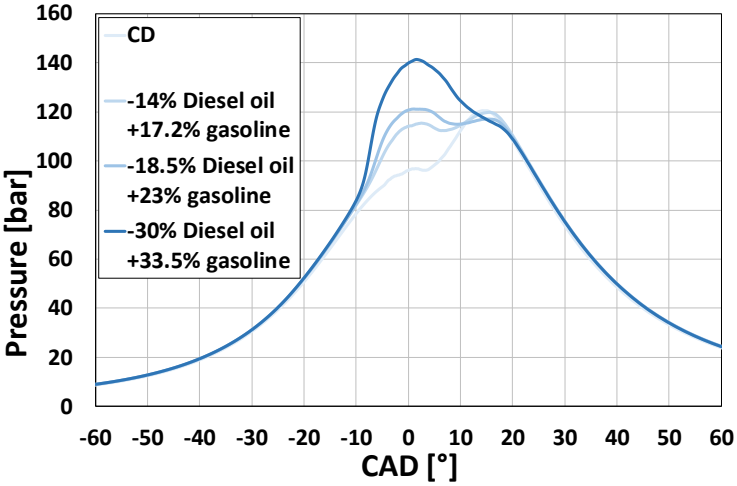

Figure 5.3b - Case with original injection law - 300 [Nm] - 1500 [rpm] pressure

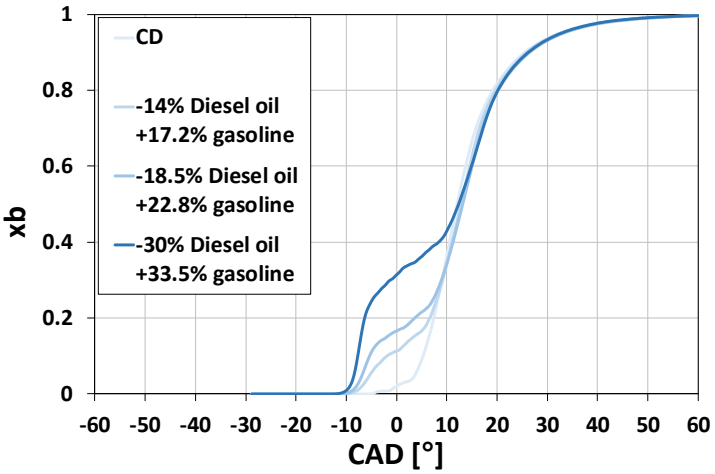

Figure 5.3c - Case with original injection law - 300 [Nm] - 1500 [rpm] burnt mass fraction xb

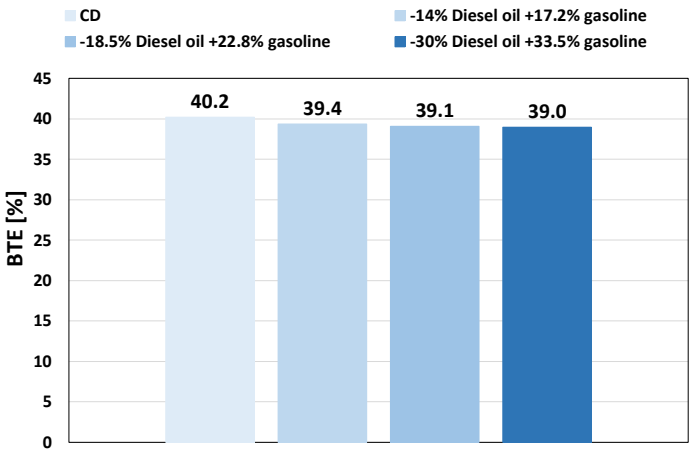

Figure 5.3d - Case with original injection law - 300 [Nm] - 1500 [rpm] BTE

To try to avoid the auto-ignition of the air-gasoline blend, the diesel fuel injection timing is increased. Even if the BTE is improved as a result, the peak pressure in the cylinder is rapidly increased, resulting in increased combustion noise.

It is therefore understood that, in addition to the amendment of the diesel injection law, the use of EGR becomes fundamental in the RCCI combustion mode, and more generally in the LTC mode, as it ensures better control of the ignition timing and RoHR.

6 Experimental analysis of diesel/NG Dual Fuel combustion

As described in Chapter 3, NG is a low carbon-content fuel due to its high hydrogen-to carbon ratio. It therefore represents a valuable low-reactivity fuel to be used in DF combustion, capable of mitigating CO_2 emissions from internal combustion engines. Moreover, NG is usually cheaper than gasoline or diesel oil and it can be also (totally or partially) substituted by bio-gas that is a renewable source of energy with CO_2 emission that can be considered globally zeroed.

For this reason, a further experimental study on DF combustion was carried out, aiming to explore the effects of using NG as the low-reactivity fuel and diesel as the high-reactivity one on combustion characteristics and emissions.

6.1 Introduction

A study was carried out to improve a thermal unit, with a nominal power of 80 [kW], for a generator set (gen-set) that could be clean and efficient, seeking to benefit from the advantages offered by the Dual-Fuel combustion mode (DF), using natural gas as a low-reactivity fuel, on high-speed (DICI) compression-ignition engines. In general, Heavy-Duty (HD) diesel engines are commercial generators, and these engines must meet increasingly stringent emission standards, so their complexity is also significant for this type of use.

On the market, this type of power generation engine consists of HD diesel engines, operating at 1,500 or 1,800 [rpm], depending on the electric frequency (50 or 60 [Hz]). The main technical specifications of some commercial thermal units are given in table 6.1[106–111]

Manufacturer	**KOHLER**	**IVECO/MTU**	**VOLVO PENTA**	**Cummins**	**HIMOINSA**	**MOTEURS Baudouin**
Combustion Type	CI	CI	CI	CI	CI	CI
Cylinders Lay-out	In-line	In-line	In-line	In-line	In-line	In-line
Number of cylinders	4	4	4	4	4	4
Turbocharger	Y	Y	Y	Y	Y	Y
Intercooler	Y	Y	Y	Y	Y	Y
High Pressure Common Rail	Y	Y	Y	Y	Y	N
Bore x Stroke [mm]	107 x 127	104 x 132	108 x 130	107 x 124	110 x 125	105 x 130
Displacement [L]	4.57	4.49	4.76	4.46	4.75	4.50
Compression Ratio	16.7:1	17.5:1	18.0:1	n.d.	17.0:1	18.0:1
Combustion System	DI	DI	DI	DI	DI	DI
Rated rpm@50 Hz	1500	1500	1500	1500	1500	1500
Max. Power at rated rpm [kW]	89.4	86	85	95	86.3	81
Max. BMEP at rated rpm [bar]	15.7	15.4	14.3	17.0	14.5	14.4
Max. fuel consumption at rated rpm [L/h]	24.2	19.0	21.5	25.0	22.3	20.7
BSFC at Max. Power, rated rpm [g/kWh]	225	183	210	218	214	212
Max. Specific Power, rated rpm [kW/L]	19.6	19.2	17.9	21.3	18.2	18

Table 6.1 - Main specifications of some gen-set engines[106-111].

The engines listed in table 6.1 have good combustion efficiency and are of robust construction suitable for this type of application. On the other hand, despite the medium-high values of Brake Mean Effective Pressure, BMEP (>14.4 [bar]), their specific power is rather low (<22 [kW/L]) and this involves space and weight. In addition, the current non-road emission standards are strict (European stage V regulations[7]) and therefore complex and expensive after-treatment systems (at least one diesel particulate filter, DPF and possibly a de-NOx device) are indispensable.

This study was conducted on a more compact thermal unit, so of small size and weight, but at the same power output, with greater efficiency and lower pollutant emissions.

The diesel engine selected runs in dual-fuel mode and it is powered by NG and diesel fuel. The use of NG reduces environmental impact, not only due to the fewer by-products of its combustion, but also because it can be easily obtained from biomass, even on the same site where the power-generating module is installed.

It should also be remembered that, until shortly before this post-pandemic economic recovery, the cost of NG was always competitive compared to that of diesel, and its use is more environmentally friendly, because less CO_2 is produced and there are opportunities to obtain fuel from biomass.

A DF NG-Diesel application is obtained with slight modifications of a standard diesel engine, in relation to which the installation of the dedicated NG fuel system is certainly essential. In this, a new design of the combustion system, including a specific diesel injector nozzle and an optimised geometry of the piston bowl, further contributes to increased efficiency and reduced production of pollutant emissions from the converted engine[8,9].

6.2 Choice of the Engine

The test was carried out on the 4-cylinder, turbocharged, common rail diesel engine, produced by FCA - VM Motori, presented in Chapter 4 of this work, the characteristics of which are summarised in table 6.2.

Engine Type	HSDI 4-S Diesel, EURO IV
Cylinders	4 in-line
Total displacement [L]	2.78
Bore x Stroke [mm]	94 x 100
Compression ratio	17.5:1
N° of valves per cylinder	4

Air Metering	Turbocharger + Intercooler
Injection system	Common Rail
Max. Injection press. [MPa]	160
Injector hole diameter [mm]	0.153
Number of injector holes	6
EGR system	High Pressure, cooler, throttle
Max. brake power [kW@rpm]	130@3800
Max. brake torque [Nm@rpm]	440@1750
Max. Peak Cylinder pressure [bar]	150
Max. Engine Speed [rpm]	4600

Table 6.2 - Main parameters of the reference engine

The engine used has a much smaller displacement than the HD diesel shown in table 6.1. However, thanks to the relatively short stroke, this engine works smoothly at 3,000 [rpm] and can therefore be coupled to a smaller electric generator, thus rotating at the same speed. In the engine condition with 12 [bar] BMEP at 3,000 [rpm], this engine delivers 83 kW, a power very similar to that of HD engines shown in table 6.1.

The advantages of the engine for this fraction of power compared to the HD units in table 6.1:

- with BMEP lower by an average of 25%, a lower thermal load;
- more compact size and lower weight, which also means the possibility to obtain the same volume of the gen-set box also with the installation of the tank.

Generally, in the design and development of a gen-set the following operating conditions are considered:

- rated speed (in this case, 3,000 [rpm]), at maximum load (in this case, corresponding to a 12 [bar] BMEP);
- rated speed (in this case, 3,000 [rpm]), at 75% of the maximum load (in this case, BMEP = 8 [bar]).

In order to assess the operating limits of DF NG-diesel combustion, also some low load conditions (BMEP = 2-4 [bar], 3,000 [rpm]) were also taken into account in this experiment. In a low-load diesel engine, the control of pollutant emissions is less critical. In fact, the low loads correspond to a lower air-fuel ratio, which results in lower peak temperature values of combustion; consequently, lower NOx and soot rates are produced.

The mass flow rates of the main pollutants as a function of the load are reported in figure 6.1, measured on the reference diesel engine at 3,000 [rpm], on which the high-pressure EGR valve was kept closed to make it dependent only on the load.

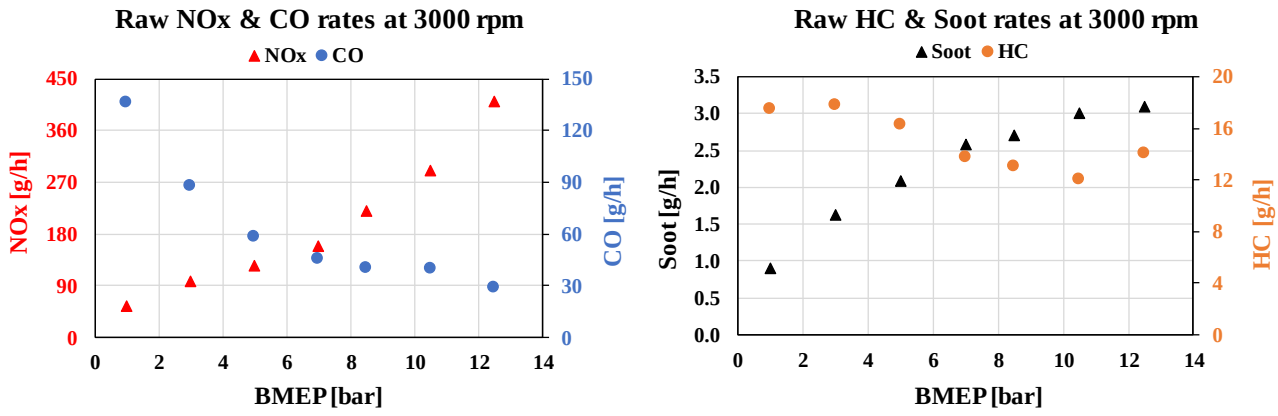

(a) (b)

Figure 6.1 - Trends of the main pollutants at 3,000 [rpm], for the reference high-speed diesel engine, without EGR.

These emission measurements show that it is not mandatory to have a DF combustion over the whole range of operating conditions for a gen-set application. In fact, low values of NOx and soot emissions are found at low load, while for the higher loads HC and CO emissions. The main physical and chemical properties of NG and gas oil used during the experimental activity are shown in table 6.3. The share of methane in NG is about 95%.

Fuel properties	**NG**	**Diesel fuel**
Lower heating value (LHV) [MJ/kg]	47	43.5
Stoichiometric air-fuel ratio	17.0	14.5
Heating value of stoichiometric mixture [MJ/kg]	2.58	2.81
Research Octane Number (RON)	≈120	-
Cetane Number (CN)	-	52
Autoignition temperature [°C]	650	200

Table 6.3 - Properties of NG and diesel fuel, employed in the study

6.3 Testing and Calibration

The experimental campaign was conducted on four different operating points, all with the same engine speed of 3,000 [rpm], but with different loads (BMEP = 2, 4, 8 and 12 [bar], corresponding to a brake torque of 44, 88, 177 and 265 [Nm], respectively).

The starting condition is always called Normal Diesel (ND): m_D is the amount of diesel fuel injected in the standard diesel mode. From this condition, the amount of NG (m_{NG}) is progressively increased, while the mass of diesel fuel injected per cycle is reduced; the closed-loop control applied to the engine pedal keeps the brake torque constant.

The amount of diesel fuel injected in standard operations, called m_D, is necessarily reduced in the transition from standard diesel mode to a DF-NG combustion. The heat released by the combustion of a mass of NG, m_{NG}, introduced in the intake manifold, complements the energy associated with the new quantity of diesel. Having defined the residual fraction of combustion of diesel fuel: $x = \frac{m'_D}{m_D}$ the amount of NG required to balance the heat of combustion, assuming complete fuel oxidation, can be expressed as

$$m_{NG} = \frac{(1-x)m_D LHV_D}{LHV_{NG}} \qquad (6.1)$$

LHV stands for Lower Heating Value and D for Diesel.

The composition of the premixed charge determines the chemical structure of the DF combustion models, namely the concentration of air, fuel vapour and exhaust gas.

Under typical operating conditions, the following simplifications are made to obtain a qualitative estimate of the relative air-fuel ratio of the premixed charge, λ_{NG}:

(a) As the charge pressure is controlled, during the transition from Diesel to DF, the mass of air delivered by the engine, m_a, should remain constant;

(b) Compared to the amount of NG, the amount of injected diesel fuel, m'_D, is always much lower;

(c) Due to its greater chemical reactivity, the diesel fuel completes its oxidation before the NG, and if with $\alpha_{s,D}$ the diesel fuel stoichiometric air-fuel ratio is defined, it subtracts from the premixed charge an amount of air equal to $(m'_D\, \alpha_{s,D})$.

Considering these assumptions, the relative air-NG ratio obtained from a given residual fraction of diesel combustion can be expressed as

$$\lambda_{\mathrm{NG}} = \frac{(\alpha - x\,\alpha_{s,D})\mathrm{LHV_{NG}}}{(1-x)\alpha_{s,NG}\mathrm{LHV_D}} \qquad (6.2)$$

where $\alpha = \mathrm{m_a}/\mathrm{m_D}$ is the ratio of air to diesel fuel in the standard diesel combustion; $\alpha_{s,NG}$ is the stoichiometric air-fuel ratio for NG.

The validity of equation 6.2 is limited to the low values of x for hypothesis (b). In fact, when the residual fraction of diesel combustion is high, a large portion of NG burns together with diesel fuel so that, if the chemical aspects are not included in an accurate calculation, it is impossible to predict the share of air consumed by each fuel. The correlation is plotted in figure 6.2.

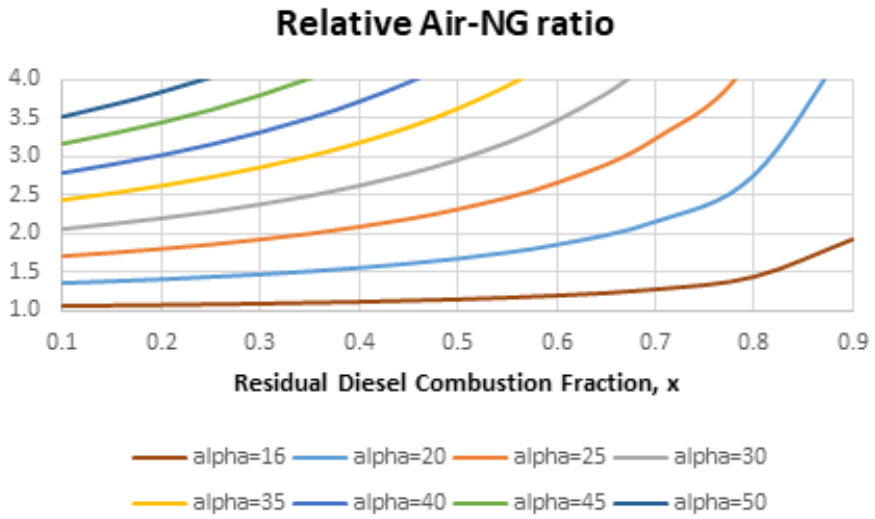

Figure 6.2 - Influence of residual diesel combustion fraction, x, and α on the average composition of the air-NG mixture, according to equation (2)

From figure 6.2, it can be inferred that when the engine is running at full load (AFR = 16-20), a high rate of diesel replacement (low x values) becomes critical as the risk of knocking approaches. For example, if the safe threshold is assumed to be lower λ_{NG} = 1.5, the corresponding minimum values of x are 0.4 (α = 20) and 0.8 (α = 16); this leads to the definition of reduced diesel mass flow thresholds of no more than 60% and 20% respectively. In addition, the replacement rate can be expected to be increased by the presence of exhaust gases in the charge (EGR), provided that α is kept constant[10].

In the same way, at low loads, the α ratio tends to be very high (>30), and this can normally lead to the production of unburnt fuel. Therefore, to cope with this problem, we can intervene

by reducing the amount of air delivered by controlling the pressure of supercharging and/ or choking the inlet flow.

When the λ_{NG} ratio is within the correct range, the process describing DF combustion is similar to that in a conventional SI engine: late injection of diesel fuel (close to TDC) triggers the flame front that propagates from the core of the combustion chamber towards the cylinder walls. In the first part of the process, the main difference compared to standard combustion occurs, as a larger amount of fuel is burnt at this stage. This behaviour is easily explained by the high chemical reactivity of the diesel fuel injected near the TDC, which burns involving a much larger amount of surrounding charge than that typically lit by a spark plug.

The X_{NG} parameter is used to assess the proportion of energy supplied by NG in relation to the heat released by the diesel in ND mode:

$$\mathrm{X}_{NG}[\%] = \frac{\mathrm{m_{NG}}.\mathrm{LHV_{NG}}}{\mathrm{m_D}.\mathrm{LHV_D}}100 \qquad (6.3)$$

By comparing the parameters $\mathrm{X}_{NG}[\%]$ and $X_D[\%] = \left(\frac{m'_D}{m_D}100\right)$ (percentage of residual energy from diesel fuel), the efficiency of the engine can be assessed, that is when the NG energy introduced is greater than the energy of the reduced diesel fuel, then BTE is lower, and vice versa.

For the first test cycle, the same injection strategy used as originally for the diesel engine is maintained, varying only the pedal position.

The four operating conditions are represented in table 4, where for each case the fraction of diesel energy subtracted $X_D[\%] - 100$ and that introduced with NG, X_{NG} are reported.

Table 6.4 shows that the amount of energy supplied by NG is generally higher than the reduction in the energy of diesel fuel, resulting in a decrease in BTE. This result was expected, because the reduction of the pedal rate leads to running the engine with diesel injection strategies that correspond to lower loads, which are not optimised for DF operations.

Operating points	**Cases**
3000 rpm – BMEP=2bar / 44 Nm	ND
	-20% Diesel fuel +46% NG
	-41% Diesel fuel +63% NG

	-60% Diesel fuel +132% NG
	-80% Diesel fuel +175% NG
3000 rpm –BMEP=4bar / 88 Nm	ND
	-20% Diesel fuel +36% NG
	-34% Diesel fuel +43% NG
	-64% Diesel fuel +86% NG
	-80% Diesel Fuel +148% NG
3000 rpm – BMEP=8bar / 177 Nm	ND
	-27% Diesel fuel +32% NG
	-46% Diesel fuel +55% NG
	-60% Diesel fuel +66% NG
	-80% Diesel fuel +93% NG
3000 rpm – BMEP=12bar / 265 Nm	ND
	-28% Diesel fuel +30% NG
	-36% Diesel fuel +42% NG
	-60% Diesel fuel +63% NG
	-80% Diesel fuel +75% NG

Table 6.4 - Review of the investigated cases

Operating points	**DF cases before calibration**	**DF cases after calibration**
3000 rpm – BMEP=2 bar	-80% Diesel fuel +175% NG	-80% Diesel fuel +135%NG
3000 rpm – BMEP=8 bar	-60% Diesel fuel +66% NG	-60% Diesel fuel +57% NG
	-80% Diesel fuel +93% NG	-80% Diesel fuel +74% NG
3000 rpm – BMEP=12 bar	-60% Diesel fuel +63% NG	-60% Diesel fuel +52% NG

Table 6.5 - DF cases before and after calibration

In the second test cycle, the Diesel injection strategy is optimised in terms of rail pressure and injection times. The pressure inside the intake manifold was optimised by setting the turbine rack correctly in one case, corresponding to the condition "80% Diesel" at 3,000 [rpm] - BMEP = 8 [bar].

The aim of the optimisation process is first of all to reduce the injection of diesel fuel as much as possible, also reducing to a minimum the amount of NG injected and necessary to cope

with the reduction of the original fuel; at the same time, respecting the main constraints, such as peak cylinder pressure limits and maximum pressure rise.

The engine brake thermal efficiency is shown in table 6.5, where the influence of the calibration can be seen. For all the cases under study, there is a strong reduction in NG energy (for example, for BMEP = 2 [bar], 80% Diesel, X_{NG} is reduced from 175% to 135%). In addition, for all BMEP cases higher than or equal to 8 [bar], compared to ND mode, the calibration leads to an improvement in BTE. For example, in the condition with BMEP = 12 [bar], at 60% reduction in diesel fuel, NG provides an amount of energy corresponding to 52% of the heat released by ND combustion. This leads to the conclusion that in optimised DF mode, the engine requires less energy from fuel to deliver a given brake torque.

6.4 Analysis of Results

Figure 6.3 shows the effect on BTE when switching from the original diesel combustion mode to the DF mode, before optimising the diesel injection strategy. The BTE trend is plotted according to the percentage of reduction of the reference diesel energy $100 - X_D[\%]$. As for almost all cases analysed, a reduction in BTE is observed, except in the case of the higher load when the higher fraction of diesel fuel with NG is replaced.

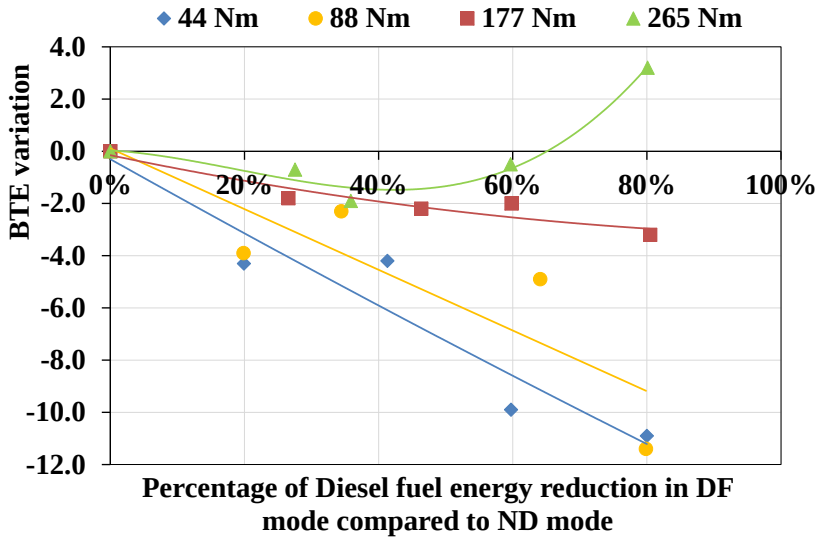

Figure 6.3 - Impact of DF combustion on BTE, without diesel injection optimisation

As shown in figure 6.4, considering the cases at the highest percentage of diesel fuel reduction (see table 6.5), the optimised diesel injection strategy leads to improved BTE.

Also, in this case the variation of BTE, compared to condition ND, is plotted according to the percentage of reduction of the reference diesel energy.

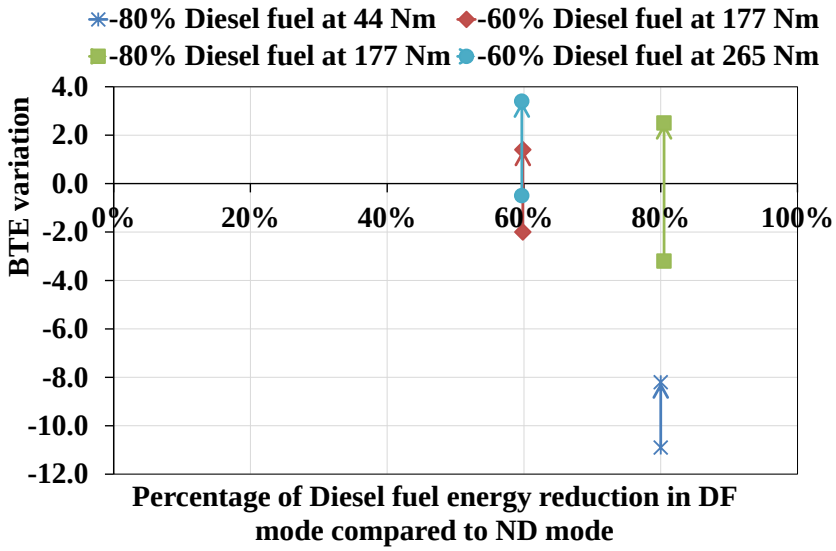

Figure 6.4 - Impact of diesel injection calibration on BTE (selection of cases at higher reduction of diesel fuel energy)

It should be noted that only the lowest load (44 [Nm], BMEP = 2 [bar]) cannot reach the value of BTE obtained in the corresponding operation ND. There is a better possibility of BTE improvement (up to 3.8%) at higher loads. In addition, it is observed that, at medium-high loads, greater efficiency is achieved when there is a higher replacement of diesel fuel: for example, at 177 [Nm] - BMEP = 8 [bar], increasing the reduction rate from 60% to 80%, the BTE improves compared to ND operation, from +1.4% to +2.5%.

In terms of BTE, for all the above considerations, it can be said that the DF-NG combustion mode with high diesel replacement rates (>60%) is absolutely convenient for BMEP equal to or higher than 8 [bar] (up to 12 [bar]).

Conversely, when operating in DF NG-diesel mode at low loads, a significant decrease in BTE is observed. However, the calibration reduces the gap between DF and ND operation, even though it cannot completely recover the lost efficiency.

Here below, the four operating points experimentally investigated are presented and discussed.

6.5 Combustion Analysis at 3,000 [rpm] – 44 [Nm] / BMEP = 2 [bar]

In this section, the operating point corresponding to the lowest investigated load is presented. Figure 6.5 shows the in-cylinder pressure and the Apparent Heat Release Rate (AHRR) for the non-calibrated DF cases and the corresponding ND case.

Applying the First Law of Thermodynamics to a constant mass of ideal gas without any hypothesis on the heat transfer, it is possible to calculate the AHRR, directly from the measured in-cylinder pressure, by means of the following formula:

$$\frac{dQ_b - dQ_{ht}}{d\theta} = \frac{k}{k-1} p \frac{dV}{d\theta} + \frac{1}{k-1} V \frac{dp}{d\theta} \qquad (6.4)$$

For the sake of simplicity, the ratio of specific heat at constant pressure and constant volume is kept constant throughout the engine cycle. However, depending on the NG concentration in the premixed charge, the coefficient value varies from case to case.

From figure 6.5 it is possible to note the progressive decrease in the maximum peak of the AHRR and the simultaneous increase of the rate of heat released during the combustion of the diesel injected through the pilot and pre-injections. The first aspect is linked to the reduction of the amount of diesel introduced by means of the main injection, while the second aspect is due to the increasing mass of NG that burns as the equivalence ratio of the premixed charge increases. Therefore, the combustion process tends to pass from diffusive to almost totally premixed, as the replacement of diesel with NG increases.

Moreover, it can be observed that the DF cases have slightly lower pressure peaks than in the ND case, except for the case with the maximum replacement of diesel with NG (-80% diesel +175% NG). In fact, in the latter case, the peak in-cylinder pressure is higher than in the other cases, due to the shift of combustion towards the compression stroke.

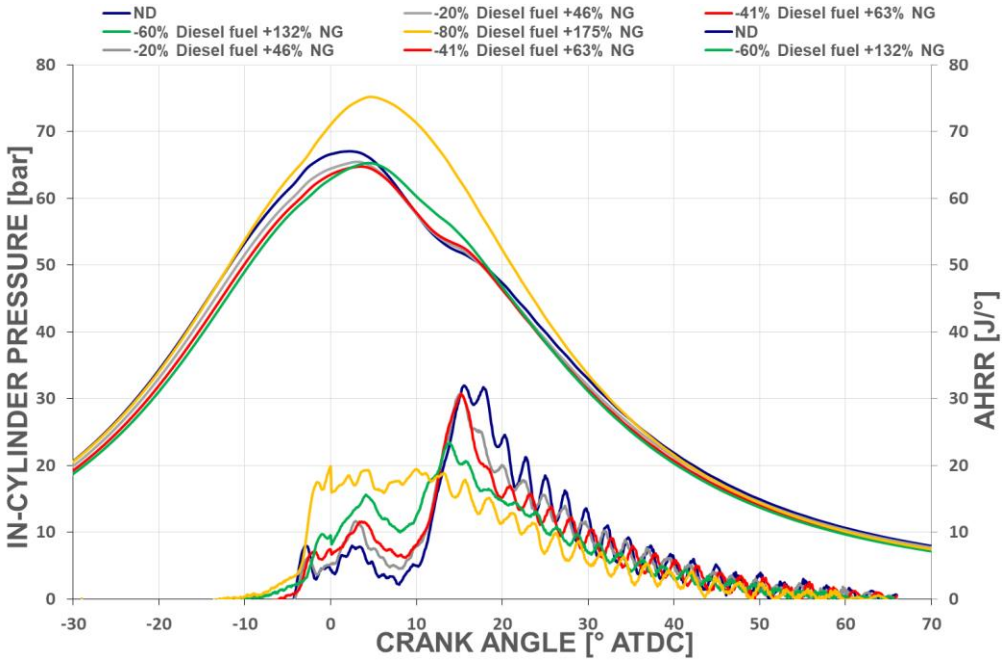

Figure 6.5 – Comparison of in-cylinder pressure and AHRR

Figure 6.6 shows the AHRR of the non-calibrated DF cases and the corresponding ND case. AHRR corresponds to the difference between the amount of energy released from combustion and the heat expelled through the walls of the combustion chamber.

Looking at figure 6.6, it can be noted that the greater the replacement of NG, the more the start of combustion is advanced.

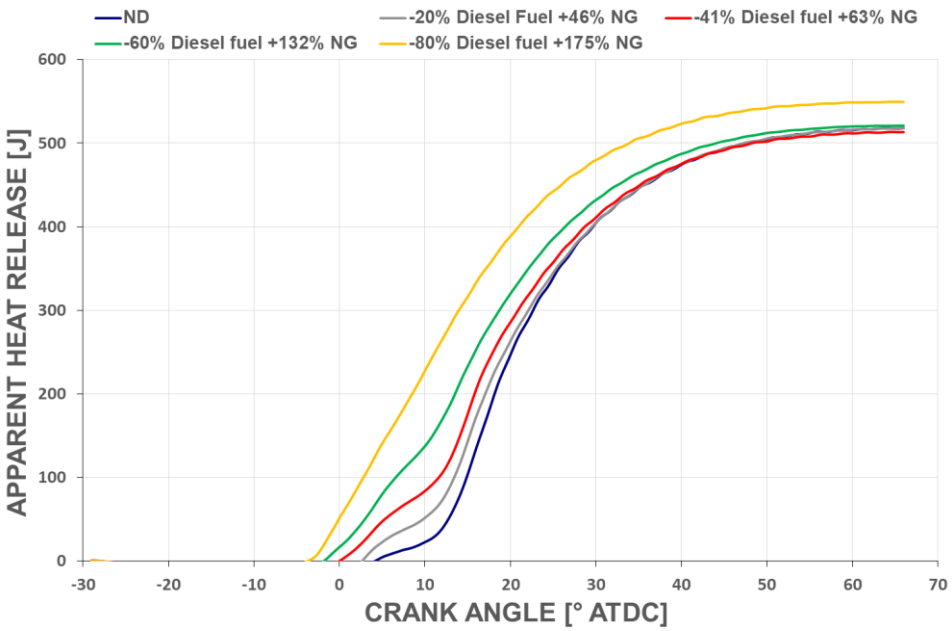

Figure 6.6 - Comparison of AHRR non-calibrated DF cases and the corresponding ND case

Figure 6.7 compares the "-80% diesel" DF cases before and after the calibration process and the ND case. It appears that the maximum value of AHR in the calibrated DF case (-80% diesel fuel +135% NG) is lower than the corresponding non-calibrated DF case (-80% diesel fuel +175% NG). This is due to the increase in the global efficiency obtained through the calibration process, i.e., by increasing the injection timing and rail pressure (see table 6.6).

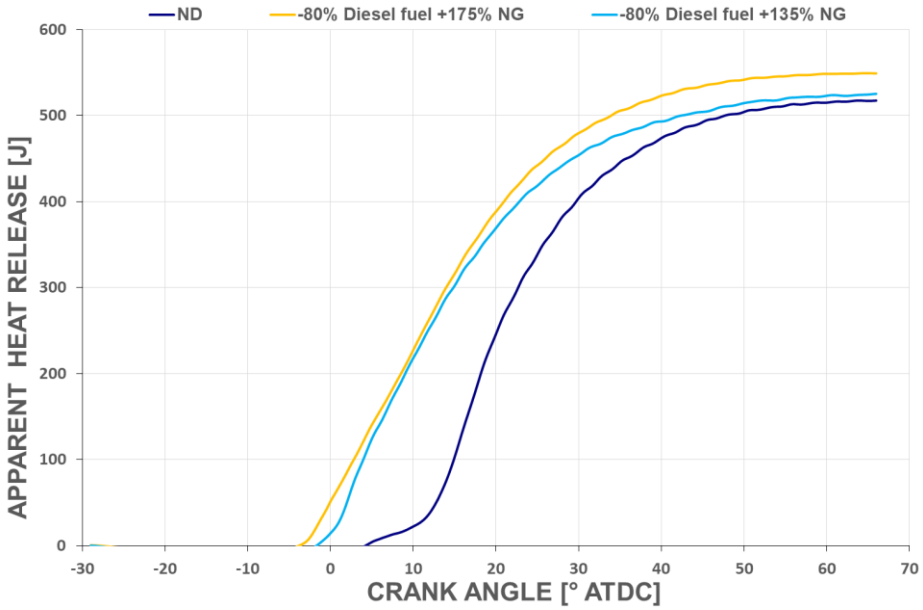

Figure 6.7 – Comparison of AHR before and after the calibration process and the ND case

	Start of injection [°CA AFTDC]	Rail pressure [bar]
-80% diesel fuel +175% NG DF case	-2	670
-80% diesel fuel +135% NGDF case	-10	1100

Table 6.6 – Optimisation parameters at 3,000 [rpm] – 44 [Nm] / BMEP = 2 [bar]

Figure 6.8 compares the DF cases before (-80% diesel + 175% NG) and after (-80% diesel + 135% NG) the calibration and the corresponding ND case. As we can see, the calibration process produces a significant increase in maximum AHR. Hence, there is a slight increase in the pressure peak of the calibrated DF case compared to the non-calibrated one. In particular, this is due to the shifting of the combustion process towards the compression stroke.

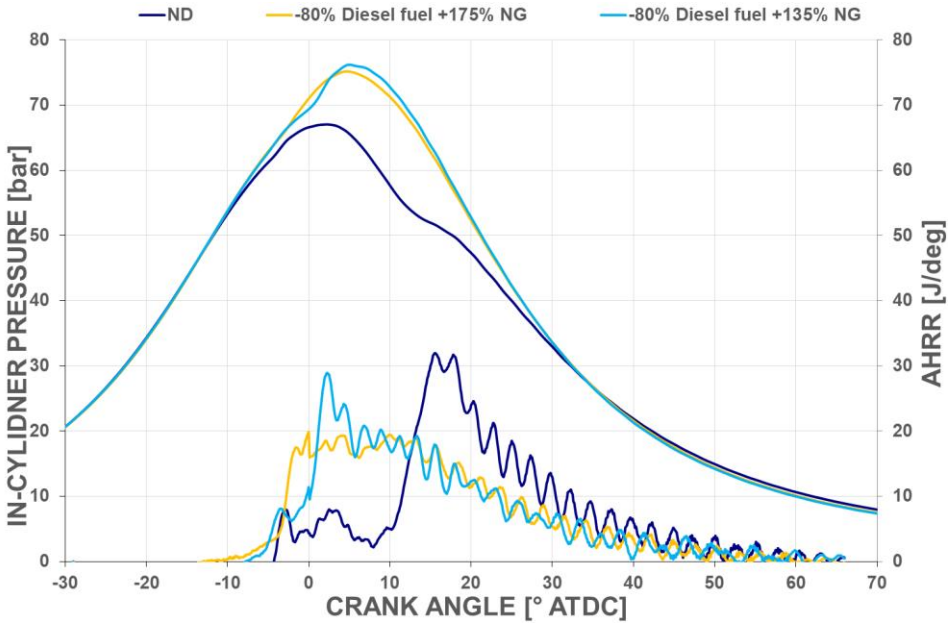

Figure 6.8 – Comparison of in-cylinder pressure and AHRR before (-80% diesel + 175% NG) and after (-80% diesel + 135% NG) the calibration and the corresponding ND case

The histogram shown in figure 6.9 compares the combustion efficiency of the DF and ND cases. Combustion efficiency is calculated according to the following formula:

$$\eta_c = \frac{(P_{in} - \frac{HC}{10^6}\frac{16}{29}\dot{m}_{air}\,LHV_{NG}\,10^3 - \frac{CO}{10^6}\frac{28}{29}\dot{m}_{air}\,LHV_{CO}\,10^3)}{P_{in}}100 \qquad (6.5)$$

where $P_{in} = \dot{m}_{NG}.LHV_{NG} + \dot{m}_{D}.LHV_{D}$ is the power introduced with NG and Diesel fuel, in [kW]; $\dot{m}_{NG}$ is the NG mass flow rate, in [g/s]; LHV_{NG} is the Lower Heating Value of NG, in [MJ/kg]; $\dot{m}_{D}$ is the Diesel fuel mass flow rate, in [g/s]; LHV_{D} is the Lower Heating Value of Diesel fuel, in [MJ/kg]; HC is the concentration of methane equivalent unburnt hydrocarbons, in ppm; $\frac{16}{29}$ is the ratio between the molar mass of methane and standard air; $\dot{m}_{air}$ is the air mass flow rate delivered to the engine, in kg/s; CO is the concentration of Carbon Monoxide, in ppm; $\frac{28}{29}$ is the ratio between the molar mass of carbon monoxide and standard air; LHV_{CO} is the Lower Heating Value of CO, in [MJ/kg].

Equation 6.5 contains an approximation, i.e., it does not include the contribution of hydrogen, which could not be measured during the tests. However, the calculation of ηc provides reliable information, at least in relative terms.

A progressive decrease in combustion efficiency is observed as the replacement of diesel with NG increases. However, a recover of a fraction of the lost efficiency is obtained passing from “-80% diesel fuel +175% NG” to “-80% diesel fuel +135% NG” DF case, thanks to the calibration process.

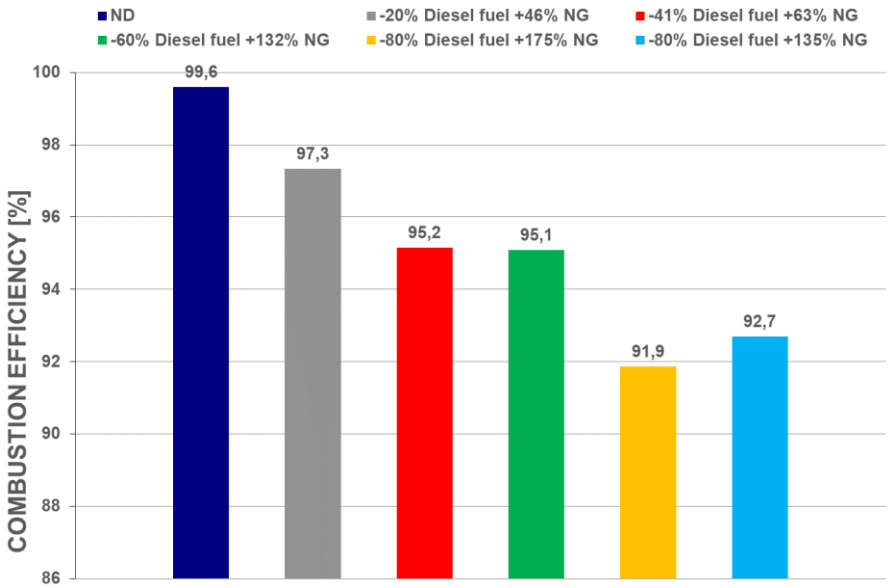

Figure 6.9 – Comparison of η_c DF and ND cases

Figure 6.10 reports the comparison among the DF and the ND cases in terms of BTE. This parameter also shows a progressive decrease as the replacement of diesel with NG increases. However, a recover of BTE was achieved passing from “-80% diesel fuel +175%

NG" DF case to "-80% diesel fuel +135% NG" DF case. However, the calibration was not sufficient to reach an overall efficiency at least equal to that one of the ND case.

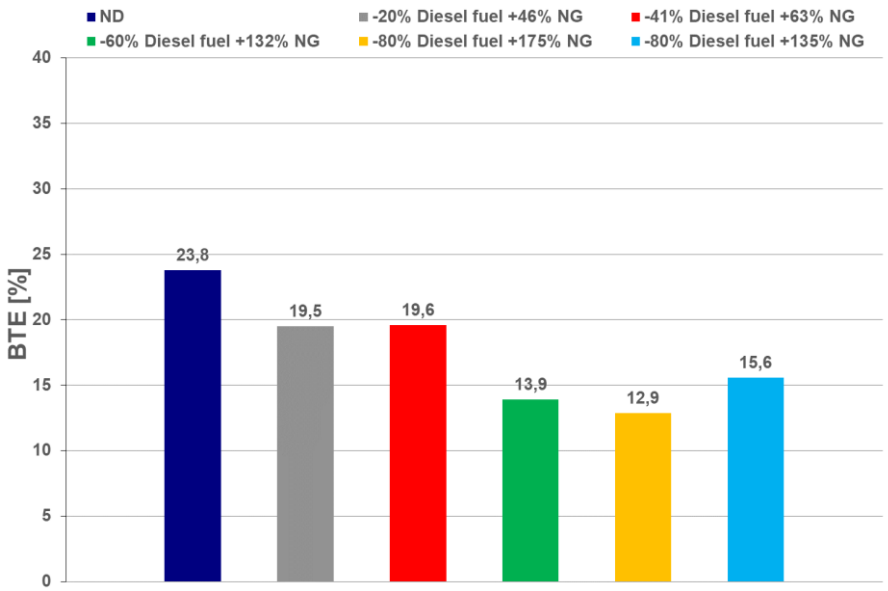

Figure 6.10 – Comparison of BTE DF and the ND cases

Figures 6.11 and 6.12 show the comparison in terms of gas and soot emissions between the DF and the ND cases.

Figure 6.11 shows a significant increase in HC and CO emissions (at least one order of magnitude) between the ND and DF cases, demonstrating that the combustion process in the non-calibrated DF cases is quite inefficient, conversely to what happens in the ND case. This is due to the overly lean premixed NG-air charge that characterises low load conditions. At the same time, there is a slight drop in CO_2 emissions, linked to the use of NG and the low combustion efficiency.

As far as the NO_x emissions are concerned, they tend to decrease up to a 60% replacement of diesel with NG in terms of energy. After that threshold, NO_x emissions increase with respect to the ND case. This is due to the strong advance of the start of combustion, and hence the increase in in-cylinder temperature.

Finally, soot emissions decrease significantly when replacing diesel with NG, which does not contain aromatics and forms a lean premixed charge with air.

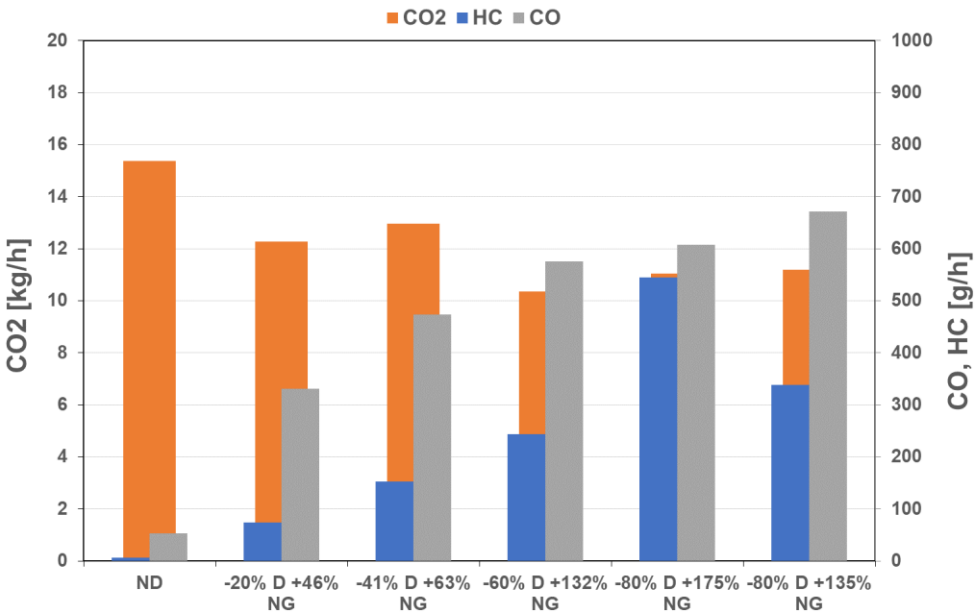

Figure 6.11 – CO_2, CO and HC emission comparison ND and DF cases

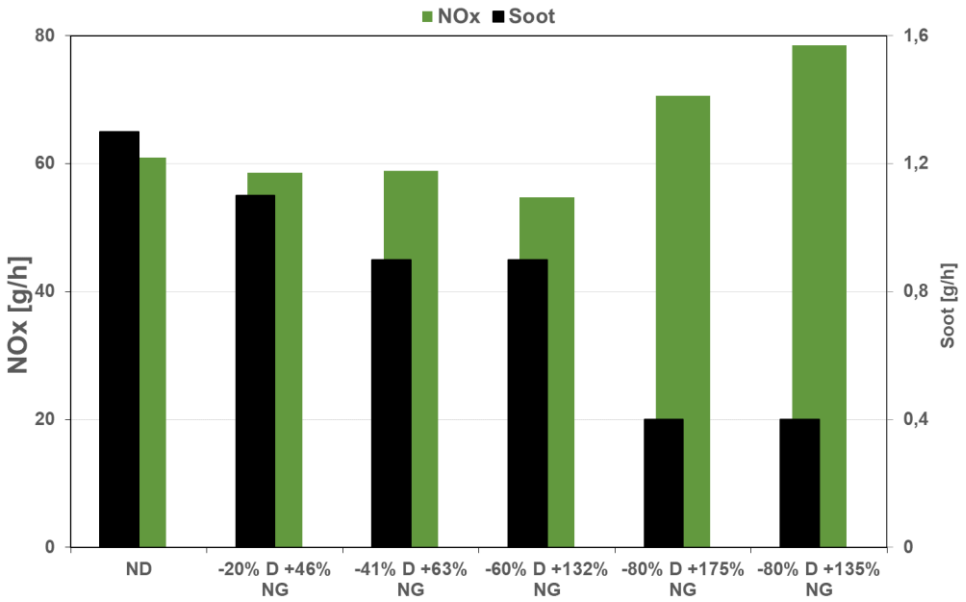

Figure 6.12 – NOx and Soot emission comparison ND and DF cases

Figures 6.13 and 6.14 show the output signal from the optical encoder (red line) and the one that controls the injector (blue line), the latter detected by a current clamp.

The two graphs allow the comparison between the injection strategies of the ND and the "-80% diesel fuel +135% NG" DF case, highlighting that, in the latter case, the main injection timing was anticipated and the duration of the main injection decreased due to the replacement of diesel with NG.

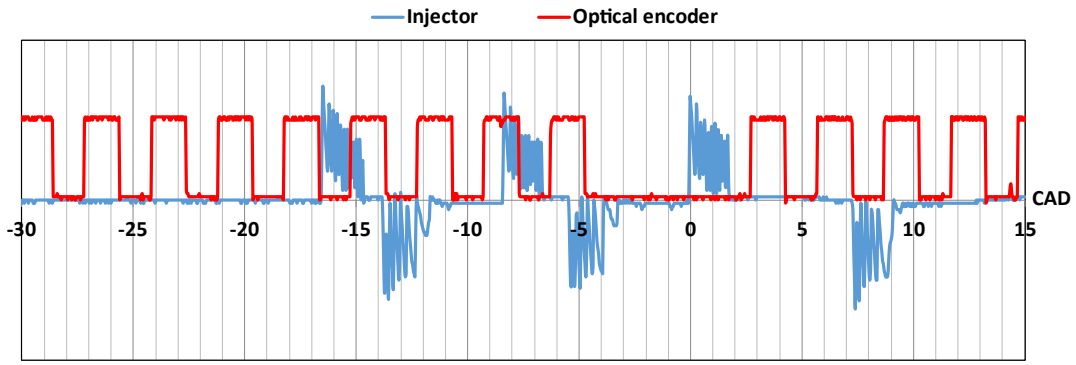

Figure 6.13 – Injection strategies ND case

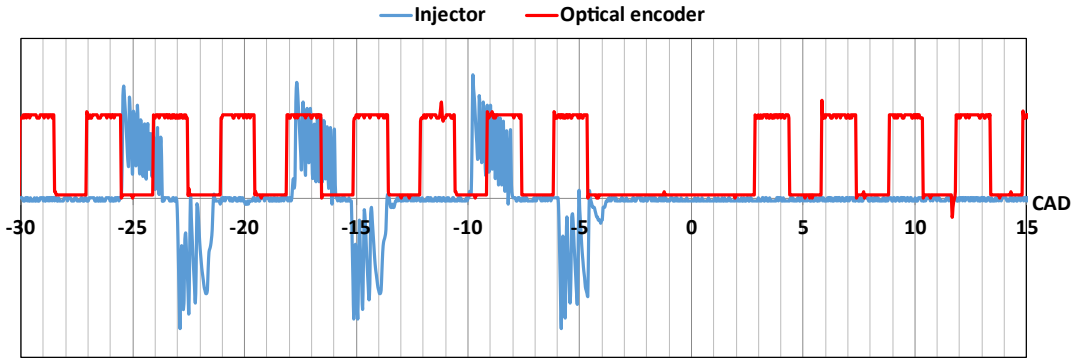

Figure 6.14 – Injection strategies “-80% diesel +135% NG” DF case

Finally, figure 6.15 reports the injection strategies and the injected volumes per cycle per cylinder of diesel for the ND case and the calibrated DF case, clearly showing the increase in injection timing and the replacement of the injected mass of the high-reactivity fuel with the low-reactivity one.

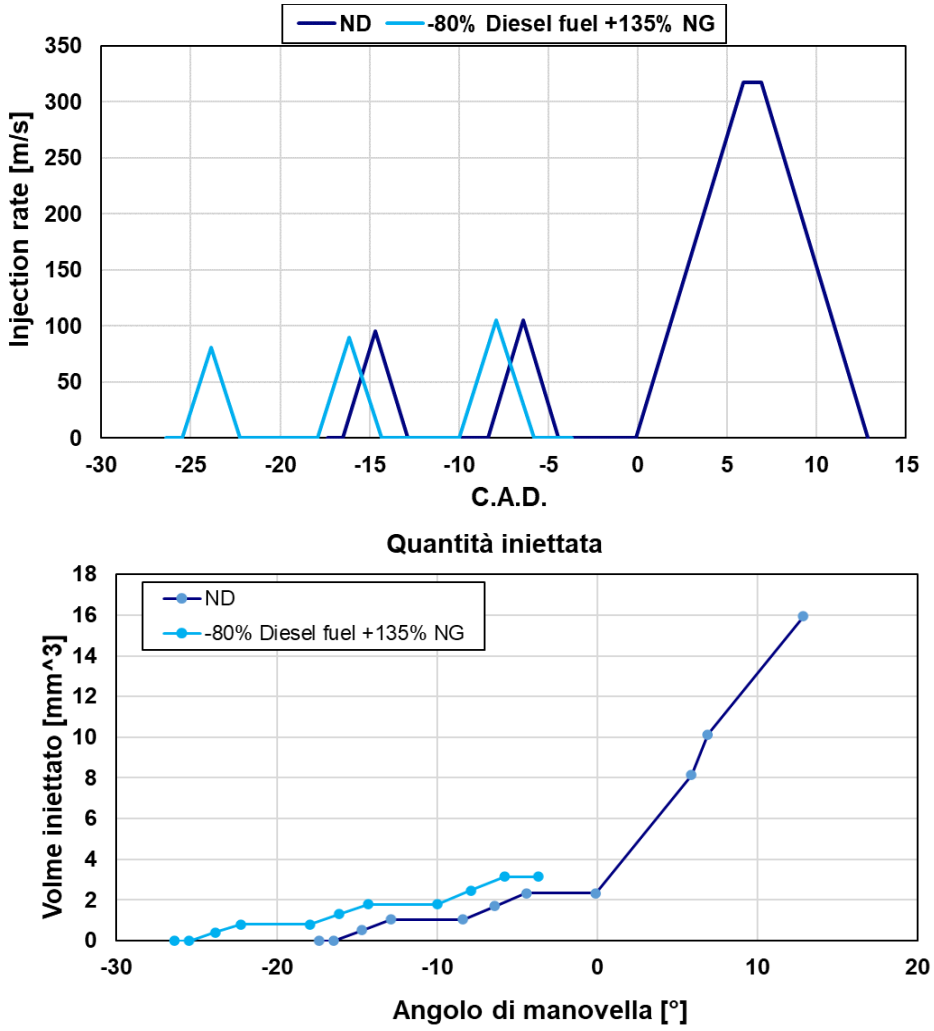

Figure 6.15 – Diesel fuel injection strategy and injected volume ND and DF cases

6.6 Combustion Analysis at 3,000 [rpm] - 88 [Nm] / BMEP = 4 [bar]

Here below, the operating point at 3,000 [rpm] - 88 [Nm] / BMEP = 4 [bar] is analysed.

Figure 6.16 shows the comparison between the DF cases and the corresponding ND case in terms of in-cylinder pressure and AHRR.

As seen in the operating point presented in the previous section (3,000 [rpm] - 44 [Nm] / BMEP = 2 [bar]), as the replacement of diesel with NG increases, we can observe a progressive drop in the maximum peak of the AHR, and a simultaneous increase in the rate of heat released during the combustion of the diesel injected through the pilot and pre-injections.

As far as the in-cylinder pressure is concerned, it slightly increases passing from ND operation to DF cases, up to a 64% replacement of diesel with NG in terms of energy. Conversely, when the high-reactivity fuel is replaced with the low-reactivity one it reaches 80% in terms of energy, and in-cylinder pressure strongly increases with respect to the ND case. This is due to the shifting of the centre of mass of the combustion process towards the compression stroke.

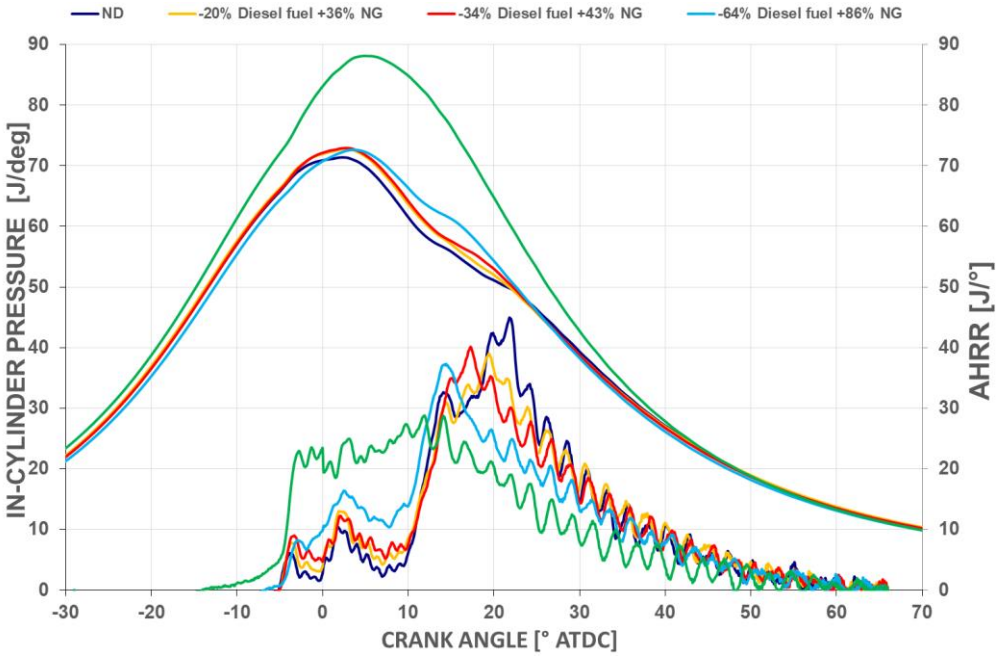

Figure 6.16 – Comparison of in-cylinder pressure and AHRR – 3,000 [rpm] / 88 [Nm]

Figure 6.17 compares the non-calibrated DF cases and the ND case in terms of AHRR.
As seen in the previous operating point, the more diesel is replaced with NG, the earlier the start of combustion. This is particularly true for the DF case characterised by the highest replacement of diesel with NG.

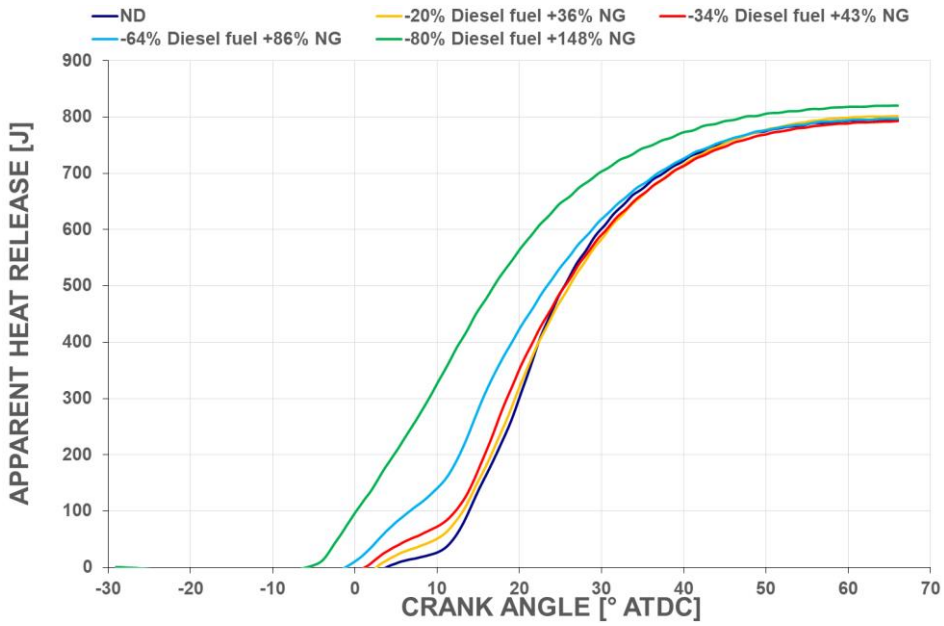

Figure 6.17 – Comparison of AHRR ND and DF cases – 3,000 [rpm] / 88 [Nm]

The histogram shown in figure 6.18 compares the ND and the DF cases in terms of combustion efficiency. Again, a progressive decrease in combustion efficiency is observed as the injected mass of NG increases, since the NG-air charge still remains excessively lean at the present load.

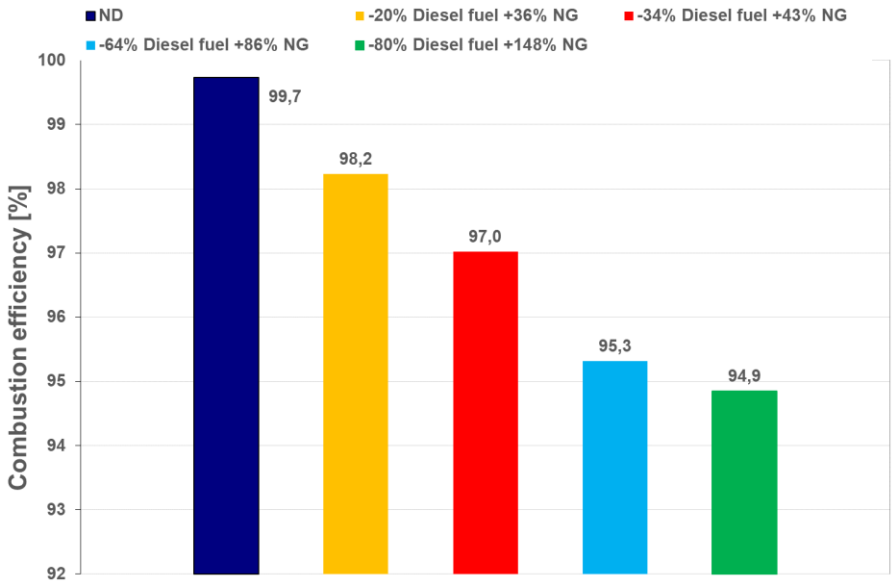

Figure 6.18 – Comparison of ηc ND and DF cases – 3,000 [rpm] / 88 [Nm]

Figure 6.19 shows the comparison among the ND and the DF cases in terms of BTE. As for the combustion efficiency, also for BTE a progressive decrease is observed as the replacement of diesel with NG increases.

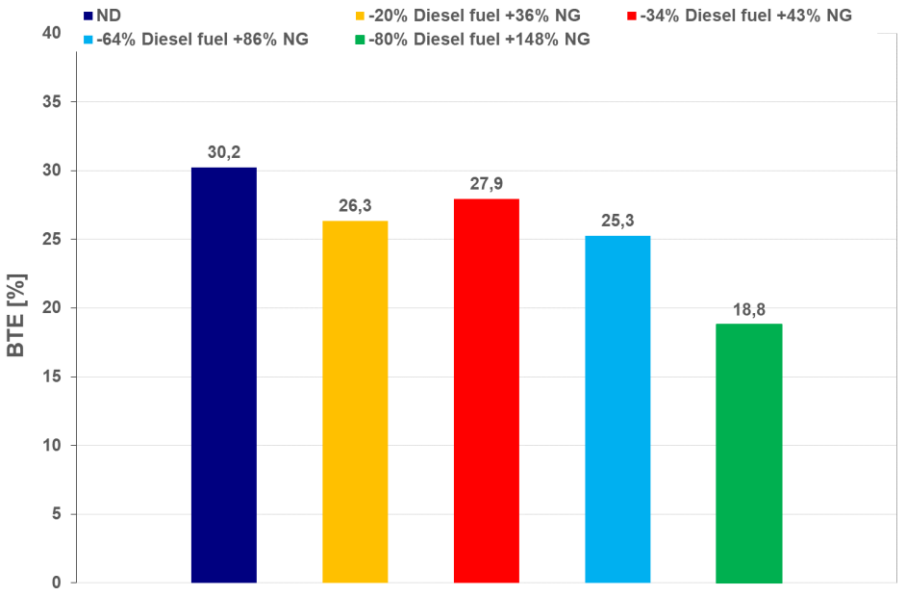

Figure 6.19 – Comparison of BTE ND and DF cases – 3,000 [rpm] / 88 [Nm]

The comparison between the ND case and the DF cases in terms of gas and soot emissions is reported in figure 6.20 and 6.21. As in the previous operating point, a significant increase in CO and HC emissions is observed. However, at this operating point, the increase in HC emissions, passing from ND to DF cases, is lower than at 3,000 [rpm] – BMEP = 2 [bar]. This is due to the fact that this load is higher than the previous one, hence the A/F ratio of the NG-air mixture is lower, which facilitates the completion of the combustion process.

A decrease in CO_2 can be noted in Figure 6.19 as the replacement of diesel with NG increases.

Finally, figure 6.21 shows a slight increase in NO_x and an improvement in soot emissions passing from ND operation to DF cases.

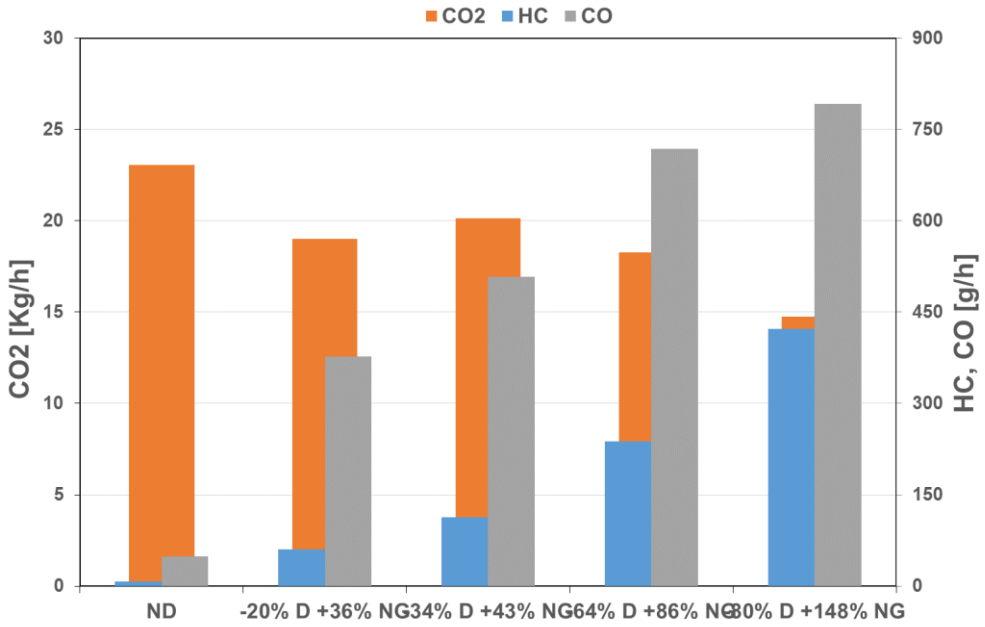

Figure 6.20 – CO_2, CO and HC Emission comparison ND and DF cases – 3,000 [rpm] / 88 [Nm]

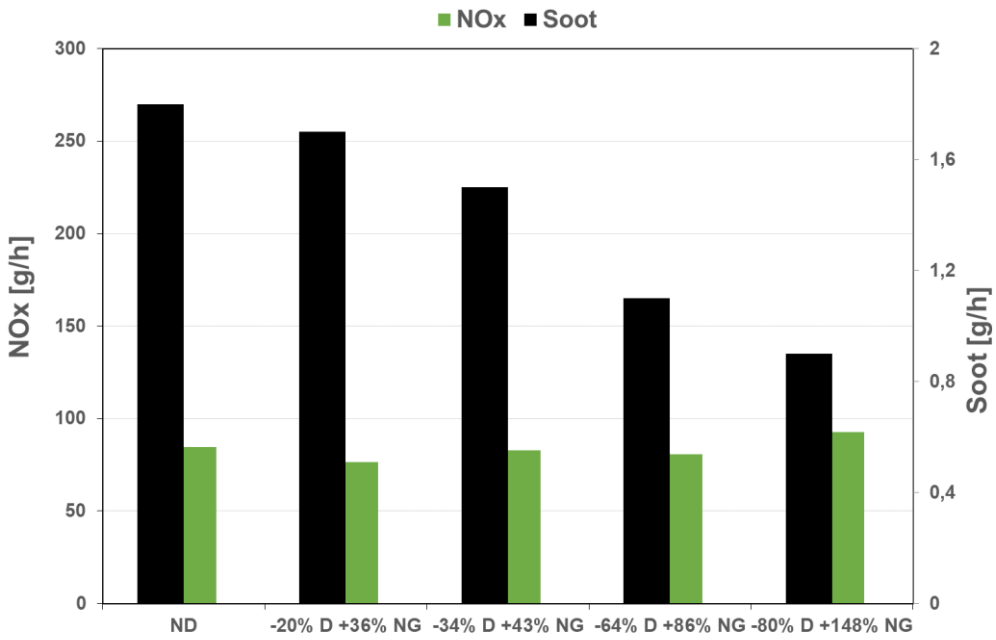

Figure 6.21 – NOx and Soot emission comparison ND and DF cases – 3,000 [rpm] / 88 [Nm]

6.7 Combustion Analysis at 3,000 [rpm] - 177 [Nm] / BMEP = 8 [bar]

The comparison between ND and DF NG-diesel modes at 3,000 [rpm] - BMEP = 8 [bar] is now reported.

The effects of different amounts of NG on in-cylinder pressure trace and on AHRR are shown in figure 6.22.

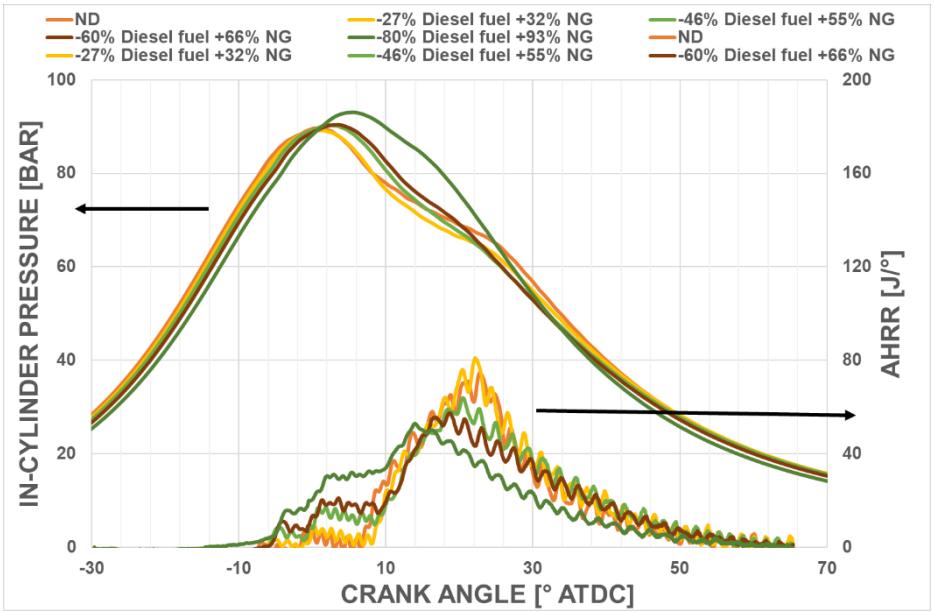

Figure 6.22 - Comparison of in-cylinder pressure and AHRR ND and DF cases - 3,000 [rpm] - BMEP = 8 [bar]. DF cases are not optimised.

The trends shown in figure 6.22, except for the maximum replacement of diesel fuel (-80%), clearly show three peaks of AHR on each curve. In the ND combustion, the first two peaks are due to the combustion of the small quantities of fuel, introduced with the pilot injection and the pre-injections, before the TDC. When the combustion is about to begin, all the fuel injected in the pilot phase is already completely vaporised and has to mix locally with the charge in the cylinder; in this way it can burn very quickly.

In this way, the conditions in the cylinder facilitate a rapid combustion of the pre-injection. Finally, the main injection corresponds to the third peak, where fuel is burned in diffusive mode. The first two peaks of AHR increase at the expense of the third when a lean mixture of NG and air is introduced inside the cylinder; this is because the integral of the AHRR curve is practically constant, representing the useful amount of heat released by combustion, to reach the given load. The growth of the first two peaks is explained by the fact that the pilot injection and the pre-injections of diesel fuel also ignite some quantities of NG that are found around the jets. Obviously, the greater the NG part contained in the charge, the greater the amount of this fuel involved in the premixed phase.

In DF NG-Diesel combustion mode, it is noted that the maximum peak of AHR tends to be lower; this affects the maximum pressure gradient in the cylinder and the associated combustion noise, which should be reduced.

Another important aspect highlighted by the trends shown in figure 6.5, for all DF modes, is the slight decrease in pressure during the compression phase, despite the constant pressure of the intake manifold. This result is explained by the higher thermal capacity of NG-air mixtures compared to pure air, which therefore affects the reduction of the polytropic index. In addition, the density of NG is lower than that of air.

From the pressure traces in figure 6.22, except for the maximum replacement rate (-80% of diesel fuel), it is noted that ND combustion is very similar to DF mode. In the case of increased fuel replacement, the peak pressure in the cylinder increases due to the earlier start of combustion. This effect is highlighted in figure 6.23, where the apparent heat release curves are plotted: the angle at which half of the energy is released is shifted from 22.6 [°ATDC] (ND) to 16.4 [°ATDC].

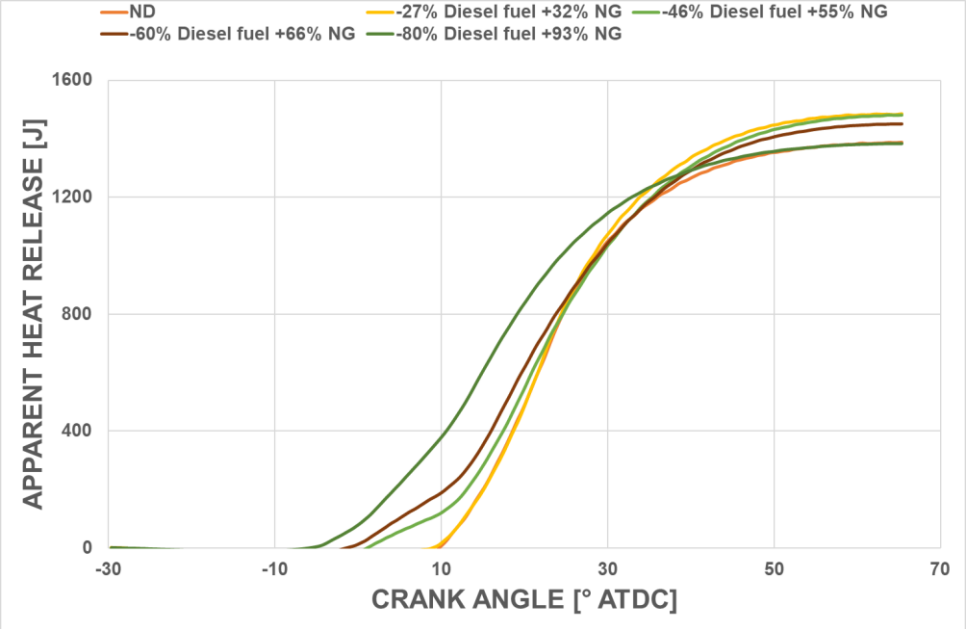

Figure 6.23 - Comparison of apparent heat release ND and DF cases
3,000 [rpm] - BMEP = 8 [bar]. DF cases are not optimised.

Figures 6.24 to 6.25 compare the combustion efficiency, BTE and emissions parameters in ND and DF modes. Two other DF cases are included, namely "-60% Diesel + 57% NG" and "-80% Diesel + 74% NG." They are the result of DF case optimisation "-60% Diesel fuel +66% NG" and "-80% Diesel fuel +93% NG" respectively. Table 6 shows the new calibration values compared to the original condition: the pressure in the rail is increased, and also the start of injection (SOI) is advanced, again compared to the condition ND. In the case of DF,

where the maximum proportion of diesel fuel (-80%) has been replaced, the calibration has led to a reduction of the charge pressure. This optimisation means that part of the combustion efficiency (and therefore BTE) is recovered, and also substantially improves the production of HC emissions.

Without a specific calibration, figure 6.25 shows that BTE also decreases in DF mode in all cases, except “-60% diesel fuel +57% NG” and “-80% diesel fuel +74% NG”. Only after the optimisation of the injection strategy, the latter two cases have higher BTE values, respectively 36.4% and 37.5% compared to ND operation (35%), despite the fact that the combustion efficiency is slightly lower. This is the result of the improved combustion phase of the DF cycle, where less complete combustion is compensated.

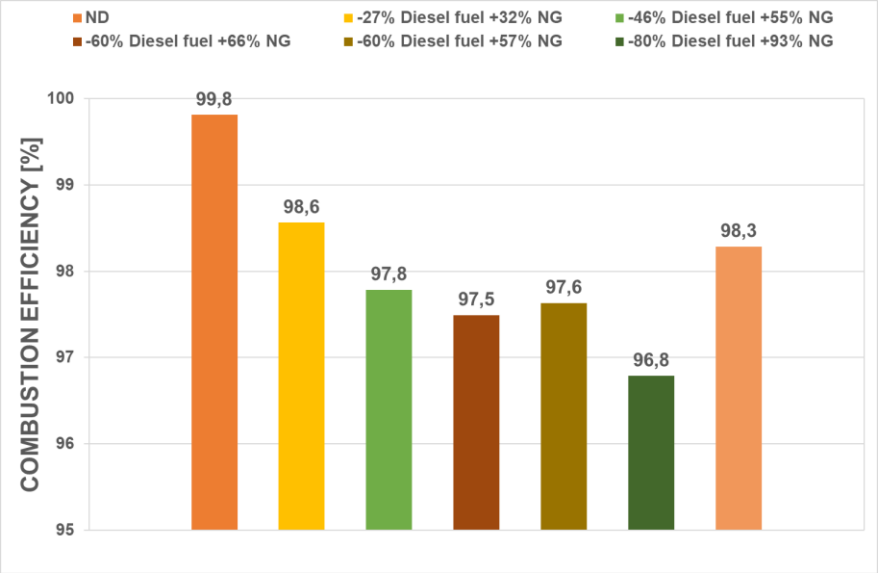

Figure 6.24 - Comparison of combustion efficiency ND and DF cases – 3,000 [rpm] - BMEP = 8 [bar]. Only “−60% Diesel fuel +57% NG” and “−80% Diesel fuel +74% NG” DF cases are optimised.

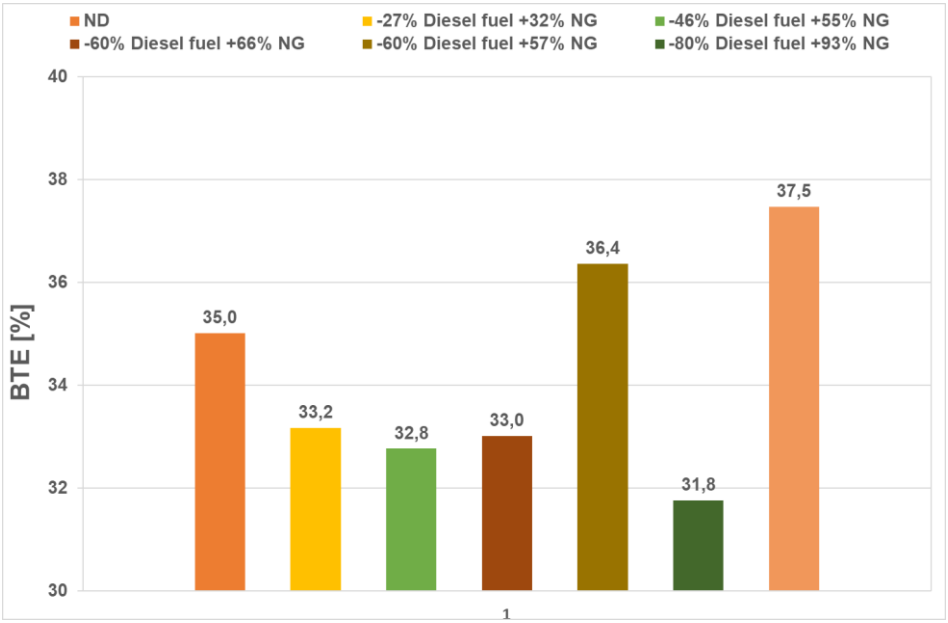

Figure 6.25 - Comparison of BTE ND and DF cases – 3,000 rpm - BMEP = 8 bar. Only "−60% Diesel fuel +57% NG" and "−80% Diesel fuel +74% NG" DF cases are optimised.

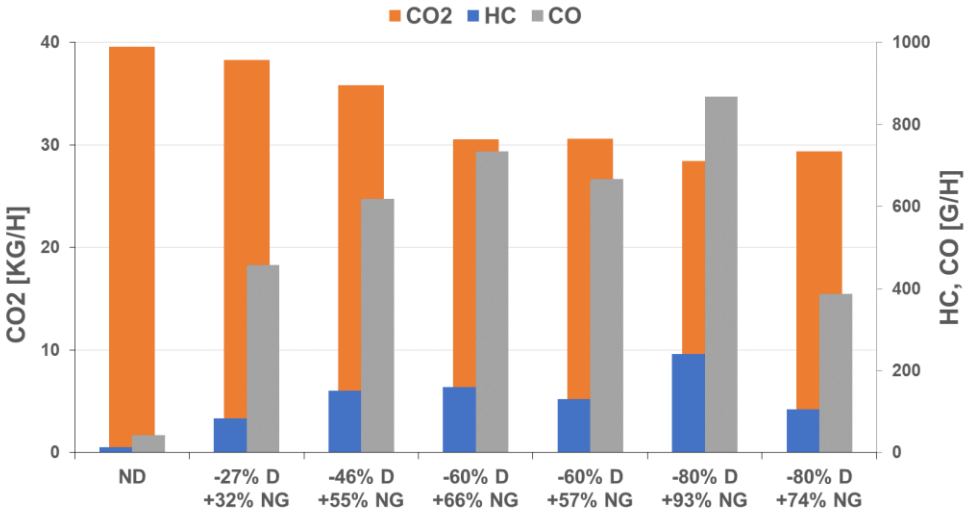

Figure 6.26a – CO_2, CO and HC emission comparison ND and DF cases – 3,000 [rpm] - BMEP = 8 [bar]. Only "−60% Diesel fuel +57% NG" and "−80% Diesel fuel +74% NG" DF cases are optimised.

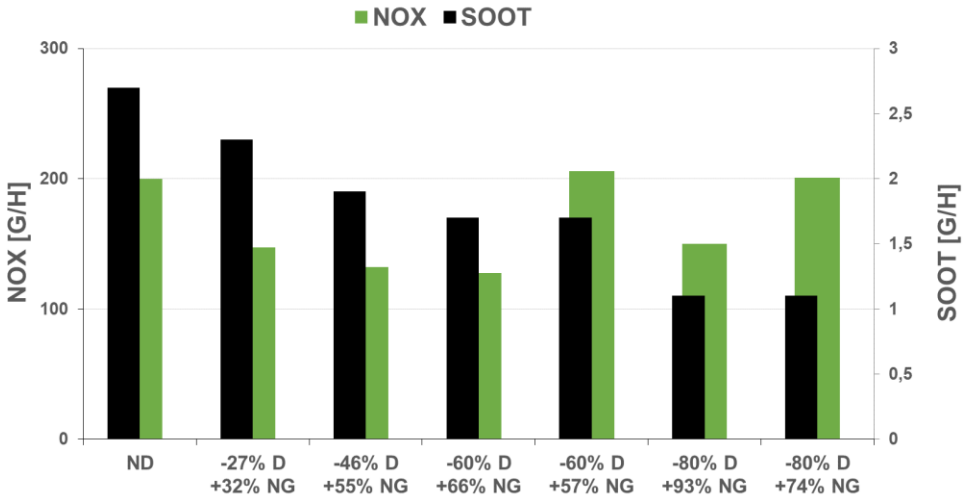

Figure 6.26b - Comparison of CO_2, HC, CO, NOx, and soot emissions ND and DF cases – 3,000 [rpm] - BMEP = 8 [bar]. Only "−60% Diesel fuel +57% NG" and "−80% Diesel fuel +74% NG" DF cases are optimised.

DF cases	SOI [° BTDC]	Rail pressure [bar]	Boost pressure [bar]
-60% Diesel fuel +66% NG	0.0	800	1.8
-60% Diesel fuel +57% NG	6.0	850	1.8
-80% Diesel fuel +93% NG	1.0	750	1.8
-80% Diesel fuel +74% NG	6.0	1050	1.4

Table 6.7 - Review of the calibration parameters for two different operating points (BMEP = 8 [bar], 3,000 [rpm], −60%/−80% Diesel fuel).

To better understand the combustion and brake thermal efficiency trends, an emission analysis was conducted.

In switching from ND operations to DF operations, a consistent increase is found, also of an order of magnitude, this can be seen in figure 6.26(a). Of course, as the diesel fuel is increasingly replaced with NG, the concentrations of CO and HC in exhaust gases increase more and more consistently.

These results are due to the very low flame velocity propagating in a homogeneous and lean mixture such as that formed with NG and air; this evidence is confirmed by many authors[11].

In addition, in this mode of operation managing a small amount of diesel, this does not ignite and does not easily burn the lean mixture of NG and air: this is due to the reduced hot spots, which are normally formed by the auto-ignition of the diesel fuel and which, in this case, do not support the combustion of the mixture.

On the other hand, as the replacement of diesel fuel increases, a trend in the decrease in CO_2 emissions is observed; this is explained by the higher hydrogen-carbon ratio characterising the methane molecule compared to diesel, but also by the higher quantities of CO and HC. The cases that have been subject to optimisation, “-60% Diesel + 57% NG” and “-80% Diesel + 74% NG” offer an interesting result in terms of CO_2, in this case reaching a reduction of 30%. This positive result is lost when CO_2 is produced with a treatment and conversion system of CO and HC.

Figure 6.26(b) shows in some cases approximately the same production, in others a reduction in NOx emissions: when improved, the maximum reduction reaches 36.2%. It must be said, however, that this advantage is cancelled when optimising the calibration to reach the maximum value of BTE, obtained in cases " 60% Diesel fuel +57% NG" and " 80% Diesel fuel +74% NG". As seen in figure 6.5, the reduction of the third peak of AHRR, which occurs in the absence of optimisation calibration, reduces the maximum temperature reached in the cylinder and therefore, the possibility of producing NOx. This trend is compensated, in calibrated cases, by the advance of the main injection timing.

Figure 6.26(b) also shows the trend of soot and immediately highlights the continuous decrease as the replacement of diesel with NG is increased. The production of soot from the diffuse combustion of diesel liquid fuel tends to decrease. The maximum reduction of this emission is from 2.7 [g/h] to about 1.1 [g/h]. In addition, the vaporisation and mixing of diesel fuel droplets improves due to the delay in the ignition of diesel fuel: this is due to the competition for oxygen that exists between diesel and NG fuel.

The effects of the calibration on in-cylinder pressure trace and on the combustion rates are shown in figures 6.27 and 6.28: two different diesel fuel replacement rates were considered (60% and 80%). The standard with the optimised injection strategy is compared in figures 6.27(c) and 6.28(c); the effects on AHRR are presented in figures 6.27(b) and 6.28(b); finally, the correlation between AHRR and the cylinder pressure trace is shown in figures 6.27(a) and 6.28(a).

What is noted for both cases, and which becomes a general rule, is that the shift of the main peak of the rate of heat release towards TDC shows improved efficiency in the thermodynamic cycle and therefore the combustion tends to complete. At the same time,

however, the pressure and peak temperature of the cylinder also increases, producing a higher rate of NOx emissions. The advance of the combustion phase leads improved efficiency in the thermodynamic cycle: thanks to the approach of the peak pressures to the TDC, a more effective use of the expansion stroke is obtained, which leads to a more developed work.

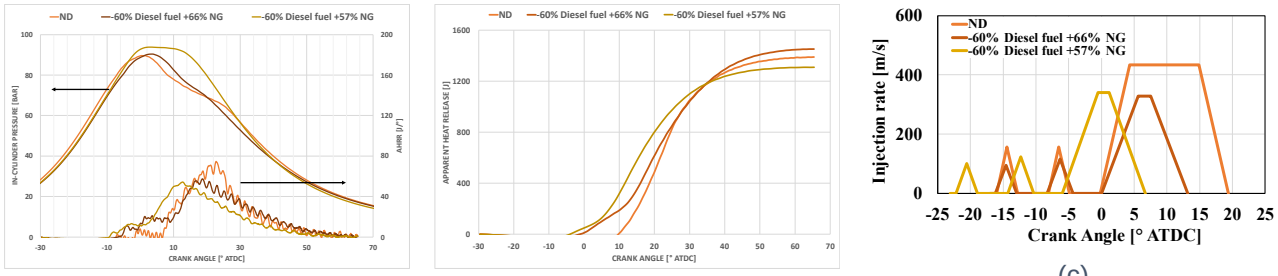

(a) (b) (c)

Figure 6.27 - Influence of Diesel fuel injection optimization (Plot c) in terms of in-cylinder pressure and apparent heat release. Operating condition: 3000 rpm - BMEP = 8 bar, “−60% Diesel fuel”.

6.8 Combustion Analysis at 3,000 [rpm] - 265 [Nm] / BMEP = 12 [bar]

Figure 6.29 illustrates the comparison between cylinder pressure and AHR in the two modes ND and DF. You always see three peaks in the evolution of the AHR. In the high load engine condition, we note the damping of the third peak that occurs in the case DF for the highest percentage of fuel replaced with NG ("60% diesel fuel +63% NG" and " 80% diesel fuel +75% NG").

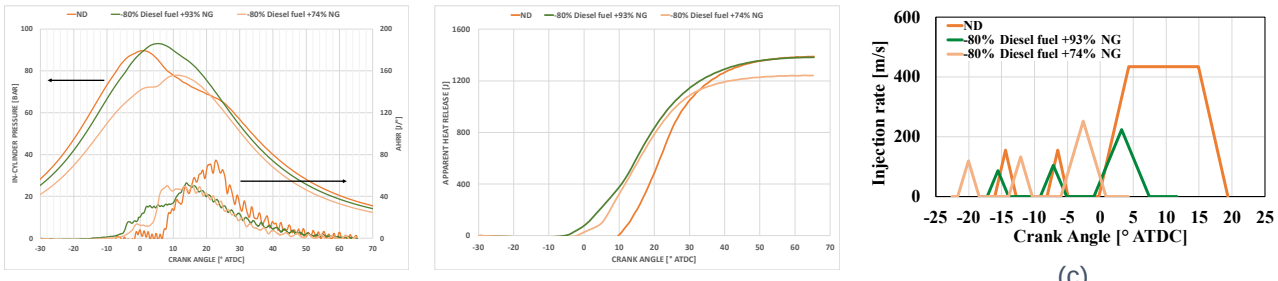

(a) (b) (c)

Figure 6.28 - Influence of Diesel fuel injection optimization (plot c) in terms of in-cylinder pressure and apparent heat release. Operating condition: 3000 rpm - BMEP=8 bar, “-80% Diesel fuel”.

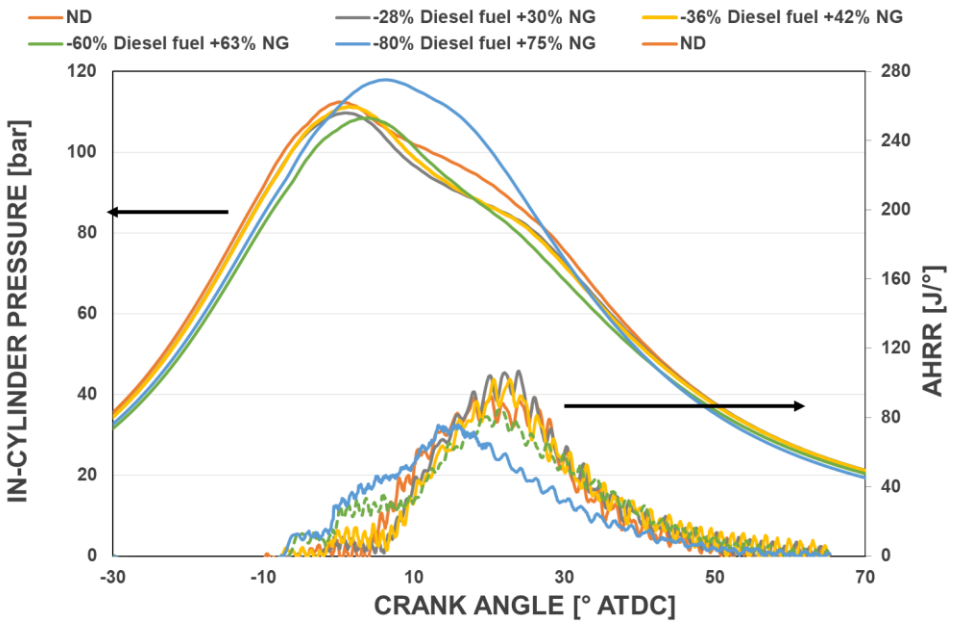

Figure 6.29 - Comparison of in-cylinder pressure and AHRR ND and DF cases - 3,000 [rpm] − BMEP = 12 [bar]. DF cases are not optimized.

It is observed that for in-cylinder pressure traces, only in case of maximum replacement of diesel fuel (-80% Diesel + 75% NG) the pressure is higher than the original case ND. In other cases of fuel replacement, the pressure is lower than the case working with diesel only. The apparent heat release curves, plotted in figure 6.30, explain this different behaviour.

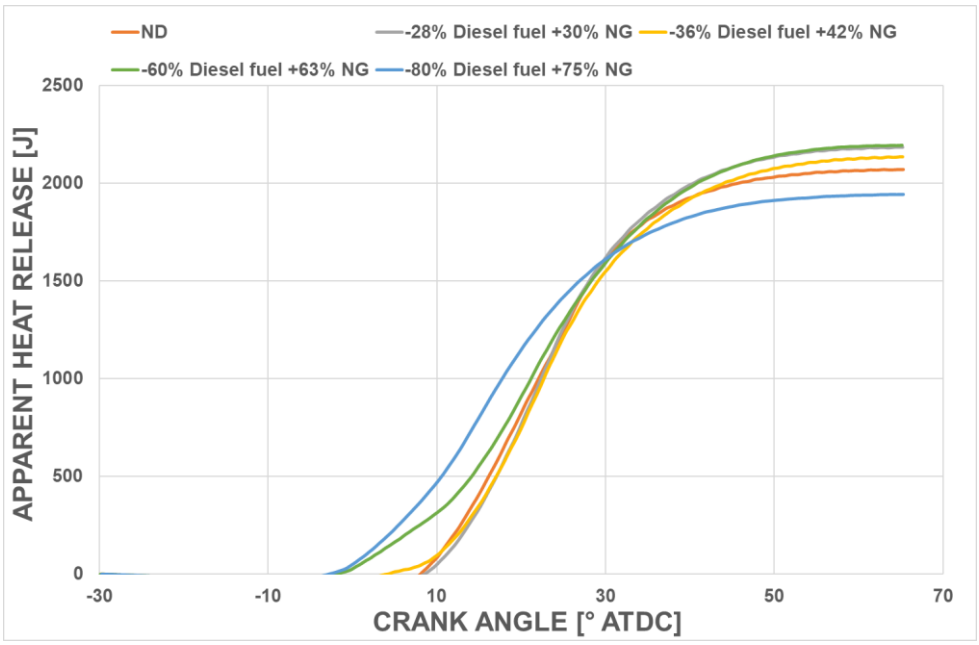

Figure 6.30 - Comparison of apparent heat release ND and DF cases - 3,000 [rpm] - BMEP = 12 [bar]. DF cases are not optimized.

The comparison between the two combustion modes, in terms of combustion efficiency and BTE, is shown in figures 6.31 and 6.32 respectively. These charts also include another DF case, namely the replacement of fuel "60% diesel fuel +52% NG." This point of view derives from the case "-60% Diesel + 63% NG", for which the pressure in the rail has been increased (from 850 to 1100 bar) and anticipated the SOI timing (from 0- to 8- this).

In figure 6.31, a deterioration in combustion efficiency is observed as the replacement of diesel fuel by NG increases. The same trend was observed with the engine point at BMEP = 8 bar (figure 6.9), although in this case the decrease is smaller. Therefore, in this case, the completion of combustion is preferred as, after the auto-ignition of diesel fuel, the NG-air mixture is more reactive. Finally, the improvement in combustion efficiency is observed by optimising the case "-60% diesel fuel +63% NG" to the case "-60% diesel fuel +52% NG": it goes from 98.3% to 98.6%, respectively, improving by 0.3%.

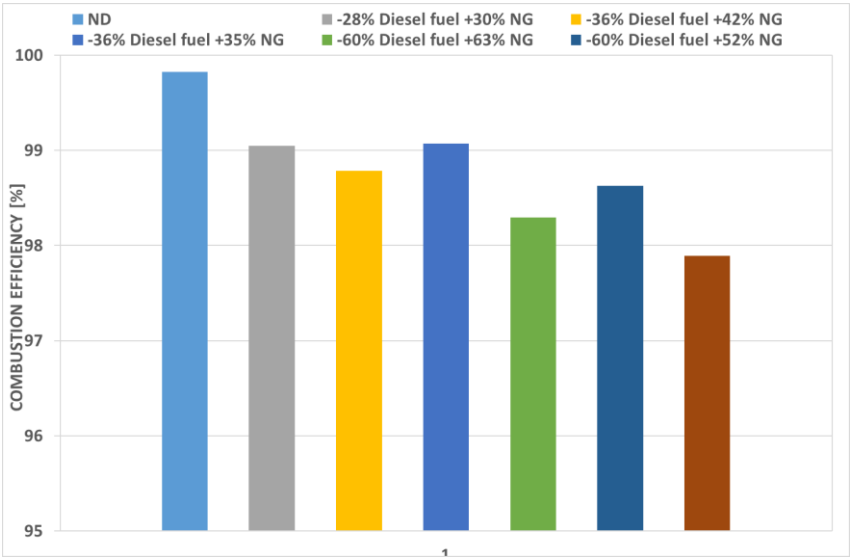

Figure 6.31 - Comparison of combustion efficiency ND and DF cases – 3,000 [rpm] - BMEP = 12 [bar]. Only “−60% Diesel fuel +52% NG” DF case is optimized.

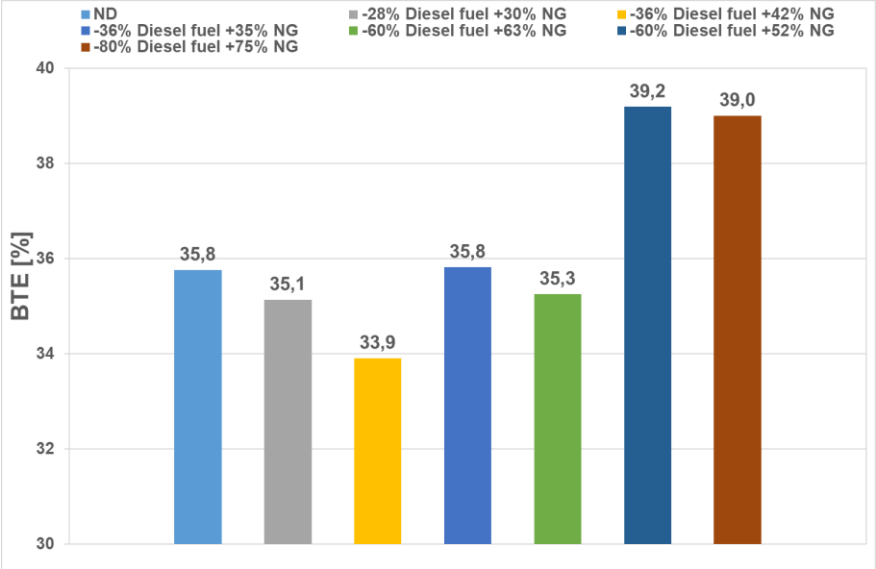

Figure 6.32 - Comparison of BTE ND and DF cases - 3,000 [rpm] - BMEP = 12 [bar]. Only "−60% Diesel fuel +52% NG" DF case is optimized.

The benefits of optimising the diesel fuel injection strategy in terms of BTE are recognised in all cases, as shown in figure 6.32. As obtained for the point at BMEP = 8 [bar], high load and high percentage of NG in the mixture, good levels of BTE are reached, even higher than the traditional ND mode. There was an improvement of 3.9% (from 35.3% to 39.2%) in the transition from "-60% diesel fuel +63% NG" to "-60% diesel fuel +52% NG" in the case.

Figure 6.33a analyses the evolution of CO_2 and reports the trends in pollutant emissions (CO, HC, soot and NOx).

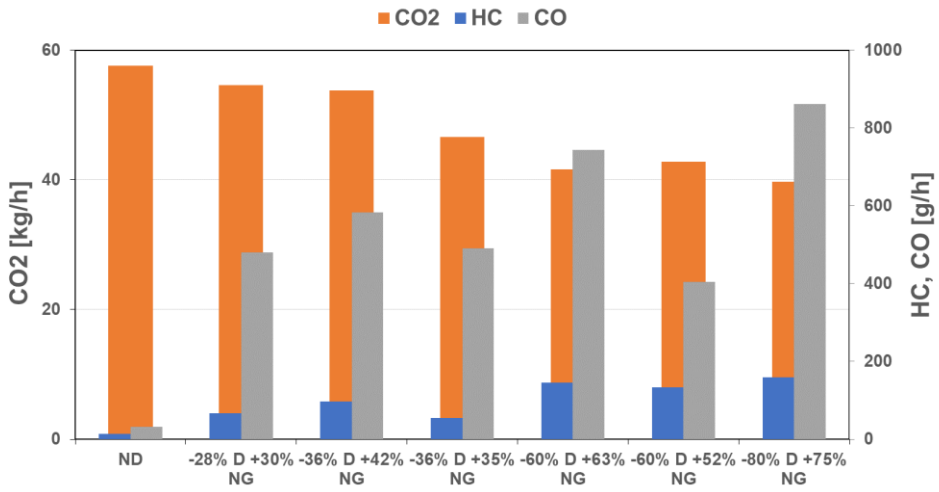

Figure 6.33a - Comparison of CO_2, HC and CO emissions ND and DF cases – 3,000 [rpm] – BMEP = 12 [bar]. Only for "−60% Diesel fuel +52% NG" DF case injection strategy is specifically optimized.

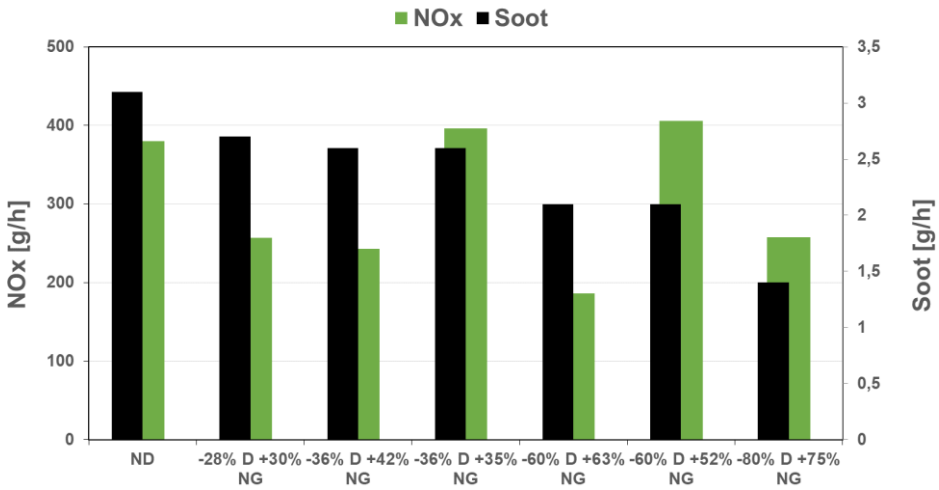

Figure 6.33b - Comparison of NOx, and soot emissions ND and DF cases – 3,000 [rpm] – BMEP = 12 [bar]. Only for "−60% Diesel fuel +52% NG" DF case injection strategy is specifically optimized.

A lower environmental impact with DF combustion mode is highlighted in figure 6.33(a), with the continuous reduction of CO_2 production, especially at medium-high diesel fuel replacements and when the fuel injection strategy is optimised. When replacing diesel with less than 30% NG there are no particular advantages in terms of CO_2 produced. The slight difference between the original ND case and the "-28% Diesel + 30% NG" case is close to the accuracy of the instrument used for measuring this combustion product.

An actual trend towards CO_2 reduction is highlighted for higher NG capacities. A deviation from this reduction trend is noted only with the case DF "-60% Diesel + 52% NG", which corresponds to greater amount of CO oxidised after the optimisation of the injection strategy.

An interesting result is the production of NOx, which tend to be lower than the ND mode, and which decreases with a maximum emission reduction of 51%, except in the case of optimisations of the diesel fuel injection strategy (-36% diesel fuel +35% NG and 60% diesel fuel +52% NG DF case). In the variation of the main injection timing strategy, as shown in figure 6.33(c), combustion is shifted to TDC [figure 6.33(b)]. As can be seen in figure 6.33(a), this produces an increase in maximum pressure and therefore in maximum temperature, which leads to an increase in NOx production. Looking at HC emissions for this point, we see how they are reduced, and, as is well known, this is due to the strong link between HC/CO and NOx emissions: when the former increase, the latter decrease, and vice versa.

In addition to the BMEP = 8 [bar] operating point, also for the BMEP = 12 [bar] operating point, soot emissions improve when the proportion of diesel replaced by NG is increased, as shown in figure 6.32(b). From the original ND operation to the maximum replacement

with NG, corresponding to the point "-80% Diesel + 75% NG", these emissions are very reduced (from 3.1 [g/h] to 1.4 [g/h]).

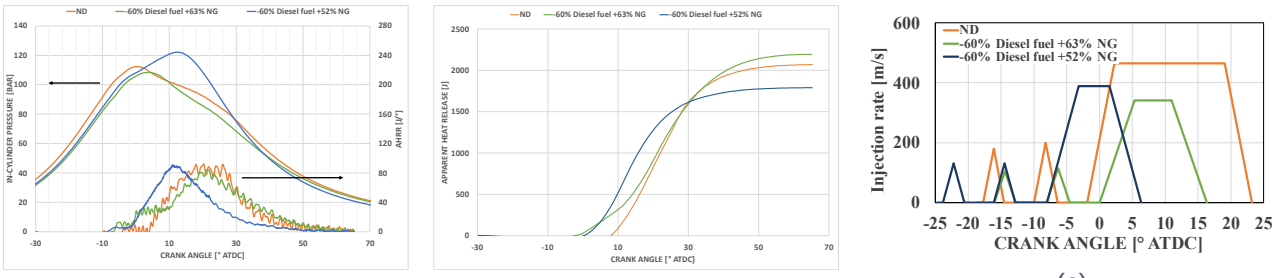

(a) (b) (c)

Figure 6.33c - Comparison of CO_2, HC, CO, NOx, and soot emissions ND and DF cases - 3000 [rpm] – BMEP = 12 [bar]. Only for “−60% Diesel fuel +52% NG” DF case injection strategy is specifically optimized.

6.9 Conclusion

The maximum replacement rates of diesel fuel with NG are taken into consideration, for which in any case regular and complete combustion is guaranteed. It is interesting to see how in the DF mode and in the medium-high load condition, the engine can be powered with only 20% diesel compared to the original operating condition.

With respect to the engine operating in the original ND condition, table 6.8 shows the percentage differences on the main emission parameters. The production of CO_2 and soot is significantly reduced, while NOx emissions improve only in the maximum load condition, with a percentage difference of -46. There is a good reduction of CO_2, up to -44%, which occurs in the condition of maximum power, while the best reduction of soot reaches about 240% (13.3 instead of 45 [mg/kWh]). On the other hand, it is reported that both the production of CO and HC are increased by an order of magnitude, in fact, as shown in the table, these are emission values downstream of the oxidising catalyst. If the average efficiency of the catalyst is around 95% for CO conversion and 90% for HC[112], it is possible to reduce these pollutants as shown in table 6.8.

	Brake Power=60 kW			Brake Power=80 kW		
	ND	DF	Diff [%]	ND	DF	Diff [%]
CO2 [g/kWh]	667	483	-38	719	500	-44
PM [mg/kWh]	45	13.3	-238	37.5	12.5	-200
NOx [g/kWh]	3.33	3.33	0	4.75	3.25	-46
CO [g/kWh]	0.67	0.25*	-167	0.38	0.38*	0
HC [g/kWh]	0.22	0.17*	-30	0.16	0.15*	-8
(*) HC and CO are calculated after the Oxidation catalyst						

Table 6.8 - Specific emissions of the gen-set engines.

It should be noted that the values in table 6.8 would allow the engine in this DF mode to fall within the thresholds set by the last Phase V of the European non-road mobile machinery legislation[113], thresholds set out in table 6.9. An important advantage is that in this DF mode the engine could work without a de-NOx after-treatment system or a particulate filter. Having taken the particulate matter (PM) as soot in first approximation in this treatment, the values shown in table 6.9, for comparison with the set limits, cannot demonstrate full compliance with the legal limits on emissions. This means that further details on particulate measurements are certainly needed. This also supports the fact that, for the new regulations in place, it is necessary to measure the number of particles, this parameter being regulated by stage V[113].

	60 kW	80 kW	Stage V limit
NOx+HC [g/kWh]	3.5	3.4	4.7
PM [mg/kWh]	13.3	12.5	15

Table 6.9 - DF engine emissions compared to the Stage V limits.

The advantage that can be obtained on the reduction of vibrations and noise should also be noted, as in DF mode a more fluid combustion is obtained. In fact, decreases in pressure were observed, in detail from 2.71 [bar/CAD] to 2.14 [bar/CAD] at BMEP = 8 [bar] and from 3.62 [bar/CAD] to 3.38 [bar/CAD] at BMEP = 12 [bar]. The emphasis on this parameter makes it possible to state that, also unlike other DF concepts, such as diesel-gasoline, this proposed DF NG-diesel application ensures stable and controllable combustion even at medium-high loads and high compression ratios[105,114].

Moving from the ND mode to the DF concept, improvement is also achieved for the BTE parameter, which increases from 35% to 37.5% at BMEP = 8 [bar] and from 35.8% to 39% at BMEP = 12 [bar].

Apart for this historical moment of increased NG prices, observing the historical trends of the prices of the two fuels, the shift to engine feeding, mostly regarding diesel oil, with the fuel NG, leads to an economic advantage.

Another inherent advantage in the use of NG is that it can be obtained from renewable sources, such as biomass, in which the production of CO_2 from combustion is recovered in its life cycle.

Using the engine at low loads, the original ND mode is already efficient and clean and therefore no further changes would be justified to optimise the DF mode in these engine conditions. However, low load is a condition rarely used in gen-set applications.

7 CFD Modelling

7.1 Introduction

In this research work, the study of combustion in compression ignition engines was conducted on the basis of experimental tests at the engine test bench and related acquisitions of significant parameters of the conditions explored. Consequently, the acquired data were used to validate the combustion model. The modelling was developed using the CFD (Computational Fluid Dynamics) 3D technique. The model obtained was used to extensively explore the operating range actually tested at the test bench, as well as to numerically test the effects on performance and on the main pollutant emissions produced when a different type of fuel is used.

Using computational fluid dynamics (CFD) it is possible to model systems where there is a fluid flow, heat transfer and related phenomena such as chemical reactions, in all those mechanical sectors where an in-depth study is required to accompany the subsequent designs and implementations:

- aerodynamics of aircraft and vehicles: lift and drag
- hydrodynamics of ships
- power plant: combustion in internal combustion engines and gas turbines
- turbomachinery: flows inside rotating passages, diffusers etc.
- electrical and electronic engineering: cooling of equipment including microcircuits
- chemical process engineering: mixing and separation, polymer moulding
- external and internal environment of buildings: wind loading and heating/ventilation
- marine engineering: loads on off-shore structures
- environmental engineering: distribution of pollutants and effluents
- hydrology and oceanography: flows in rivers, estuaries, oceans
- meteorology: weather prediction
- biomedical engineering: blood flows through arteries and veins

The ultimate aim of developments in the CFD field is to provide a capability comparable with other CAE (computer-aided engineering) tools such as stress analysis codes. In the past, the main reason why CFD has lagged behind is the complexity of the underlying behaviour, which precludes a description of fluid flows that is at the same time economical and sufficiently complete. The availability of affordable high-performance computing hardware

and the introduction of user-friendly interfaces have led to a recent upsurge of interest, and CFD has entered into the wider industrial community in the last years.[115]

The development of CFD has taken place over a long period of time, has involved many economic investments, but its usefulness has spread and its costs are now accessible to many users, thanks to the important advantages in terms of:

- Less time in the design of components,
- Achieving major complexities in the field of fluids, for which conducting experimental campaigns may be difficult to bring back to reality and therefore also entail excessive expenditure,
- Details to be achieved, also by means of a precise geometric parameterisation,
- The possibility to compare different solutions in a short time.

There are commercial and open CFD codes. The formers are used for the various specific sectors, especially in the industrial sector, where the source code is not modified by the user and usually the calculation grid is the result of an automated process.

The use of a closed code specific to an industrial sector facilitates the simulation work of the user who develops his own product, but does not adapt to academic developments especially if unconventional problems are studied. Academic research can certainly use the closed code, but in the case of, for example, studies on different combustion processes or in general the study of problems where it is necessary to develop physical models it is essential to use the open code.

For the present work, an open version of KIVA-3V developed by a collaboration between Unimore and Chalmers University has been used.

7.2 Kiva 3V introduction

The KIVA-3V code is an open source and is based on Fortran language, initially developed in the Los Alamos National Laboratory. The first version of the code has been veveloped in the 70ies to simulate generic reactive flow and successively it has been adapted to the internal combustion engine modelling[116]. The resulting development resulted in the first version of KIVA-3V, which was presented in a 1985 SAE document[117].

7.3 Kiva-3V CFD modelling theory

The code has always been used in the field of research and therefore improvements and new adaptations have been made over time, for example, in the combustion of diesel fuel

alone, rather than double fuel mixtures or in the use of hydrogen. The collaboration between Unimore and Chalmers University has developed in depth the simulation of chemical reactions that could reliably describe combustion in a diesel cycle[116].

More validation has been considered in order to calibrate the numerical model compared to the experimental data. The fluid computing domain is discretized by a block-structured mesh. These meshes allow achieve the required solution in the contour layers using much less elements than unstructured ones. The highest mesh resolution results in the application of mesh cells with high aspect ratio. The structured mesh is constructed with numerical blocks. Each numeric block is a polygon with at least 4 angles and 4 sides that are coupled opposite each other. The structured mesh inside the block consists of two mesh systems. The number of mesh elements on opposite sides shall be equal. The following figure shows an example of a structural mesh:

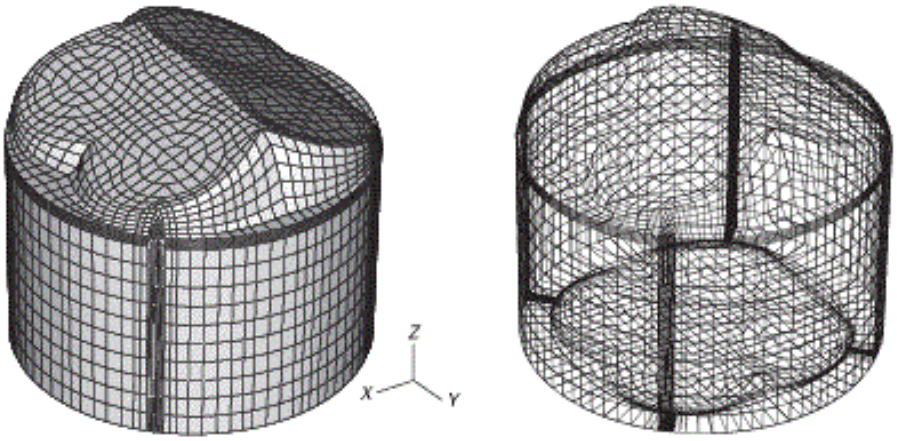

Figure 7.1 - A structured non-orthogonal mesh for a pent-roof i.c. engine geometry[118]

The mesh used in this study has been generated using the K3-prep pre-processor, included in the KIVA3V package.

7.4 Models implemented

The main sub-models implemented in the custom version of the used code are:

- turbulence model: k – ε RNG model
- break-up model: Hybrid KH-RT model
- collision model: Droplet trajectories
- evaporation model: Single component
- combustion model: Diesel PaSR / coupled chemical kinetics

- flame propagation: TFC/Premix code for aspirated fuel

In general, the software solves the mass, quantity and energy conservation equations for multicomponent quantities in the gas phase, considering them compressible and reactive. As already said the turbulence is modelled by the most used model of turbulence k - ε RNG, while for the heat exchange is followed the approach of Launder and Spalding. The Hybrid Kelvin-Helmholtz Rayleigh-Taylor (KH-RT)[117] model forms the process of break-up process of Diesel fuel droplets, while the Partly Stirred Reactor Model (PaSR) is used to reproduce DF combustion, coupled with the flame propagation model (TFC).[116,118,119]
Measurements of ignition delay times in shock tube experiments and flame propagation data for constituent components of NG allow the development and validation of chemical kinetic mechanisms for NG-diesel mixtures. The SENKIN Code was used to calculate the ignition delay at constant volume conditions.[120,121]

Combustion is instead modeled following two different approaches, on the one hand there is the PaSR (Partially Stirred Reactor) model in order to model the interaction between turbulence and chemistry, while as customization of the software have been implemented libraries for a complete resolution of the chemistry associated with oxidation phenomena that occur during combustion. In particular, the chemical kinetic mechanisms are written in a Chemkin-II package, that is, they are represented by reagents and products and in particular for each reaction the reaction rate is calculated by means of a modified Arrhenius equation:

$$k = AT^{b}e^{\frac{-E_a}{RT}} \qquad (7.1)$$

Parameters *A*, *b* and E_a should then be specified for each reaction. These parameters are in turn determined on the basis of shock-tube experiments in which the auto-ignition delay times and the velocity of propagation of the flame front are measured. With regard to the chemical species used, natural gas was modelled as a blend of methane, while for diesel it is advisable to use the DOS (Diesel Oil Surrogate) model. Real Diesel is composed of a large number of aliphatic and aromatic compounds, so a complete chemical kinetics mechanism would be extremely complex: "surrogate" fuels are therefore more practical for engine simulations.

The DOS model is based on: a single component liquid fuel (equivalent chemical formula: $C_{14}H_{28}$) having the same main properties of real diesel and a two-component vapour model consisting of a blend of n-heptane (C_7H_{16}) and toluene (C_7H_8). The mechanism developed to simulate the DF combustion is made up of 81 species and 421 reactions.

8 Numerical optimisation of the diesel injection strategy on a light-duty diesel engine operated in DF NG-diesel combustion mode

8.1 Introduction and aim

In order to achieve a wider vision of the NG-diesel DF combustion concept, the results obtained from the test bench for the Dual Fuel combustion have been used to validate the numerical model of the engine and then this model has been used to investigate the influence of the injection strategy on the Dual Fuel combustion. The operating point at 3000 rpm - 265 Nm (BMEP = 12 bar) is considered.

This calculation work is reported in “Numerical Optimization of the Injection Strategy on a Light Duty Diesel Engine Operating in Dual Fuel (CNG-Diesel) Model”[122].

8.2 3D-CFD engine model used

The customised version of the code KIVA-3V already presented was used for this modelling study[123].

For the computational analysis discussed here, the sector mesh at TDC is represented in figure 8.1. Conventionally the cylinder head is reconstructed in the model as a flat surface: neglecting the influence of geometric details, it is of the same order of magnitude as with the uncertainties on boundaries and initial conditions. The squish height was adjusted to match the correct compression ratio of the studied engine. A minimum of 5 cell layers were imposed in the squish region at TDC. Outside this region, the classic cell size is about 0.5-1.0 mm. The mesh consists of about 110,000 cells at BDC and about 25,000 at TDC.

It has also been demonstrated in previous analyses[124] that a good compromise between accuracy and computational cost is ensured by using the meshing criteria above.

The initial and boundary conditions are extracted from the experimental campaign on DF mode with the use of NG fuel, presented in the relevant chapter of this thesis. The initial flow field implemented is derived from calculations made in a previous numerical investigation on the same baseline engine[121].

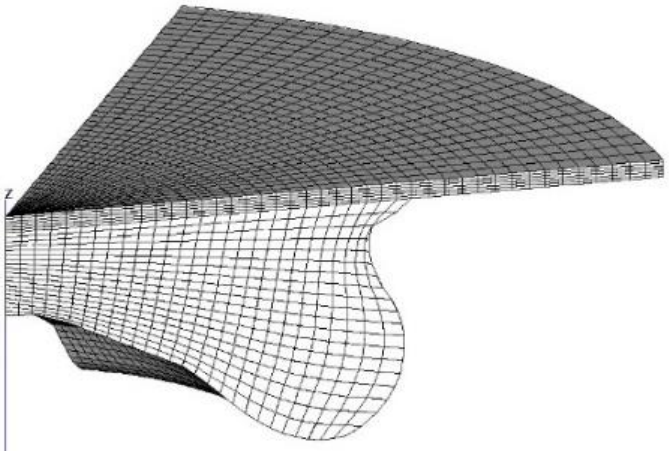

Figure 8.1 - Sector mesh at TDC

The natural gas is defined by a mixture of methane (≈95 %), ethane, propane and nitrogen, while the Diesel Oil Surrogate (DOS) model describes the diesel fuel. In the DOS model, the properties of the actual diesel fuel are used for the liquid phase, while for the fuel vapour a mixture of 70/30 % n-heptane (n-C_7H_{16}) and toluene (C_7H_8) is used[39]. Finally, the combustion mechanism for NG-diesel blends includes 81 species and 421 reactions.

8.3 KIVA-3V engine model validation

As mentioned above in 10.1, the engine point corresponding to the highest load 3,000 [rpm] - 265 [Nm] / BMEP = 12 [bar] on which to concentrate the numerical analysis is considered. The following points are taken for the validation of the 3D-CFD model (how they are referred to here is indicated in brackets):

- ND case;
- “-36% diesel fuel +35% NG” DF case (NG35),
- “-60% diesel fuel +52% NG” DF case (NG52),
- “-80% diesel fuel +75% NG” DF case (NG75).

With respect to DF operation, the BTE value of the DF cases studied here is equal or higher (see figure 10.2).

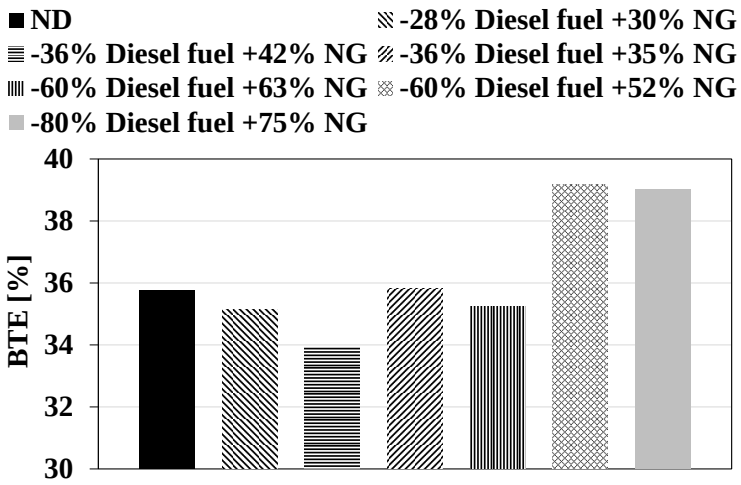

Figure 8.2 - Comparison between ND and DF operations in terms of BTE at 3,000 [rpm] - BMEP = 12 [bar]. Only "−60% Diesel fuel +52% NG" DF case is optimised.

To model the actual pressure flow in the cylinder with the best precision, the Heat Release Rate (RoHR) and the raw emissions corresponding to the cases are considered, and a single setting is necessarily defined for the calibration parameters. For reductions in diesel energy of more than 60%, the soot emissions were not validated, due to the low concentrations produced by the engine on this pollutant in this condition: in fact, the values measured are close to the lower threshold of the measuring instrument.

Calibration parameters such as heat transfer, the diesel injection strategy (SOI of pilot, pre and main injections; injection duration; diesel mass distribution among the injections) and the diesel break-up (fuel temperature; KH and RT break-up models time constants) are considered to validate the model.

In the following figure 8.3, the numerical trends of the pressure in the cylinder and of the Rohr are reported compared with the real data: it is possible to state that there is a good correspondence. Diesel injection strategies are reported for each validation case.

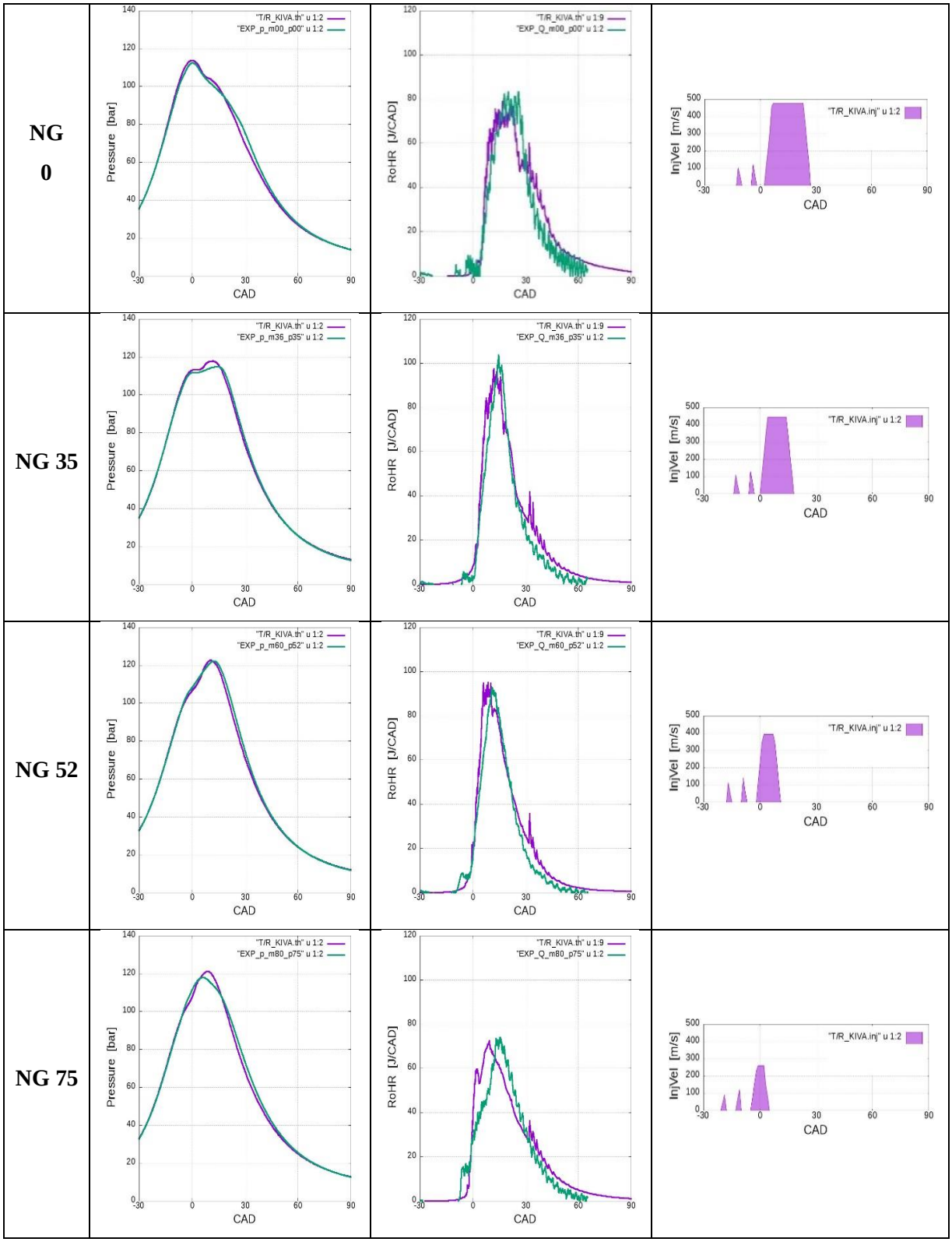

Figure 8.3 - Comparison between experimental and numerical results in terms of in-cylinder pressure and RoHR. The third row shows the diesel injection velocity

The comparisons between the calculated and measured gaseous emissions are shown below (figure 8.4). A good level of repeatability is certainly noted for CO_2 emissions. Conversely, for the calculation of CO and UHC emissions, the 3D-CFD model reports the

link to the percentage of NG replacement. There is also an error affecting the absolute values calculated by the model.

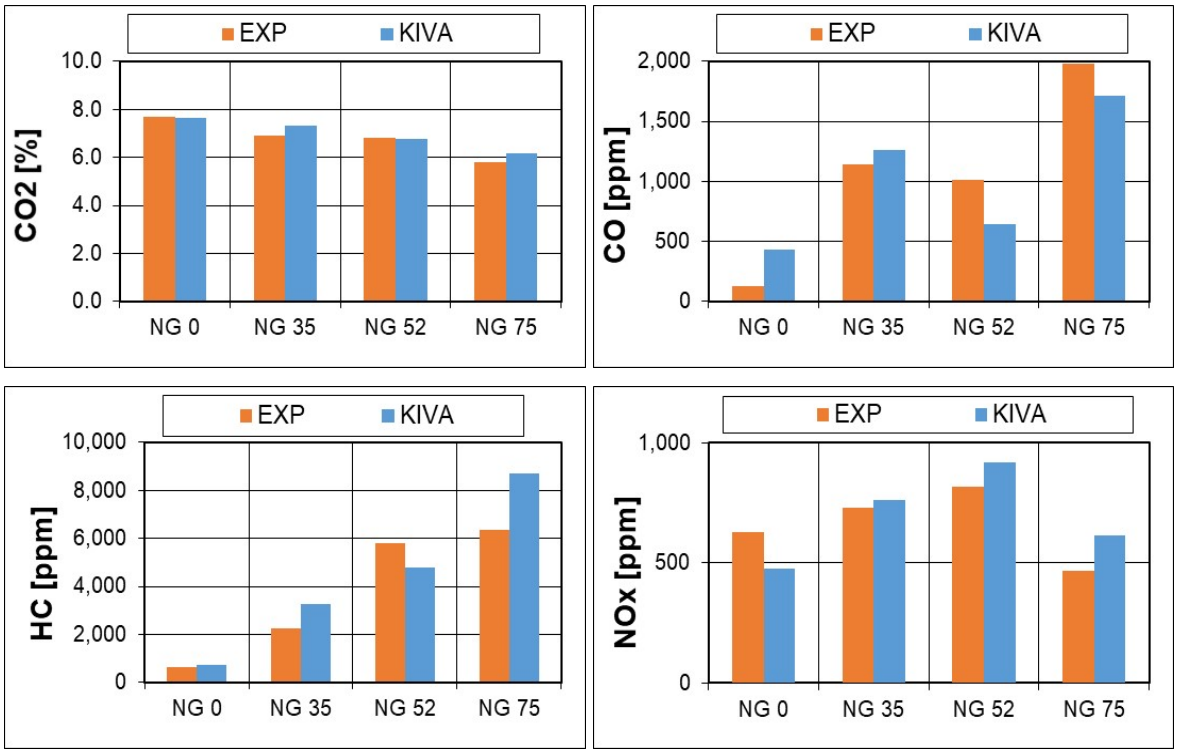

Figure 8.4 - Comparison between experimental and numerical results in terms of CO_2, CO, UHC and NOx emissions

For the calculation of NOx emissions, these are slightly underestimated when compared to the actual ND case. On the other hand, they are slightly overestimated as the NG replacement rates rise.

Figure 8.5 shows the calculation of soot emission by the model. As mentioned above, no specific calibration was carried out on a pollutant. However, the calculations show the continuous reduction of this pollutant as the share of NG increases to replace diesel, reflecting the trend of experimental acquisitions.

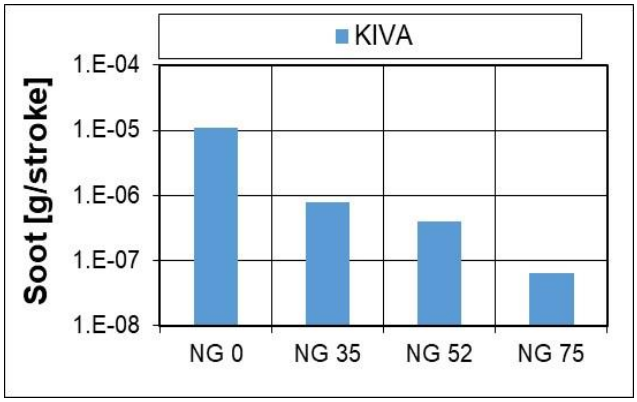

Figure 8.5 - Soot concentrations calculated by the numerical model

8.4 Influence of the diesel injection strategy on DF NG-diesel combustion at medium-high load and high NG replacement rate

The effects of different injection strategies are studied with the calibrated KIVA model. In particular, two different variants of the original injection law are considered, studying the median DF case, i.e., NG52 – 3,000 [rpm] - 265 [Nm] / BMEP = 12. The pre and pilot injections are eliminated in an alternative manner and, in order to keep the injected fuel mass constant, the duration of the main injection is increased proportionally.

The following combinations were considered and compared:

- injections (referred to as “inj 111”): pilot, pre and main injections;
- injections (referred to as “inj 011”): pre and main injections;
- 2 injections (referred to as “inj 101”): pilot and main injections;
- 1 injection (referred to as “inj 001”): only main injection.

In both directions, the injection timing is shifted by steps of 2 Crank Angle Degrees (CAD). The calculations of the simulation carried out for the two conditions on the parameters indicated are shown below (figures 8.6-9) (in-cylinder pressure and temperature and Rate of Heat Release), Gross Indicated Mean Effective Pressure (referred to as IMEP*, defined as the specific indicated work, calculated between IVC and EVO) and emissions (NOx, CO, CO_2 and Soot).

IMEP* corresponds to the Indicated Mean Effective Pressure evaluated between Intake Valve Closing (IVC) and Exhaust Valve opening (EVO):

$$\mathrm{IMEP}^* = \frac{1}{V_d}\int_{\mathrm{IVC}}^{\mathrm{EVO}} \mathrm{pdV}$$

where V_d is the unit displacement.

The following considerations are made.

Even though there are slight differences in the first part of the combustion, the exclusion of pre and pilot injections is not decisive on the in-cylinder pressure traces and the heat release curves. With pre and pilot injections, the auto-ignition process is accelerated, which leads to a slightly more fluid pressure gradient (figure 8.6).

Excluding pre-injections, there are no evident changes in terms of IMEP, gross NOx emissions and CO_2; conversely, due to slightly less complete combustion, there is an increase in CO and soot emissions (CO: +92%; soot: one order of magnitude greater); This result is the elimination of pre and/or pilot injections, greater mass of diesel injected during the main injection to compensate, and consequently a richer mixture is generated locally (figure 8.7).

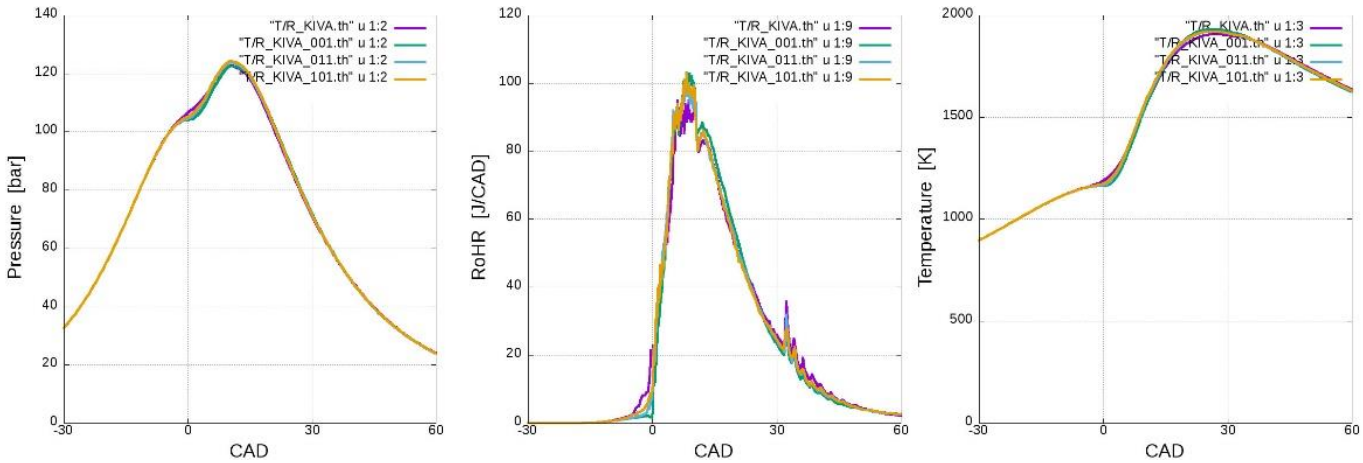

Figure 8.6 - Operating point NG52, influence of injection strategies on DF combustion on in-cylinder pressure, Rate of Heat Release, in-cylinder temperature, gross Indicated Mean Effective Pressure

Inj 111 (red lines): pre, pilot and main injections

Inj 001 (green lines): only main injection

Inj 011 (blue lines): pre and main injections

Inj 101 (yellow lines): pilot and main injections

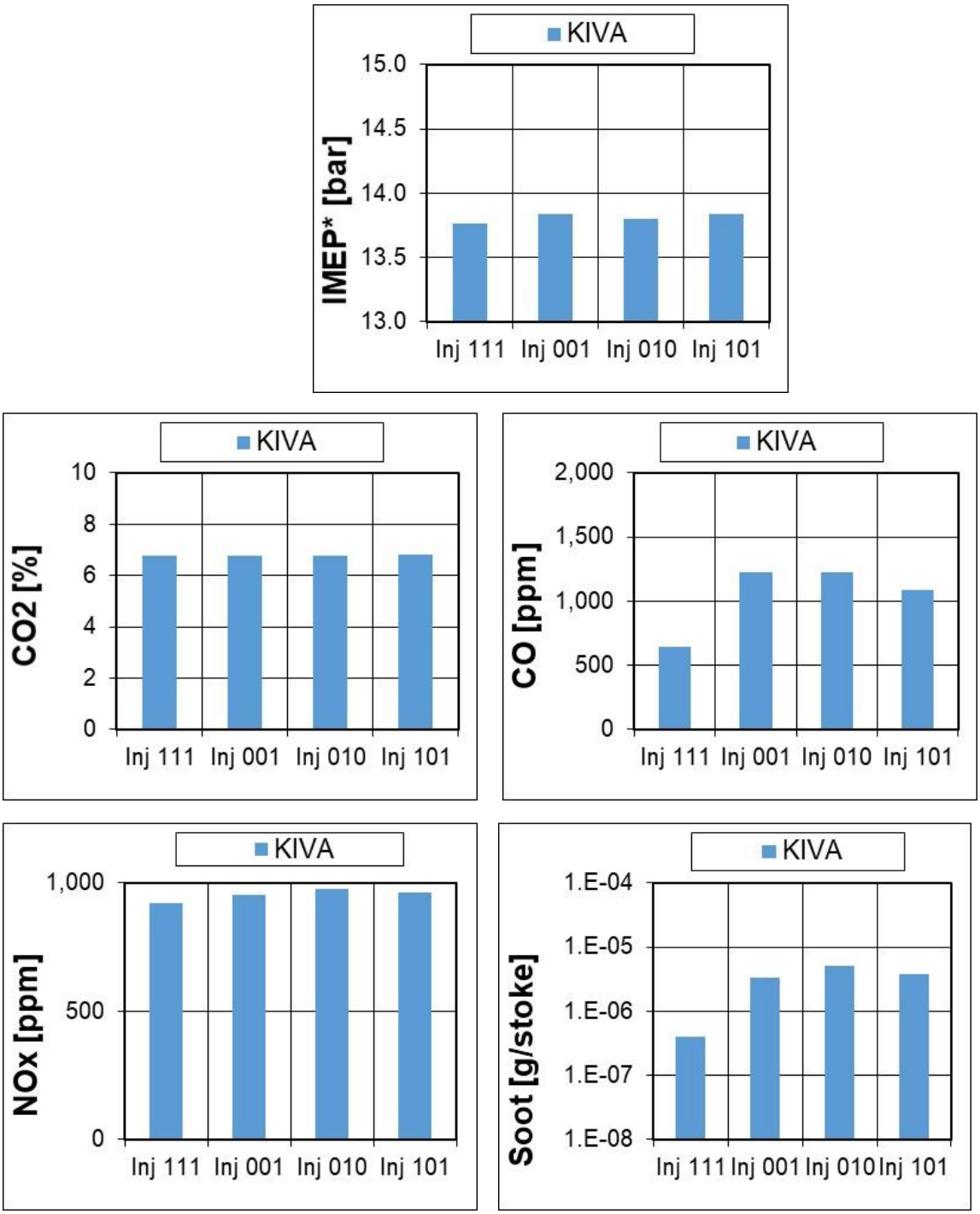

Figure 8.7 - Operating point NG52, influence of injection strategies on DF combustion on CO_2 and pollutant emissions

When the diesel injection law is anticipated, the combustion process begins in advance and is shorter (figure 8.8). There is a shift towards the TDC of Rohr and, at the same time, a higher peak value. As a result, there is a peak increase in both pressure in the cylinder and temperature, while these move towards the TDC. This leads to an increase in NOx emissions (+11%) (figure 8.9). On the other hand, anticipating the diesel injection law has a

positive effect on IMEP* (+2%), while CO, CO_2 and soot emissions do not change significantly. Opposite trends are observed if the diesel injection law is delayed.

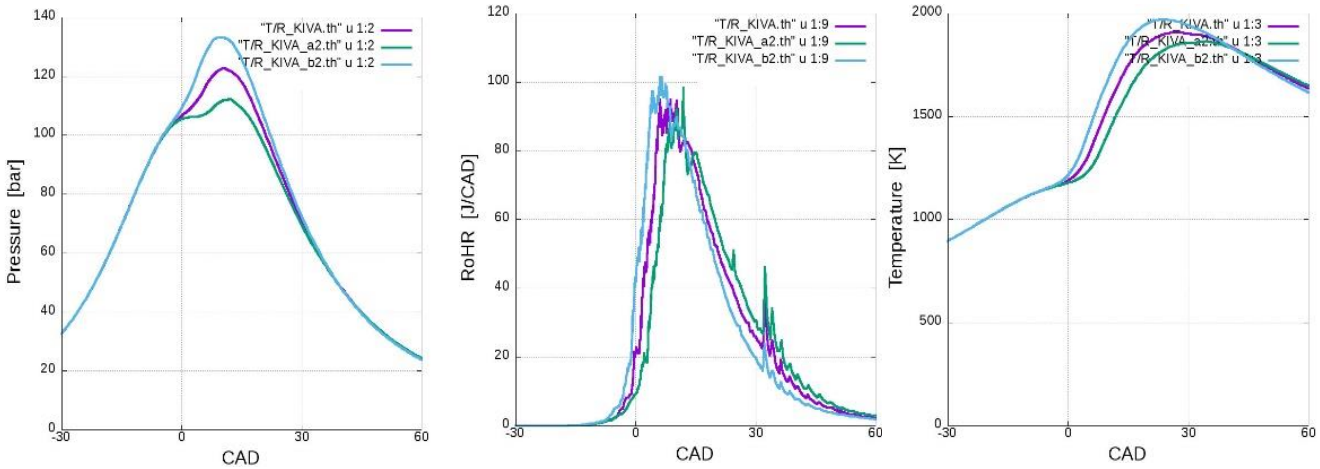

Figure 8.8 - Operating point NG52, influence of diesel injection timing on DF combustion on in-cylinder pressure, Rate of Heat Release, in-cylinder temperature, gross Indicated Mean Effective Pressure

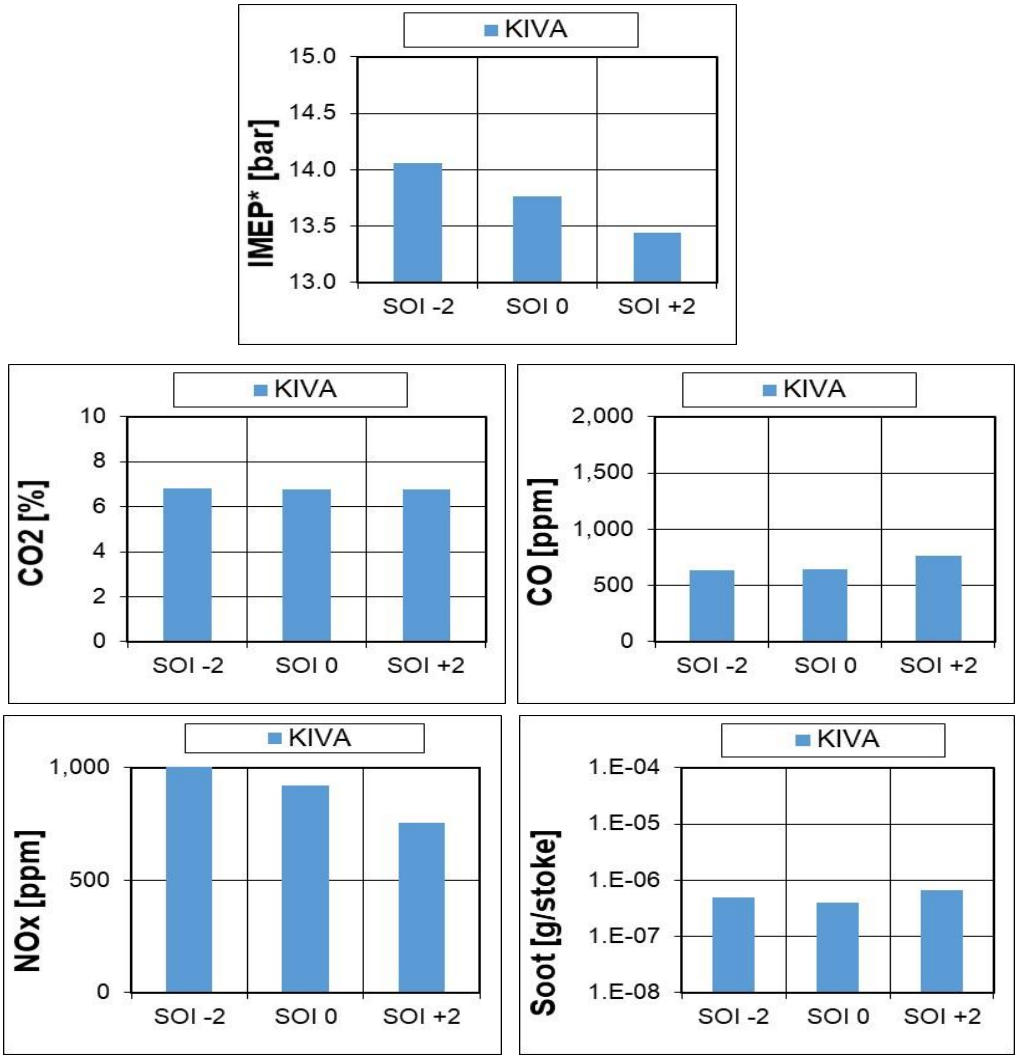

Figure 8.9 - Operating point NG52, influence of diesel injection timing on DF combustion on CO_2 and pollutant emissions

8.5 Conclusions

With the validated model KIVA-3V, it is therefore possible to predict, with good precision, the in-cylinder pressure compared to the same parameter acquired experimentally, the parameter RoHR and CO_2 emissions. In addition, the model allows dependence on the replacement rate of NG for the remaining CO, UHC and NOx emissions, but not on the absolute values.

Anticipating the triple diesel injection law (pilot, pre, main), normally adopted in the engine point taken into account in this validation, 3000 rpm - 265 [Nm] / BMEP = 12 [bar], and with the replacement rate of diesel with NG equal to -60% diesel fuel + 52% NG, leads to an improvement in performance (improvement IMEP*: +2%), at the expense of higher NOx emissions (+11%).

9 Interchangeability between NG and biogas in DF operation using diesel as the high reactivity fuel

9.1 Introduction and aim

In this chapter, renewable fuel such as biogas is considered. The choice of these fuels is strategic in terms of the containment of greenhouse gases if we consider the CO_2 balance in the biomass life cycle.

Table 9.1[39] shows the ranges within which the main biogas elements and the relative ranges of values of the main characteristics may vary:

Constituents	**Range**
CH_4 [vol. fraction - %]	30÷73
CO_2 [vol. fraction - %]	20÷40
N_2 [vol. fraction - %]	5÷40
O_2 [vol. fraction - %]	0÷5
H_2 [vol. fraction - %]	1÷3
H_2S [vol. fraction - %]	0÷0.01
Properties	**Values**
Density [kg/m^3]	0.65-0.91
Octane number [-]	130
Auto-ignition temperature [°C]	632-813
Lower Heating Value [MJ/Nm^3]	10÷25

Table 9.1 - Chemical and physical characteristics of biogas[39]

The use of biogas in place of NG in DF combustion mode was studied using the KIVA-3V model. In this specific case, 3D-CFD analysis was conducted for the dual biogas-diesel feed, taking three different biogas mixtures, comparing the DF NG-diesel operation in the engine point corresponding to 3,000 [rpm] - 177 [Nm] / 8 bar BMEP; the "-80% Diesel + 74% NG" DF case was used as reference.

A comparison was also made between biogas-diesel DF operation and a biogas-powered SI generator to assess the benefits in terms of CO_2 and BTE emissions.

This analysis is published in “Application to micro-cogeneration of an innovative dual fuel compression ignition engine running on biogas”.[125]

9.2 3D-CFD model description and validation

First, simulations were carried out taking into account the same low-reactivity NG fuel used in the previous section, consisting of methane (96%), ethane, propane and nitrogen; then pure methane (CH_4) and 3 different biogas compositions were tested (BG50, BG65 and BG75).

- 75 vol% CH_4 / 25 vol% CO_2 (BG75),
- 65 vol% CH_4 / 35 vol% CO_2 (BG65);
- 50 vol% CH_4 / 50 vol% CO_2 (BG50).

The main characteristics of the 5 different mixtures are shown in table 9.2.

By a combination of experimental measurements, all simulations were considered to have the same initial physical conditions (in-cylinder pressure, temperature, turbulent kinetic energy, turbulence length scale and swirl ratio).

This is used to isolate the effects of the CO_2 in the premixed charge on the performance.

In addition, to ensure the same energy at the premixed charge, the same CH_4 mass is adopted in the simulations of biogas-diesel combustion DF and CH_4-diesel combustion DF, taken as a reference. In this way, when the presence of CO_2 in the premixed charge increases, the air mass is reduced, which results in a reduction of AFR.

		NG	**CH_4**	**BG50**	**BG65**	**BG75**
Composition [vol %]	N_2	1.0%	0.0%	0.0%	0.0%	0.0%
	CH_4	96.0%	100.0%	50.0%	65.0%	75.0%
	C_2H_6	2.5%	0.0%	0.0%	0.0%	0.0%
	C_3H_8	0.5%	0.0%	0.0%	0.0%	0.0%
	CO_2	0.0%	0.0%	50.0%	35.0%	25.0%
Density	kg/m^3	0.694	0.668	1.255	1.079	0.962
LHV	MJ/kg	49.00	50.00	13.31	20.12	26.05
LHV	MJ/Nm^3	34.00	33.40	16.70	21.71	25.05
WI[126]	MJ/Nm^3	44.71	44.76	16.33	22.89	27.98

Table 9.2 - Fuels considered: composition and main properties

The comparison between the simulation and experiments for cases CH_4 and NG is reported in the following figure 9.1-2. For NG, the code correctly reproduces the combustion process for this operating point, as evidenced by the in-cylinder pressure trace and heat release curve.

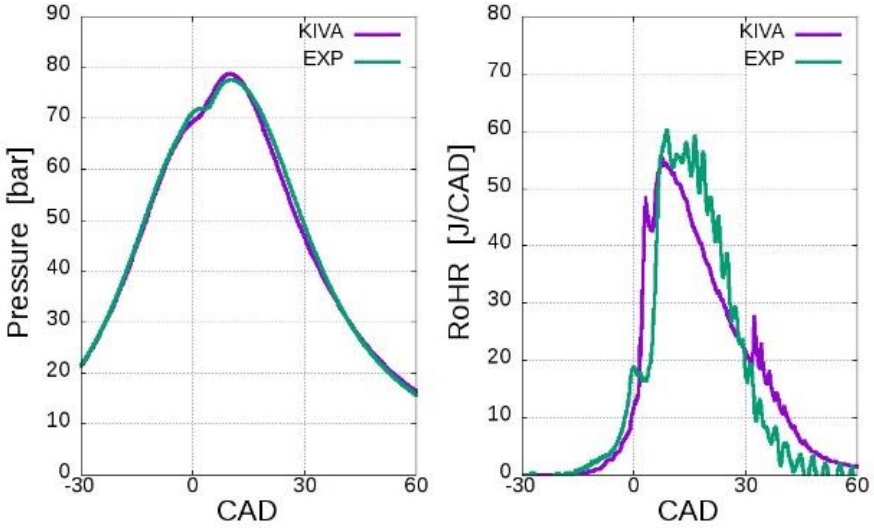

Figure 9.1-2 - Comparison between simulations and experiments: in-cylinder pressure (left) and Rate of Heat Release (right) for the case NG

In the following figure 9.1-2, the comparison between the model and the experimental one is reported using CH_4: as expected from the previous result, there is no evident difference when passing from NG (96% of the methane) to pure methane.

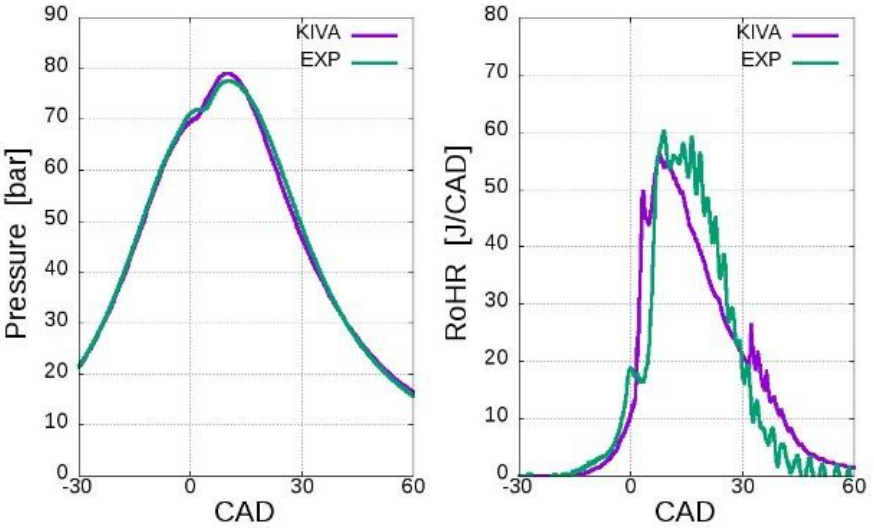

Figure 9.3-4 - Comparison between experimental and numerical results: in-cylinder pressure and RoHR; premixed charge: CH_4-air mixture

As shown in table 9.2, the biogas mixture properties are not so similar to those of NG and CH_4, with particular reference to the LHV and the Wobbe Index (WI). The WI parameter

gives an indication of how similar gaseous fuels can be, and thus interchangeable in SI engines: close values in this index are due to the comparability of AFR and laminar flame velocity[13]. While it is possible to increase the amount of pre-mixed fuel to balance lower values of LHV for biogas mixtures, more expedients are needed to compensate for the difference between different WI values.

9.3 Results and discussions

The diagrams below (figure 9.5-6) compare the curves with the three different biogas mixtures, BG50 (50% CH_4), BG65 (65% CH_4) and GB75 (75% CH_4) and the base curve (100% CH_4), for what concerns in-cylinder pressure and RoHR.

As the percentage of CO_2 increases, in the first part of the combustion the RoHR decreases slightly, while its peak clearly decreases. As a result, the peak in-cylinder pressure is reduced (drops from 79 [bar] up to 72.5 [bar]) with a slight elongation of the combustion phase. This results in a deterioration of the combustion efficiency (about -4% for BG50, about -2% for BG65 and about -1% for BG75) and of IMEP* (about -7% for BG50, about -4% for BG65 and about -2% for BG75). The reason for this lies in the presence of CO_2 in the biogas that acts as an inert gas.

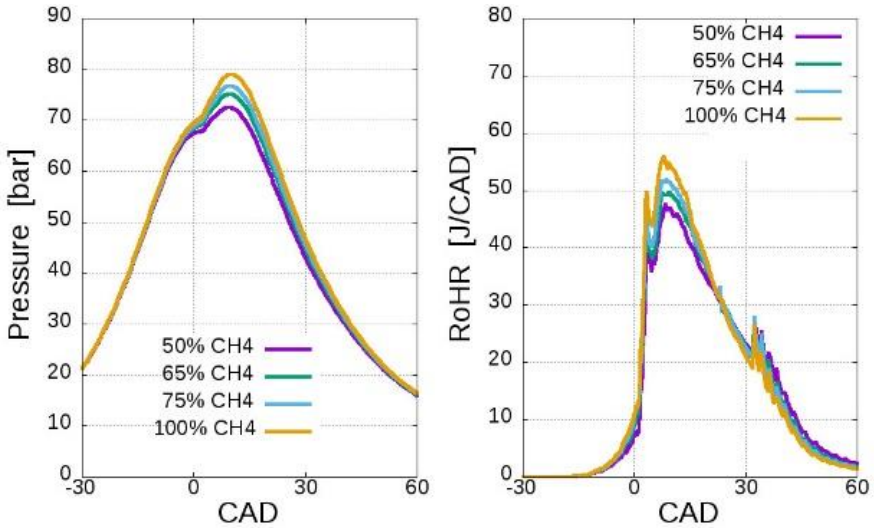

Figure 9.5-6 - Comparison between BG50 (50% CH_4), BG65 (65% CH_4), BG75 (75% CH_4) and 100% CH_4: in-cylinder pressure (left) and Rate of Heat Release (right).

Compared to the reference case ("-80% Diesel fuel +74% NG" DF case at 3,000 [rpm] – 177 [Nm] / 8 [bar] BMEP), Start of Injection (SOI) was anticipated by 1, 2, 3 and 4 CAD for all cases, with the aim of recovering the lost efficiency due to the presence of CO_2. The following figures 9.7-12 show the simulation results for BG50, BG65 and BG75 respectively.

Advancing the law on diesel injection (purple lines: reference case), the Rohr moves towards the TDC. The peak in-cylinder pressure is higher because the combustion process becomes faster and more impulsive.

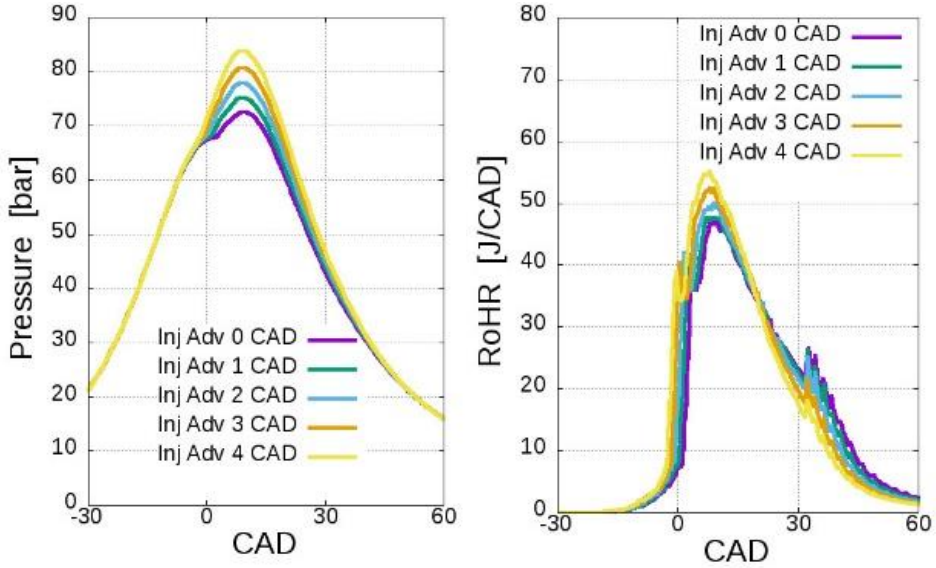

Figure 9.7-8 - Influence of Start of Injection on in-cylinder pressure (left) and Rate of Heat Release (right) for the case BG50.

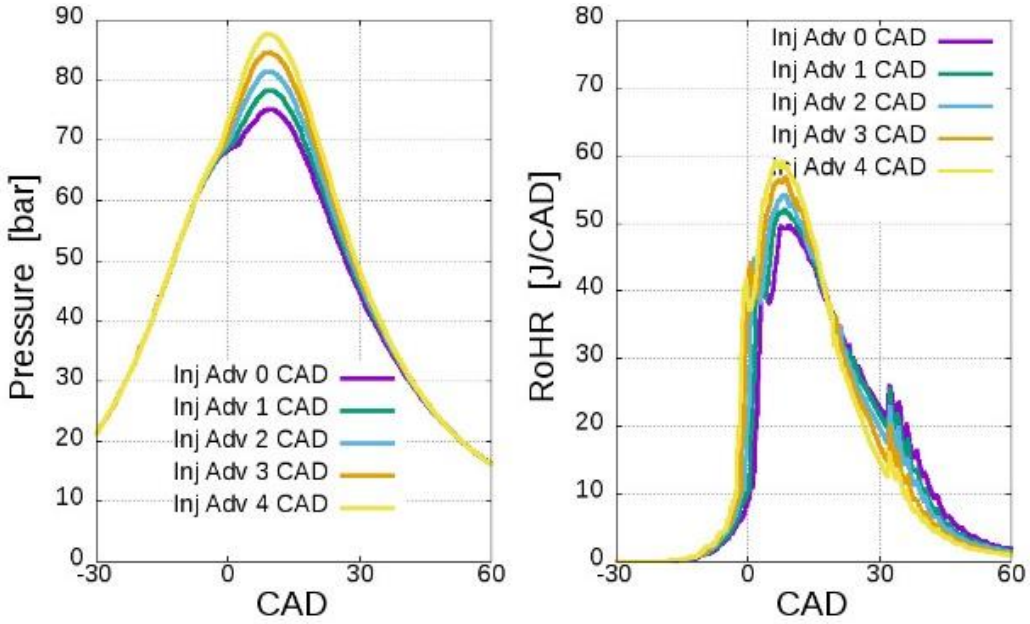

Figure 9.9-10 - Influence of Start of Injection on in-cylinder pressure (left) and Rate of Heat Release (right) for the case BG65.

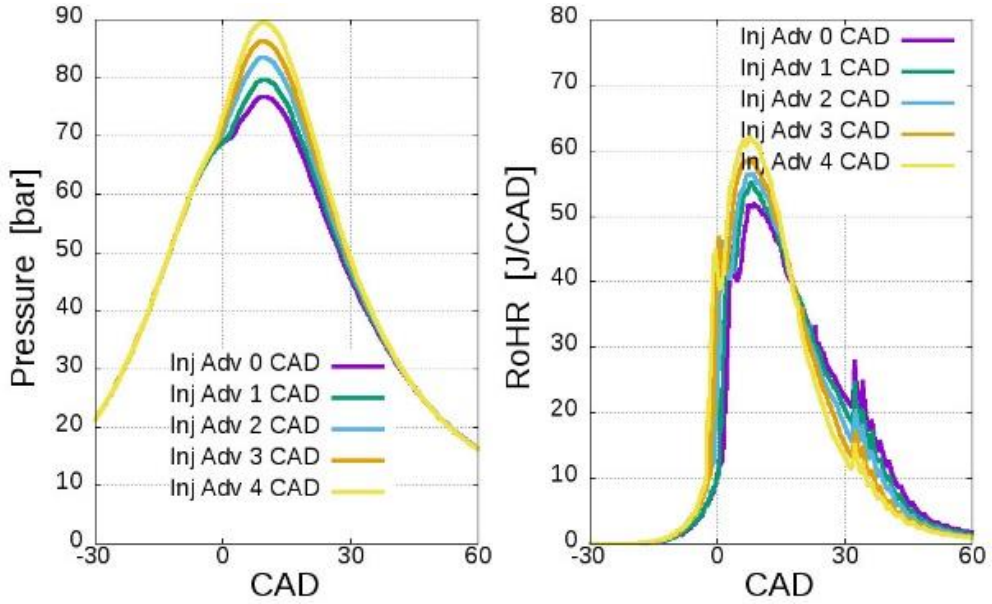

Figure 9.11-12 - Influence of Start of Injection on in-cylinder pressure (left) and Rate of Heat Release (right) for the case BG75.

Finally, figures 9.13-16 compare the combustion efficiency, the in-cylinder peak pressure and the gross Indicated Mean Effective Pressure (IMEP*) as results of all simulations.
Unlike in the previous section, the IMEP* parameter is calculated as the pressure volume integral from -40°CA to +60°CA ATDC rather than between IVC and EVO.
Performance recovery is observed by advancing the diesel injection strategy. In fact, for the BG75 case, the same combustion efficiency and IMEP* as in the reference case were achieved with an advance of 1 CA, while for the BG65 and BG50 cases it was necessary to anticipate by 2 and 4 CA respectively. In this way, the combustion process was accelerated and consequently the completion of the combustion and the increase in the production of work output are encouraged.

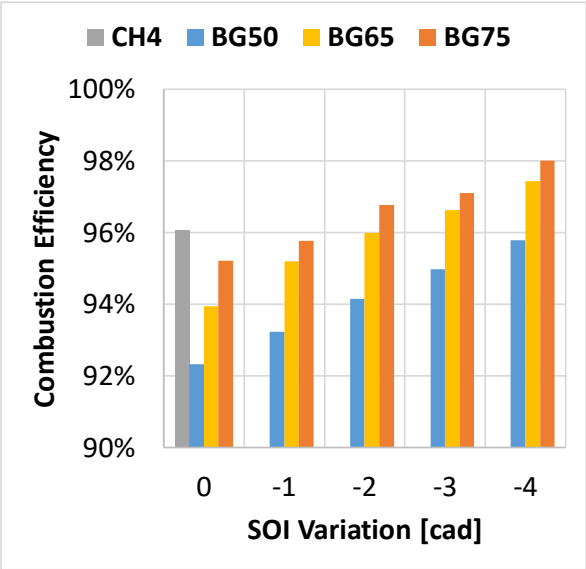

Figure 9.13 - Influence of SOI advance on combustion efficiency peak in-cylinder pressure

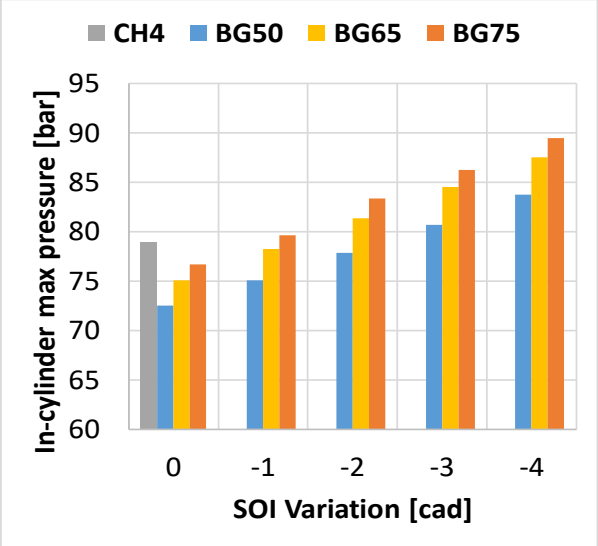

Figure 9.14 - Influence of SOI advance on peak in-cylinder pressure

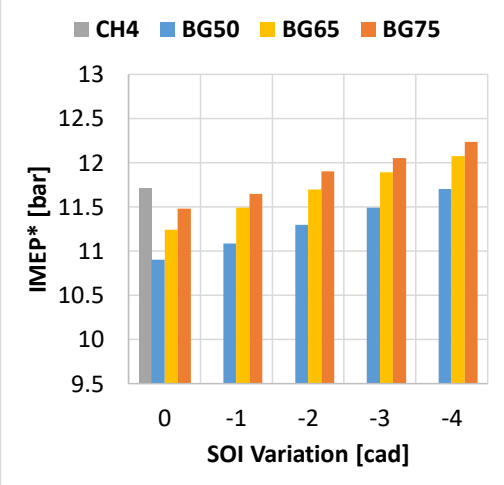

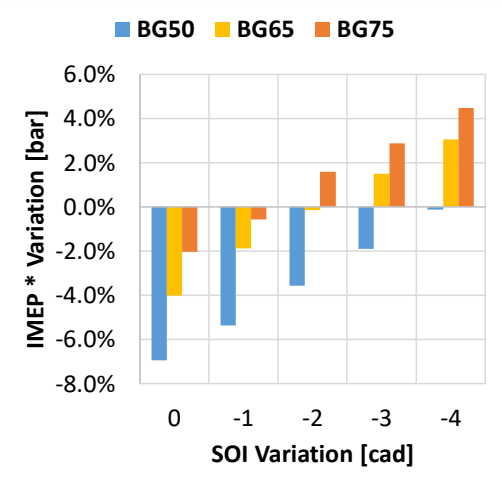

Figure 9.15-16 - Influence of SOI on IMEP* and IMEP* variation with reference to the CH4 case

9.4 Comparison with a conventional SI engine

The results reported in this analysis are compared with a group of commercial SI generators, running on biogas, in order to put the analysis into context and evaluate the practical benefits of the proposed DF concept. The engine taken into consideration has a power comparable to that at the highest load investigated during the experimental activity, as reported in section 4 (i.e., 83 [kW]). The main characteristics are shown in table 9.3 below[127]:

Manufacturer	HIMOINSA
Combustion Type	SI
Cylinders Lay-out	In-line
Number of cylinders	6
Air metering	Naturally aspirated
Bore x Stroke [mm]	130x150
Displacement [L]	11.946
Compression Ratio	12:1
Injection system	PFI
Rated rpm@50 Hz	1500
Max. Power at rated rpm [kW]	82.5
Max. BMEP at rated rpm [bar]	5.5
Fuel consumption at Max. Power, rated rpm [Nm^3/h]	36.8
BSFC at Max. Power, rated rpm [g/kWh]	513.8
Max. Specific Power, rated rpm [kW/L]	6.9

Table 9.3 - SI gen-set running on biogas: parameters of the reference[133]

The maximum power value reported above refers to a biogas mixture composed of 65% by volume of methane and 35% by volume of CO_2. Thus, the G65 case with SOI optimised above is considered, also for the proposed DF CI engine. As already mentioned, timing optimisation allows the same combustion efficiency and IMEP* as the basic NG engine.

For the SI generator set the table shows a fuel consumption of 36.8 [Nm^3/h] at the maximum power of 82.5 [kW]. Fuel consumption is also reported for other partial loads[127]:

- load 75% (61.9 [kW]): fuel consumption = 29.9 [Nm^3/h],
- load 50% (41.3 [kW]): fuel consumption = 23 [Nm^3/h],
- load 25% (20.6 [kW]): fuel consumption = 15.9 [Nm^3/h].

On the DF biogas-diesel engine, a single operating condition was studied, corresponding to 3,000 [rpm] and 177 [Nm] / 55.5 [kW], and some hypotheses to extrapolate the performance on different loads are listed below:

- the speed of 3,000 [rpm] is always maintained,
- the correct engine calibration, as a diesel injection strategy and boost pressure, maintains the same combustion and thermodynamic efficiency, measured for the reference case,
- with constant engine revolution speed and combustion mode maintained, Friction Mean Effective Pressure (FMEP) should remain constant.

The comparison between the two engines DF biogas-diesel is reported in figure 9.17. A greater BTE is observed over the entire power range, due to the greater thermodynamic and pumping efficiency that the CI engine guarantees. For throttle losses of the SI engine, higher at low loads, the improvement achieved in these conditions reaches 34%. At the point corresponding to 3,000 [rpm] - 177 [Nm] / 55.5 [kW], fuel economy of 21% is achieved.

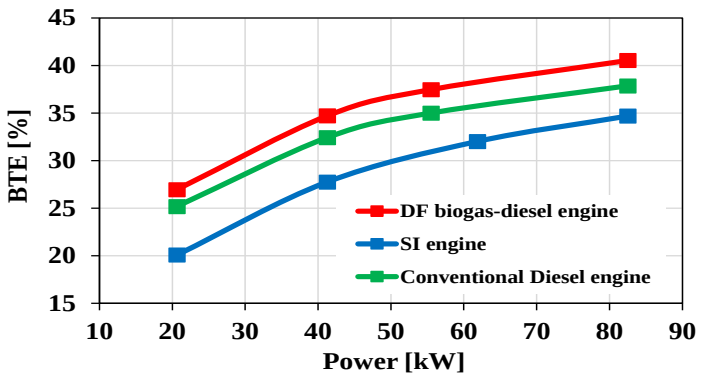

Figure 9.17 - Comparison DF biogas-diesel engine - SI generator set engine - conventional diesel engine

9.5 Conclusions on model descripted

These simulation results confirm that the composition of the biogas does not affect the engine performance in DF mode, without any intervention on combustion strategies. However, in order to keep the fuel energy in the cylinders constant, the biogas flow rate must be carefully regulated when the CO_2 increases in the fuel blend. At the same time, reliable and cost-effective techniques exist to monitor the biogas composition, as described in[128].

However, the slight fall of BTE is compensated by the optimisation of the injection timing. A higher burning rate is observed, which improves both the combustion efficiency and the IMEP, thanks to the increase in injection advance.

In conclusion, the CFD results show that, by optimising the injection timing, it is possible to cancel the dependence of the performance of the DF engine on the biogas composition.

Compared to a conventional SI engine that delivers the same biogas power, the proposed dual-fuel CI engine offers the following advantages:

- Due to the increased efficiency of the thermodynamic cycle (higher compression ratio), BTE increases by about 20% for lower thermal losses and pumping;
- Due to the lower biogas consumption, a 20% reduction in CO_2 emissions;
- Simpler engine control system due to reduced sensitivity to biogas composition;
- Since the combustion chamber may remain the same, as it is not necessary to replace the pistons and install the ignition system, fewer components have to be changed in order to transform a diesel engine into a biogas engine;
- Reduced overall dimensions.

9.6 Application to micro-cogeneration of an innovative dual fuel compression ignition engine running on biogas

For the advantages presented here, an application study has been carried out for which the publication "Application to micro-cogeneration of an innovative dual fuel compression ignition engine running on biogas" has been published where it has been considered to be a medium-sized agricultural and zoo-technical holding whose activities include livestock farming, the cultivation of fields for animal feed and the production of milk and cheese. This company can also produce good quality biogas from cattle manure, agricultural waste and specific crops as fuel to power an engine for the cogeneration of thermal and electrical energy.

The typical electrical and thermal demand during one year of production has been taken into consideration and analyzed and the main purpose of the analysis has been the understanding of the best motor size and its hourly and seasonal management for maximise the use of its renewable sources (biogas or biomethane) and reduce the purchase of electricity and natural gas.

In figure 9.18 and 9.19, both winter and summer, the profiles of the thermal energy demand of a typical day are reported: the period in which the crop drying process is active is shown in the first graph, while the second one reports the required thermal profile for all the remaining 156 days of the year.

The main thermal uses are shown in Table 9.4.

Utilities	Thermal power [kW]
Crop drying	530
Heating and domestic water	25
Cheese production and milk pasteurization	37

Table 9.4. - Main thermal users of the farm

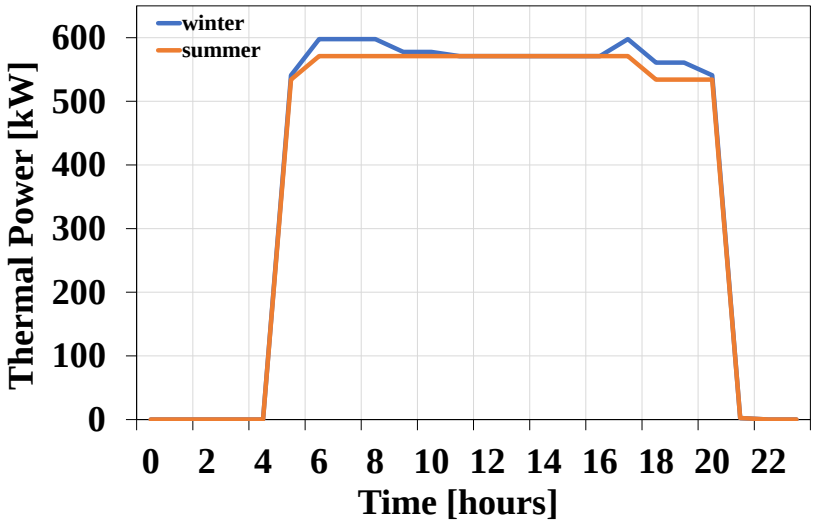

Figure 9.18 - Thermal power demand of the farm with crop drying process

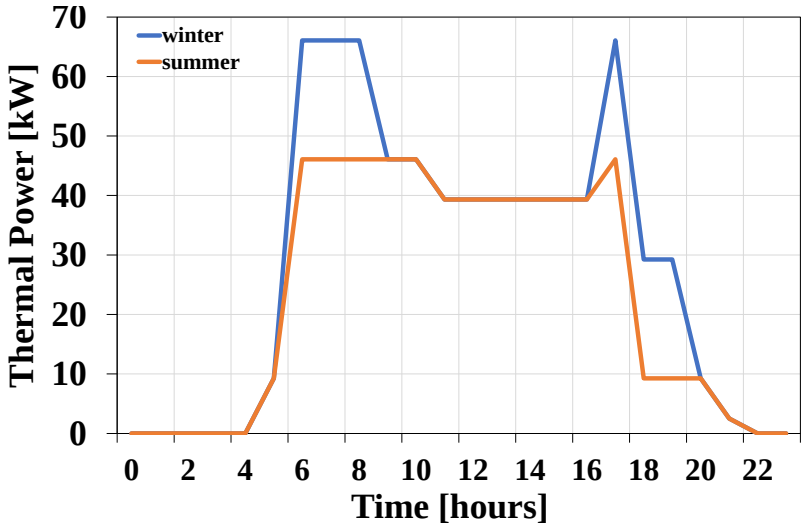

Figure 9.19 - Thermal power demand of the farm without crop drying process

The production needs of the company are fully covered by a maximum available power supply of 100 kW. Table 9.5 shows the main electrical utilities of the farm.

Users	Electric power [kW]
Dryer ancillaries	12
Grain grinding	10
Mixer	3
Feeders	6
Well pump	3

Stable ventilation and milking	6.75
Manure ramp	3
Waste collection	3
Waste separation	2.2
Lighting	2.6
Cheese production	10
Washing - cleaning	3
Circulation pumps	2
Manure treatment for fertilization	8
Milk storage	11
Milk shaker	3.5

Table 9.5 - Main electrical utilities of the farm

Figure 9.20 shows, both for winter and summer, the electricity demand profiles resulting from a typical company day.

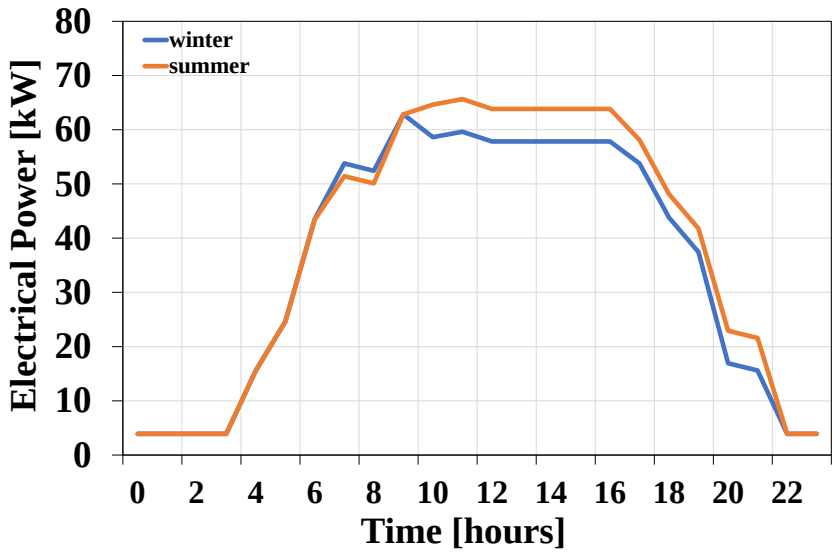

Figure 9.20 - Electrical power demand of the farm

The reference engine for the implementation of cogeneration is the one presented in the previous section, operating in DF mode, powered by CNG as low reactivity fuel.

It has been chosen to limit the maximum electrical power that can be supplied by the engine to 50 kWe, despite the company's peak electrical power is about 65 kWe.

The full-load operating point considered in this study is 3.000 rpm-177 Nm/8 bar BMEP (corresponding to 55,5 kW), and is among the points considered in the CNG-powered experiment presented in the previous section.

9.7 Economic analysis

The biogas that feeds the DF engine working as a micro-cogenerator, can be auto-produced in the company thanks to the installation of a plant on site.

In addition, the farm can be made completely independent from the supply of external fuel, thus reducing the cost of purchasing energy, if the biogas is used to replace the combustion of NG in the crop drying system.

It's good to make an economic analysis to understand the convenience of installing a biogas plant, as well as the cost of the micro-cogeneration system.

The annual cost for the purchase of energy to achieve its production processes is about 200.000 €, and these are divided as follows:

- electricity: 55.000 € (considered current average specific cost in Italy = € 0,18/kWh);
- GN: 140.000 € (considered current average specific cost in Italy = 0,7 €/Nm^3).

From the analyzed thermal energy needs profiles, considering that the dryer has an efficiency of 60%, 1.700.000 kWht are needed for the drying process of the crops, which correspond to a consumption of 181.000 Nm^3 of GN, for an annual cost of 126,000 €.

Biogas production takes place in an anaerobic digester that is fed mainly by cattle manure and partly by crops. The cattle manure allows a specific production of about 300 Nm^3/tonss, while that allowed by the crops is about 500 Nm^3/tons[19]. Assuming an average dejection per animal of about 10 tonnes/year, the average annual manure availability of the farm is over 1.800 tonnes, but only a limited part of it is used for biogas production. The thermal demand of the dryer is reduced because crops are used in the digester. In particular, keeping the working period of 200 days and 16 h/day, the thermal power required decreases from 530 kW to 502 kW. For the production of biogas, the annual quantities of cattle manure and crops destined for the relevant installation are shown in Table 9.6.

	Quantity [ton/year]	**Biogas production [Nm^3/year]**
Cattle manure	576	173,000
Crops	87	43,250

Table 9.6 - Annual amounts of cattle manure and crops employed for biogas production

For the electricity demand of the biogas plant, the electricity demand of the farm increases by 12%.

Having an electrical power absorbed by 2 kW auxiliaries, the micro-cogeneration system can ensure a maximum electrical power of 48 kW, while the peak thermal power is about 55 kW. Anaerobic digestion requires about 25% of the heat produced by the system.

With the use of this self-production plant, are reported in figure 9.21 the new profiles of demand for electricity, while in figure 9.22 and 9.22 are reported the new profiles of thermal power.

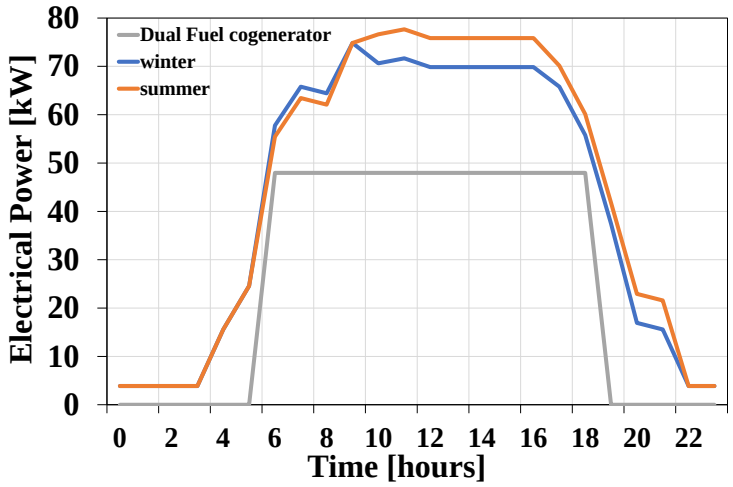

Figure 9.21 - Electricity supplied by the micro-cogenerator (grey line) and electricity demand of the farm with biogas plant (blue and orange lines)

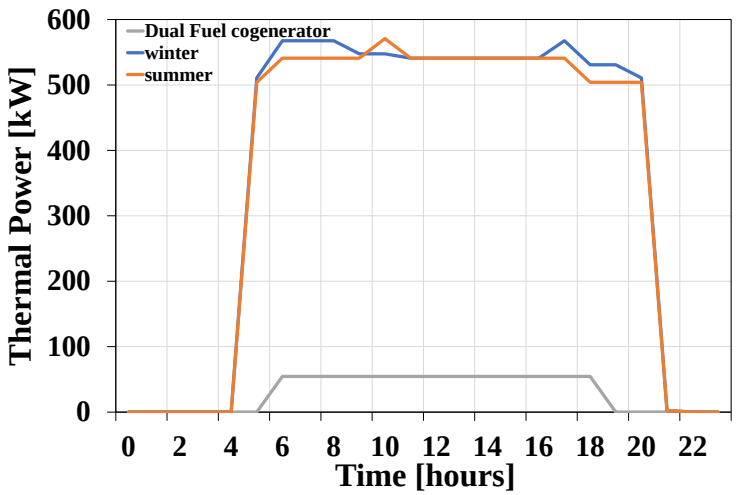

Figure 9.22 - Thermal power supplied by the micro-cogenerator (grey line) and thermal power demand of the farm with biogas production plant (blue and orange lines)

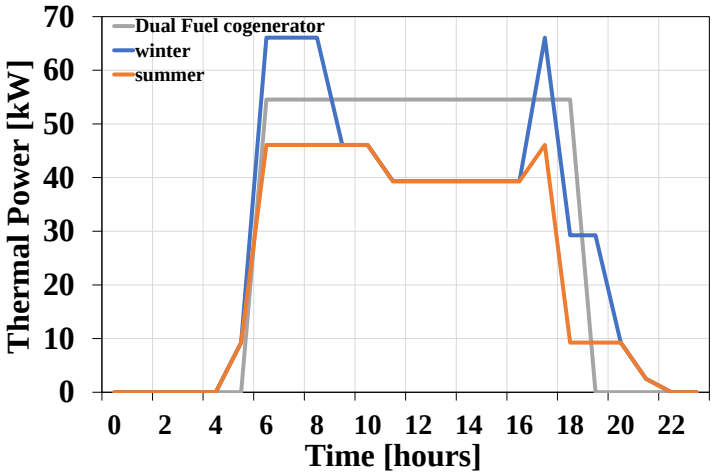

Figure 9.23 - Thermal power demand of the farm with biogas production plant (blue and orange lines), without crop drying process and thermal power provided by micro-cogeneration (grey line)

Savings are 22,450 €/year, as the purchase of electricity from the public grid is reduced by 50% in one year (from 308,000 kWh to 152,000 kWh), thanks to micro-cogeneration.

Micro-cogeneration also provides 10% of the thermal energy needed during the crop drying period. Thanks to the production of biogas, the expenditure for NG, previously equal to 140.000 €/year, is completely eliminated, although the purchase of diesel is more than doubled (from 4.200 €/year to 10.200 €/year).

We still have to consider a loss of about 7.500 €/year for a harvest quota no longer available for sale.

The maintenance costs of the biogas plant and micro-cogeneration system should be taken into account in the economic balance sheet. With ordinary maintenance rates of 200 €/kWe and extraordinary maintenance rates of 50 €/kWe, this expense is about 13.000 €/year.

Therefore, the investment involves a cash flow of 136.000 €/year.

Taking into account also the connection to the public electricity grid and the authorization procedures, the entire plant (biogas plant and micro-cogeneration system) requires an investment of 450,000 €. Considering a precautionary discount rate of 1%, the resulting cash flow, calculated over 10 years, leads to an effective net value of € 750,000 and allows an economic return in 5.3 years. Still considering an expenditure of about 100.000 € after 10 years for the complete replacement of the micro-cogeneration system and some components of the biogas plant, the actual net value after 15 years will be 1.340.000 € (figure 9.24).

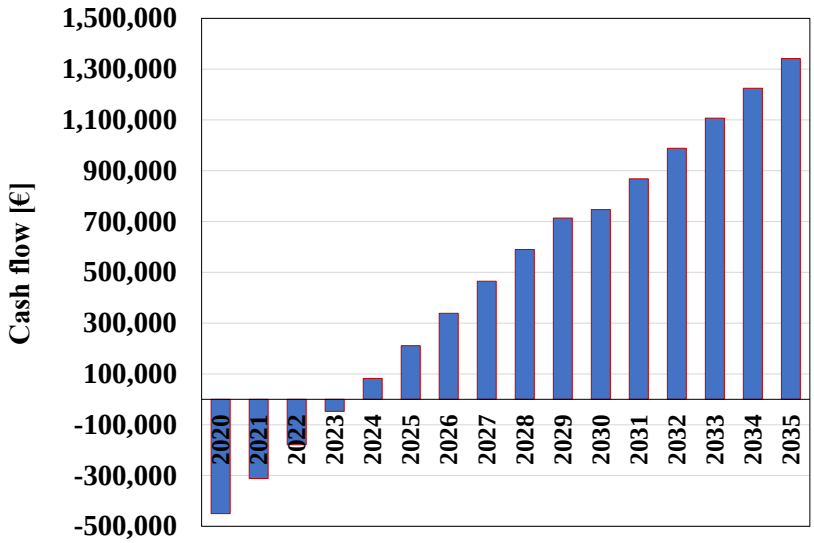

Figure 9.24 - Net actual value

The new dual-fuel self-produced biogas-powered unit, compared to a conventional diesel engine, can reduce fuel costs and significantly reduce soot emissions.

Therefore, the micro-cogeneration associated with an anaerobic digester for biogas production, for the case study considered, after 15 years can provide a net effective value of € 1.340.000.

Compared to a conventional SI engine that delivers the same biogas power, the proposed dual-fuel CI engine brings the following advantages:

- thanks to the increased efficiency of the thermodynamic cycle (higher compression ratio), increase of BTE by about 20% for lower thermal losses and pumping;
- thanks to the lower biogas consumption, a 20% reduction in CO2 emissions;
- simpler engine control system for reduced sensitivity to biogas composition;

- since the combustion chamber may remain the same, as it is not necessary to replace the pistons and install the ignition system, to transform a diesel engine into a biogas engine a smaller number of components must be changed;
- reduced overall dimensions.

The new dual-fuel self-produced biogas-powered unit, compared to a conventional diesel engine, can reduce fuel costs and significantly reduce soot emissions.

10 Numerical Investigation of Dual Fuel combustion on a Compression Ignition Engine fuelled with Hydrogen/Natural Gas blends

10.1 Introduction

A solution that can further reduce the carbon footprint of internal combustion engines is represented by the use of hydrogen.

The use of hydrogen as the only source of power for internal combustion engines is a challenge for the control of its combustion, characterised by its high flame speed that produces rapid increases in the pressure in the combustion chamber[129]. On the contrary, the use of hydrogen in a mixture with other fuels, one of which can be natural gas, leads to more controllable combustion. Moreover, hydrogen can be easily transported in gas pipelines mixed with natural gas, without the need to build infrastructures dedicated to its individual transport.

This has given impetus to some studies aimed at analysing the effects on combustion and emissions of hydrogen-natural gas mixtures, with different relationships between the two fuels. Among these, of particular interest are studies in which such mixtures are used as low reactivity fuel in dual-fuel engines.

With this in mind, a numerical analysis of the dual-fuel hydrogen-natural gas and diesel combustion on the reference engine, previously described in Chapter 4, was carried out with the aim of evaluating the effects in terms of performance and pollutant emissions.

As for the case presented on the CNG, the work described in this chapter consists in a 3D-CFD analysis carried out by the same version of KIVA-3V, to understand what may be the effects of the different H_2-NG mixtures on the particularities of combustion of a light turbocharged compression ignition engine.

From the experimental campaign conducted, the model was validated under operating conditions corresponding to:

- 3,000 [rpm] - Brake Mean Effective Pressure (BMEP) = 2 [bar] / 44 [Nm] and in this operating condition was considered the replacement -80% Diesel fuel +135% NG;
- 3,000 [rpm] - Brake Mean Effective Pressure (BMEP) = 8 [bar] / 177 [Nm] and in this operating condition was considered the replacement -80% Diesel fuel +74% NG;
- 3,000 [rpm] - Brake Mean Effective Pressure (BMEP) = 12 [bar] / 265 [Nm] and in this operating condition was considered the replacement -60% Diesel fuel +52% NG.

A series of simulations were created based on these conditions in DF H_2/NG-diesel mode, where the influence of a fraction of H_2 mole ranging from 0% to 50% was investigated.
It is assumed that the combustion simulations are carried out at closed valves, starting at the Intake Valve Closing (IVC, -130 [CA °AFTDC]) and stopping at the Exhaust Valve Opening (EVO, 112 [CA °AFTDC]).
In order to minimise the computational effort, the restart function is used when the influence of the diesel injection strategy has been evaluated: in this way, the compression stroke is simulated only once, from IVC to -40 [CA °AFTDC], while, starting from the last point, all other calculations are carried out, those characterised by different injection laws.
For the validation of the model, the parameter of the specific work transferred from gas to piston in the range from -40 [CA°] to 114 [CA°] after TDC (EVO) is also considered. The formula used for the calculation of this parameter, referred to as gross Indicated Mean Effective Pressure (IMEP*), is as follows:

$$IMEP^* = \frac{\int_{-40\ CA°\ AFTDC}^{EVO} pdV}{V_d}$$

where the displacement of the engine unit is represented by V_d, while in-cylinder pressure and volume are p and V.

10.2 Combustion model validation (3,000 [rpm] - BMEP = 2 [bar] / 44 [Nm], case −80% Diesel fuel +135% NG)

The first engine condition considered (3,000 [rpm] - BMEP = 2 [bar]), in this case with the replacement in energy terms of 80% of diesel with 135% of NG, optimised in the parameters related to the rail pressure and the Start of Injection (SOI), which also led to the reduction of the amount of NG injected.
With regard to the validation of the numerical model, both for ND and DF operations, the following figures 10.1(a-d) show the comparison between the numerical and experimental results on cylinder pressure and on the apparent heat release rate (AHRR). The experimental trends are quite close to the numerical ones.

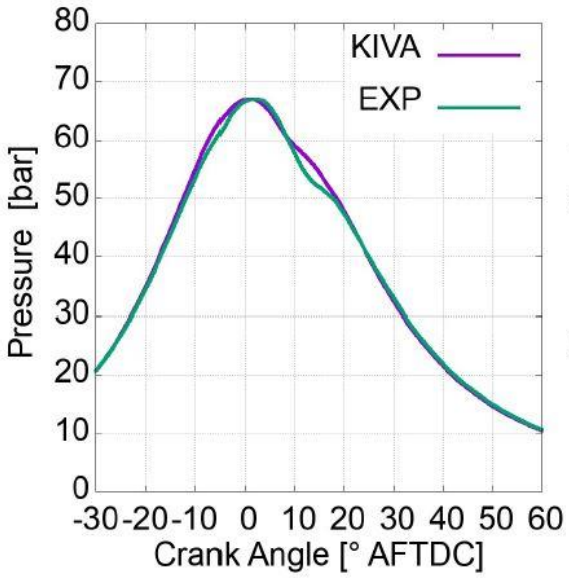

(a) - ND in-cylinder pressure

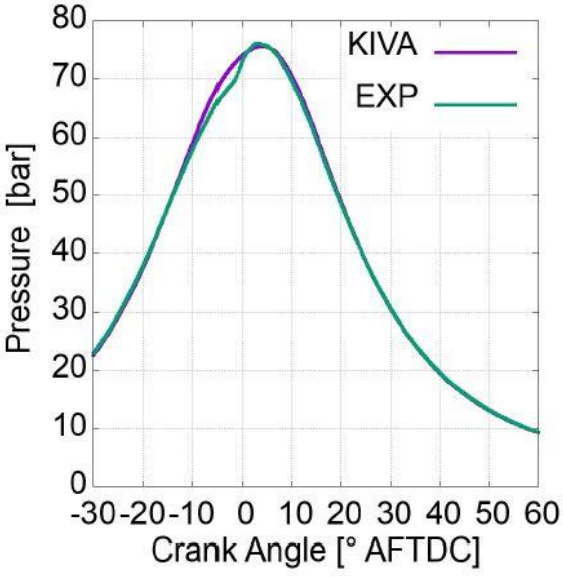

(b) - DF NG/diesel in-cylinder pressure (-80%ND +135NG% case)

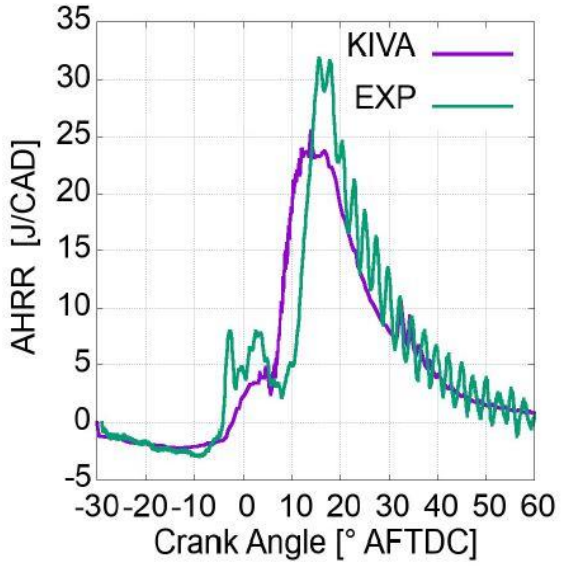

(c) - ND AHRR

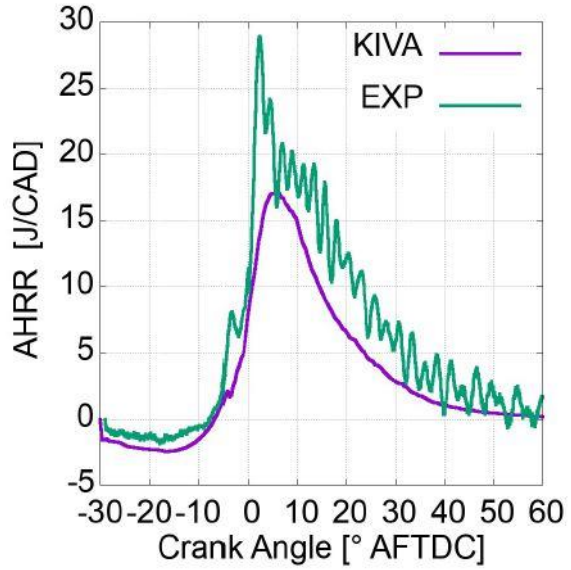

(d) - DF NG/Diesel AHRR (-80%ND +135NG% case)

Figure 10.1 (a-d) - ND and DF NG-diesel operation at 3,000 [rpm] – 177 [Nm], case −80% Diesel fuel +74% NG. Comparison between experimental and numerical in-cylinder pressure and AHRR

The following table 10.1 shows a comparison between IMEP* and peak in-cylinder pressure parameters between simulation and experiments. The consistency of the numerical model is confirmed for both combustion modes.

		ND	DF
Numerical IMEP*	[bar]	6.64	5.82
Experimental IMEP*	[bar]	6.67	5.75
IMEP* difference	[%]	-0.446	1.294
Numerical peak in-cylinder pressure	[bar]	67.07	75.65
Experimental peak in-cylinder pressure	[bar]	67.04	76.20
Peak in-cylinder pressure difference	[%]	0.022	-0.720

Table 10.1 - Comparison between experimental and numerical IMEP* and peak in-cylinder pressure for ND and DF NG-diesel cases at 3,000 [rpm] – BMEP = 2 [bar]

10.2.1 H2-NG blend simulations

As seen in the chapter describing the NG-DF experimental results, the 44 [Nm] operating point is a particular condition in which, compared to ND mode, it was necessary to insert a higher energy content with NG instead of diesel fuel. Therefore, the operation in DF mode with only NG is already disadvantageous at the start, as the combustion is difficult to proceed with: the combustion efficiency is in fact very low.

The volumetric fractions of the various components used to represent Low-Reactivity Fuels mixtures (LRF) H_2-NG are examined in table 10.2 below.

		NG	5vol% H_2	10vol% H_2	20vol% H_2	30vol% H_2	40vol% H_2	50vol% H_2
Composition [vol%]	CH_4	96.000	91.200	86.400	76.800	67.200	57.600	48.000
	C_2H_6	2.500	2.375	2.250	2.000	1.750	1.500	1.250
	C_3H_8	0.500	0.475	0.450	0.400	0.350	0.300	0.250
	N_2	1.000	0.950	0.900	0.800	0.700	0.600	0.500
	H_2	0.000	5.000	10.000	20.000	30.000	40.000	50.000

Table 10.2 - Composition of the H_2-NG blends analysed

In the following table 10.3, for this case, the characteristics of interest of the in-cylinder conditions to vary the percentage of hydrogen replaced are given. The dosage of the mixture is extremely lean, so in this situation, with its low ignition energy, hydrogen helps the completion of combustion.

The parameters given in this table are: the mass of each main fuel component; the actual Air-Fuel (A/F) ratio of the premixed charge, $(A/F)_{premix}$; the correspondent stoichiometric value $((A/F)_{st,premix}$ and the relative A/F ratio λ_{premix}; the total A/F ratio (considering the injected diesel fuel), $(A/F)_{tot}$; the correspondent values of stoichiometric A/F$((A/F)_{st,tot}$ and Lambda λ_{tot}.

	CH_4 [mg]	H_2 [mg]	$(A/F)_{premix}$ [-]	$(A/F)_{st,premix}$ [-]	λ_{premix} [-]	$(A/F)_{tot}$ [-]	$(A/F)_{st,tot}$ [-]	λ_{tot} [-]	H_2 Energy Fract. [%]	H_2 Mass Fract. [%]
NG	15.10	0.00	49.56	16.84	2.94	23.57	16.46	2.58	-	-
5vol%H_2	14.62	0.10	50.02	16.95	2.95	23.66	16.55	2.58	1.34%	0.58%
10vol%H_2	14.46	0.21	50.30	17.08	2.94	23.79	16.66	2.58	2.77%	1.21%
20vol%H_2	13.87	0.45	51.37	17.37	2.95	24.10	16.89	2.59	6.02%	2.68%
30vol%H_2	13.28	0.74	52.37	17.72	2.95	24.43	17.18	2.58	9.79%	4.45%
40vol%H_2	12.42	1.08	54.21	18.16	2.98	24.84	17.54	2.60	14.41%	6.73%
50vol%H_2	11.55	1.50	55.90	18.76	2.98	25.45	18.01	2.60	19.90%	9.60%

Table 10.3 - Main features of the H_2-NG blends analysed

10.2.2 Results and Discussion

Influence of hydrogen content and start of injection

From the comparison between the pressure traces (figure 10.2(a)) and the AHRR (figure 10.2(b)) for the various replacements, in this case hydrogen does not lead to a dramatic increase in pressure peaks; also in terms of heat release, the combustion is not shortened, if anything the effect significantly increases the area under the traces of the AHRR and therefore the heat released by combustion.

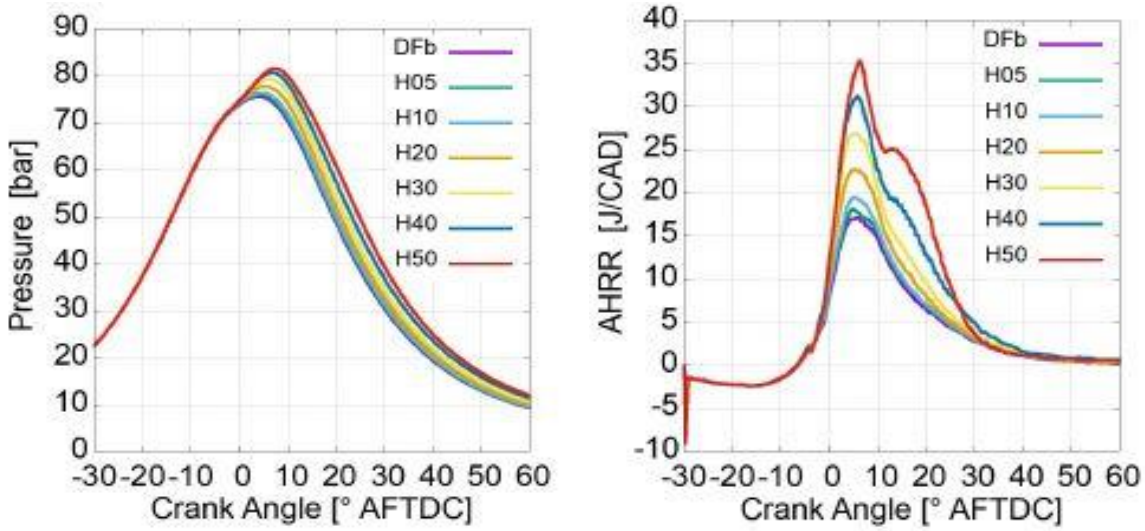

(a) *(b)*

Figure 10.2 - In-cylinder pressure (a) and Apparent Heat Release Rate (b) for different Hythane blends

A sweep of the diesel Start Of Injection (SOI) angle was studied to understand how this could have an effect on limiting the effects of H_2 enrichment on the peak in-cylinder pressure and PPRR. In particular, the diesel injection law was advanced up to 3 CAD and delayed up to 6 CAD, with steps of 1 CAD and keeping the DFb case as a reference.

There are 70 cases from the simulation of all H_2-NG mixtures, and for each SOI value (10 SOI and 7 mixtures). The simulation results were used to construct the contour maps shown in figures 10.3-6.

IMEP* values as a function of H_2 vol% and SOI diesel are represented in the colours shown in figure 10.3 (a-b). The value of IMEP* corresponding to the DFb case is represented by the continuous red line.

In this case, advancing the injection could be effective to further increase combustion efficiency and IMEP*. Below, the performance parameters are processed to define a possible strategy that can lead to improvement.

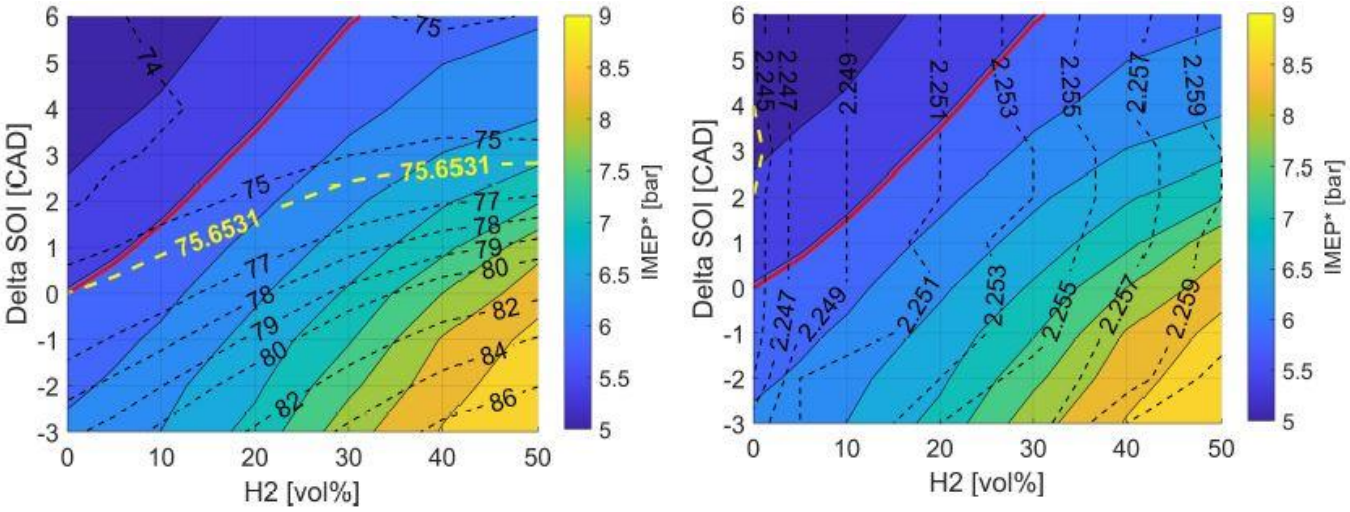

Figure 10.3 - Contour maps of IMEP* for different H_2 vol%-delta SOI combinations with peak in-cylinder pressure (a) and PPRR (b) levels superimposed

From the map in figure 10.3(a), it can be deduced that there is room for improvement in terms of IMEP*. The region to the left of the reference level (red line), where the IMEP* values are lower, is very narrow.

In addition, even in this case the iso-maximum reference pressure passes through areas where the IMEP* assumes values higher than the reference one: this means that all the points identified between the two curves, IMEP* and maximum pressure of case ND, offer the two-fold advantage of an increase in IMEP* with a low-pressure peak. In addition, the increase in IMEP* grows very rapidly, moving horizontally on the map, i.e., with the increase in the percentage of hydrogen replaced; in the same direction, the maximum pressure reached in-cylinder shows a much smaller growth. Therefore, it is deduced that the effect of hydrogen is excellent, always remembering the operating limit of hythane at 30% by volume. To obtain the highest IMEP* points we have to exploit the injection timing, but the maximum pressure increases faster.

As was already apparent from the pressure traces in figure 10.2(a), hydrogen does not generate high pressure gradients: as proof of this, in figure 10.2(b) we can see a very modest increase in the PPRR values, almost entirely dependent on the percentage of hydrogen replacement, in fact the iso-PPRR are almost vertical. In conclusion, from the observation of these two maps, it is possible to say firstly that there are large areas for which it is possible to move the parameters H_2 and injection timing to obtain better efficiency values, without affecting the structural strength of the engine; this is because both the pressure peak and its gradient reach low values.

The trends in combustion efficiency and overall efficiency, as shown in the maps in figure 10.4(a)-4(b) respectively, are very similar. In this engine condition, as already mentioned, there is overall low efficiency with the only replacement of NG compared to the base case ND, as it presents a highly lean mixture, hydrogen is the aid that facilitates the completion of combustion. In addition, the higher heat release, compared to the base case, is converted into pressure and therefore into useful work. Thus, facilitating the completion of combustion leads to better performance parameters.

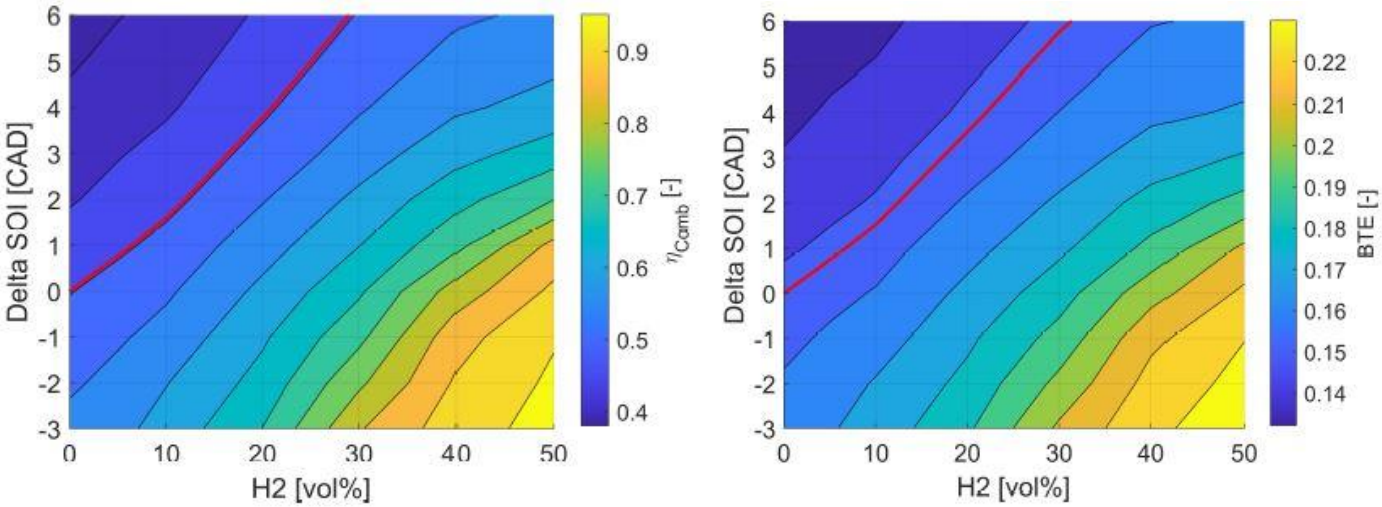

(a) (b)

Figure 10.4 - Contour maps of Combustion Efficiency (a) and BTE (b)

From the maps of the combustion parameters reported below, it is noted that the variation in the percentage of hydrogen results in practically no change in the CA50 (figure 10.5(a)). This is because, in this case, there is a twofold effect: on one hand, the H_2 speeds up the combustion, and at the same time there is more fuel involved, which tends to lengthen it, balancing the effects. Conversely, the dependence on the timing is practically linear, as the combustion is shifted depending on the moment in which it is injected.

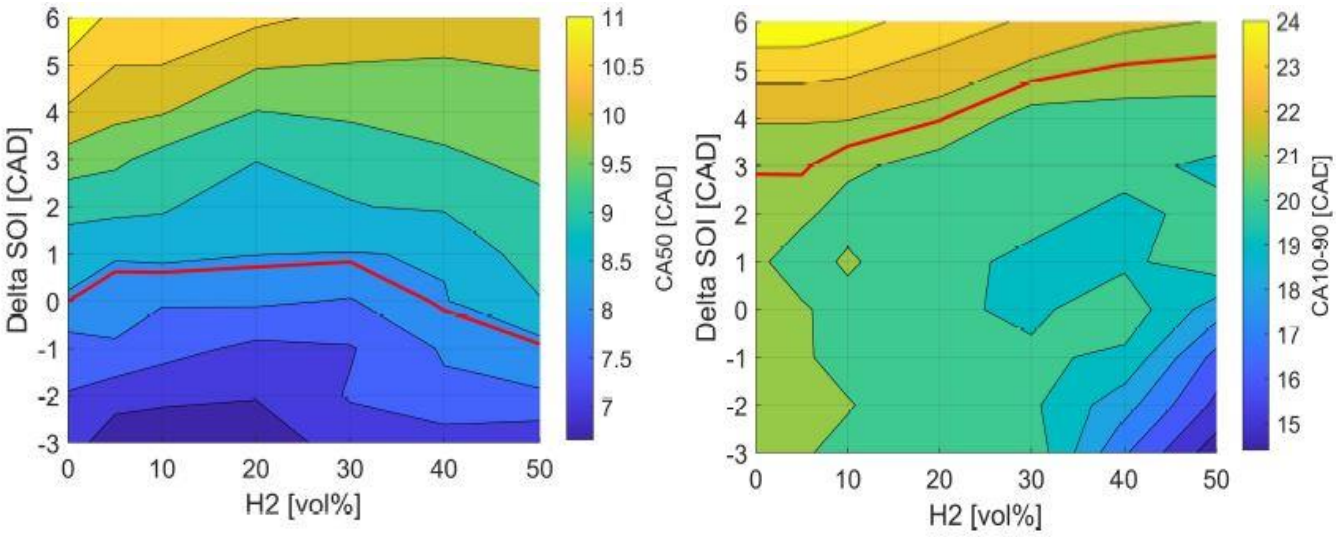

(a) (b)

Figure 10.5 - Contour maps of CA50 (a) and combustion duration CA10-90 (b)

Although the map of the duration of combustion represented in figure 10.5(b) presents trends that partly differ to those seen so far for the combustion duration parameters, the conclusions are similar to what just expressed for the parameter CA50, on the 50% burning position, that is to say the burning duration remains almost constant due to the two contrasting effects mentioned above.

Emissions

The specific gaseous emissions are reported in figures 10.6 (a-d) and are calculated as the ratio of the emission mass flow rate to the engine brake power (P).

Specifically, P is evaluated as follows:

$$P = IMEP^* V_d \frac{n}{2} \eta_i^* \qquad (2)$$

where V_d is the total displacement in, n is the engine speed and η_i^* is a correction parameter, calculated according the following formula:

Engine friction and pumping losses affect efficiency; for the following reasons, it can be considered independent of cases:

- Friction losses mainly depend on engine speed, which doesn't change, and on in-cylinder peak pressures, that are quite similar;
- Pumping losses are related to the mass flow rate delivered by the engine, that is kept almost constant throughout the cases.

The effect on carbon monoxide represented in the map in figure 10.6(b) reflects the effect of hydrogen on the combustion efficiency. Since CO is an incomplete combustion product, this will be the higher the fewer oxidation reactions are completed. And this situation is facilitated in the very lean dosing condition seen in this engine condition. From figure 10.4(a) moreover, it can be deduced that, with the highest replacements of H_2 and with the highest values of injection timing, it is possible to increase the efficiency from the situation base, from around 50%, up to approximately 90%.

Similar considerations can be made for unburned hydrocarbons represented in figure 10.6(c); at the same injection timing, for replacements up to the threshold of 30% of H_2 these are more than halved. In the same way, it is already possible to obtain an optimal containment of these emissions at the lowest replacement values if we act on the timing.

With the replacement of H_2 it could be expected that, due to violent heat releases associated with high temperature values, favourable conditions for dissociation reactions producing NOx are reached. In this case, these conditions would also benefit from a predominantly lean environment.

But looking at the figure 10.6(d), the trend of nitrogen oxides seems to be promising. In fact, even for the highest percentages of H_2replacement, the increase is extremely modest; this is probably due to the fact that low load is reached at low temperature values, even for the strong excess of air; nevertheless, hydrogen promotes combustion, which occurs and is maintained at lower temperature values, compared to other cases where sudden releases of heat occur. From the map it is then deduced how it is possible to reduce nitrogen oxides also by acting on injection delays, even for the highest H_2 replacements.

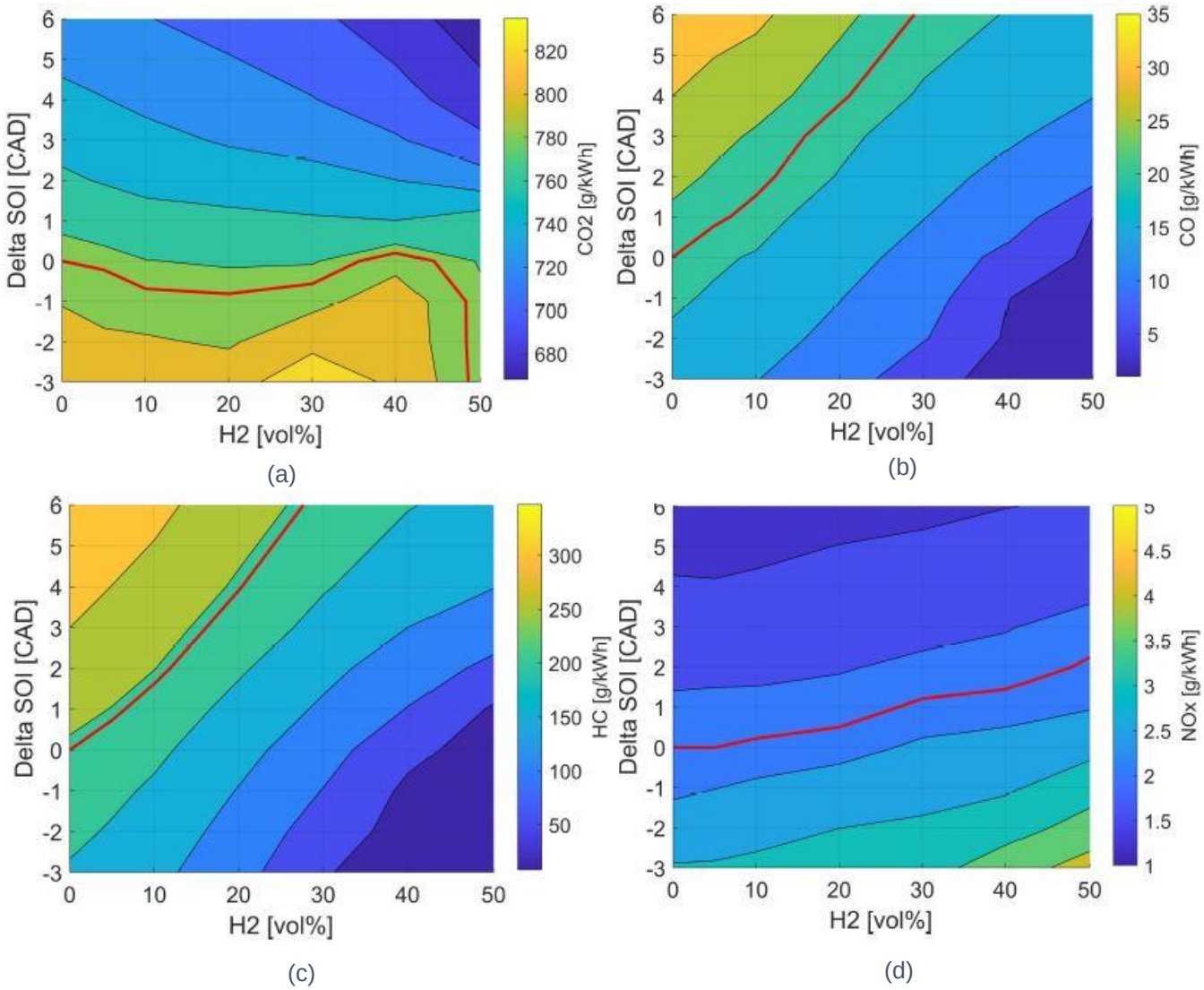

Figure 10.6 - Contour maps of CO2 (a), CO (b), UHC (c) and NOx (d)

10.2.3 Engine performance and emissions of selected operating points

Following the analysis of the maps above, the variation of the replacement rate and the injection timing, also for this condition at 44 [Nm], three significant points were chosen for the identification of a possible calibration that can lead to an improvement with respect to the basic condition:

- 30%H_2 - DeltaSOI = +2,5CA represented in figure 10.7(a): it was chosen to maintain a constant maximum pressure value;
- 30%H_2 – DeltaSOI = -3CA represented in figure 10.7(b), was considered to maximise overall efficiency, not exceeding the limit of volumetric concentration of hydrogen in the mixture of hythane;

- 5%H_2 - DeltaSOI = -3CA, to carry out a comparison on the emissions of CO and HC.

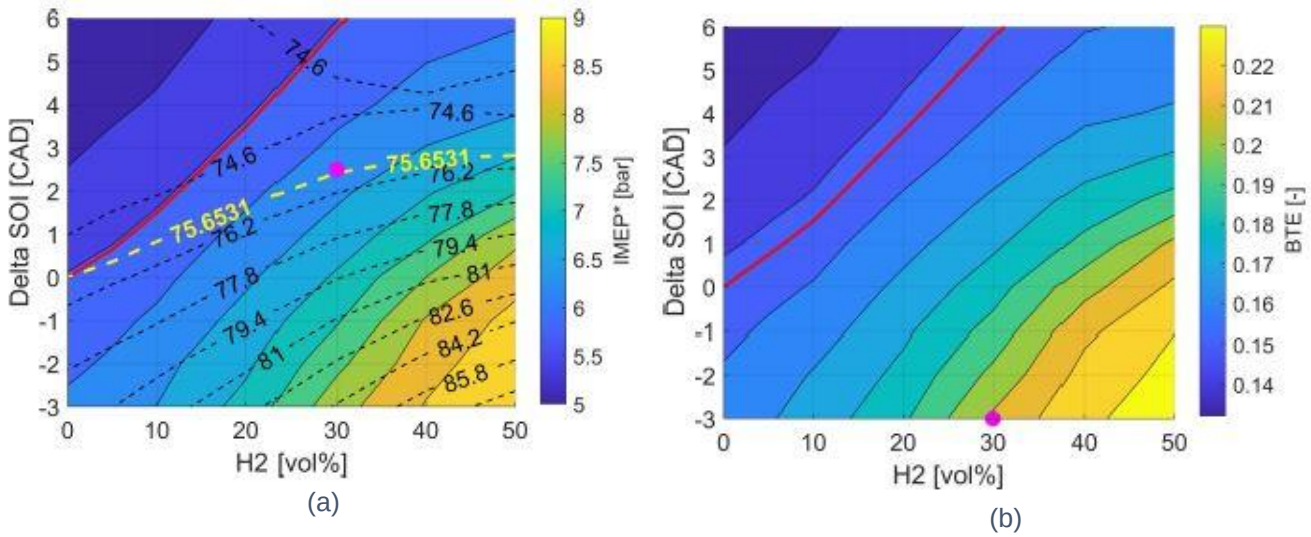

Figure 10.7 - Representation of points of interest on maps

Figure 10.7(a) is the combination that maintains the maximum pressure value equal to the base case, but increases the IMEP*: 30% H_2 and DeltaSOI = +3 CA. From figure 10.7(b), high replacements and high advances are used to return in the zone to maximum attainable BTE. For the low replacement point, reference should be made to CO maps in figure 10.6(b) and unburned hydrocarbons in figure 10.6(c).

The graphs in figure 8 show that in all three cases the effect of hydrogen on the performance parameters is positive, the main effect is on the increase in combustion efficiency. Clearly the point 30%H_2 DeltaSOI = -3 CA has better performance, for the other two points the increases are more limited.

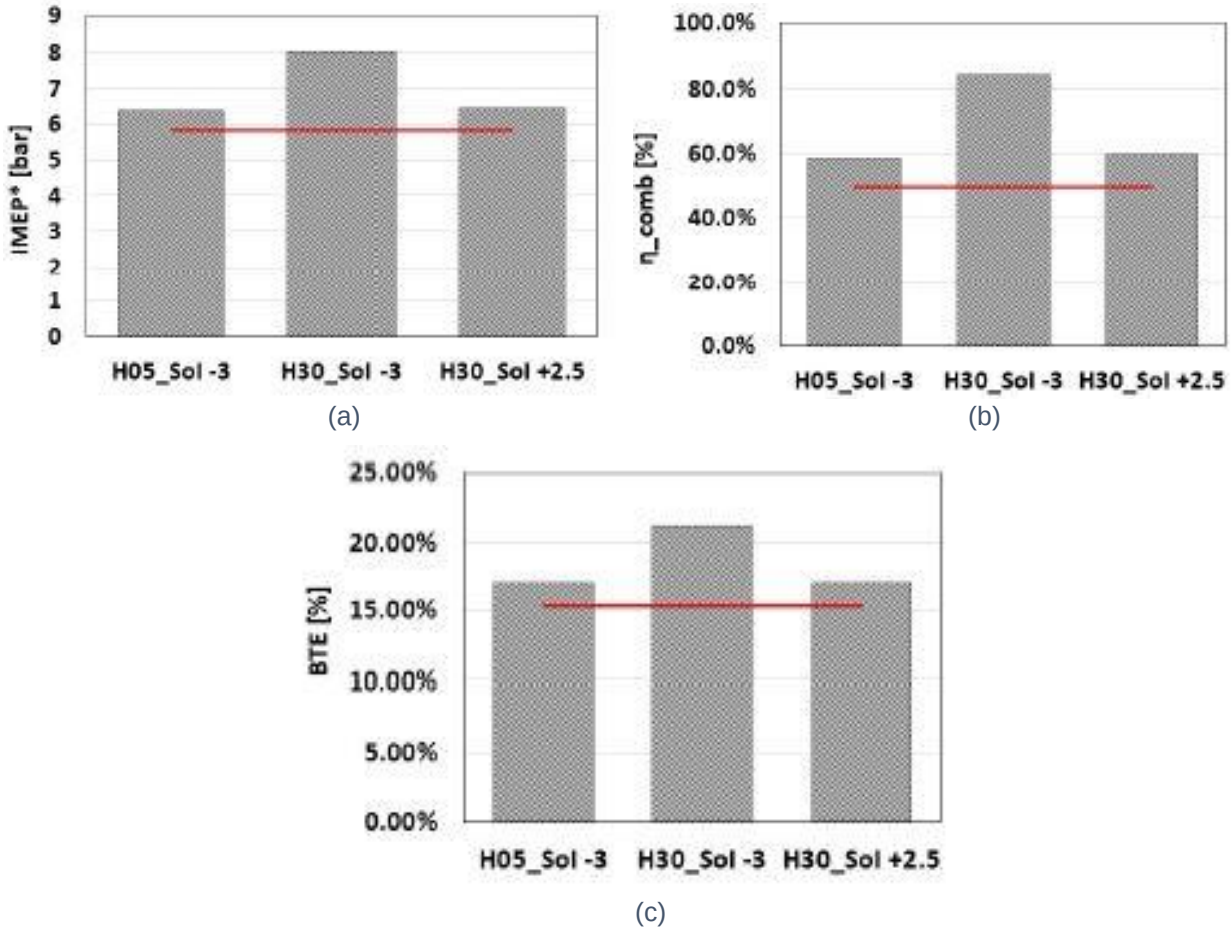

Figure 10.8 - Comparison of the performance parameters in the different significant points: (a) IMEP*, (b) ηcomb, (c) BTE

In terms of peak pressure (figure 10.9(a)), there is an increase for the 5% replacement, as well as for 10%; PPRR increases in all cases, but keeps well below the threshold value of 5 [bar/CAD]. From the observation of figure 10.8, the point 30% H_2 - DeltaSOI = -3 CA seems to offer better performance values. However, even for the other two points, the values reached are all acceptable in terms of structural strength and engine noise.

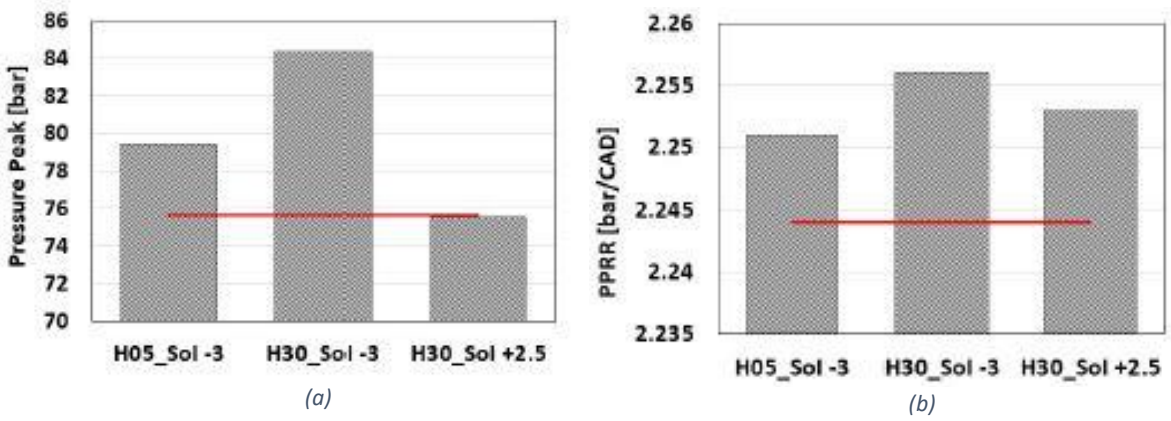

Figure 10.9 - Comparison of pressure peaks and PPRR at different significant points

Compared to the base case, the combustion parameters trend does not differ much and the differences remain substantially slight. As already mentioned, hydrogen tries to promote combustion, that in this low load condition, would proceed slower than other engine conditions in the base DF situation, involving greater mass of reagents in the cylinder and trying to speed up combustion.

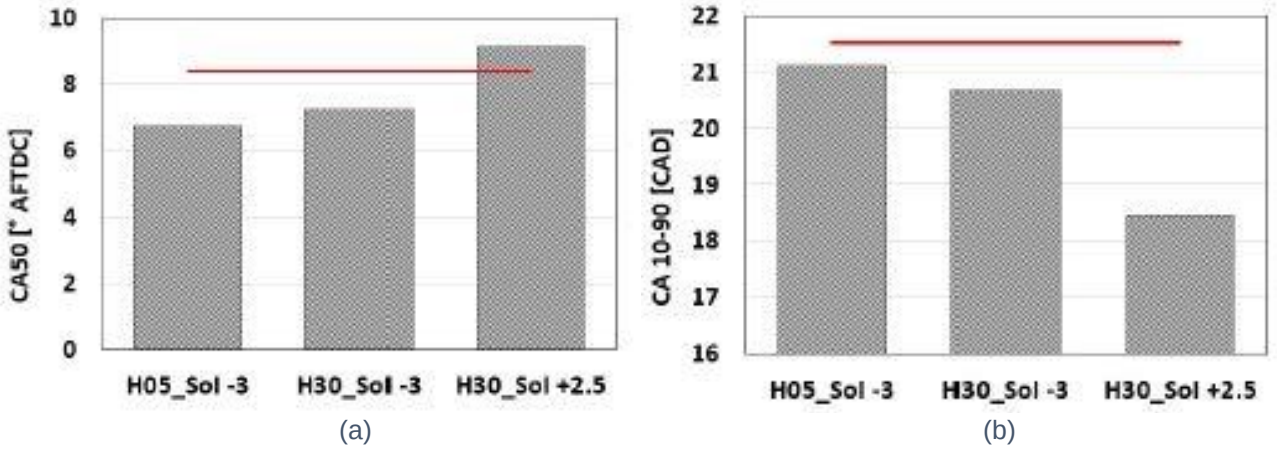

Figure 10.10 - Comparison of combustion parameters at different significant points: (a) CA50, (b) CA 10-90

With regard to emissions (figure 10.11), the effect of hydrogen is to facilitate the completion of combustion, reducing the products of partial combustion. However, in some cases, an increase in CO_2 is observed (figure 10.11(a)), as combustion takes place in a more complete way, so the products of partial combustion are reduced to the advantage of those of complete combustion. This is further supported by an increase in IMEP* and combustion efficiency for all three significant points.

Finally, the specific emission of nitrogen oxides in two out of three cases shows a modest increase, probably due to a local rise in ambient temperatures (figure10.11(d)).

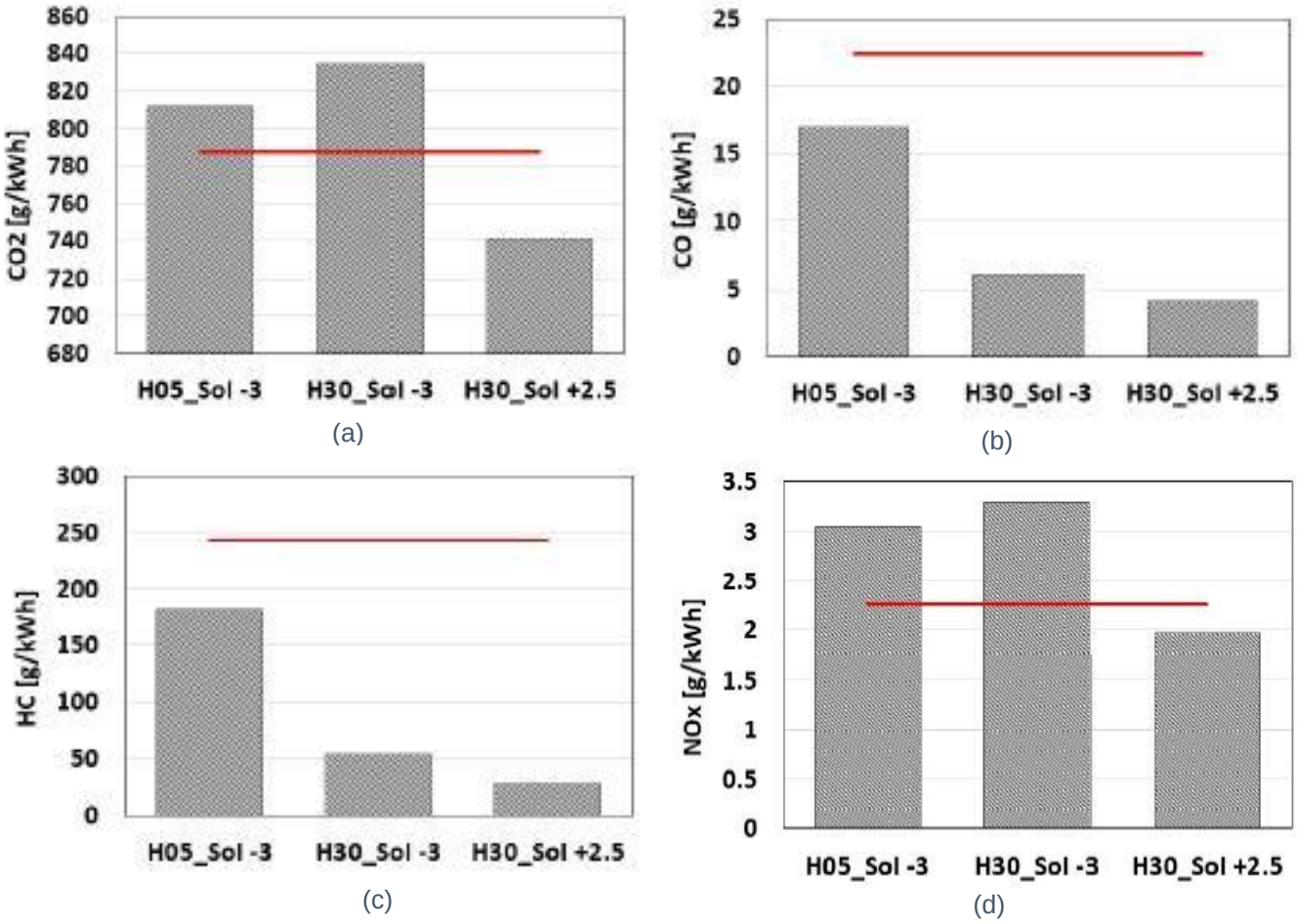

Figure 10.11 - Comparison of emissions at different significant points

10.2.4 Conclusion of 3,000 [rpm] - BMEP = 2 [bar] / 44 [Nm], case –80% Diesel fuel +135% NG

At this low engine load, it can be concluded that the effect of hydrogen helps to complete that lean combustion that, in the base case, has difficulty in being completed. In general, all the significant points analysed foresee almost exclusively advantages, excluding the small increase in nitrogen oxides and carbon dioxide, which can be contained at the highest replacements by delaying the injection compared to the base case (30%H_2 DeltaSOI = +2.5CAD). If on the other hand the aim is to maximise power and efficiency, it is necessary to intervene with the maximum percentage of replacement of H_2 and advancing the injection. With regard to the case with low hydrogen replacement, similar performances are obtained to those of the case with the greater delay and with 30% of hydrogen replacement, although the pollutant emissions worsen.

The choice between these two calibration cases should therefore take into account the actual percentage of hydrogen that is allowed to be mixed in hythane.

10.3 Combustion model validation (3,000 [rpm] - BMEP = 8 [bar] / 177 [Nm], case –80% Diesel fuel +74% NG)

The second engine condition considered (3,000 [rpm] - BMEP = 8 [bar] / 177 [Nm]), in this case with the replacement in energy terms of 80% of diesel with 74% NG and optimised in the parameters related to the rail pressure and the Start of Injection (SOI), allowed the reduction of the amount of NG injected.

Table 5 shows the main parameters for both the DF NG-diesel mode and the normal diesel mode in this engine condition.

With regard to the validation of the numerical model, both for ND and DF operations, the following figures 10.12(a-d) compare the numerical and experimental results on cylinder pressure and apparent heat release rate (AHRR). We can see how the experimental trends are quite in agreement with the numerical ones.

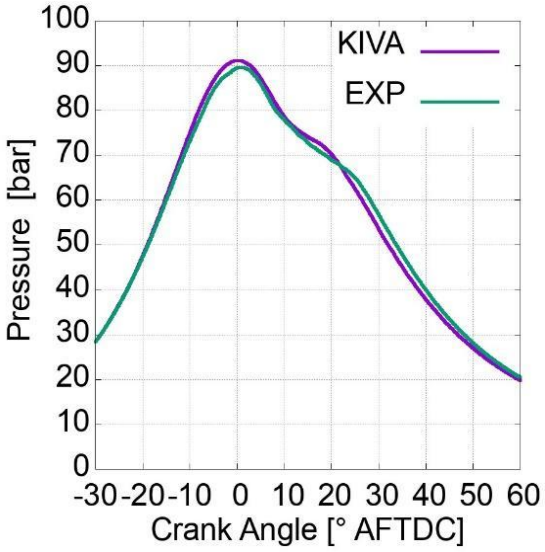

(a) - ND in-cylinder pressure

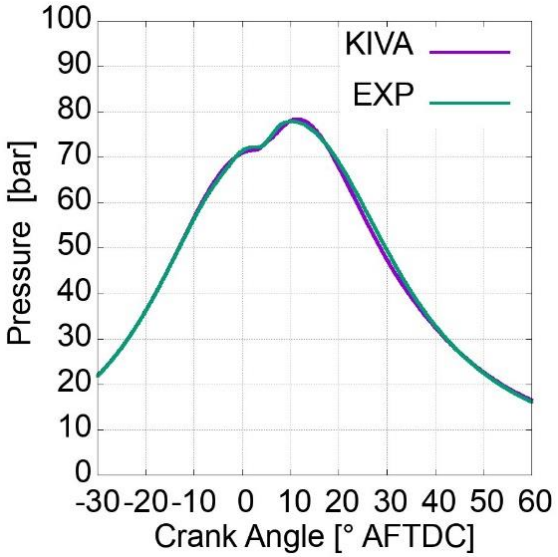

(b) - DF NG/diesel in-cylinder pressure (-80%ND +74NG% case)

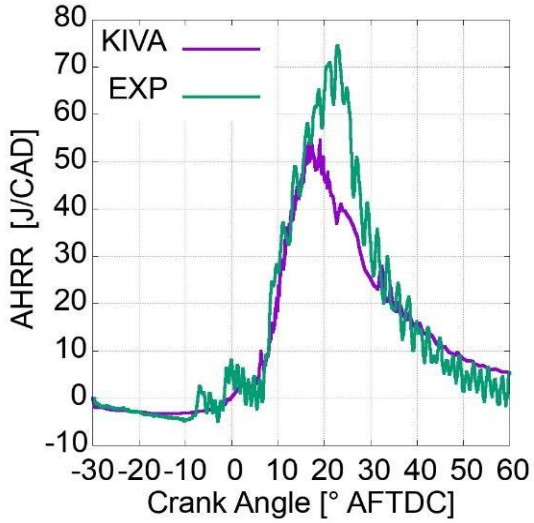

(c) - ND AHRR

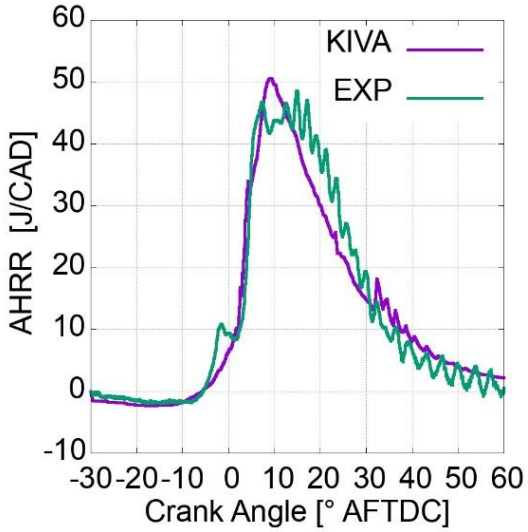

(d) - DF NG/Diesel AHRR (-80%ND +74NG% case)

Figure 10.12 - ND and DF NG-diesel operation at 3,000 [rpm] – 177 [Nm], case −80% Diesel fuel +74% NG. Comparison between experimental and numerical in-cylinder pressure and AHRR

The following table 10.4 shows a comparison between IMEP* and peak in-cylinder pressure parameters in both the simulation and the experiments. The consistency of the numerical model is confirmed for both combustion modes.

		ND	DF
Numerical IMEP*	[bar]	12.65	11.69
Experimental IMEP*	[bar]	13.13	11.64
IMEP* difference	[%]	-3.683	+0.467
Numerical peak in-cylinder pressure	[bar]	91.13	78.44
Experimental peak in-cylinder pressure	[bar]	89.64	77.44
Peak in-cylinder pressure difference	[%]	+1.665	+0.655

Table 10.4 - Comparison between experimental and numerical IMEP* and peak in-cylinder pressure for ND and DF NG-diesel cases at 3,000 [rpm] – BMEP = 8 [bar]

10.3.1 H2-NG blend simulations

With the calibrated numerical model, for the engine condition considered here at 3,000 [rpm] / BMEP = 8 [bar]/177[Nm], the influence of the composition of an H_2-NG mixture on the performance and emissions produced was assessed.

	CH_4 [mg]	H_2 [mg]	$(A/F)_{premix}$ [-]	$(A/F)_{st,premix}$ [-]	λ_{premix} [-]	$(A/F)_{tot}$ [-]	$(A/F)_{st,tot}$ [-]	λ_{tot} [-]	H_2 Energy Fract. [%]	H_2 Mass Fract. [%]
NG	23.39	0.00	30.78	16.84	1.83	23.57	16.23	1.45	-	-
5vol%H_2	23.07	0.16	30.94	16.95	1.82	23.66	16.31	1.45	1.21%	0.51%
10vol%H_2	22.67	0.33	31.19	17.08	1.83	23.79	16.40	1.45	2.52%	1.08%
20vol%H_2	21.77	0.71	31.78	17.37	1.83	24.10	16.60	1.45	5.46%	2.37%
30vol%H_2	20.78	1.17	32.42	17.72	1.83	24.43	16.85	1.45	8.93%	3.96%
40vol%H_2	19.60	1.70	33.22	18.16	1.83	24.84	17.16	1.45	13.00%	5.89%
50vol%H_2	18.06	2.37	34.42	18.76	1.83	25.45	17.56	1.45	18.08%	8.44%

Table 10.5 - Main features of the H_2-NG blends analysed

Table 10.5 shows that, both for the premixed charge and for the injection of diesel fuel, the lambda is much higher than 1.83 and 1.45 respectively. Therefore, the engine always works in lean conditions. In addition, for the different mixtures, the parameters λ_{premix} and λ_{tot} are very similar. In fact, as the H_2 fraction increases in the H_2-NG mixture, there is a simultaneous increase in (A/F) and $(A/F)_{st}$. The energy and mass of H_2, in relation to the energy and mass of the associated mixture H_2-NG-diesel, are reported in the last two

columns of table 10.5. Note that the mass fraction of H_2 is less than half of its energy fraction, as the lower heating value (LHV) of H_2 is more than twice that of NG.

10.3.2 Results and Discussion

Influence of hydrogen content and start of injection

The results of combustion simulations with different H_2 volumetric fractions are now presented and discussed.

The in-cylinder pressure and AHRR as a function of the volumetric fraction of H_2 in the H_2-NG mixture (0% baseline Dual Fuel (DFb) case - 50%) is shown in figure 10.13(a-b). The peak pressure in the cylinder always increases with the increase in the amount of H_2: for the case with 30 vol% of H_2 (H30) the increase is about 12 [bar] (+20.5%) and, for the case with 50 vol% of H_2 (H50), about 34 [bar] (+43%). The increase in the concentration of H_2 also leads to the increase in the Peak Pressure Rise Rate (PPRR): for the DFb case, the PPRR is about 2.15 [bar/CAD], for H30 this parameter rises to 3.40 [bar/CAD] and for H50 to 6.30 [bar/CAD]. The close correlation between the peaks of AHRR and PPRR is highlighted. As expected, without changing the Start of Combustion (SOC) angle, the addition of H_2 speeds up the combustion process, reducing its duration.

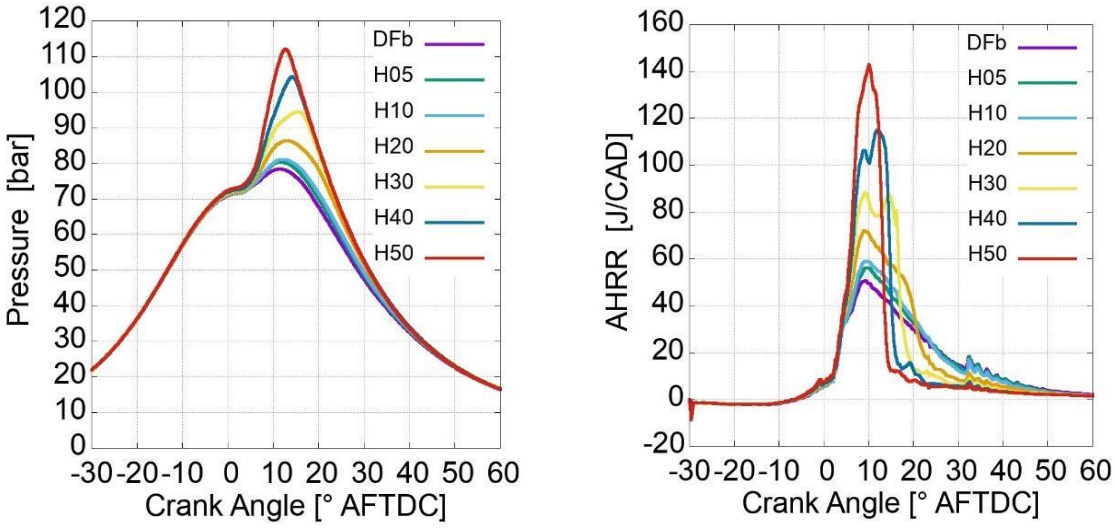

Figure 10.13 - In-cylinder pressure (a) and Apparent Heat Release Rate (b) for different Hythane blends (DF NG-diesel operation at 3,000 [rpm] – 177 [Nm], case −80% Diesel fuel +74% NG)

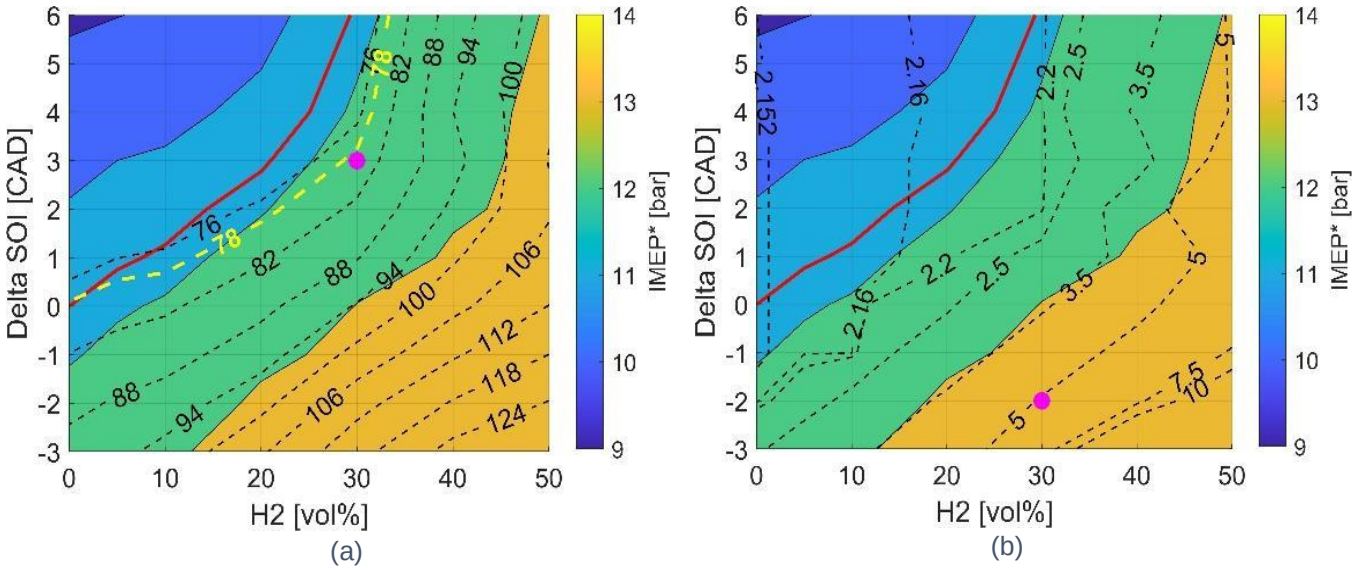

Figure 10.14 - Contour maps of IMEP* for different H_2 vol%-delta SOI combinations with peak in-cylinder pressure (a) and PPRR (b) levels superimposed

In figure 10.14(a), dotted lines indicate peak in-cylinder pressure values as a function of H_2 vol% and diesel SOI and are superimposed to the IMEP* contour map; the peak cylinder pressure value of the case DFb is represented by the yellow dotted line.

Figure 10.14(a) shows that as the H_2 concentration and injection timing increase, IMEP* increases. In addition, IMEP* goes from 11.7 bar to 13.0 [bar] (+11.3%) passing from H0 to H30 and keeping the same SOI of the DFb case. The peak in-cylinder pressure and PPRR are also increased.

In addition, a good compromise can be reached, moving along the solid red line (same IMEP* of DFb) and reaching 30% of H_2, obtaining a slight advantage over the peak in-cylinder pressure. Similarly, thanks to the increase of up to 30% of H_2, we move along the yellow dotted line (same peak cylinder pressure of DFb), thus obtaining a slight increase in IMEP*.

Therefore, it can be deduced from these considerations that it is possible to define the region between the solid red line and the yellow dotted line as a "sweet spot", where compared to the DFb case, the engine operates with greater efficiency and less mechanical stress.

From figure 10.14(b), falling beyond the graph domain as its value is equal to 2.15 [bar/CAD], the curve corresponding to the DFb case is not represented. However, most H_2 vol%-Delta SOI combinations are acceptable if a PPRR limit of 5 [bar/CAD] is taken. It can be noted that the limit of 5 [bar/°] can be reached with H30, at an IMEP* (therefore thermal efficiency) much higher than DFb, if a peak cylinder pressure of up to 110 [bar] is accepted.

Figures 10.15(a-b) represent the trends of the combustion parameters CA50 and CA10-90 as a function of H_2 vol%-Delta SOI and show how, as the mole fraction H_2 increases, combustion occurs more quickly: in fact, both parameters decrease as H_2 concentration increases, at the angle SOI corresponding to DFb. The SOI diesel also conditions both the CA50 and the CA10-90: both decrease with the earlier start of combustion, because the flame propagation is facilitated by the higher combustion temperature.

The BTE parameters and combustion efficiency η_{comb} as a function of H_2 vol% and Delta-

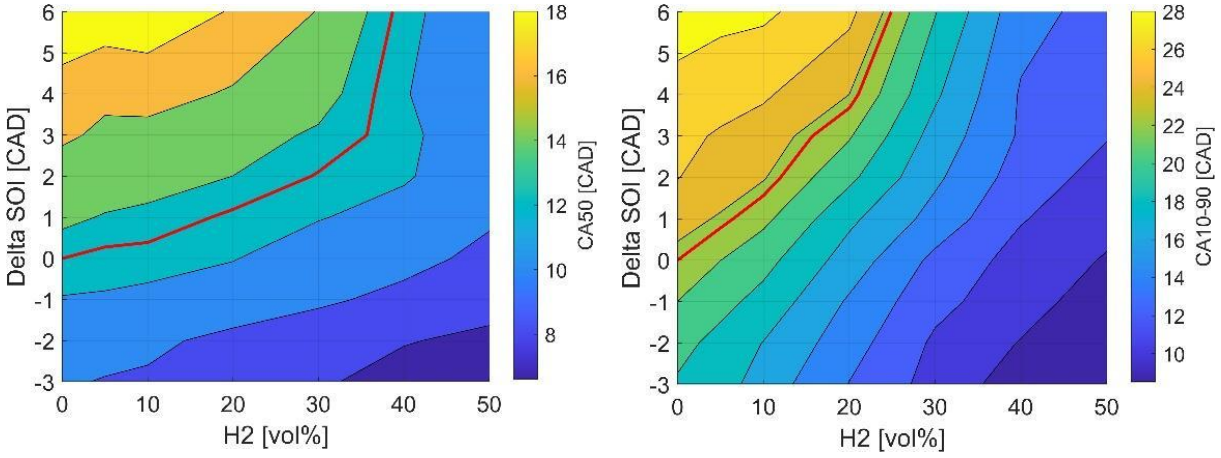

(a) (b)

Figure 10.15 - Contour maps of CA50 (a) and combustion duration CA10-90 (b)

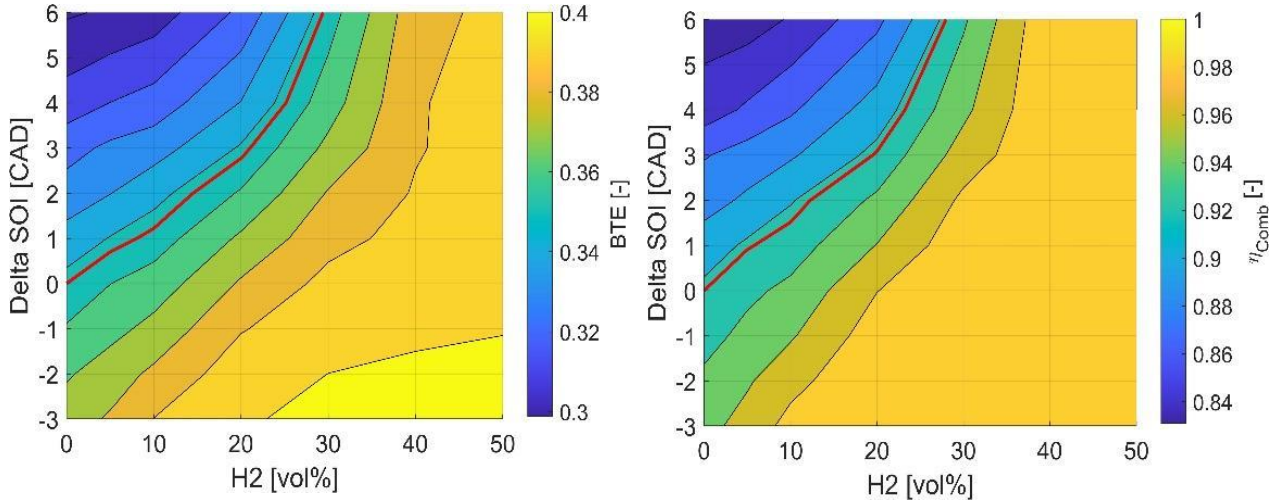

(a) (b)

Figure 10.16 - Contour maps of BTE (a) and Combustion Efficiency (b)

SOI are shown in the following figures 10.16(a-b) respectively. The combination of faster combustion, combined with greater efficiency of the thermodynamic cycle, and more complete combustion (higher η_{comb}) (figure 10.16(b)), improves the BTE precisely thanks to the presence of H_2.

Emissions

Figure 10.17(a) shows that as the mole fraction of H_2 increases, specific CO_2 emissions decrease. Improvement of BTE and reduction of carbon content in the H_2-NG mixture are the main reasons for this.

Moreover, the reduction of CO and UHC is always due to more complete combustion (see figure 10.17(b-c)). The result is consistent with figure 10.16(b), where increasing the H_2 content improves η_{comb}.

There are increasing NOx emissions (figure 10.17(d)), due to higher in-cylinder peak temperatures as the H_2 mole fraction increases, which speeds up the combustion process.

SOI is also decisive for these trends, as the completion of combustion is facilitated by an early start, and while this on one hand reduces CO and UHC emissions, on the other hand it increases NOx, due to higher temperatures.

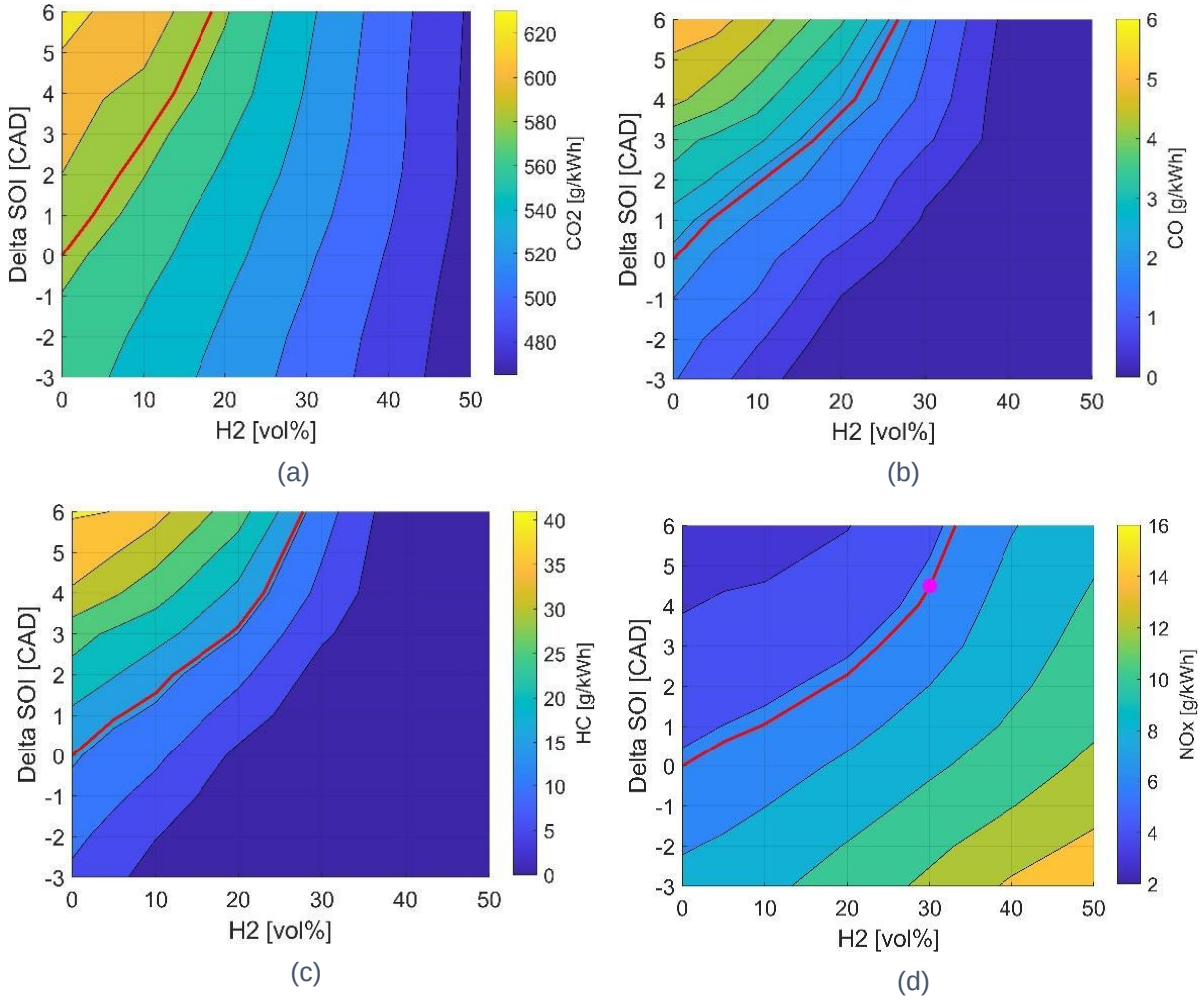

Figure 10.17 - Contour maps of CO2 (a), NOx (b), CO (c) and UHC (d)

10.3.3 Engine performance and emissions of selected operating points

Using the figures shown so far, it is possible to study combinations in fractions of H_2 mole and diesel SOI that can produce the above-mentioned advantages. Then three operating conditions are identified, and compared with the DFb case, all with reference to the maximum acceptable level of H_2 in hythane mixtures (30 vol%).

On the basis of figure 10.14(a) the first operating condition is defined: the "safety region" between the red solid line and the yellow dotted line is defined, and the delayed injection of 3 CAD (Delta_SOI) is chosen. Remaining within the limits of in-cylinder peak pressure, the resulting IMEP* is higher than the reference case. As all the combinations have the same input energy value, as mentioned initially, an increase in terms of IMEP* is equivalent to an improvement in BTE. This operating point is called "H30_SOI +3".

The PPRR parameter determines the limits to be observed on engine noise and vibrations and is therefore considered to define the second operating point. According to literature, the upper limit for PPRR is defined at 5 [bar/CAD], a value used in this study. Thus, the

intersection between the curve PPRR = 5 [bar/CAD] and the coordinate of 30 vol% H_2 determines the second operating point. This corresponds to a further diesel injection advance of 2 [CAD] and is highlighted by a red point in Figure 10.5(b). The above operating condition is referred to as "H30_SOI -2".

Finally, for the definition of the third operating point, NOx emissions are considered. This point is characterised by the same specific NOx emissions as the DFb case, which can be obtained with 30 vol% H_2 and Delta_SOI equal to 4.5 [CAD] (delayed injection); this is shown as a red dot in figure 10.17(d).

Figures 10.18-21 show comparisons of the three operating points. The horizontal red line represents the DFb case, which is thus compared.

IMEP*, η_{comb} and BTE parameters are represented in figures 10.18(a-c), which show better performance than DFb case for all selected DF H_2-NG/diesel cases.

Both η_{comb} and BTE improve when diesel injection is advanced, this leads to increased output work. Therefore, the condition defined by "H30_SOI -2" leads to the highest increase in IMEP* (11.7%), η_{comb} (8.1%) and BTE (13.3%).

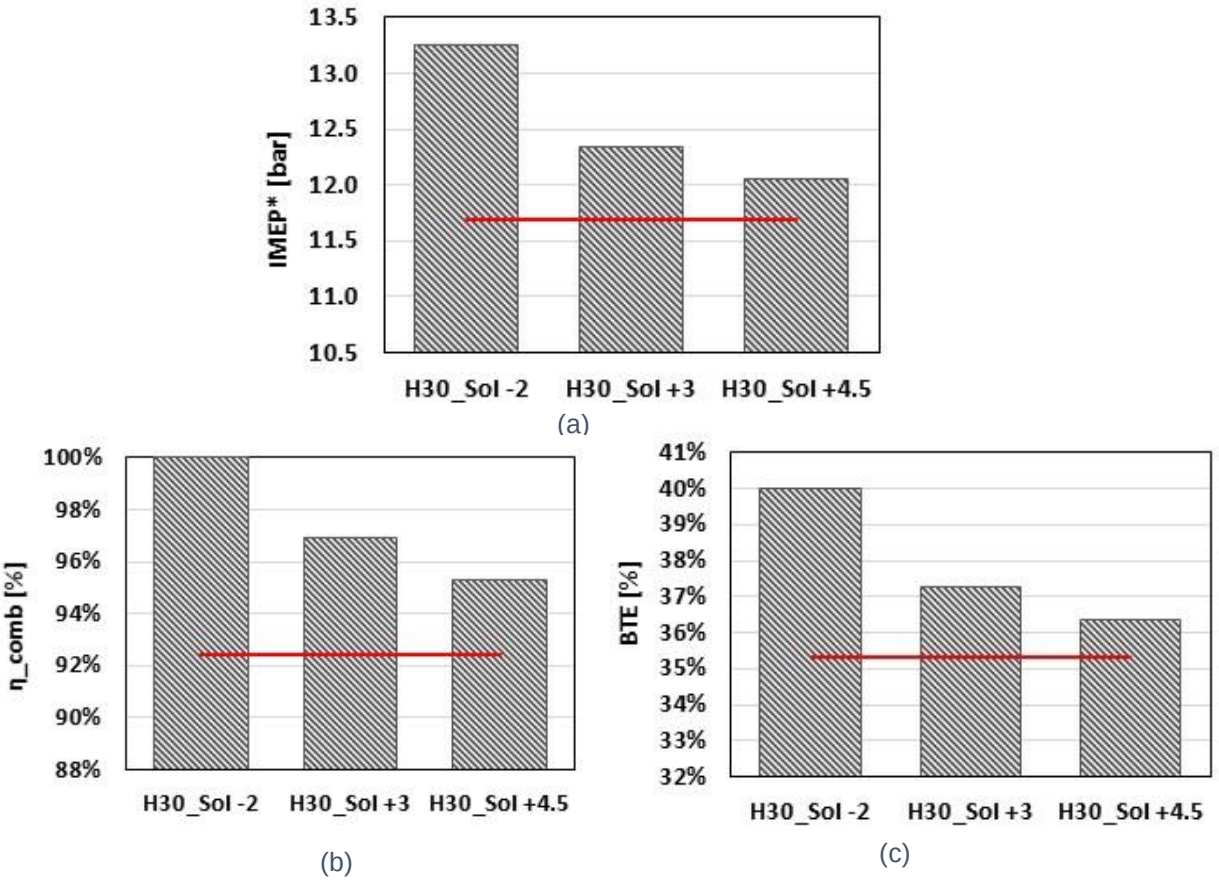

Figure 10.18 - Comparison between “H30_SOI -2”, “H30_SOI +3”, “H30_SOI +4.5” cases in terms of IMEP* (a), combustion efficiency (b) and BTE (c)

As we might expect, when the diesel injection is advanced, CA50 approaches the TDC (see figure 10.19a). Moreover, as the diesel injection advance increases, the duration of combustion expressed by CA10-90 decreases (figure 10.19b), however always less than that in the case DFb.

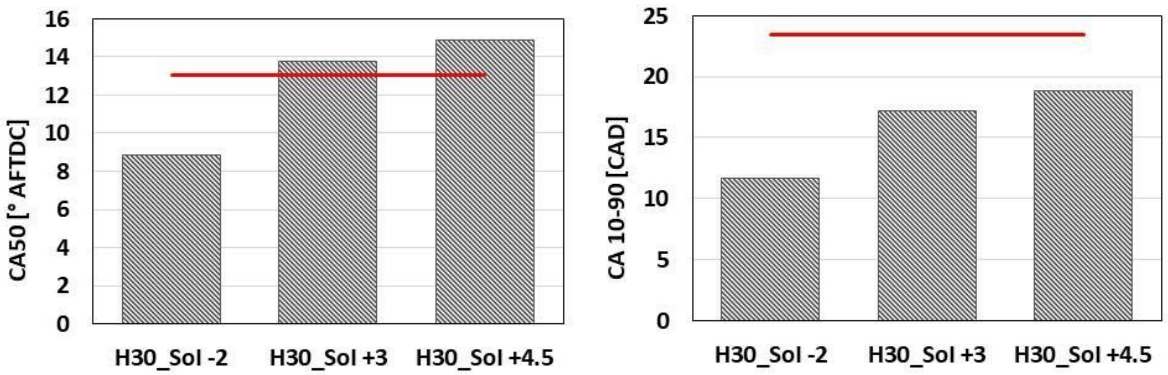

Figure 10.19 - Comparison between “H30_SOI -2”, “H30_SOI +3”, “H30_SOI +4.5” cases in terms of CA50 (a) and CA10-90 (b)

The same or even lower peak in-cylinder pressure and PPRR, compared to the DFb case, is shown by the cases "H30_SOI +3" and "H30_SOI +4,5", while a higher in-cylinder peak pressure and PPRR occurs for "H30_SOI -2" (see figure 10.20(a-b)). In particular, between the case Dfb and the case "H30_SOI -2" an increase in in-cylinder peak pressure is calculated from 80 [bar] to about 110 [bar], and an increase in PPRR of about 150% (from 2.2 [bar/CAD] to 5.1 [bar/CAD]).

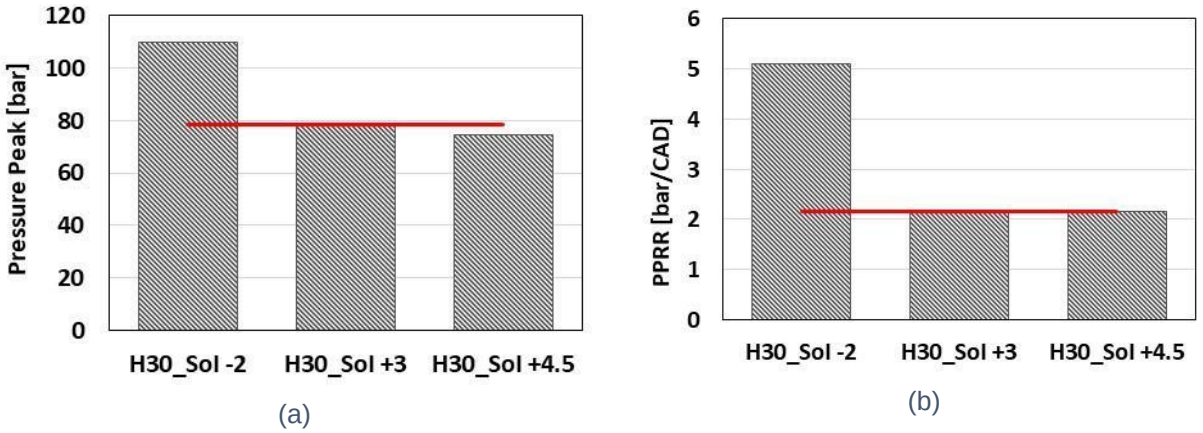

Figure 10.20 - Comparison between “H30_SOI -2”, “H30_SOI +3”, “H30_SOI +4.5” cases in terms of peak pressure (a) and PPRR (b)

Higher NOx emissions (+84%) than in the DFb case are calculated in the "H30_SOI -2" case, characterised by a more advanced and faster combustion process. Conversely, NOx emissions close to those of the DFb case are shown for H30_SOI +3 and H30_SOI +4.5.
Finally, compared to the DFb case, lower CO, UHC and CO_2 emissions are shown for all selected DF H_2-NG /diesel cases. The maximum benefit is obtained by advancing the diesel injection law by 2 [CAD] (H30_SOI -2), for the trends shown by η_{comb} and BTE. In fact, in this condition, while CO_2 emissions are reduced by about 12%, compared to DFb, CO and UHC tend to zero.

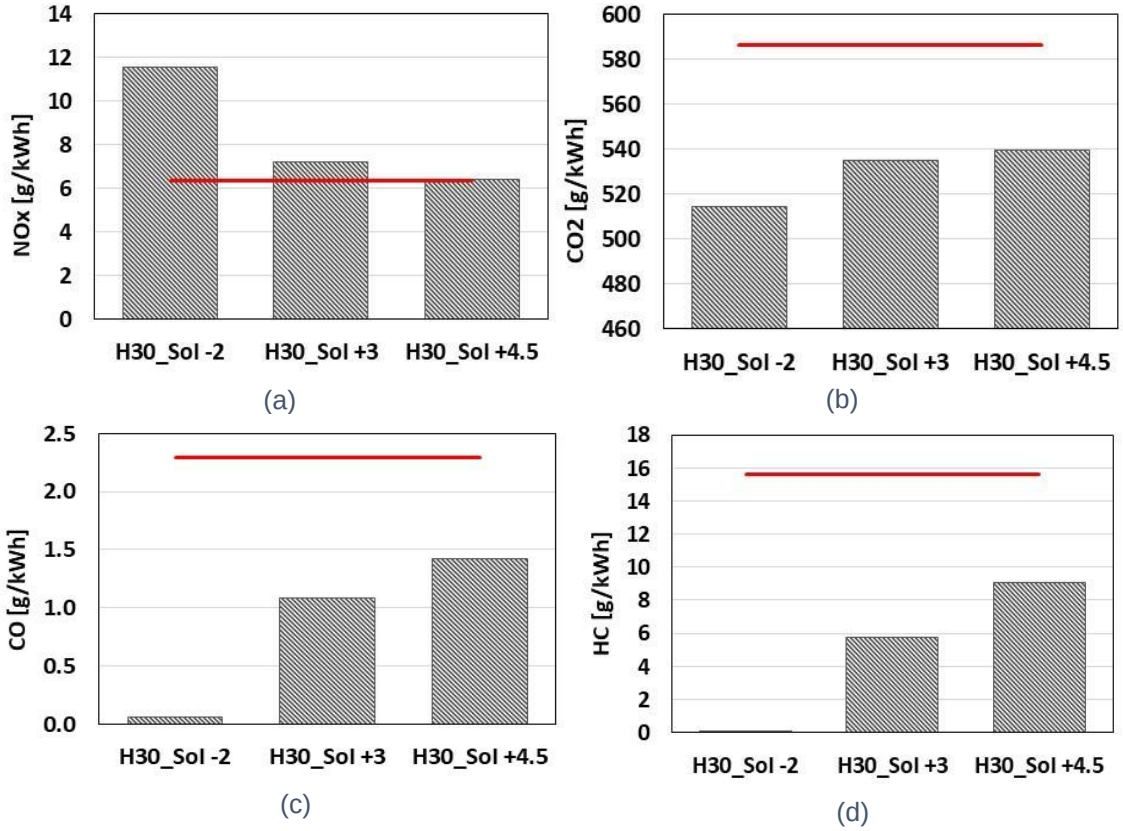

Figure 10.21 - Comparison between “H30_SOI -2”, “H30_SOI +3”, “H30_SOI +4.5” cases in terms of NOx (a), CO2 (b), CO (c) and HC (d)

To understand in more detail how the addition of hydrogen and SOI diesel can influence DF combustion, the O_2 mass fraction and CH_4 mass fraction are shown on three cut planes at various angles of the crank (figure 10.A1).
In detail, the following cutting planes in Figure A1 show the contour maps of the mass fraction of O_2 for the cases Diesel, DFb and H30_SOI+3:

- “O”: cut plane normal to the cylinder axis;
- “M”: cut plane coincident with the symmetry plane of the sector mesh;
- “B”: cut plane coincident with a cyclic boundary of the sector mesh.

It is shown that DF cases are able to exploit the O_2 present in the core and in the periphery of the combustion chamber to a greater extent than the diesel case, therefore a higher and faster consumption of O_2, due to the presence of low-reactivity fuel, NG or H_2-NG mixture in DFb and H30_SOI+3 cases respectively.
Moreover, thanks to the addition of hydrogen in the premixed charge, it is clear that the case "H30_SOI+3" is characterised by a faster combustion process than the case "DFb". In fact, although compared to the DFb case the SOI of the H30_SOI+3 case is delayed by 3 [CAD], the consumption of O_2 in the H30_SOI+3 case is already higher than in the DFb case.

Figure 10.A2 shows the contour maps of CH_4 mass fraction for DFb, H30_SOI+3 and H30_SOI-2 cases on the same cutting planes shown in figure 10.A1.
The following considerations can be drawn from the analysis of Figure A2:
Compared to DF cases, the oxidation of CH_4 in the diesel case is slower. In addition, in the diesel case, the higher CH_4 fraction located on the periphery of the combustion chamber is not involved in the combustion process.
Therefore, as demonstrated by the comparison of H30_SOI+3 and H30_SOI-2 cases, the faster and more complete the combustion process the more the SOI advances.

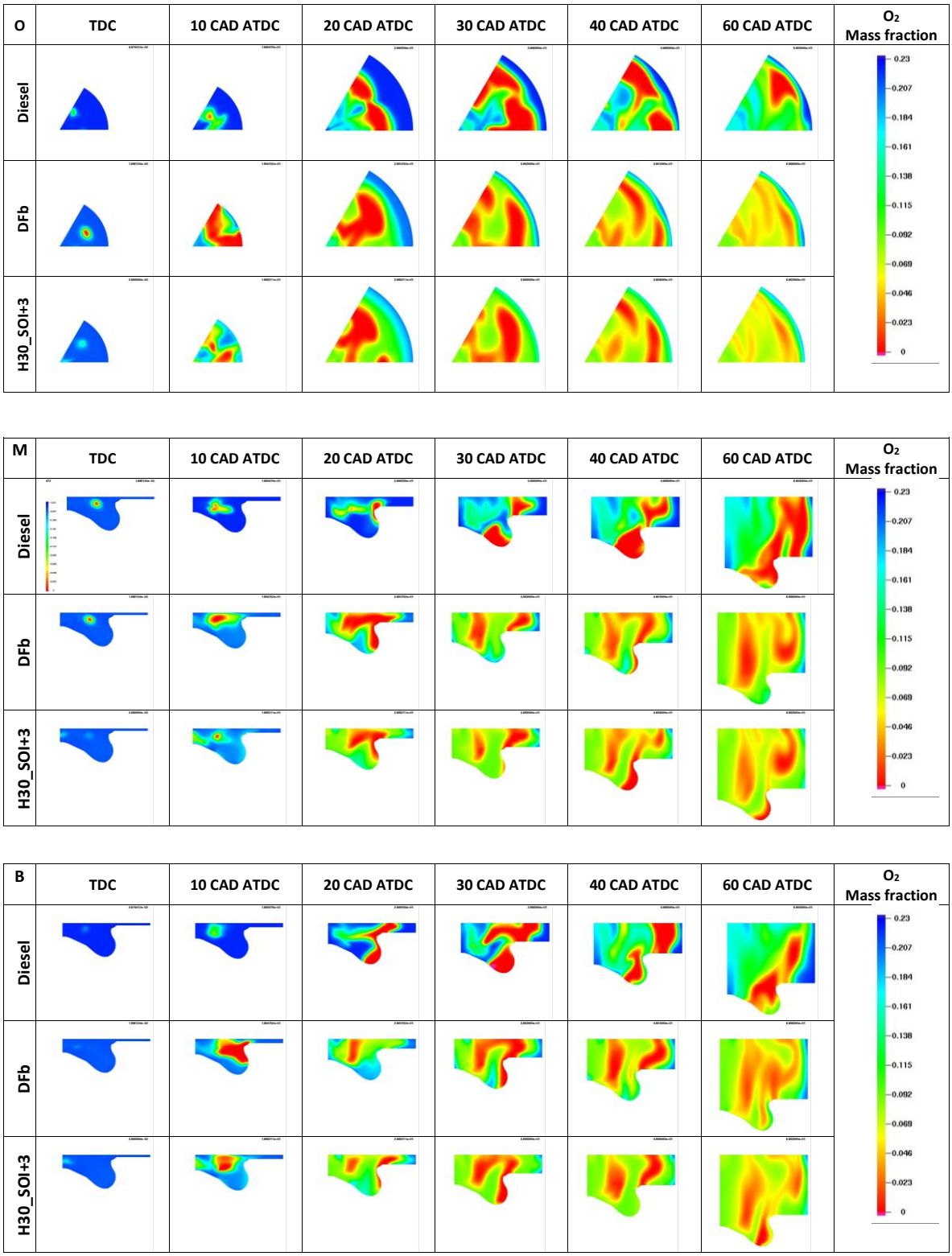

Figure 10.A1 - Comparison between “Diesel”, “DFb” and “H30_SOI +3” cases in terms of O2 mass fraction viewed on different cut planes ("O”: cut plane normal to the cylinder axis; “M”: cut plane coincident with the symmetry plane of the sector mesh; “B”: cut plane coincident with a cyclic boundary of the sector mesh), at different crank angles

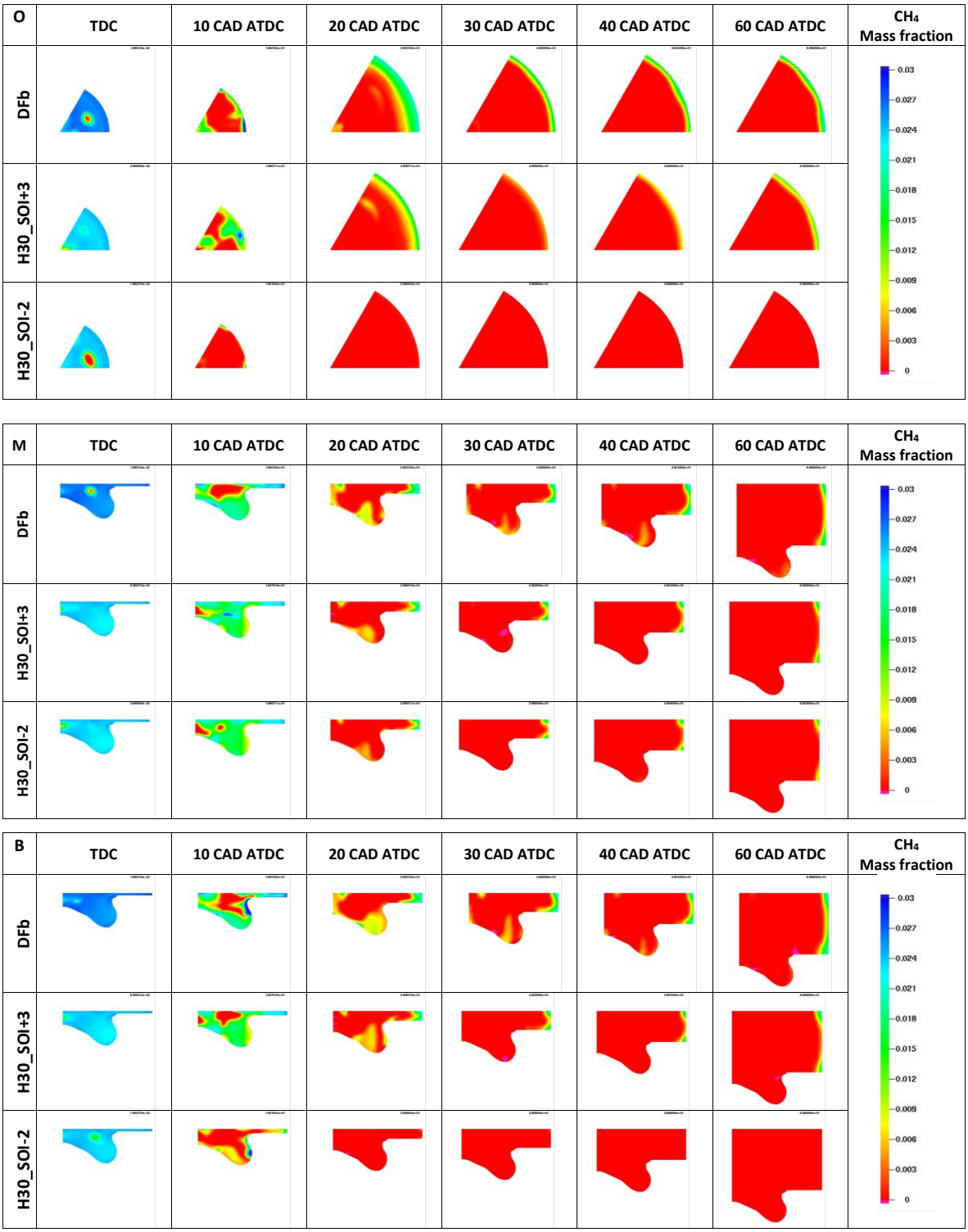

Figure 10.A2. Comparison between “DFb”, “H30_SOI +3” and “H30_SOI-2” cases in terms of CH4 mass fraction viewed on different cut planes ("O": cut plane normal to the cylinder axis; “M”: cut plane coincident with the symmetry plane of the sector mesh; “B”: cut plane coincident with a cyclic boundary of the sector mesh), at different crank angles

10.3.4 Conclusion of 3,000 [rpm] - BMEP = 8 [bar] / 177 [Nm], case –80% Diesel fuel +74% NG

It was observed from the simulation results that the combustion process is accelerated with H_2 enrichment. Consequently, compared to the DFb case, with the 50% by volume replacement of H_2 and maintaining the same SOI, the BTE can increase up to 12.6%, while the specific UHC and CO emissions are drastically reduced, Thanks to the improvement of the BTE and the lower carbon content of the premixed charge. At the same operating state, the specific of CO_2 emissions are also reduced by 19.7%. Increased peak cylinder pressure, PPRR and NOx emissions are the main drawbacks of hydrogen enrichment.
However, these deficiencies are eliminated by proper calibration of the SOI, which maintains the advantage over the standard DF NG-diesel combustion. For example, by replacing 30% vol of H_2 and reducing the injection advance by 4.5 [CAD], BTE, UHC, CO and CO_2 improve, while in-cylinder peak pressure, PPRR and NOx emissions do not change.

10.4 Combustion model validation (3,000 [rpm] - BMEP = 12 [bar] / 265 [Nm], case –60% Diesel fuel +52% NG)

Now the engine point 3,000 [rpm] - BMEP = 12 [bar] / 265 [Nm] is taken into account, the case with the replacement in energy terms of 60% diesel with 52% NG, concerning the experimental point at which 63% NG was initially introduced and optimised in performance by reducing this percentage.
Table 10.6 shows the main parameters for both the DF NG-diesel mode and the normal diesel mode in this engine condition.

With regard to the validation of the numerical model, the following figures 10.22(a-d) show the comparison between the numerical and experimental results on cylinder pressure and on the apparent heat release rate (AHRR) for the 3,000 [rpm] - BMEP = 12 [bar] / 265 [Nm] point, for the original ND and DF case with replacement 60% Diesel fuel +52% NG.

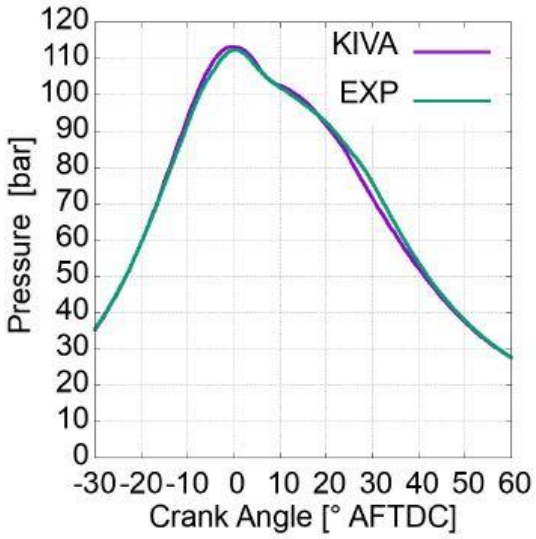

a – ND in-cylinder pressure

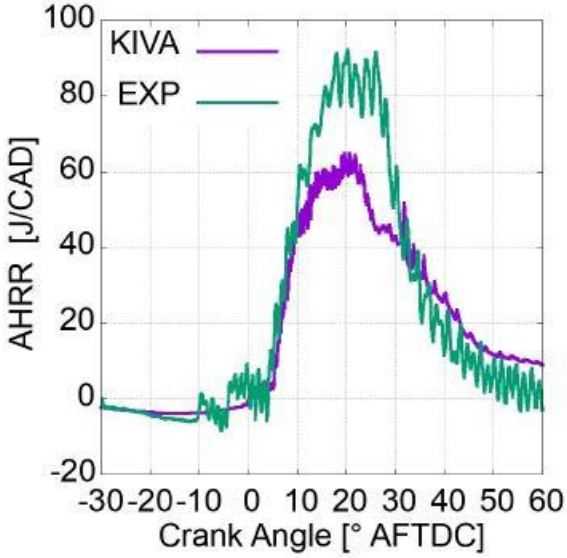

(b) – ND AHRR

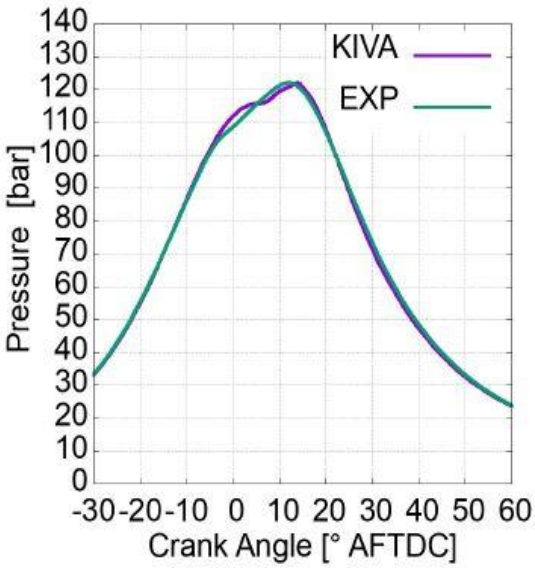

c - ND in-cylinder pressure (-60%ND +52NG% case)

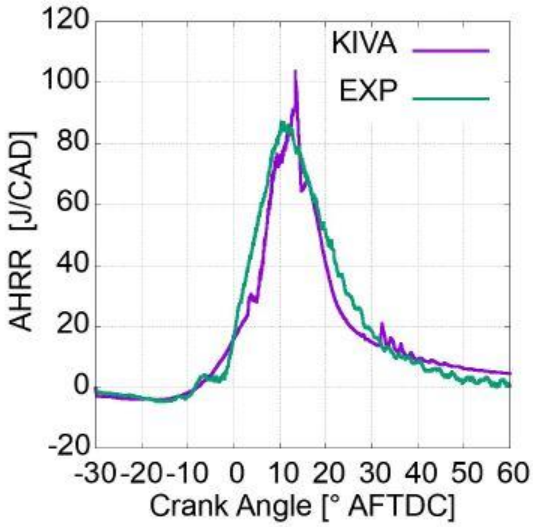

(d) - DF NG/Diesel AHRR (-60%ND +52NG% case)

Figure 10.22 - ND and DF NG-diesel operation at 3,000 [rpm] – 265 [Nm], case −60% Diesel fuel +52% NG. Comparison between experimental and numerical in-cylinder pressure and AHRR

In this engine condition at maximum load in dual-fuel combustion, the experimental numerical alignment gives very precise results, moreover also from comparing the traces of pressure in figure 10.22(c) and of the Apparent Heat Release Rate in figure 10.22(d) the overlap is optimal. The results of subsequent simulations are therefore considered reliable.

		ND	DF
Numerical IMEP*	[bar]	17.93	17.27
Experimental IMEP*	[bar]	18.09	17.37
IMEP* difference	[%]	-0.854	-0.580
Numerical peak in-cylinder pressure	[bar]	113.26	122.14
Experimental peak in-cylinder pressure	[bar]	112.41	122.14
Peak in-cylinder pressure difference	[%]	+0.753	+0.0005

Table 10.6 - Comparison between experimental and numerical IMEP* and peak in-cylinder pressure for ND and DF NG-diesel cases at 3,000 [rpm] – BMEP=12 [bar] \ 265 [Nm]

Table 10.7 shows the main characteristics of the mixture at low reactivity; it can be noted that even at higher load you always work in lean conditions.

	CH_4 [mg]	H_2 [mg]	$(A/F)_{premix}$ [-]	$(A/F)_{st,premix}$ [-]	λ_{premix} [-]	$(A/F)_{tot}$ [-]	$(A/F)_{st,tot}$ [-]	λ_{tot} [-]	H_2 Energy Fract. [%]	H_2 Mass Fract. [%]
NG	23.59	0.00	45.83	23.59	2.72	23.57	15.66	1.58	-	-
5vol%H_2	23.17	0.16	46.31	23.33	2.73	23.66	15.71	1.59	0.88%	0.36%
10vol%H_2	22.74	0.33	46.77	23.07	2.73	23.79	15.77	1.59	1.83%	0.75%
20vol%H_2	21.87	0.71	47.66	22.59	2.74	24.10	15.90	1.59	3.95%	1.63%
30vol%H_2	20.87	1.17	48.72	22.04	2.75	24.43	16.07	1.59	6.46%	2.71%
40vol%H_2	19.72	1.72	49.92	21.44	2.75	24.84	16.27	1.58	9.47%	4.04%
50vol%H_2	18.18	2.38	51.86	20.56	2.76	25.45	16.52	1.58	13.11%	5.70%

Table 10.7 - Main features of the H_2-NG blends analysed

This operating point represents a high load condition, the effect of hydrogen is clearly visible both in terms of pressure trace and heat release in figures 10.23a-23b. For the highest percentages of replacement, the effect is a release of very violent heat and an ignition of a significant part of the charge very early: it is noted that, in the traces of pressure, compression cannot be distinguished from combustion. The high temperatures and

pressures in the chamber greatly facilitate the ignition of the hydrogen portion, which once ignited causes an extremely short heat release.

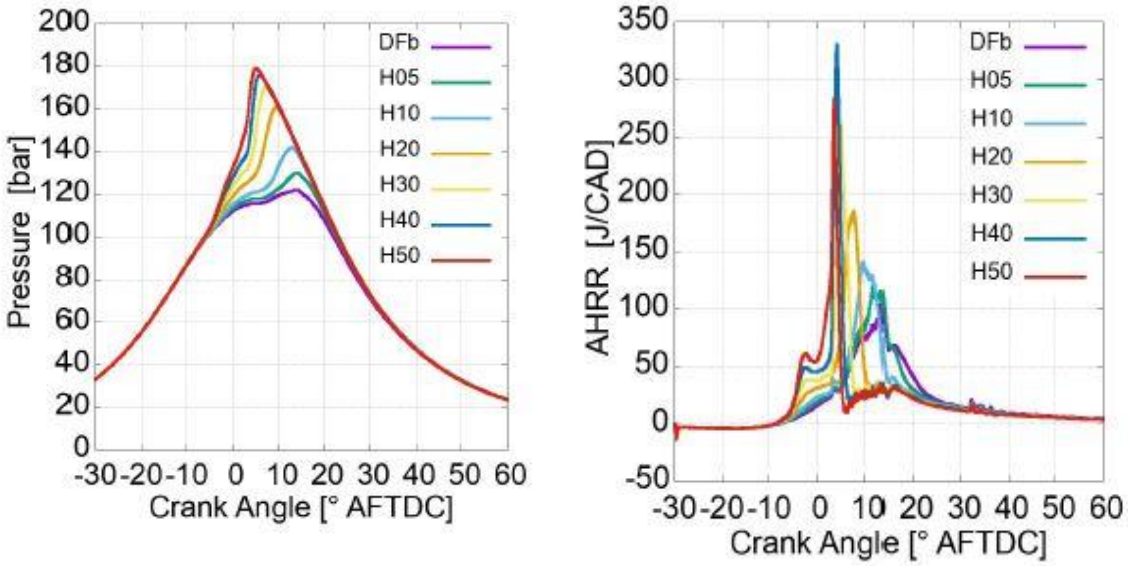

(a) (b)

Figure 10.23 - In-cylinder pressure (a) and Apparent Heat Release Rate (b) for different Hythane blends (DF NG-diesel operation at 3,000 [rpm] – 265 [Nm], case −60% Diesel fuel +52% NG)

For this engine condition, therefore, we can already exclude operation with high hydrogen replacements, as these would certainly affect the structural resistance of the engine both in terms of peak pressure and gradient at the maximum point, Moreover, it is possible that in reality such a violent heat release behaves similarly to a detonation or that it cannot be converted to pressure, with everything dissipated through the head. In this first analysis, we can try to limit these growths by operating with longer injection delays.

Performance parameters

Looking at the map in figure 10.24, we see an increase in IMEP* that tends to stabilise at the maximum value already with low replacements by adjusting the timing; in contrast, the isopressure curves are very close to each other, this means a rapid increase in this parameter, in particular by increasing the percentage of replacement.

The maximum reference ISO-pressure of 122 [bar] in this case is almost superimposed on the IMEP reference* (red line), in this case more than in the others it is fundamental to keep the pressure peak contained and therefore to operate in points that are found in the region between the yellow dotted line and the red line: the margins of improvement without impacts on the structural strength of the engine are very small. In general, from this map it is possible

to understand that every increase in terms of converted work is paid off by a significant increase in pressure peak.

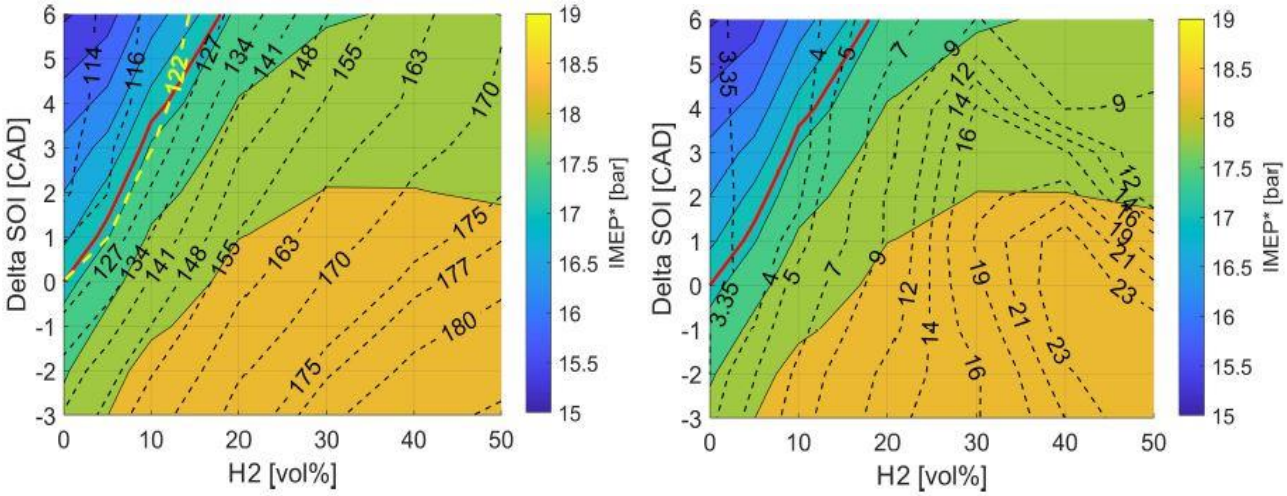

Figure 10.24 - Contour maps of IMEP* for different H_2 vol%-delta SOI combinations with peak in-cylinder pressure (a) and PPRR (b) levels superimposed

It is always necessary to add to the analysis of the peak pressure also that relative to the PPRR value, in this case the iso-PPRR for the reference case does not appear in the map in figure 10.24(b) as it remains beneath the Y axis. The representative curve was considered to be PPRR = 3.35 [bar/CAD] against a base case value of 3.34 [bar/CAD].

It can be seen that in the case of the pressure gradient the margins are even smaller, in fact in this case any point that is not the base case will record a much steeper peak, which tends to become more and more vertical as the replacement percentage increases.

Referring again to the maximum value of PPRR = 5 [bar/CAD], the previously mentioned operating region between the maximum iso-pressure and the base case iso-IMEP* is all below the limit in terms of PPRR.

The trends in combustion efficiency and overall efficiency, shown in the maps in figure 10.25(a)-25(b) respectively, leave no room for major advantages. As for the combustion efficiency, it already has a very high value in the base case, hydrogen will therefore have a "catalyst" role of combustion making it faster, in particular already from comparisons on the AHRR in figure 10.23b we can see how the release phase is very narrow, even if in the final phase the release is modest: probably, the duration of the total combustion will be similar but combustion speed will increase in the first phase.

With reference to the overall performance, combinations are possible that increase the value even if modestly: from the map in figure 10.25(b) we can see a large region where the BTE actually increases, however the increase is much more vertical in areas where there is a lower BTE than in the base case, areas of little interest.

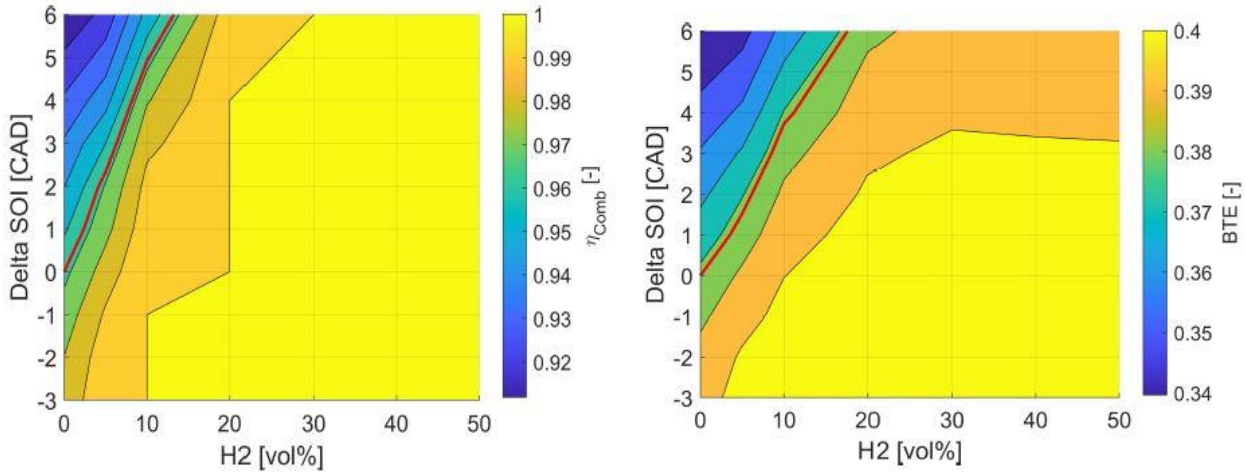

(a) (b)

Figure 10.25 - Contour maps of BTE (a) and Combustion Efficiency (b)

Combustion parameters

The following is an analysis of the combustion parameters in order to confirm the considerations made on the performance parameters.

As already expected from the observation of the AHRR, the position of the MFB50, in figure 10.26(a), is strongly anticipated according to the percentage of hydrogen replacement, in this case the hydrogen ignites very early, burning very quickly and also sending a significant share of fuel into combustion.

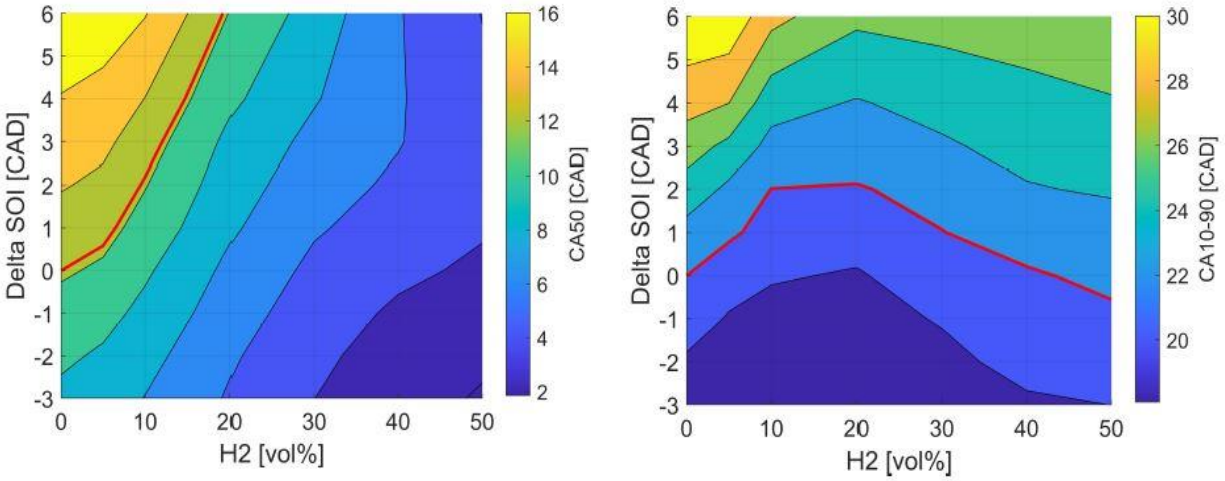

(a) (b)

Figure 10.26 - Contour maps of CA50 (a) and combustion duration CA10-90 (b)

What occurs on the other hand happens in terms of combustion duration, represented in figure 10.26(b), may seem in some way to be against the trend, with an increase in combustion speed; however, if you carefully observe the comparison between the heat releases in figure 10.23(b), it is noted that even for cases with higher replacement portions a more significant part of the heat is released in a range of increasingly narrower engine angles, however for the same cases much lower heat release is still observed after 5 CA AFTDC.

In terms of combustion parameters, therefore, it can be concluded that for this point hydrogen concentrates the bulk of the heat release in an increasingly reduced time, and anticipated to increase the percentage of replacement while maintaining an almost constant duration of combustion, the latter tends to have a stronger dependence on the injection displacement.

Emissions

In this case, it has been seen that hydrogen does not offer the benefits obtained in terms of performance for the other engine points, it is therefore necessary to make sure that there may be an advantage instead in terms of polluting emissions.

Figure 10.27(a) shows the contour map relating to the specific CO_2 emission, we note that there is no benefit in terms of IMEP*, while more in terms of carbon dioxide emissions. This decrease in specific emissions as replacement increases is due to the fact that, compared to the base case, a part of the fuel that burns does not produce carbon dioxide and therefore, in this case, a decrease in the amount of CO_2 emitted to the exhaust is observed in a directly proportional manner to the specific emission, as with a good approximation the output power remains constant with the increase in hydrogen.

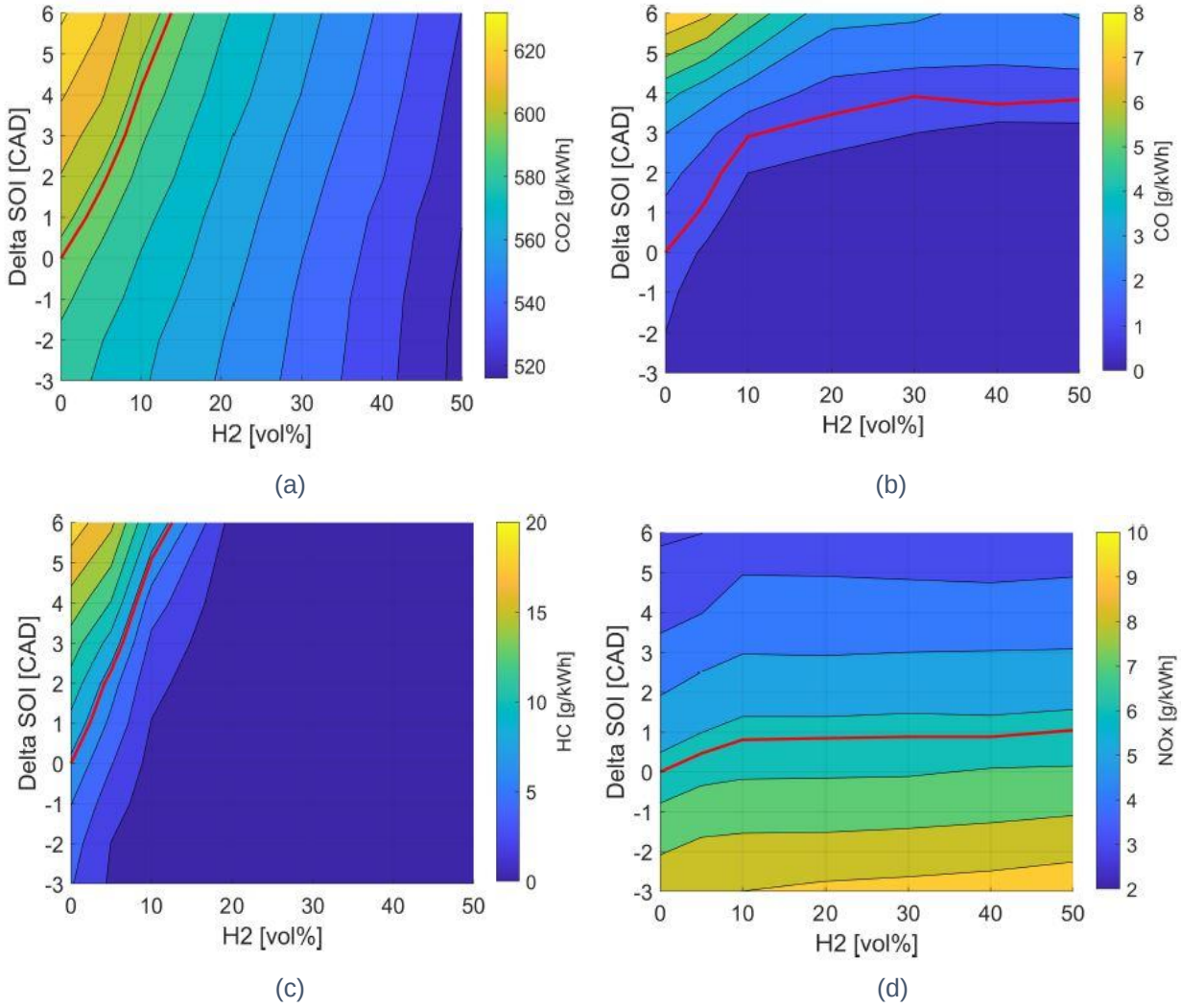

Figure 10.27 - Contour maps of CO_2 (a), CO(b), UHC(c) and NOx (d)

Carbon monoxide is an indicator of incomplete combustion; already in the base case, the combustion efficiency reached high values and the possible replacement of hydrogen offers very limited benefits in terms of carbon monoxide emission. This consideration is confirmed in figure 10.27(b), where it is possible to note a very low emission already on the red line

and that it is almost cancelled for any hydrogen replacement value. Even a small amount of hydrogen helps the completion of combustion from a point of view of the chemical reactions. The same considerations can be made for the unburned hydrocarbons represented in figure 10.27(c); the red line, corresponding to the base case, is very close to a large region where the unburned hydrocarbons are almost zero: in general, hydrogen offers very few benefits on emissions related to incomplete combustion products since the base situation is already close to optimal.

Finally, the specific emission of nitrogen oxides (fig.10.27(d)) is not particularly affected by hydrogen replacement, rather it shows a dependence on the timing of combustion, decreasing for the longest delays. This is probably due to a "balance" between two contrasting phenomena:

- as the percentage of hydrogen replacement increases, the heat release is more and more violent, surely leading to higher temperatures;
- however, the heat release becomes more and more restricted.

Nitrogen oxides are formed in the period of time in which the temperature exceeds the target temperature of formation by about 2,200 [K], and when it falls below this value the production stops; therefore, the addition of hydrogen promotes temperature but only for a very short time, and therefore the emission will remain constant to compensate for this behaviour.

10.5 3D Post Processing of Results for Case 265[Nm] −60% Diesel fuel +52% NG

From the maps presented in the previous paragraph you can see that the margins of improvement for this point are extremely narrow:

- referring to the maps in which the iso curves represent maximum pressure, figure 10.24(a), and iso-PPRR, figure 10.24(b), it is seen that the regions with maximum pressure equal or less than the base case and value of the PPRR less than the target of 5 [bar/CAD] are very narrow;
- From another point of view, when analysing the maps of combustion efficiency, figure 10.25(a), or BTE, Figure 10.25(b), it is observed that the base case already has maximum combustion efficiency and that the margins for BTE improvement are around one percent;
- Considering emissions, only a significant decrease in carbon dioxide is observed, for other pollutants no significant reductions can be achieved.

Moreover, referring to the pressure traces and the heat rate release, respectively in figure 10.23(a)-23(b), we note, in addition to an increase in peak pressure, an extremely violent

and concentrated heat release. Starting from these considerations, however, it was chosen to analyse a point that maximises BTE, but proceeding with 3D post-processing in order to explain the AHRR trend. The chosen point has a 30% hydrogen replacement and an SOI delay of 2 [CAD]; below is the pressure trace to the Apparent Heat Release Rate compared to the base case.

In particular, from the developments of the AHRR in figure 10.28(b), the already observed trend is confirmed, moreover it is particularly anticipated and can make us think of an auto-ignition of the charge, a phenomenon that tends to self-exalt, and can lead to knocking, resulting in thermomechanical failure of the engine block.

In order to understand whether it is indeed auto-ignition, we first need to consider the injection timing, shown in figure 10.29.

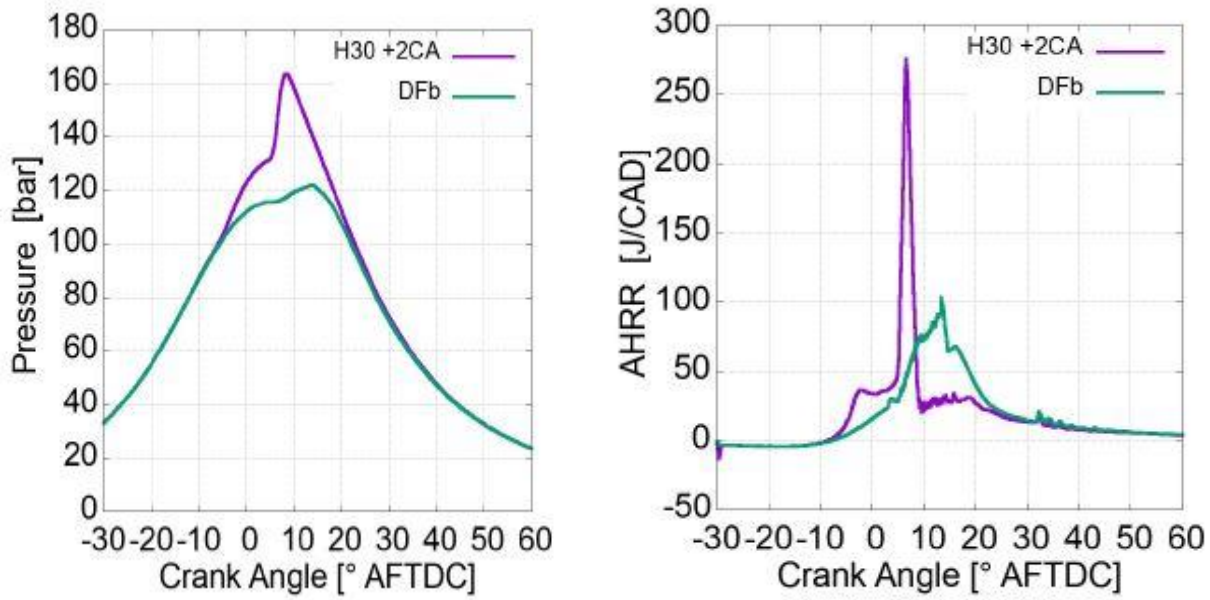

(a) - Pressure traces

(b) - Apparent Heat Release Rate

Figure 10.28 - Comparison of pressure traces (a) and AHRR (b) between the base case and the case 30%H_2 and DeltaSOI = +2CAD

Looking at the graph of the AHRR in figure 10.28(b) the heat release starts before the upper point, earlier than in the base case, although at this point it was considered an injection delay. Moreover, in figure 10.29 we can see how the heat release peak is during the first phases of the main injection. These considerations make the hypothesis of auto-ignition increasingly plausible, however, in order to confirm and have an even more in-depth view of what occurs in the chamber in table 10.11, the temperature distribution on the plane passing through the injection axis at several significant engine angles is reported.

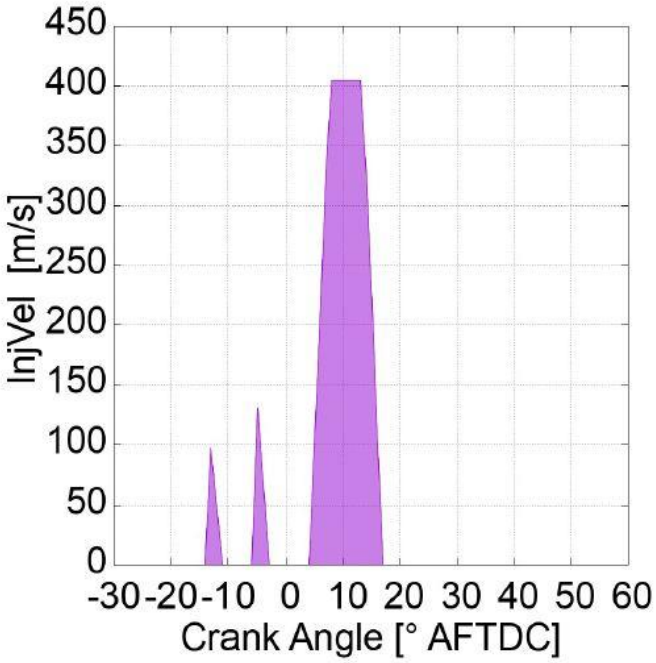

Figure 10.29 - Injection rates diagram

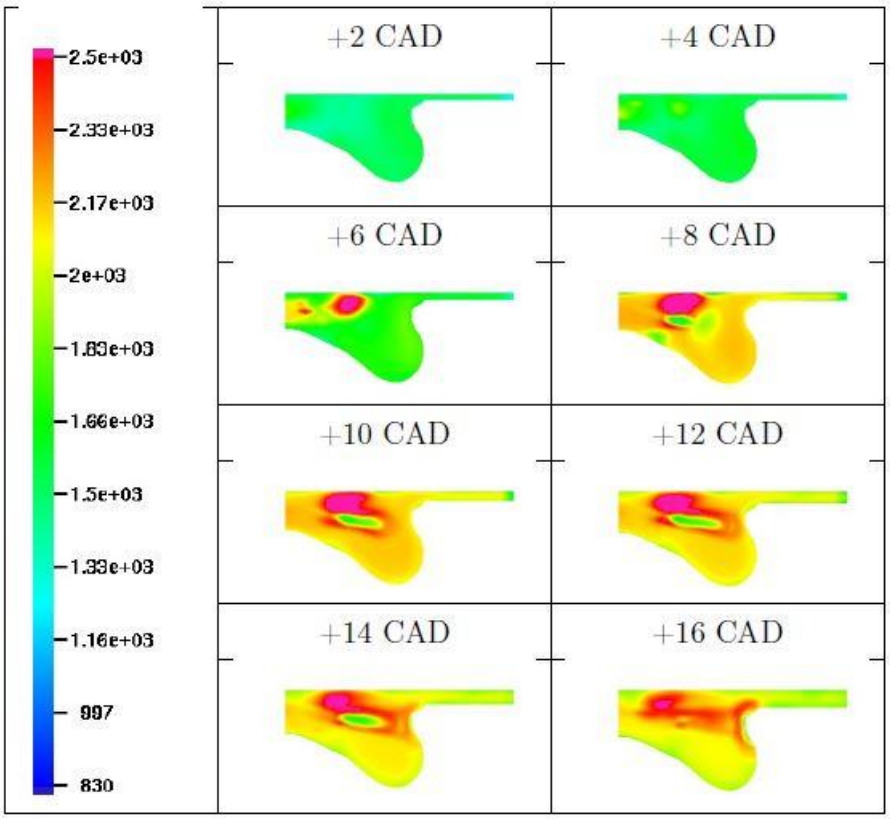

Table 10.8 - 3D Images of Temperature Distribution in Room for 265m60p52 case

Observing the +6 [CAD] and +8 [CAD] instants, it is observed that the temperature instantaneously goes from that of end compression to over 2,100 [K], a temperature that is

characteristic of combustion. In addition, it is noted that up to +4 [CAD], the temperature increases due to the effect of compression, at +6 [CAD] there is the development of a first flame kernel that could be attributed to the pilots. However, such a dramatic rise in temperatures and such a large portion of the charge is due exclusively to an auto-ignition phenomenon.
In the following moments, however, it is noted that inside the combustion zone an elongated area, clearly not burned, takes shape, which represents the spray of diesel combined with a portion of methane. This result further confirms the fact that it is not the main injection that ignites the charge. We should also remember that in the moments +6, +8 [CAD], the main injection starts at very low speed and with very little mass.

10.6 Conclusion of 3,000 [rpm] - BMEP = 8 [bar] / 265 [Nm], case −60% Diesel fuel +52% NG

In conclusion, for this point the results show firstly that hydrogen does not offer significant room for improvement, but the main effect is that it causes auto-ignition phenomena on the charge. These conditions therefore make the use of hydrogen at high loads too risky; we could envisage acting on the percentage of EGR as a future development. However, in the first analysis this could affect performance and therefore lose even that small advantage which can be obtained with hythane.

10.7 Conclusions and future developments

In conclusion, the effect of hydrogen on combustion has strong dependence on engine load. At high loads, the main problem is represented by the auto-ignition phenomena in the premixed charge; in this case hydrogen has extremely violent heat releases, with too fast combustion. This makes hydrogen unusable in these conditions. Moreover, the analyses carried out show that any improvements in performance and emissions are extremely limited. Conversely, for medium and low loads, hytane operation has proven to be advantageous.
In the medium load case, for all the significant points analysed, an increase in performance was observed together with a decrease in specific emissions, except for nitrogen oxides. These can be maintained at levels equal to those of the initial dual-fuel case, resulting in the highest efficiency increases. In addition, higher increases in work produced are also paid off

in terms of increased stress and operating roughness with higher pressure peaks. In the low-load case, the role of hydrogen is crucial for the completion of combustion.

The low-load point with dual-fuel operation strategy tested on the bench had very low combustion efficiency, the replacement of hydrogen for this case increases the energy released by combustion, thus with the main effect not so much on the peak as on the expansion phase, which is shifted upwards. This has very positive implications in terms of the useful work produced by combustion, significantly increasing overall efficiency. In general, it has therefore been seen that the effect on the peak pressure caused by the rapid hydrogen combustion can be limited by acting on the injection delay.

This analysis is limited to the closed-valve engine cycle part, from IVC to EVO, as the software is unable to manage valve handling. A very interesting development is certainly represented by the simulation of the intake phase because, due to its very low density, hydrogen could affect the volumetric efficiency.

In addition, the EGR level was kept constant in all simulations, a subsequent analysis with different percentages of exhaust gas recirculation could be interesting, in particular for the effect this has on nitrogen oxides and on controlling the mixture reactivity. Finally, starting from experimental tests carried out at the same load, but at different rotational speeds, firstly the predictivity of the model could be tested and secondly the behaviour of hydrogen as the engine speed changes could be investigated.

CONCLUSIONS

Environmental and energy problems underlie today's international and geo-political context. Government policies are offering strong impulses to tackle the dangerous consequences of these issues. Studies and experiments are underway to take the best advantage of consolidated technologies, but, above all, to develop new ones, in order to reduce the environmental impact of energy conversion systems, maintaining high performance levels and ensuring high reliability.

Internal combustion engines have achieved very high performance, low costs and high reliability, following more than a century of developments, and the technology they are equipped with makes it possible to achieve very high levels of efficiency: the large marine diesel 2-stroke engines have overall efficiencies of more than 50%, while hybrid engines reach even higher values, for example Formula 1 power-units. In addition, the environmental impact of engines can be significantly reduced by using, on one hand, appropriate emission reduction systems, and, on the other hand, fuels with low-carbon content or bio-fuels, in order to reduce or eliminate CO_2 emissions, recognised as one of the main greenhouse gases.

The studies carried out during the three-year PhD programme moved in this direction. In particular, investigations were carried out on innovative combustion techniques at low temperature, and introducing different fuels in a diesel engine. In detail, to understand the worth of new power solutions and related control strategies, experimental tests and 3D CFD combustion simulations were carried out.

The experimental tests were initially carried out in dual-fuel mode with gasoline to understand what characteristics a combustion with two well-known fuels with different reactivity could offer. Some improvements in terms of overall engine performance (BTE) were observed in combustion at low loads, after an optimisation of the diesel injection profile and without the use of EGR. While, at high loads, even implementing changes to the diesel injection law, it was not possible to manage combustion effectively, since, in this engine condition, gasoline tends to auto-ignite before diesel injection. Therefore, it was understood that it was probably necessary to use EGR.

The results from subsequent experimental tests with natural gas showed advantages in terms of performance and exhaust emissions produced. Diesel fuel was reduced to an 20% energy content compared to the original amount, replaced with natural gas, while optimisations were made to diesel injection profile. Medium and high load conditions were tested, and reduced NOx emissions were recorded at maximum load conditions, with a

difference of up to 46% compared to the base situation; in the same way, CO_2 levels were reduced by around 40%, while soot levels fell drastically at both medium and high load. Improvements were also recorded in BTE, increased by 2.5 percent at medium load and around 3 percent at high load, after appropriate re-calibration of the diesel injection system. Therefore, the results obtained were encouraging, particularly in the gen-set application studied, where excellent results can be obtained in the normal-use engine conditions for these applications.

The numerical CFD 3D simulations performed, validated through comparison with the experimental tests carried out with natural gas, were used to investigate the use of other low-reactivity fuels, such as biogas and hythane (a blend of methane and hydrogen).

Modelling using hythane showed that there are significant margins for the application of this blend in dual-fuel mode. The calculations show a general increase in combustion speed, as this is completed in less time than the use of methane. By choosing appropriate combinations of hydrogen percentage and diesel injection timing, at low and medium loads, operating areas in which BTE is appreciably increased were identified. The higher loads, on the other hand, do not seem to allow any improvement in comparison with the use of natual gas, and, moreover, the rise in pressure in the combustion chamber, in these engine conditions, is very high and therefore difficult to manage.

By enriching natural gas with hydrogen, reductions in CO and HC emissions were observed at low loads, while an increase in NOx were observed, although these can still be contained by changing both the injection law and the percentage of hydrogen in the mixture. Also at medium load, NOx levels were not lower than the base case.

In general, these results offer important indications on the use of hydrogen mixed with methane gas; in fact, through appropriate combustion control strategies, such as injection timing and the quantities introduced in the mixture, good results can be obtained in terms of performance and emissions. Further investigations could also be conducted on combustion with hythane adding the use of EGR, in order to slow combustion especially at high loads.

Calculations were also made using biogas as a pre-mixed fuel, to observe engine performance variation according to the percentage of CO_2 naturally contained in its mixture. The calculations carried out with biogas demonstrate that engine performance can be maintained almost constant at different CO_2 concentrations, properly changing the diesel injection timing. Therefore, in a cogeneration application, such as the one studied and reported in the published article “Application to Micro-Cogeneration of an Innovative Dual Fuel Compression Ignition Engine Running on Biogas”, we can expect that, in addition to

the benefits in terms of efficiency offered from the compression ignition engine, it is possible to further improve performance by appropriately modifying the injection laws according to the CO_2 content in biogas.

Many other fuelling methods can be envisaged for this type of application. One of these is biomethane, i.e., methane derived from biogas, which is also considered for development in the current national energy policy. Mixed with hydrogen, its use could lead to the improvements described in the previous steps. The dependence on fossil fuels would also be totally eliminated, if we consider that the pilot injection of diesel fuel is replaced by biodiesel, i.e., a fuel of natural origin, as described in this work, and hydrogen made available from renewable sources.

Therefore, compression ignition engines powered in dual-fuel mode can really be a carbon-neutral energy conversion system when totally powered by non-fossil bio-fuels. Moreover, this technology can be easily and with low cost applied to existing compression ignition engines, with the further advantage of a drastic reduction of their soot emission. It can be concluded that dual-fuel technology applied to diesel engines can be an excellent solution in this historical time of energy transition, alongside other technologies that will not be widely applied until they have reached the necessary reliability.

Further developments are needed, especially in pilot applications to confirm studies such as these that have adopted experiments on innovative combustion techniques and related calculations on potential fuel mixtures with reduced environmental impact.

References

(1) AR6 Climate Change 2021 The Physical Science Basis.Pdf.
(2) CLIMATE CHANGE 2021: Ecco come e perché il clima è cambiato fino ad oggi https://www.ingenio-web.it/31657-climate-change-2021-ecco-come-e-perche-il-clima-e-cambiato-fino-ad-oggi (accessed 2021 -11 -26).
(3) Trewin, B. Annex I: Observational Products. In *Climate Change 2021: The Physical Science Basis. Contribution of Working Group I to the Sixth Assessment Report of the Intergovernmental Panel on Climate Change*; Masson-Delmotte, V., Zhai, P., Pirani, A., Connors, S. L., Péan, C., Berger, S., Caud, N., Chen, Y., Goldfarb, L., Gomis, M. I., Huang, M., Leitzell, K., Lonnoy, E., Matthews, J. B. R., Maycock, T. K., Waterfield, T., Yelekçi, Ö., Yu, R., Zhou, B., Eds.; Cambridge University Press, 2021.
(4) Bp-Stats-Review-2021-Full-Report Https://Www.Bp.Com/Content/Dam/Bp/Business-Sites/En/Global/Corporate/Pdfs/Energy-Economics/Statistical-Review/ (Accessed 2021 -11 -26).
(5) deputati, C. dei. Cambiamenti climatici - Ambiente e gestione del territorio - Politica estera e questioni globali https://temi.camera.it/leg18/temi/tl18_cambiamenti_climatici.html (accessed 2022 -04 -18).
(6) Dec, J. E. A Computational Study of the Effects of Low Fuel Loading. **2002**.
(7) Basic Research Needs for Clean and Efficient Combustion of 21st Century Transportation Fuels. 208.
(8) Zhao, F. Automotive Spark-Ignited Direct-Injection Gasoline Engines. *Progress in Energy and Combustion Science* **1999**, 126.
(9) Westbrook, C. K. Chemical Kinetics of Hydrocarbon Ignition in Practical Combustion Systems. *Proceedings of the combustion institute* **2000**, *28* (2), 1563–1577.
(10) Saxena, S.; Bedoya, I. D. Fundamental Phenomena Affecting Low Temperature Combustion and HCCI Engines, High Load Limits and Strategies for Extending These Limits. *Progress in Energy and Combustion Science* **2013**, *39* (5), 457–488.
(11) Dec, J. E. Advanced Compression-Ignition Engines—Understanding the in-Cylinder Processes. *Proceedings of the combustion institute* **2009**, *32* (2), 2727–2742.
(12) Westbrook - 2013 - Biofuels Combustion.Pdf.
(13) Yao, M.; Zheng, Z.; Liu, H. Progress and Recent Trends in Homogeneous Charge Compression Ignition (HCCI) Engines. *Progress in Energy and Combustion Science* **2009**, *35* (5), 398–437. https://doi.org/10.1016/j.pecs.2009.05.001.
(14) Neely, G. D.; Sasaki, S.; Huang, Y.; Leet, J. A.; Stewart, D. W. New Diesel Emission Control Strategy to Meet US Tier 2 Emissions Regulations. SAE Technical Paper. **2005**.
(15) Alkidas, A. C. Combustion Advancements in Gasoline Engines. *Energy Conversion and Management* **2007**, *48* (11), 2751–2761. https://doi.org/10.1016/j.enconman.2007.07.027.
(16) Lu, X.; Han, D.; Huang, Z. Fuel Design and Management for the Control of Advanced Compression-Ignition Combustion Modes. *Progress in Energy and Combustion Science* **2011**, *37* (6), 741–783.
(17) Shim, E.; Park, H.; Bae, C. Comparisons of Advanced Combustion Technologies (HCCI, PCCI, and Dual-Fuel PCCI) on Engine Performance and Emission Characteristics in a Heavy-Duty Diesel Engine. *Fuel* **2020**, *262*, 116436. https://doi.org/10.1016/j.fuel.2019.116436.
(18) Karim, G. A. *DUAL-FUEL DIESEL ENGINE*; CRC Press, 2015.
(19) Noehre, C.; Andersson, M.; Johansson, B.; Hultqvist, A. *Characterization of Partially Premixed Combustion*; SAE Technical Paper 2006-01–3412; SAE International: Warrendale, PA, 2006. https://doi.org/10.4271/2006-01-3412.
(20) Kalghatgi, G. T.; Risberg, P.; Ångström, H.-E. Advantages of Fuels with High Resistance to Auto-Ignition in Late-Injection, Low-Temperature, Compression Ignition Combustion. *SAE Transactions* **2006**, *115*, 623–634.
(21) Manente, V.; Tunestal, P.; Johansson, B.; Cannella, W. J. Effects of Ethanol and Different Type of Gasoline Fuels on Partially Premixed Combustion from Low to High Load; 2010. https://doi.org/10.4271/2010-01-0871.

(22) Bessonette, P. W.; Schleyer, C. H.; Duffy, K. P.; Hardy, W. L.; Liechty, M. P. Effects of Fuel Property Changes on Heavy-Duty HCCI Combustion. *SAE Transactions* **2007**, *116*, 242–254.
(23) Inagaki, K.; Fuyuto, T.; Nishikawa, K.; Nakakita, K.; Sakata, I. *Dual-Fuel PCI Combustion Controlled by In-Cylinder Stratification of Ignitability*; SAE Technical Paper 2006-01–0028; SAE International: Warrendale, PA, 2006. https://doi.org/10.4271/2006-01-0028.
(24) Kokjohn, S. L.; Hanson, R. M.; Splitter, D. A.; Reitz, R. D. Experiments and Modeling of Dual-Fuel HCCI and PCCI Combustion Using In-Cylinder Fuel Blending. *SAE International Journal of Engines* **2010**, *2* (2), 24–39.
(25) Reactivity controlled compression ignition (RCCI) combustion - ProQuest https://www.proquest.com/openview/57272c7ceb20144d01baaf3f03fa00d9/1?pq-origsite=gscholar&cbl=18750 (accessed 2022 -02 -16).
(26) Akansu, S. Internal Combustion Engines Fueled by Natural Gas?Hydrogen Mixtures. *International Journal of Hydrogen Energy* **2004**, *29* (14), 1527–1539. https://doi.org/10.1016/j.ijhydene.2004.01.018.
(27) Chandra, R.; Vijay, V. K.; Subbarao, P. M. V.; Khura, T. K. Performance Evaluation of a Constant Speed IC Engine on CNG, Methane Enriched Biogas and Biogas. *Applied energy* **2011**, *88* (11), 3969–3977.
(28) Nwafor, O. M. I. Effect of Choice of Pilot Fuel on the Performance of Natural Gas in Diesel Engines. *Renewable Energy* **2000**, *21* (3–4), 495–504.
(29) Papagiannakis, R. G.; Rakopoulos, C. D.; Hountalas, D. T.; Rakopoulos, D. C. Emission Characteristics of High Speed, Dual Fuel, Compression Ignition Engine Operating in a Wide Range of Natural Gas/Diesel Fuel Proportions. *Fuel* **2010**, *89* (7), 1397–1406.
(30) Abd Alla, G. H.; Soliman, H. A.; Badr, O. A.; Abd Rabbo, et M. Effect of Pilot Fuel Quantity on the Performance of a Dual Fuel Engine. *Energy Conversion and Management* **2000**, *41* (6), 559–572.
(31) Performance and Exhaust Emissions in a Natural-Gas Fueled Dual-Fuel Engine https://www.jstage.jst.go.jp/article/jsmeb/44/4/44_4_641/_article/-char/ja/ (accessed 2022 -02 -16).
(32) Papagiannakis, R. G.; Hountalas, D. T. Experimental Investigation Concerning the Effect of Natural Gas Percentage on Performance and Emissions of a DI Dual Fuel Diesel Engine. *Applied Thermal Engineering* **2003**, *23* (3), 353–365.
(33) Hardy, W. L.; Reitz, R. D. A Study of the Effects of High EGR, High Equivalence Ratio, and Mixing Time on Emissions Levels in a Heavy-Duty Diesel Engine for PCCI Combustion. **2006**.
(34) Kalsi, S. S.; Subramanian, et K. Effect of Simulated Biogas on Performance, Combustion and Emissions Characteristics of a Bio-Diesel Fueled Diesel Engine. *Renewable Energy* **2017**, *106*, 78–90.
(35) Nathan, S. S.; Mallikarjuna, J. M.; Ramesh, A. An Experimental Study of the Biogas–Diesel HCCI Mode of Engine Operation. *Energy Conversion and Management* **2010**, *51* (7), 1347–1353.
(36) Feroskhan, M.; Ismail, S. Investigation of the Effects of Biogas Composition on the Performance of a Biogas–Diesel Dual Fuel CI Engine. *Biofuels* **2016**, *7* (6), 593–601.
(37) Feroskhan, M.; Ismail, S. Evaluating the Effect of Intake Parameters on the Performance of a Biogas–Diesel Dual-Fuel Engine Using the Taguchi Method. *Biofuels* **2020**, *11* (4), 441–449.
(38) Barik, D.; Murugan, S.; Sivaram, N. M.; Baburaj, E.; Sundaram, P. S. Experimental Investigation on the Behavior of a Direct Injection Diesel Engine Fueled with Karanja Methyl Ester-Biogas Dual Fuel at Different Injection Timings. *Energy* **2017**, *118*, 127–138.
(39) Yoon, S. H.; Lee, C. S. Experimental Investigation on the Combustion and Exhaust Emission Characteristics of Biogas–Biodiesel Dual-Fuel Combustion in a CI Engine. *Fuel processing technology* **2011**, *92* (5), 992–1000.
(40) Sabari Girish, G.; Vijayakothandaraman, R.; Prabhu, A. Experimental Investigation on a CI Engine Fuelled with Bio Gas and Rice Straw Additives. *International Journal of Ambient Energy* **2019**, *40* (6), 610–612.
(41) Vijin Prabhu, A.; Manimaran, R.; Jeba, P.; Babu, R. Effect of Methane Enrichment on the Performance of a Dual Fuel CI Engine. *International Journal of Ambient Energy* **2021**, *42* (3), 325–330.

(42) Debabrata, B.; Murugan, S. Investigation on Combustion Performance and Emission Characteristics of a DI (Direct Injection) Diesel Engine Fueled with Biogas-Diesel in Dual Fuel Mode. *Energy (Oxford)* **2014**, *72*, 760–771.
(43) Rahman, K. A.; Ramesh, A. Studies on the Effects of Methane Fraction and Injection Strategies in a Biogas Diesel Common Rail Dual Fuel Engine. *Fuel* **2019**, *236*, 147–165.
(44) Mahla, S. K.; Singla, V.; Sandhu, S. S.; Dhir, A. Studies on Biogas-Fuelled Compression Ignition Engine under Dual Fuel Mode. *Environmental Science and Pollution Research* **2018**, *25* (10), 9722–9729.
(45) Shan, X.; Qian, Y.; Zhu, L.; Lu, X. Effects of EGR Rate and Hydrogen/Carbon Monoxide Ratio on Combustion and Emission Characteristics of Biogas/Diesel Dual Fuel Combustion Engine. *Fuel* **2016**, *181*, 1050–1057.
(46) Verma, S.; Das, L. M.; Kaushik, S. C.; Bhatti, S. S. The Effects of Compression Ratio and EGR on the Performance and Emission Characteristics of Diesel-Biogas Dual Fuel Engine. *Applied Thermal Engineering* **2019**, *150*, 1090–1103.
(47) Ajav, E. A.; Singh, B.; Bhattacharya, T. K. Thermal Balance of a Single Cylinder Diesel Engine Operating on Alternative Fuels. *Energy conversion and management* **2000**, *41* (14), 1533–1541.
(48) Zhang, Z. H.; Cheung, C. S.; Chan, T. L.; Yao, C. D. Experimental Investigation of Regulated and Unregulated Emissions from a Diesel Engine Fueled with Euro V Diesel Fuel and Fumigation Methanol. *Atmospheric Environment* **2010**, *44* (8), 1054–1061.
(49) Zhang, Z. H.; Tsang, K. S.; Cheung, C. S.; Chan, T. L.; Yao, C. D. Effect of Fumigation Methanol and Ethanol on the Gaseous and Particulate Emissions of a Direct-Injection Diesel Engine. *Atmospheric Environment* **2011**, *45* (11), 2001–2008.
(50) Ferrari, G. *Motori a Combustione Interna*, I.; Società Editrice Esculapio, 2016.
(51) Thiyagarajan, S.; Edwin Geo, V.; Martin, L. J.; Nagalingam, B. Carbon Dioxide (CO2) Capture and Sequestration Using Biofuels and an Exhaust Catalytic Carbon Capture System in a Single-Cylinder CI Engine: An Experimental Study. *Biofuels* **2018**, *9* (6), 659–668.
(52) Bp-Stats-Review-2021-Full-Report.Pdf.
(53) Dall'etanolo di canapa a quello da cianobatteri: l'evoluzione dei biocarburanti e delle biofabbriche - Microbiologia Italia https://www.microbiologiaitalia.it/batteriologia/levoluzione-dei-biocarburanti-e-delle-biofabbriche/ (accessed 2022 -02 -20).
(54) Hansen, A. C.; Zhang, Q.; Lyne, P. W. Ethanol–Diesel Fuel Blends—-a Review. *Bioresource technology* **2005**, *96* (3), 277–285.
(55) Agarwal, A. K. Biofuels (Alcohols and Biodiesel) Applications as Fuels for Internal Combustion Engines. *Progress in energy and combustion science* **2007**, *33* (3), 233–271.
(56) Larson, E. D. A Review of Life-Cycle Analysis Studies on Liquid Biofuel Systems for the Transport Sector. *Energy for Sustainable Development* **2006**, *10* (2), 109–126. https://doi.org/10.1016/S0973-0826(08)60536-0.
(57) IEA – International Energy Agency https://www.iea.org (accessed 2022 -03 -01).
(58) Reif, K. Gasoline Engine Management. *Bosch Professional Automotive Information, DOI* **2015**, *10*, 978–3.
(59) *Transport, Energy and CO2*; International Energy Agency (IEA), 2009.
(60) JRC, R. E.; HASS, H.; LARIVÉ, J.-F.; JRC, L. L.; MAAS, H.; Rickeard, D. Well-to-Wheels Report Version 4. a JEC Well-to-Wheels Analysis. *Institute for Energy and Transport, Joint Research Centre, Luxembourg: Publications Office of the European Union* **2014**, *2014*.
(61) EPA Analysis of the Exhaust Emission Impacts of Biodiesel Presentation to the Mobile Source Technical Review Subcommittee. 27.
(62) Wu, G.; Ge, J. C.; Choi, N. J. A Comprehensive Review of the Application Characteristics of Biodiesel Blends in Diesel Engines. *Applied Sciences* **2020**, *10* (22), 8015. https://doi.org/10.3390/app10228015.
(63) Lee, I.; Johnson, L. A.; Hammond, E. G. Use of Branched-Chain Esters to Reduce the Crystallization Temperature of Biodiesel. *Journal of the American Oil Chemists' Society* **1995**, *72* (10), 1155–1160.
(64) Crua, C.; de Sercey, G.; Heikal, M. R. Dropsizing of Near-Nozzle Diesel and RME Sprays by Microscopic Imaging. **2012**, 9.

(65) Kaplan, C.; Arslan, R.; Sürmen, A. Performance Characteristics of Sunflower Methyl Esters as Biodiesel. *Energy Sources* **2006**, *28* (8), 751–755.
(66) Senatore, A.; Cardone, M.; Rocco, V.; Prati, M. V. *A Comparative Analysis of Combustion Process in DI Diesel Engine Fueled with Biodiesel and Diesel Fuel*; SAE Technical Paper, 2000.
(67) Hwang, J.; Qi, D.; Jung, Y.; Bae, C. Effect of Injection Parameters on the Combustion and Emission Characteristics in a Common-Rail Direct Injection Diesel Engine Fueled with Waste Cooking Oil Biodiesel. *Renewable Energy* **2014**, *63*, 9–17.
(68) Kalligeros, S.; Zannikos, F.; Stournas, S.; Lois, E.; Anastopoulos, G.; Teas, C.; Sakellaropoulos, F. An Investigation of Using Biodiesel/Marine Diesel Blends on the Performance of a Stationary Diesel Engine. *Biomass and Bioenergy* **2003**, *24* (2), 141–149.
(69) Westbrook, C. K.; Pitz, W. J.; Curran, H. J. Chemical Kinetic Modeling Study of the Effects of Oxygenated Hydrocarbons on Soot Emissions from Diesel Engines. *The journal of physical chemistry A* **2006**, *110* (21), 6912–6922.
(70) Hwang, J.; Jung, Y.; Bae, C. Comprehensive Assessment of Soot Particles from Waste Cooking Oil Biodiesel and Diesel in a Compression Ignition Engine. *SAE International Journal of Fuels and Lubricants* **2015**, *8* (2), 290–297.
(71) Lapuerta, M.; Armas, O.; Rodriguez-Fernandez, J. Effect of Biodiesel Fuels on Diesel Engine Emissions. *Progress in energy and combustion science* **2008**, *34* (2), 198–223.
(72) Youn, I. M.; Park, S. H.; Roh, H. G.; Lee, C. S. Investigation on the Fuel Spray and Emission Reduction Characteristics for Dimethyl Ether (DME) Fueled Multi-Cylinder Diesel Engine with Common-Rail Injection System. *Fuel processing technology* **2011**, *92* (7), 1280–1287.
(73) Park, S. H.; Lee, C. S. Combustion Performance and Emission Reduction Characteristics of Automotive DME Engine System. *Progress in energy and combustion science* **2013**, *39* (1), 147–168.
(74) Arcoumanis, C.; Bae, C.; Crookes, R.; Kinoshita, E. The Potential of Di-Methyl Ether (DME) as an Alternative Fuel for Compression-Ignition Engines: A Review. *Fuel* **2008**, *87* (7), 1014–1030.
(75) Sorenson, S. C.; Glensvig, M.; Abata, D. L. Dimethyl Ether in Diesel Fuel Injection Systems. *SAE transactions* **1998**, 438–449.
(76) Park, S. H.; Lee, C. S. Applicability of Dimethyl Ether (DME) in a Compression Ignition Engine as an Alternative Fuel. *Energy Conversion and Management* **2014**, *86*, 848–863.
(77) Kim, M. Y.; Yoon, S. H.; Ryu, B. W.; Lee, C. S. Combustion and Emission Characteristics of DME as an Alternative Fuel for Compression Ignition Engines with a High Pressure Injection System. *Fuel* **2008**, *87* (12), 2779–2786.
(78) Egnell, R. Comparison of Heat Release and NOx Formation in a DI Diesel Engine Running on DME and Diesel Fuel. *SAE Transactions* **2001**, 492–506.
(79) Teng, H.; McCandless, J. C.; Schneyer, J. B. Thermochemical Characteristics of Dimethyl Ether—an Alternative Fuel for Compression-Ignition Engines. *SAE transactions* **2001**, 96–106.
(80) Yao, M.; Zheng, Z.; Xu, S.; Fu, M. Experimental Study on the Combustion Process of Dimethyl Ether (DME). *SAE transactions* **2003**, 2422–2429.
(81) Jeon, J.; Kwon, S. I.; Park, Y. H.; Oh, Y.; Park, S. Visualizations of Combustion and Fuel/Air Mixture Formation Processes in a Single Cylinder Engine Fueled with DME. *Applied energy* **2014**, *113*, 294–301.
(82) Beer, T.; Grant, T. Life-Cycle Analysis of Emissions from Fuel Ethanol and Blends in Australian Heavy and Light Vehicles. *Journal of Cleaner Production* **2007**, *15* (8–9), 833–837.
(83) Hardenberg, H. O.; Ehnert, E. R. Ignition Quality Determination Problems with Alternative Fuels for Compression Ignition Engines. *SAE Transactions* **1981**, 3782–3788.
(84) Demirbas, A.; Gullu, D. Acetic Acid, Methanol and Acetone from Lignocellulosics by Pyrolysis. *Energy Edu. Sci. Technol* **1998**, *1* (2), 111–115.
(85) Nichols, R. J. The Methanol Story: A Sustainable Fuel for the Future. **2003**.
(86) He, B.-Q.; Shuai, S.-J.; Wang, J.-X.; He, H. The Effect of Ethanol Blended Diesel Fuels on Emissions from a Diesel Engine. *Atmospheric Environment* **2003**, *37* (35), 4965–4971.
(87) Ecklund, E. E.; Bechtold, R. L.; Timbario, T. J.; McCallum, P. W. State-of-the-Art Report on the Use of Alcohols in Diesel Engines. *SAE transactions* **1984**, 684–702.
(88) Demirbas, A. *Methane Gas Hydrate: As a Natural Gas Source*; Springer, 2010.

(89) Wei, L.; Geng, P. A Review on Natural Gas/Diesel Dual Fuel Combustion, Emissions and Performance. *Fuel Processing Technology* **2016**, *142*, 264–278.
(90) Lhuillier, C.; Brequigny, P.; Contino, F.; Mounaïm-Rousselle, C. Combustion Characteristics of Ammonia in a Modern Spark-Ignition Engine. In *Conference on Sustainable Mobility*; 2019.
(91) Makareviciene, V.; Sendzikiene, E.; Pukalskas, S.; Rimkus, A.; Vegneris, R. Performance and Emission Characteristics of Biogas Used in Diesel Engine Operation. *Energy Conversion and Management* **2013**, *75*, 224–233.
(92) Bari, S. Effect of Carbon Dioxide on the Performance of Biogas/Diesel Duel-Fuel Engine. *Renewable energy* **1996**, *9* (1–4), 1007–1010.
(93) Crookes, R. J. Comparative Bio-Fuel Performance in Internal Combustion Engines. *Biomass and Bioenergy* **2006**, *30* (5), 461–468.
(94) Henham, A.; Makkar, et M. Combustion of Simulated Biogas in a Dual-Fuel Diesel Engine. *Energy Conversion and Management* **1998**, *39* (16–18), 2001–2009.
(95) Bordelanne, O.; Montero, M.; Bravin, F.; Prieur-Vernat, A.; Oliveti-Selmi, O.; Pierre, H.; Papadopoulo, M.; Muller, T. Biomethane CNG Hybrid: A Reduction by More than 80% of the Greenhouse Gases Emissions Compared to Gasoline. *Journal of Natural Gas Science and Engineering* **2011**, *3* (5), 617–624.
(96) Subramanian, K. A.; Mathad, V. C.; Vijay, V. K.; Subbarao, P. M. V. Comparative Evaluation of Emission and Fuel Economy of an Automotive Spark Ignition Vehicle Fuelled with Methane Enriched Biogas and CNG Using Chassis Dynamometer. *Applied Energy* **2013**, *105*, 17–29.
(97) Yang, L.; Ge, X.; Wan, C.; Yu, F.; Li, Y. Progress and Perspectives in Converting Biogas to Transportation Fuels. *Renewable and Sustainable Energy Reviews* **2014**, *40*, 1133–1152.
(98) Dimitriou, P.; Tsujimura, T. A Review of Hydrogen as a Compression Ignition Engine Fuel. *International Journal of Hydrogen Energy* **2017**, *42* (38), 24470–24486.
(99) SinghYadav, V.; Soni, S. L.; Sharma, D. Performance and Emission Studies of Direct Injection CI Engine in Duel Fuel Mode (Hydrogen-Diesel) with EGR. *International journal of hydrogen energy* **2012**, *37* (4), 3807–3817.
(100) De Morais, A. M.; Justino, M. A. M.; Valente, O. S.; de Morais Hanriot, S.; Sodré, J. R. Hydrogen Impacts on Performance and CO2 Emissions from a Diesel Power Generator. *international journal of hydrogen energy* **2013**, *38* (16), 6857–6864.
(101) Sandalcı, T.; Karagöz, Y. Experimental Investigation of the Combustion Characteristics, Emissions and Performance of Hydrogen Port Fuel Injection in a Diesel Engine. *International journal of hydrogen energy* **2014**, *39* (32), 18480–18489.
(102) Wu, H.-W.; Wu, Z.-Y. Investigation on Combustion Characteristics and Emissions of Diesel/Hydrogen Mixtures by Using Energy-Share Method in a Diesel Engine. *Applied Thermal Engineering* **2012**, *42*, 154–162.
(103) Suzuki, Y.; Tsujimura, T. *The Combustion Improvements of Hydrogen/Diesel Dual Fuel Engine*; SAE Technical Paper, 2015.
(104) Agarwal, A. K.; Singh, A. P.; Maurya, R. K. Evolution, Challenges and Path Forward for Low Temperature Combustion Engines. *Progress in energy and combustion science* **2017**, *61*, 1–56.
(105) Reitz, R. D.; Duraisamy, G. Review of High Efficiency and Clean Reactivity Controlled Compression Ignition (RCCI) Combustion in Internal Combustion Engines. *Progress in Energy and Combustion Science* **2015**, *46*, 12–71. https://doi.org/10.1016/j.pecs.2014.05.003.
(106) KOHLER Engines, “KOHLER G2-165 Technical Datasheet”, Accessed July 2020, Http://Www.Kohlerpower.Com/Onlinecatalog/Pdf/G2165.Pdf.
(107) MTU, “MTU 4R0113 DS94 Technical Datasheet”, Accessed July 2020, Https://Www.Mtu-Solutions.Com/Eu/En/Products/Power-Generation-Products-List.Html.
(108) VOLVO PENTA, “VOLVO PENTA TAD550GE Technical Datasheet”, Accessed July 2020, Https://Www.Volvopenta.It/Industrialpowergeneration/It-It/Products/Engines/Ranges/Prime-Power-Pg.Html.
(109) Cummins, “Cummins QSB5-G4 Technical Datasheet”, Accessed July 2020, Https://Www.Cummins.Com/g-Drive-Engines/Diesel-Electronic-b-Series.

(110) HIMOINSA, “HIMOINSA HHW-95 T5 Technical Datasheet”, Accessed July 2020, Https://Www.Himoinsa.Com/Eng/Electric-Generators/488/Generator-Set--90kva--Open-Skid.Html.
(111) MOTEURS Baudouin, “MOTEURS Baudouin 4M11G90/5 Technical Datasheet”, Accessed July 2020, Https://Www.Baudouin.Nl/Wp-Content/Themes/Baudouin/Files/Gensets/Specs/4M11/PowerKit%20Datasheet%204M11G90-5.Pdf.
(112) Yamamoto, H.; Uchida, H. Oxidation of Methane over Pt and Pd Supported on Alumina in Lean-Burn Natural-Gas Engine Exhaust. *Catalysis today* **1998**, *45* (1–4), 147–151.
(113) Shao, Z.; Dallmann, T.; Bandivadekar, A. European Stage V Non-Road Emission Standards. 9.
(114) Benajes, J.; García, A.; Monsalve-Serrano, J.; Boronat, V. Achieving Clean and Efficient Engine Operation up to Full Load by Combining Optimized RCCI and Dual-Fuel Diesel-Gasoline Combustion Strategies. *Energy Conversion and Management* **2017**, *136*, 142–151.
(115) Versteeg e Malalasekera - 2007 - An Introduction to Computational Fluid Dynamics t.Pdf.
(116) Golovitchev, V. I.; Montorsi, L.; Rinaldini, C. A.; Rosetti, A. CFD Combustion and Emission Formation Modeling for a HSDI Diesel Engine Using Detailed Chemistry. In *Internal Combustion Engine Division Fall Technical Conference*; 2006; Vol. 42606, pp 349–358.
(117) Gustavsson, J.; Golovitchev, V. I. *Spray Combustion Simulation Based on Detailed Chemistry Approach for Diesel Fuel Surrogate Model*; SAE Technical Paper, 2003.
(118) Golovitchev, V. I.; Nordin, N.; Jarnicki, R.; Chomiak, J. 3-D Diesel Spray Simulations Using a New Detailed Chemistry Turbulent Combustion Model. *SAE transactions* **2000**, 1391–1405.
(119) Ehleskog, R.; Golovitchev, V.; Denbratt, I.; Andersson, S.; Rinaldini, C. A. Experimental and Numerical Investigation of Split Injections at Low Load in an HDDI Diesel Engine Equipped with a Piezo Injector. *SAE Transactions* **2006**, 932–946.
(120) Golovitchev, V. I.; Imren, A. Development of Dual Fuel Combustion Models for Direct Injected Heavy Duty Diesel Engines. *Diesel fuels: characteristics, performances and environmental impacts. Nova Pusblisher* **2013**.
(121) Mattarelli, E.; Rinaldini, C. A.; Golovitchev, V. I. CFD-3D Analysis of a Light Duty Dual Fuel (Diesel/Natural Gas) Combustion Engine. *Energy Procedia* **2014**, *45*, 929–937.
(122) Cantore, G.; Mattarelli, E.; Rinaldini, C. A.; Savioli, T.; Scrignoli, F. Numerical Optimization of the Injection Strategy on a Light Duty Diesel Engine Operating in Dual Fuel (CNG/Diesel) Mode. *International Journal of Heat and Technology* **2019**, *37* (3), 682–688.
(123) Amsden, A. A.; Findley, M. *KIVA-3V: A Block-Structured KIVA Program for Engines with Vertical or Canted Valves*; Lawrence Livermore National Lab.(LLNL), Livermore, CA (United States), 1997.
(124) Mattarelli, E.; Rinaldini, C. A.; Savioli, T. Dual Fuel (Natural Gas Diesel) for Light-Duty Industrial Engines: A Numerical and Experimental Investigation. *Natural Gas Engines* **2019**, 297–328.
(125) Legrottaglie, F.; Mattarelli, E.; Rinaldini, C. A.; Scrignoli, F. Application to Micro-Cogeneration of an Innovative Dual Fuel Compression Ignition Engine Running on Biogas. *International Journal of Thermofluids* **2021**, *10*, 100093.
(126) Regulation No 49 of the Economic Commission for Europe of the United Nations (UN/ECE)) https://eur-lex.europa.eu/legal-content/EN/TXT/HTML/?uri=CELEX:42013X0624(01)&from=EN (accessed 2021 -04 -11).
(127) Himoinsa. HIMOINSA a Yanmar Company, Generator Sets, Lighting towers https://www.himoinsa.com/ (accessed 2022 -03 -03).
(128) Rahmouni, C.; Tazerout, M.; Le Corre, O. A Method to Determine Biogas Composition for Combustion Control. *SAE Transactions* **2002**, 700–709.
(129) Verhelst, S.; Wallner, T. Hydrogen-Fueled Internal Combustion Engines. *Progress in Energy and Combustion Science* **2009**, *35* (6), 490–527. https://doi.org/10.1016/j.pecs.2009.08.001.